



Universidade do Minho
Escola de Engenharia

Hugo Manuel Martins Machado

**Thermo-economic model of a photovoltaic
plant integrated with H₂ production**

outubro de 2023



Universidade do Minho
Escola de Engenharia

Hugo Manuel Martins Machado

Thermo-economic model of a photovoltaic plant integrated with H2 production

Dissertação de Mestrado em Engenharia Mecânica
Área Especialização em Tecnologias Energéticas e
Ambientais

Trabalho efetuado sob a orientação de:
Professor Doutor José Carlos Teixeira
Professora Doutora Ana Cristina Ferreira

DIREITOS DE AUTOR E CONDIÇÕES DE UTILIZAÇÃO DO TRABALHO POR TERCEIROS

Este é um trabalho académico que pode ser utilizado por terceiros desde que respeitadas as regras e boas práticas internacionalmente aceites, no que concerne aos direitos de autor e direitos conexos.

Assim, o presente trabalho pode ser utilizado nos termos previstos na licença abaixo indicada.

Caso o utilizador necessite de permissão para poder fazer um uso do trabalho em condições não previstas no licenciamento indicado, deverá contactar o autor, através do RepositóriUM da Universidade do Minho.

Licença concedida aos utilizadores deste trabalho



Atribuição

CC BY

<https://creativecommons.org/licenses/by/4.0/>

AGRADECIMENTOS

Após a conclusão do projeto de dissertação, resta-me expressar uma palavra de enorme gratidão a um grupo específico de pessoas.

Ao meu orientador, Professor Doutor José Carlos Teixeira, manifesto o meu apreço pela disponibilidade e excelentes conselhos proporcionados, que me permitiram uma diversificada aprendizagem nos campos abordados neste projeto.

À minha orientadora, Professora Doutora Ana Cristina Ferreira, quero expressar um enorme agradecimento. Pela sua dedicação incansável ao longo de todos os meses de trabalho, tornou a conclusão deste projeto possível.

Expresso também o meu agradecimento à Voltalia, que me concedeu a oportunidade de desenvolver este projeto. Em particular, quero expressar a minha gratidão ao Engenheiro Tiago Costa, pela sua total disponibilidade e ajuda ao longo destes meses de trabalho.

DECLARAÇÃO DE INTEGRIDADE

Declaro ter atuado com integridade na elaboração do presente trabalho acadêmico e confirmo que não recorri à prática de plágio nem a qualquer forma de utilização indevida ou falsificação de informações ou resultados em nenhuma das etapas conducente à sua elaboração.

Mais declaro que conheço e que respeitei o Código de Conduta Ética da Universidade do Minho.

ABSTRACT

In the current context, there is a growing global concern regarding environmental degradation. Governments and non-governmental organizations across the globe have adopted precautionary strategies and policies aimed at the mitigation of greenhouse gas emissions. These efforts are verified through substantial investments in renewable energy. However, some pivotal considerations arise. Firstly, weather-related fluctuations affect the production of some clean energy sources. Second, aligning intermittent renewable systems with grid demands presents a colossal challenge.

Hence, there is an imperative need to develop an integrated system for renewable power plants. This necessitates the implementation of both daily and seasonal energy balancing strategies, encompassing the storage of surplus energy generated during favourable periods. This surplus energy is then deployed during periods when renewable sources alone are inadequate to meet grid demand. One proposed solution is focused on the utilization of hydrogen. This system entails the storage of clean energy to convert intermittent production into chemical energy, thereby preventing wastage. In this regard, a mathematical model was developed to optimize energy usage from a photovoltaic power plant. The primary objective was to maximize energy utilization.

The design of the photovoltaic power plant, which produces 3.9 GWh/year, aimed to generate electricity that directly met predefined consumption requirements. In the absence of such requirements, surplus electricity could be employed for water electrolysis to produce hydrogen. This provided flexibility in meeting consumption needs, whether through direct electricity or previously generated and stored hydrogen.

The proposed and simulated model was analysed from the thermodynamic and economic point of view. Regarding the surplus energy storage, the model effectively handles excess power by injecting only 5.58 MWh into the electrical grid and purchasing 0.162 GWh from it. Moreover, the project exhibits positive returns exceeding its initial costs, with a net present value of 5.2 million euros, making it a financially appealing investment.

Keywords: Power-to-X, green hydrogen, energy storage, photovoltaic.

RESUMO

A degradação ambiental é atualmente bastante significativa e é uma preocupação que se encontra mundialmente difundida. Assim sendo, governos e organizações não-governamentais em todo o mundo adotam estratégias e políticas preventivas que visam a redução das emissões de gases com efeito estufa. Tais iniciativas refletem-se em investimentos significativos para a adoção de energias renováveis. Porém, existem considerações fundamentais que deverão ser denotadas. Em primeiro lugar, as flutuações climáticas têm impacto na produção de determinadas fontes de energia renovável. Em segundo lugar, conciliar sistemas intermitentes de energia renovável com o requerido pela rede representa um desafio de grande magnitude.

Por conseguinte, existe urgência no desenvolvimento de um sistema integrado para centrais de energia renovável. Para tal, é fundamental a implementação de estratégias de equilíbrio energético, diárias e sazonais, que englobem o armazenamento do excesso de energia gerada durante os períodos favoráveis. A mesma seria utilizada em períodos em que as fontes de energia renovável, por si só, não satisfazem o requerido pela rede.

A solução proposta centra-se na criação de um sistema que envolve o armazenamento de energia renovável em hidrogénio, através da conversão da energia elétrica em energia química. Nesse sentido, foi desenvolvido um modelo matemático, capaz de otimizar o uso de energia de uma central fotovoltaica, cujo principal objetivo focou-se em maximizar a utilização de energia. O projeto da central fotovoltaica, que produz 3.9 GWh/ano, teve como diretriz a conformidade com os requisitos de consumo predefinidos. Na ausência desses requisitos, a eletricidade excedente poderia ser utilizada na eletrólise da água de modo a produzir hidrogénio. Isso possibilita uma correta resposta às exigências de consumo.

Por sua vez, o modelo foi alvo de uma avaliação técnica e económica. No que diz respeito ao armazenamento da energia, o modelo gere de forma eficiente os recursos de energia excedente, com a injeção de apenas 5.58 MWh na rede nacional elétrica e a compra de 0.162 GWh à mesma. Além disso, o projeto apresenta retornos promissores que superam os seus gastos iniciais, apresentando um valor atual líquido de 5.2 milhões de euros.

Palavra-chave: *Power-to-X*, hidrogénio verde, retenção de energia, fotovoltaico

CONTENT

| | |
|--|-------|
| Abstract | v |
| Resumo..... | vi |
| Content..... | vii |
| List of Figures..... | xi |
| Tables List..... | xviii |
| 1. Introduction..... | 1 |
| 1.1 Motivation and contextualization | 1 |
| 1.1.1 Global environmental and social concerns..... | 1 |
| 1.1.2 European Union policies | 3 |
| 1.1.3 Decarbonization: renewable energies integration | 4 |
| 1.1.4 Incorporation of hydrogen as a strategic vector | 5 |
| 1.2 Proposed objectives | 6 |
| 1.3 Dissertation structure..... | 7 |
| 2. Hydrogen value chain..... | 8 |
| 2.1 Feedstock and hydrogen production | 12 |
| 2.1.1 Feedstocks for water electrolysis..... | 12 |
| 2.1.2 Production methods..... | 14 |
| 2.1.3 Classification of hydrogen by colours | 16 |
| 2.1.4 Classification of hydrogen by European Commission..... | 19 |
| 2.1.5 Categories comparison..... | 20 |
| 2.2 Hydrogen storage | 21 |
| 2.2.1 Compression and liquefaction: methods comparison | 23 |
| 2.2.2 Technical considerations for gaseous hydrogen storage..... | 26 |
| 2.2.3 Technical considerations for underground storage..... | 27 |
| 2.2.4 Technical considerations for cryo-compressed storage | 30 |
| 2.2.5 Characteristics of hydrogen storage vessels..... | 31 |
| 2.3 Hydrogen transportation..... | 34 |

| | | |
|-------|--|----|
| 2.3.1 | Technical considerations for gaseous hydrogen transportation | 35 |
| 2.3.2 | Technical considerations for pipeline transportation..... | 37 |
| 2.3.3 | Technical considerations for liquid hydrogen transportation | 39 |
| 2.4 | Hydrogen applications..... | 40 |
| 3. | Component characterization of a PV power plant integrated with hydrogen production | 47 |
| 3.1 | PV power production unit | 47 |
| 3.1.1 | PV panels and solar tracker system | 47 |
| 3.1.2 | Combiner string box..... | 48 |
| 3.1.3 | Maximum power point tracking | 49 |
| 3.2 | Green hydrogen production systems based on electrolysis | 51 |
| 3.2.1 | Electrolysis process | 51 |
| 3.2.2 | Types of electrolyzers..... | 54 |
| 3.2.3 | Auxiliary components of electrolysis | 60 |
| 3.2.4 | Behaviour of electrolyzers connected to renewable energies | 61 |
| 3.3 | Compressor..... | 64 |
| 3.3.1 | Compression efficiency | 65 |
| 3.3.2 | Performance characteristics of a reciprocating compressor | 67 |
| 3.4 | Fuel cell..... | 69 |
| 3.4.1 | Fuel cell general operation..... | 70 |
| 3.4.2 | Types of fuel cells | 71 |
| 3.4.3 | Fuel cells efficiency | 76 |
| 3.5 | PV-electrolyser connection system design..... | 79 |
| 3.5.1 | Direct connection | 79 |
| 3.5.2 | Indirect connection | 80 |
| 4. | System description and mathematical model | 83 |
| 4.1 | Profile of industry energy consumption..... | 84 |
| 4.2 | Location of the power plant installation | 85 |

| | | |
|-------|--|-----|
| 4.3 | Input of meteorological data..... | 86 |
| 4.4 | System description | 88 |
| 4.4.1 | PV power plant..... | 89 |
| 4.4.2 | Hydrogen production unit..... | 91 |
| 4.4.3 | Compressor | 94 |
| 4.4.4 | Hydrogen storage..... | 96 |
| 4.4.5 | Fuel cell | 97 |
| 4.4.6 | Battery..... | 98 |
| 4.4.7 | Hydrogen flow parametrization..... | 99 |
| 4.5 | Mathematical modelling | 100 |
| 4.5.1 | Energy pathway efficiency | 100 |
| 4.5.2 | Electrolyser state..... | 102 |
| 4.5.3 | Transition criteria | 103 |
| 4.5.4 | Energy distribution..... | 104 |
| 5. | Results and discussion..... | 114 |
| 5.1 | Reference case simulation..... | 115 |
| 5.1.1 | Energy distribution analysis | 115 |
| 5.1.2 | Simulation of a daily profile in December..... | 115 |
| 5.1.3 | Simulation of a daily profile in August | 122 |
| 5.1.4 | Monthly analysis | 125 |
| 5.2 | Sensitivity analysis | 130 |
| 5.2.1 | Analysis of electrolyser capacity | 130 |
| 5.2.2 | Analysis of hydrogen storage capacity..... | 133 |
| 5.2.3 | Analysis of industry demand increase | 134 |
| 5.2.4 | Analysis of the increase in hydrogen storage capacity and industry demand..... | 136 |
| 5.3 | Improved system operating scenario..... | 138 |
| 5.3.1 | High demand | 138 |
| 5.3.3 | Annual analysis..... | 141 |

| | | |
|-------|---|-----|
| 5.3.4 | Analysis of industry demand..... | 146 |
| 6. | Economic analysis | 151 |
| 6.1 | Assessing initial investment and operating costs..... | 151 |
| 6.2 | Revenues | 155 |
| 6.3 | Calculation of avoided costs..... | 156 |
| 6.4 | Analysis of economic viability..... | 158 |
| 7. | Conclusions and Prospects for future work..... | 160 |
| 7.1 | Conclusions..... | 160 |
| 7.2 | Prospects for future work..... | 161 |
| | References..... | 162 |
| | Appendices | 175 |
| | Appendix 1 – Components of the projected model | 175 |
| | Appendix 2 – Data base | 177 |
| | Appendix 3 – Photovoltaic resolution methodology..... | 178 |
| | Appendix 4 – Economic analysis..... | 179 |
| | Annexes | 181 |
| | Annex 1 – Conference of the Parties (COP)..... | 181 |
| | Annex 2 – Manufacturer's information | 183 |

LIST OF FIGURES

Figure 1 - Share of world total final energy consumption by source in 2019..... 2

Figure 2 - Comprehensive view of a hydrogen supply chain framework..... 9

Figure 3 – Example of a centralized water electrolyser..... 10

Figure 4 – Example of a decentralized water electrolyser..... 10

Figure 5 – Most common storage and transportation methods. The blue lines represent pathways where a change of state occurs. 11

Figure 6 – General hydrogen production processes. Adapted from Al-Qahtani et al. (2021a). 14

Figure 7 – Scale of TRL (European Space Agency, 2023)..... 17

Figure 8 – Summary of the categorization of hydrogen by colours, and comparison of its carbon dioxide emissions, environmental impact, and cleanliness of the compound produced. FF stands for fossil fuels and RE for renewable energies (Germescheidt et al., 2021). 19

Figure 9 - Energy density for different fuels. Adapted from Escamilla et al. (2022)... 22

Figure 10 - Hydrogen storage technologies (Hassan et al., 2021). 23

Figure 11 – Example of a hydrogen liquefaction facility (T & Ch, 2012)..... 24

Figure 12 - Example of a cylinder storage tank for hydrogen gas (India Hydrogen Alliance, 2021)..... 27

Figure 13 – Illustration of underground hydrogen storage through a salt cavern (Wolter, 2020). 28

Figure 14 - Example of a common vessel for liquid hydrogen: (1) inner vessel (tank) for liquid hydrogen; (2) outer vessel (casing); (3) thermal insulation; (4) casing safety diaphragm; (5) pressure gauge; (6) safety devices (valve and diaphragm) of the inner vessel; (7) pipe for gas discharge; (8) drain and fill pipe; (9) level indicator; (10) evaporator (or receiver with compressed gaseous hydrogen or helium); (11) branch pipe for sampling liquid hydrogen; (12) vacuum control in the insulating space (Kotowicz et al., 2017)..... 32

Figure 15 – Example of a spherical liquid hydrogen storage tank (Kyodo, 2023)..... 32

Figure 16 - Categorization of pressure vessels (Hassan et al., 2021)..... 33

| | |
|---|----|
| Figure 17 - Example of liquid hydrogen being transported via ship (Collins Leigh, 2022). | 34 |
| Figure 18 - Example of hydrogen being transported via train (Diermann, 2020)..... | 34 |
| Figure 19 – Example of a truck trailer coupled with hydrogen gas storage bundled tubes (AIChE Academy, 2020). | 35 |
| Figure 20 – Illustration of a hydrogen pipeline (Nguyen, 2023). | 38 |
| Figure 21 – Example of a truck trailer coupled with liquid hydrogen storage tank (Furui CIT, 2022)..... | 40 |
| Figure 22 - Hydrogen demand across sectors and regions. Adapted from IEA, (2022). | 41 |
| Figure 23 - Dissemination of hydrogen applications (Fonseca et al., 2019). | 44 |
| Figure 24 – Types of trackers for PV system (Kang et al., 2019)..... | 48 |
| Figure 25 – Example of a string combiner box..... | 49 |
| Figure 26 – I-V curves for different a) irradiance, and b) temperature. Adapted from (Tajuddin et al., 2015). | 49 |
| Figure 27 – Example of varying conditions and MPP trajectory response (Firak & Djukić, 2010)..... | 50 |
| Figure 28 - Influence of temperature on thermodynamic parameters of water electrolysis. Adapted from Hussain (2021). | 52 |
| Figure 29 – Example of an alkaline electrolyser cell functional principle (Shiva Kumar & Lim, 2022). | 55 |
| Figure 30 - Example of an PEM electrolyser cell functional principle (Shiva Kumar & Lim, 2022)..... | 57 |
| Figure 31 - Example of a solid oxide electrolyser cell functional principle (Shiva Kumar & Lim, 2022). | 58 |
| Figure 32 – Example of an electrolyser installation supplied by a power plant. The blocks with dashed borders represent examples of elements that integrate some categorization of the auxiliary components and may be present in the installation. | 60 |
| Figure 33 – Experimental results of an electrolyser for different operation conditions. a) variation of current, voltage, temperature, and pressure over time. b) Evolution of hydrogen flow f_{H2} , hydrogen transferred to the oxygen current (HTO), and oxygen transferred to the hydrogen current (OTH) over time (Kojima et al., 2023)..... | 61 |

| | |
|---|----|
| Figure 34 – Family tree of compressors categorization (Brun & Kurz, 2019). | 64 |
| Figure 35 – Comparison of the efficiency of drive systems for a steady torque application (Banerjee, 1998). | 66 |
| Figure 36 – Induction motor and a DC motor efficiency for the same application (Calzada-Lara & Álvarez, 2015). | 67 |
| Figure 37 – Reciprocating compressors efficiency. Adapted from (Hollingsworth et al., 2018). | 68 |
| Figure 38 – Example of mass flow variation over a range of speeds of a reciprocating compressor operating with R-12 refrigerant. Adapted from (Mccovern, 1988). | 68 |
| Figure 39 – Example of isentropic efficiency variation over a range of speeds of a reciprocating compressor operating with carbon dioxide as a refrigerant (Ma et al., 2012). | 69 |
| Figure 40 – Scheme of the working principle of hydrogen fuel cell (Haseli, 2018). ... | 70 |
| Figure 41 – Example of the proton exchange fuel cell in operation (Li et al., 2019). .. | 71 |
| Figure 42 – Working principle of an alkaline fuel cell (Khlifi & Toukebri, 2022). | 72 |
| Figure 43 – Working principle of a PEMFC (Khlifi & Toukebri, 2022). | 73 |
| Figure 44 – Working principle of a PAFC (Khlifi & Toukebri, 2022). | 74 |
| Figure 45 – Working principle of a SOFC (Khlifi & Toukebri, 2022). | 75 |
| Figure 46 – Representation of direct and indirect PV-electrolyser connection. Adapted from Phan Van et al. (2023). | 79 |
| Figure 47 - Examples of possible adjustments in the series-parallel electrolyser cells configuration that can be made to achieve a match between the MPL with the electrolyser load line (I-V) (Phan Van et al., 2023). | 80 |
| Figure 48 – Representation of a direct a) and indirect b) connection between the PV system and the electrolyser. Adapted from (Garrigós et al., 2014). | 81 |
| Figure 49 – Outline of the PV plant integrated with hydrogen production model. ... | 83 |
| Figure 50 - Daily profile of the electrical demand of the industry. | 85 |
| Figure 51 – Location of the modelled installation, from a general and close distance. | 85 |
| Figure 52 – System main components. | 88 |
| Figure 53 - Representation of the most important components of the photovoltaic plant and their respective connections. | 89 |

| | |
|---|-----|
| Figure 54 – Representation of the real PV power plant and the projected power plant. The blue rectangle represents the projected PV panels, while the black ones represent the actual PV panels. | 91 |
| Figure 55 – Layout of the PV system. The grey area represents the available area for the PV panels implementation. The red area was designated as a restricted zone. The blue rectangles represent the PV panels. The purple area represents the substation. The black lines represent the fences, and the grey lines represent the roads. | 91 |
| Figure 56 – Representation of the core elements of the electrolyser ME 450/1400 from H-TEC systems. | 94 |
| Figure 57 - Representation of the chosen hydrogen diaphragm compressor option from the Minnuo Group. | 95 |
| Figure 58 - Representation of the chosen hydrogen storage option from the Honghua (Shandong) Steel Group. | 97 |
| Figure 59 – Illustration of a battery GRES-225-100. | 98 |
| Figure 60 – General representation of the hydrogen flow. | 99 |
| Figure 61 – Illustration of the order of importance regarding the energy application. | 100 |
| Figure 62 – Representation of the energy measurement points of the electrolyser device. | 105 |
| Figure 63 – Electrolyser energy supply when the PV power plant cannot meet the energy demand. | 110 |
| Figure 64 – Meteorological data for the power plant location. GHI stands for global horizontal irradiance, DHI represents the diffuse horizontal irradiance, and Tavg the average of temperature. | 115 |
| Figure 65 - Daily profile of energy distribution produced by the PV power plant. Data for December 16 th | 116 |
| Figure 66 – Illustration of industry demand and its respective energy source supplier. Data for December 16 th | 117 |
| Figure 67 – The hydrogen inlet on the fuel cell device at each hour of the day. Data for December 16 th | 117 |

Figure 68 - a) The hydrogen that is stored at the beginning of each hour in the stationary storage tanks. Data for December 16th. b) The electrolyser hydrogen produced each hour..... 118

Figure 69 – Representation of the source and its respective amount of energy to meet the compressor's demand. Data for December 16th..... 119

Figure 70 – Energy that is stored at the beginning of each hour in the battery. Data for December 16th. 120

Figure 71 – Representation of the electrolyser state in each hour of the day. Data for December 16th. The values are coded as: 0 for idle, 1 for standby, and 2 for the production state..... 120

Figure 72 - Energy available to meet the electrolyser’s demand. Data for December 16th..... 121

Figure 73 - Energy available to meet the fuel cell’s demand. Data for December 16th. 122

Figure 74 - Daily profile of energy distribution produced by the photovoltaic power plant. Data for August 16th..... 123

Figure 75 - The hydrogen stored at the beginning of each hour in the stationary storage tanks. Data for August 16th..... 124

Figure 76 - Illustration of industry demand and its respective energy source supplier. Data for August 16th. 124

Figure 77 – Comparison of hydrogen production, storage, and consumption in December versus August..... 125

Figure 78 - Energy distribution comparison between December and August from the photovoltaic power plant..... 126

Figure 79 - Industry demand and its energy source supplier compared between December and August..... 127

Figure 80 - Representation of annual hydrogen production, storage, and consumption. 128

Figure 81 - Representation of the annual industry demand and its energy source supplier..... 129

Figure 82 – Annual energy distribution from the photovoltaic power plant..... 129

| | |
|--|-----|
| Figure 83 – Representation of the annual energy sold to the grid. Data from the electrolyzers study. | 131 |
| Figure 84 – Annual hydrogen production. Data from the electrolyser analysis. | 131 |
| Figure 85 –Number of cold starts for low-capacity and standard electrolyser registered in December. | 132 |
| Figure 86 - Comparison of hydrogen production, storage and consumption between December and August. | 133 |
| Figure 87 - Energy distribution comparison between December and August from the PV power plant. | 134 |
| Figure 88 - Daily profile of the electrical demand of the industry. | 134 |
| Figure 89 - Comparison of hydrogen production, storage and consumption between December and August. | 135 |
| Figure 90 - Comparison of energy bought from the grid between December and August. | 135 |
| Figure 91 - Energy distribution comparison between December and August from the PV power plant. | 136 |
| Figure 92 - Comparison between December and August of the energy sold to the grid. | 137 |
| Figure 93 - Comparison between December and August of the energy bought from the grid. | 137 |
| Figure 94 - Comparison of hydrogen production, storage and consumption between December and August. | 139 |
| Figure 95 - Industry demand and its energy source supplier compared between December and August. | 140 |
| Figure 96 - Energy distribution comparison between December and August from the photovoltaic power plant. | 141 |
| Figure 97 - Representation of annual hydrogen production, storage, and consumption. | 142 |
| Figure 98 – Annual profile of tank of hydrogen tank’s occupancy of the final high demand model. | 143 |
| Figure 99 - Annual profile of Energy bought from the electrical grid. | 144 |
| Figure 100 - Annual energy distribution from the PV power plant. | 144 |

| | |
|---|-----|
| Figure 101 - Industry annual demand and its energy source supplier. | 145 |
| Figure 102 – Annual energy consumption of the model, and grid-acquired energy. | 146 |
| Figure 103 - Representation of annual hydrogen production and storage. | 147 |
| Figure 104 - Variation of hydrogen mass stored throughout the year. | 148 |
| Figure 105 - Industry annual demand and its energy source supplier. | 148 |
| Figure 106 - Annual energy consumption of the model, and grid-acquired energy. | 149 |
| Figure 107 - Illustration of the distribution of CAPEX for each component of the final model..... | 152 |
| Figure 108 - Example of a Monofacial Si-mono photovoltaic module (Solar Jinko, 2023)..... | 175 |
| Figure 109 - Architectural design of a single axis’s solar tracker. | 175 |
| Figure 110 – Example of a string box (Schneider Electric, 2016)..... | 175 |
| Figure 111 – Illustration of inverter devices (Solar Industry, 2023). | 176 |
| Figure 112 – Illustration of a power transformer. | 176 |
| Figure 113 - Example of a spreadsheet of the database with information about the electrolyser..... | 177 |
| Figure 114 – Example of an electrolyser efficiency spreadsheet of the database. .. | 177 |

TABLES LIST

| | |
|--|----|
| Table 1 – Higher and lower heating values of common fossil fuels and hydrogen | 8 |
| Table 2 – Electrolysis process feedstocks and the corresponding levelized cost of hydrogen | 13 |
| Table 3 – Inputs of general hydrogen productions methods. Adapted from F. Zhang et al. (2016)..... | 15 |
| Table 4 – Description of general production method. Adapted from Zhang et al. (2016) | 15 |
| Table 5 – Technical information of compressed hydrogen storage | 29 |
| Table 6 – Information about storage cylinders from the past and the present (Hassan et al., 2021)..... | 33 |
| Table 7 - Technical information of hydrogen gas transportation found in literature | 39 |
| Table 8 – Technical information of liquid hydrogen transportation found in literature | 40 |
| Table 9 – General characteristics of water electrolysis technologies (Shiva Kumar & Lim, 2022)..... | 59 |
| Table 10 – Fuel cell advantages and disadvantages and application (Gechev & Punov, 2022; Hadi Tawil & Hareb, 2008) | 77 |
| Table 11 – Efficiencies of each type of fuel cell, according to literature | 78 |
| Table 12 – Summary of the location characteristics of the installation | 86 |
| Table 13 – Output data from a TMY..... | 86 |
| Table 14 - Information about which year provided the meteorological data for each month of the TMY | 87 |
| Table 15 – PV panel characteristics..... | 89 |
| Table 16 –The electricity produced by the PV power plant, and the energy demand required by industry on June 2 nd of 2019. | 92 |
| Table 17 – Technical information of electrolyser ME 450/1400 from H-TEC Systems | 93 |
| Table 18 - Technical characteristics of the compressor provided by Shanghai Sollant | 95 |
| Table 19 – Technical characteristics the selected storage tank..... | 97 |

| | |
|--|-----|
| Table 20 – Technical information of the utilised fuel cell provided from Doosan..... | 98 |
| Table 21 - Representation of hydrogen of mass and volume flow at different conditions..... | 99 |
| Table 22 – Efficiencies of photovoltaic power plant to components | 101 |
| Table 23 - Efficiencies of grid to components..... | 101 |
| Table 24 – Presentation of the designed models and corresponding studies conducted. | 114 |
| Table 25 – Representation of the main technical parameters of the standard and low-power electrolyser | 130 |
| Table 26 - Model response concerning the operational state of the electrolyser throughout the day. The “1” represents the operation mode and “0” the idle state..... | 132 |
| Table 27 - Summary of CAPEX of the low demand final model | 151 |
| Table 28 - Summary of OPEX..... | 152 |
| Table 29 - Calculation of the weighted average price of electricity | 153 |
| Table 30 - Price of electricity and deionized water | 153 |
| Table 31 - Electricity demand by components and its supply source..... | 154 |
| Table 32– Annual COGS..... | 154 |
| Table 33 - Water required in one year of hydrogen production | 155 |
| Table 34 - Revenues originated by the sale of hydrogen and PV electricity..... | 155 |
| Table 35 - Representation of the CAPEX, OPEX and COGS for the natural gas power plant..... | 156 |
| Table 36 - Carbon dioxide emissions for one year of operation..... | 157 |
| Table 37 - Natural gas operating costs..... | 157 |
| Table 38 - Economic study characterization | 158 |
| Table 39 - NPV and the IRR of the project | 159 |
| Table 40 - Representation cash flow calculation of the year one and fifteen of the study | 179 |
| Table 41 – Representation of annual cash flows in the economic study, and the respective accumulated values | 180 |
| Table 42 - History of Conference of the Parties (COP)..... | 181 |

LIST OF ABBREVIATIONS AND ACRONYMS

Symbols

| | | |
|------------|-----------------------------|--|
| CF | Cash flow | |
| Ct | Count number of time | - |
| D | Photovoltaic production | - |
| E | Energy | kWh |
| \dot{E} | Specific energy | kWh/kg |
| e^- | Electron | - |
| HHV | High heating value | kWh/kg |
| ie | Interest rate | |
| LHV | Low heating value | |
| Lr | Load ratio | - |
| m | Mass | kg |
| \dot{m} | Mass flow | kg/h |
| P | Power | J/s |
| Q | Heat | J |
| \dot{q} | Volumetric flow | m ³ /h |
| S | Electrolyser state | - |
| t | Lifetime | |
| T | Absolute temperature | K |
| V | Voltage | V |
| W | Work | J |
| ΔG | Gibbs free energy variation | kJmol ⁻¹ |
| ΔH | Enthalpy variation | kJmol ⁻¹ |
| ΔS | Entropy variation | kJ · K ⁻¹ mol ⁻¹ |
| η | Efficiency | - |
| ρ | Density | kg/m ³ |

Subscripts

| | |
|--------|----------------------------|
| acc | Alternating current cables |
| act | Activation |
| aux | Auxiliary equipment |
| bat | Battery |
| c | Calculated |
| $comp$ | Compressor |

| | |
|-------------|----------------------------------|
| <i>con</i> | Concentration |
| <i>cons</i> | Consumption of the device |
| <i>conv</i> | Direct current converter |
| <i>cp</i> | Capacity |
| <i>crit</i> | Criterion for state shift |
| <i>cs</i> | Cold start |
| <i>dcc</i> | Direct current cables |
| <i>e</i> | End |
| <i>ele</i> | Electrolyser |
| <i>elec</i> | Electrical |
| <i>ep</i> | Equipment Point |
| <i>F</i> | Faraday |
| <i>f</i> | cylinder walls |
| <i>FC</i> | Fuel Cell |
| <i>G</i> | Electrical Grid |
| <i>Hf</i> | Hydrogen facilities |
| <i>hs</i> | Hot start |
| <i>i</i> | Hour |
| <i>idl</i> | Idle |
| <i>ind</i> | Industry |
| <i>inv</i> | Inverter |
| <i>isen</i> | Isentropic |
| <i>L</i> | Lack |
| <i>m</i> | Electrical motor |
| <i>max</i> | maximum |
| <i>min</i> | minimum |
| <i>mnt</i> | Maintain the state of the device |
| <i>MQ</i> | crank journal |
| <i>MS</i> | crank pin |
| <i>MT</i> | piston pin |
| <i>NG</i> | Natural Gas |
| <i>ohm</i> | ohmic |
| <i>out</i> | Output |
| <i>ov</i> | Overall |
| <i>P</i> | Potential |
| <i>p</i> | Produced |
| <i>pc</i> | Control Point |
| <i>pr</i> | Device operation energy range |

| | |
|-----------------------|----------------------------------|
| <i>prod</i> | Production |
| <i>PV</i> | Photovoltaic Power Plant |
| <i>r</i> | Real |
| <i>rev</i> | Reversible |
| <i>s</i> | Beginning |
| <i>sby</i> | Standby |
| <i>st</i> | Storage |
| <i>T</i> | Total |
| <i>th</i> | Thermal |
| <i>tk</i> | Hydrogen storage tanks |
| <i>tran</i> | Transformer |
| <i>xs</i> | Excess |
| <i>adb</i> | Adiabatic |
| <i>DH₂</i> | Dedicated to hydrogen production |
| <i>H₂</i> | Hydrogen |
| <i>0</i> | Neutral thermal |

Abbreviations

| | |
|-------|--|
| AFC | Alkaline Fuel Cell |
| CAPEX | Capital Expenditure |
| CCS | Carbon Capture System |
| CCUS | Carbon Capture, Utilization, and Storage |
| COGS | Cost of Goods Sold |
| COP | Conference of the Parties |
| FCEVs | Fuel Cell Electric Vehicles |
| GHG | Greenhouse Gases |
| H-DR | Iron Reduction |
| IEA | International Energy Agency |
| IRENA | International Renewable Energy Agency |
| IRR | Internal Rate of Return |
| NPV | Net Present Value |
| OPEX | Operating Expenditure |
| PEM | Proton Exchange Membrane |
| PEMFC | Proton Exchange Membrane Fuel Cell |
| SDG | Sustainable Development Goals |
| SMR | Steam Reforming |
| SOEC | Solid Oxide Electrolysis Cell |

SOFC

Solid Oxide Fuel Cell

UNFCCC

United Nations Framework Convention on Climate
Change

1. INTRODUCTION

In this chapter, it is presented the motivation, the objectives and the structure of the dissertation.

1.1 Motivation and contextualization

1.1.1 Global environmental and social concerns

Despite the well-developed and countless alternatives to convert raw materials into power, energy is, nowadays, one of the most discussed topics due to its role for the perpetuity of civilizations and economies worldwide. When compared to the recent past, population growth is at a slower pace and data shows that the current increase is of 1.10% per year, representing an additional 83 million people annually. Yet, the perspective for the population in 2030 and 2050 is 8.6 and 9.8 billion, respectively (United Nations, 2017). Consequently, the energy demand will constantly increase due to the needs of mobility/transportation, building appliances and at the industrial sector. The anticipated energy consumption by the year 2050 is projected to reach 500 Exajoules (EJ), indicating a notable increase of 13%, when compared to the energy consumption levels observed in 2022 (DNV, 2022).

There is a huge implication with the facts presented above, mainly due to the massive utilization of fossil fuels. The combustion of fossil fuels is inherently associated with the emission of Greenhouse Gases (GHG), which consequently leads to undesirable climate change experienced worldwide. In addition, another negative aspect is the effect of pollutant emissions in human health (Xu et al., 2022). In terms of suspended particles, there are several areas in the world with an average value of PM_{2.5}¹ concentrations higher than recommended levels, and approximately 85% of the global population lives in those areas, which makes air pollution the fourth leading cause of human life degradation (Cohen et al., 2017). Finally, it is important to mention that these non-renewable fuels are represented by a finite quantity

¹ PM_{2.5} (fine particulates) - suspended particles with a diameter less than 2.5 micrometres.

available for human use. Although more reserves of these resources are found annually, their extraction is becoming increasingly costly due to the difficulty in accessing and extract them. It also should be noted that their distribution across the world is not homogeneous and, therefore, it is not expected to faithfully match the increasing energy demand (Dincer & Acar, 2014a).

According to the International Energy Agency (IEA), the final energy consumption in 2019, worldwide, was 418 EJ. By analysing the Figure 1, it becomes evident that 66.3% of the total energy resources used was directly obtained from fossil fuels. Furthermore, fossil fuel power plants accounted for 62% of the electricity consumed (82.3 EJ). Additionally, non-renewable fuel sources accounted for 85.9% of the world's energy supply. To provide an example, regarding the industry sector, it is anticipated that the heat demand will increase by 1.7% annually until 2030. As a result, the consumption of fossil fuels will rise unless other alternative options are explored (*Solar Heat for Industry*, 2017).

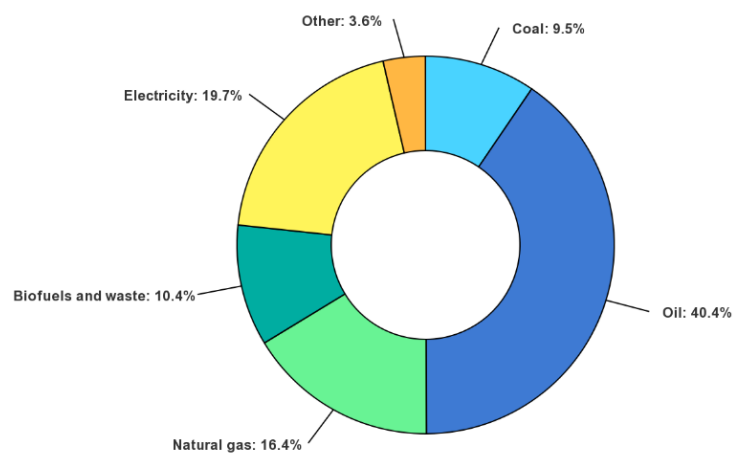


Figure 1 - Share of world total final energy consumption by source in 2019. (Energy Agency, 2021).

Based on these facts and forecasts, it became crucial for most of governmental and nongovernmental organizations around the world to adopt preventive measures and policies with the aim to reduce GHG emissions (Ehsan & Preece, 2022). The objective is to promote global sustainability by implementing renewable energies and focusing on more eco-friendly processes (Wappler et al., 2022a).

1.1.2 European Union policies

Nowadays, the lives of 2.4 billion people, which represent 9.5% of the population, are still at risk due to the lack of access to clean energy solutions or even electricity. Combined with the concerns about climate change, this fact led to the establishment of the 17 global Sustainable Development Goals (SDG), developed by the United Nations General Assembly, especially the Goal 7 and Goal 13. The Goal 7 aims to ensure access to reliable, sustainable and clean energy for all. To achieve this, it is necessary to explore alternative, sustainable and environmentally friendly fuels, as well as, intensify the development and use of renewable energies. The Goal 13 aims to countries to outline and implement plans to reduce GHG emissions (United Nations, 2022).

Moreover, numerous protocols on sustainable development are actively engaged by European countries. For instance, the Conference of the Parties (COP) is one of the primary recurring assemblies that specifically addresses these environmental issues. These meetings bring together countries that are signatories to the United Nations Framework Convention on Climate Change (UNFCCC). For instance, COP21, in 2015, emerged as one of the most significant milestones in decarbonization, as 181 parties signed the Paris Agreement. The main purpose of the arrangement was to ensure that the global average temperature increase should be contained (lower than 2°C) and, if possible, below 1.5°C when compared to pre-industrial levels (European Commission, 2018). Since then, several conferences of the countries participating in the UNFCCC have taken place, where measures and rules have been adjusted with the aim of all participating parties keeping on the path to accomplish the aforementioned agreement (United Nations, 2023). Moreover, some reports have been published, such as Special Report on Global Warming of 1.5 °C (IPCC, 2019), which emphasize the importance of scaling down the GHG emissions.

According to the Hydrogen Roadmap report, Europe aims to eliminate approximately 2.800 Mt of carbon dioxide (CO₂) emissions by the year 2050 (Fuel Cells and Hydrogen 2 Joint Undertaking, 2019). Around 60% of this emissions' reduction are expected to come from the implementation of the Paris Agreement and energy efficiency measurements. However, additional efforts beyond the existing plans would be required to address the remaining 1.100 Mt of CO₂ emissions.

Furthermore, in 2020, the European Union designed a trajectory to follow in its battle against climate change. This is known as the “European Green Deal” (European Commission, 2019), a sustainable investment plan worth one trillion euros, focused on climate change mitigation and economic growth, combined with sustainable management of energy resources. For this purpose, the European Commission has enhanced the environmental targets ambition for 2030, formulating climate, energy, transport, and taxation policies that are suitable for achieving a reduction of net GHG emissions by at least 55% by 2030 (European Commission, 2023). In other words, there has been continuous investment to apply renewable energies, increasing energy efficiency, promoting decarbonization and achieving a reduction in fossil fuel consumption. With the “European Green Deal”, European member states positioned themselves as extremely committed to decarbonization (Panarello & Gatto, 2023).

However, according to the Sustainable Development Goals Report (United Nations, 2022), the current national undertakings made by countries are not enough to achieve the target of limiting global warming to 1.5 °C. Additionally, it highlights that if countries only adhere to their existing commitments, GHG emissions are projected to increase by nearly 14% in the next decade. To counteract this trend, it is imperative that new solutions emerge to reduce the dependency on fossil fuels (Wappler et al., 2022b).

In conformity with the “European Green Deal” (European Commission, 2019), the shift towards achieving climate neutrality will not evolve only renewable energies. Innovative technologies and infrastructure, including Carbon Capture, Utilization and Storage (CCUS), energy storage, smart grids, fuel cells, and alternative fuels like hydrogen, are necessary for achieving the goals of decarbonization.

1.1.3 Decarbonization: renewable energies integration

The comprehensive analysis of the potential for hydrogen to contribute to the decarbonization of the European economy was explicitly presented in the report entitled “Hydrogen Road Map Europe” (Fuel Cells and Hydrogen 2 Joint Undertaking, 2019), which was developed collaboratively with the input of 17 companies and organizations. Based on the contents of this document, the European Union requires a substantial increase in renewable power generation and an extensive electrification of the final consumption grid.

Nevertheless, there are two imperative points to consider. On one hand, some of these clean energies have fluctuations in the production of electricity due to the unpredictability of weather conditions. On the other hand, the disparity of grid requirements is a very important issue when it comes to choosing the energy supplier. Since some renewable systems only provide energy when the climate circumstances are favourable, this type of equipment by itself can not satisfy the grid peaks (Lagioia et al., 2023). For these reasons, it is imperative to search for a new system that can be integrated with existing power plants. This integration will enable solar, hydro, and wind power to become grid-friendly, making it possible to achieve peak-shaving. In other words, renewable power plants require the implementation of daily and seasonal balancing strategies. This balance involves storing the surplus energy generated by renewable sources and use it when renewable sources alone are insufficient to meet the grid demand.

One of the solutions proposed is based on hydrogen. This type of system consists of storing clean energy so that intermittent production can be transformed into chemical energy and not be wasted (Fuel Cells and Hydrogen 2 Joint Undertaking, 2019; Luo et al., 2022).

1.1.4 Incorporation of hydrogen as a strategic vector

Hydrogen is not a novel discovery in the energy field, in the eighteenth and nineteenth centuries, scientists such as Antoine Lavoisier and William Grove published their research about the description of the chemical element and its applications (Winter, 2005). The large-scale availability of this chemical element allowed to be one of the earliest molecules detected and catalogued/reported. In other words, hydrogen integrates most components presents in nature: water, chemical compounds, organic matter, and the atmosphere. Thus, it is the most abundant element in the globe (Von Zuben et al., 2022a).

Moreover, hydrogen has the ability to work as an energy storage medium from daily to seasonal periods. Subsequently, it can be converted into electricity or used as fuel for several applications, including vehicular mobility, supply heat demand and supporting industrial processes. In accordance with the IEA, the decrease of solar and wind investment costs have amplified the possibility of incorporating hydrogen into the energy mix. For instance, in 2023, the photovoltaic (PV) capital costs are 75% lower than in 2010, which translates a possible alternative to achieve a cheaper electrolytic hydrogen production. This

can play a crucial factor in the energy transition and towards the hydrogen integration as a strategic vector (Fuel Cells and Hydrogen 2 Joint Undertaking, 2019; IEA, 2019a).

According to the International Renewable Energy Agency (IRENA), a global intergovernmental agency for energy transformation, the production of hydrogen through renewable power plants will allow to use it as a storage way, being projected to reach a capacity of 2000 TWh by 2050. This will provide the flexibility for the increased implementation of renewable energies, such as solar PV. Furthermore, it is expected that hydrogen and its byproducts, such as ammonia and methanol, will play a significant role in the overall final energy consumption, accounting for a share of approximately 12% by 2050. Consequently, nearly 30% of electricity consumption will be applied to the production of green hydrogen. To fully comprehend this transformation, the current capacity of hydrogen electrolyzers is 0.3 GW. To achieve the aforementioned targets, the equipment will need to have a capacity of 5000 GW (IRENA, 2021).

1.2 Proposed objectives

The main objective of this dissertation is to develop a mathematical model that, based on technical and economic criteria, enables decision-making regarding the final application of the energy generated by a PV power plant. The purpose is to maximize the energy use. The PV power plant sizing should consider the electricity production that directly meets specific consumption requirements, which are based on a defined profile of an industrial facility. In the absence of energy consumption by the industry facility, the electricity can be used to produce hydrogen through water electrolysis. Consequently, the industry consumption can be met either by the electricity generated directly from the PV panels or by converting the previous surplus energy, which was stored in the form of compressed hydrogen, into electricity. As a last resource, the electrical grid can supply the remaining industrial energy demand. Based on this overall objective, the following specific objectives have been defined:

1) Modelling and size a PV power plant integrated with a hydrogen production unit and storage cylinders by identifying and sizing all the components and systems of the installation.

2) Study the electricity production profile based on the PV power plant sizing. For this objective, the pvDesign® software will be used.

3) Develop a thermodynamic model that allows identifying the potential for green hydrogen production and storage through PV production.

4) Simulate the energy production, based on the defined thermodynamic model: estimate the potential for hydrogen production and respective storage, determine the amount of energy that can be injected into the grid and for self-consumption.

5) Perform a sensitivity analysis should be conducted considering seasonal effects throughout the year consumption needs of the industry.

6) Improve the thermodynamic model to obtain a system capable of taking advantage of the renewable energy produced by the PV power plant and by performing the seasonal energy storage.

7) Perform an economic analysis of the full system operation, taking into account the Capital Expenditure (CAPEX) and Operational Expenditure (OPEX).

1.3 Dissertation structure

This dissertation is divided into seven main chapters. The first one describes the motivation and context of the problematic, as well as, the research objectives. The second and third chapters constitute the literature review. Specifying, the second chapter details the hydrogen value chain: feedstocks, hydrogen production, storage, transportation and applications. The third chapter depicts the characterization of PV power plants integrated with hydrogen production. The fourth chapter is focused on the development of a PV power plant integrated with hydrogen production model, including the description of the system components, as well as the thermodynamic system modelling. The fifth chapter refers to the results and discussion for a reference simulation scenario. A sensitivity analysis was also performed to achieve an improved operating scenario. Lastly, an economic analysis regarding the developed model was carried out on sixth chapter, with the assessment of the initial investment and operating expenses, the revenues, the calculation of avoided costs, and the current economic viability of the projected installation. The final chapter presents the conclusion and the prospects for future work.

2. HYDROGEN VALUE CHAIN

As previously mentioned, there is a huge pressure from the prevailing policies to change the energetic matrix by replacing non-renewable fuels with green power and achieving near or even net-zero end-use emissions by 2050. One of the key paths is based on hydrogen due to its promising physical and chemical properties. Firstly, the high potential and efficiency to convert hydrogen into other forms of energy and, secondly, the fact that hydrogen does not have carbon in its molecular constitution. Hydrogen adoption as a fuel for power systems is becoming more and more attractive due to the current pollution concerns (Xu et al., 2022). Additionally, as can be checked in Table 1, hydrogen has a Higher Heating Value (HHV), three to four times higher than common hydrocarbon fuels such as methane and gasoline (Dincer & Acar, 2014b).

Table 1 – Higher and lower heating values of common fossil fuels and hydrogen

| Fuel | HHV [kJ/g] | LHV [kJ/g] |
|----------|------------|------------|
| Hydrogen | 141.9 | 119.9 |
| Methane | 55.5 | 50 |
| Gasoline | 47.5 | 44.5 |
| Diesel | 44.8 | 42.5 |
| Methanol | 20 | 18.1 |

Both cleanliness and sustainable application of renewable energy sources are being recognized as effective solutions to reduce carbon emissions and environmental pollution (Yang et al., 2021), while accomplishing agreements such as the “European Green Deal” and the European Climate Law (Crespi et al., 2022). The significant integration of renewable energy sources is leading to a substantial level of electricity curtailment, primarily resulting from a seasonal mismatch in electricity supply, particularly at large scale systems (Jiang et al., 2022). Hence, by 2050, one of the most significant technical challenges in attaining carbon neutrality is large-scale energy storage (Escamilla et al., 2022).

As previously analysed, a possible solution is based on the use of hydrogen as an energy carrier. It appears to be a promising option for mitigating the seasonal electricity instability in the power system (Escamilla et al., 2022). Hydrogen can enhance the power sector with the integration of renewable technologies through storage and later use (Riera et al., 2023a). The main goal of incorporating hydrogen into the energy system, especially in the

electricity distribution network, is to improve the network stability by minimizing the energy loss factor. The energy loss factor is defined as the energy generated that cannot be recovered and is irreversibly wasted (Frankowska et al., 2023).

The hydrogen supply chain can be divided into production, transportation, storage, distribution, and application. The different alternatives for all these stages can be observed in Figure 2 (Riera et al., 2023b; Sens et al., 2022).

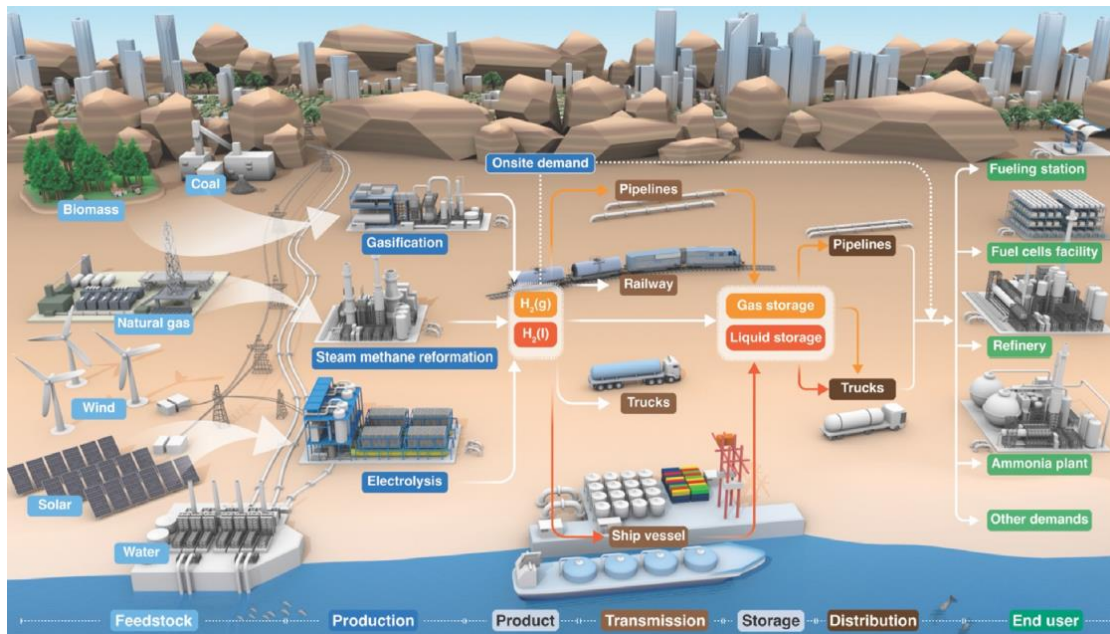


Figure 2 - Comprehensive view of a hydrogen supply chain framework.

(Riera et al., 2023b)

Hydrogen can be obtained through a variety of technologies and feedstocks, including renewable energies, such as biomass, wind, and solar, as well as fossil fuels, like coal and natural gas. As a result, the production process can vary depending on the availability of the energy sources. For instance, the production processes include gasification, steam methane reforming and electrolysis (Winter, 2005; Xu et al., 2022).

Besides that, the hydrogen supply chain can be classified according to the position of the production units. Hydrogen production can take place on-site (i.e., centralized), or near the utilization zone (i.e., decentralized). These two alternatives are represented in Figure 3 and Figure 4, respectively. The centralised option requires the transportation of hydrogen from the production site to the place of its utilization. In contrast, decentralized production does not include the stage of transportation since hydrogen is already produced in the location of its application. To simplify, electrolyzers may or may not be in proximity to the energy source, which, in the case of Figure 3 and Figure 4, is a solar or wind power plant.

Thus, a decentralized scenario implies a complex distribution grid which is required to supply the compound to the end-use point. In that case, the electrolysis device is placed near the point of application, thereby avoiding the need for a complex distribution network for hydrogen (Riera et al., 2023b; Sgarbossa et al., 2023).

Between these two scenarios, the selection of the most appropriate hydrogen supply chain should take into consideration several factors. According to Sgarbossa et al. (2023), the cost of transporting small quantities of hydrogen makes centralized production economically unviable when compared to near end-use production, decentralised production. However, as the operation scales up and the amount of produced hydrogen increases, the centralized option becomes more financially lucrative.

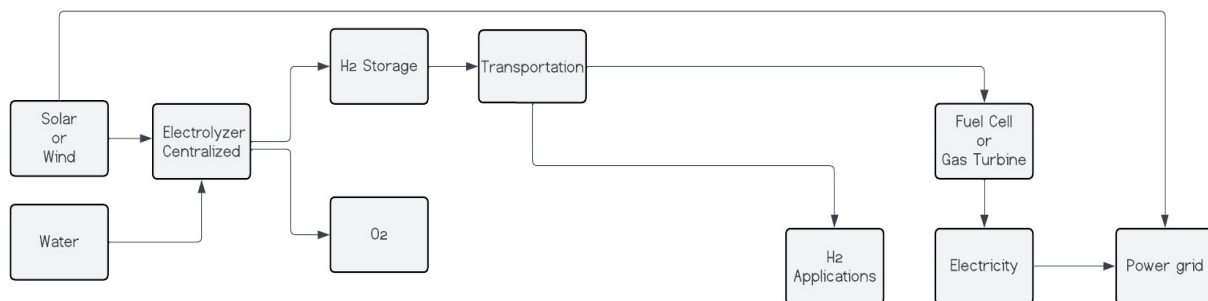


Figure 3 – Example of a centralized water electrolyser.

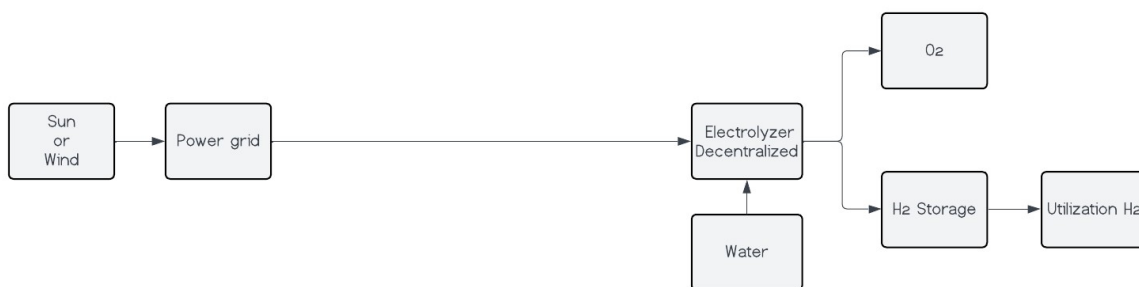


Figure 4 – Example of a decentralized water electrolyser.

Regarding the hydrogen transportation, there are several ways to connect the production to the storage facilities or end use consumption, which encompass road transportation, maritime transport, pipeline, and railway transport. Furthermore, the hydrogen can be handled in either a gaseous or liquid state, depending on the quantities and type of transportation used (Reuß et al., 2017).

Regarding the storage stage, it can be divided into two options: physical storage and material-based chemical storage. Physical storage is further categorized into three main

groups: compressed gas storage, liquefied storage, and cryo-compressed storage. Material-based storage is divided into adsorption storage and absorption storage (Hassan et al., 2021). Further discussion on this topic will be provided in subchapter 2.2. In Figure 5 the most common methods to transport and store hydrogen are represented.

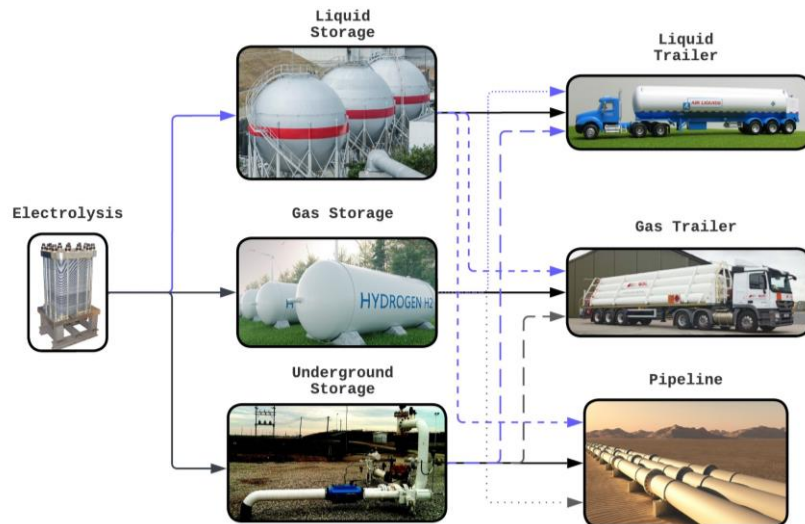


Figure 5 – Most common storage and transportation methods. The blue lines represent pathways where a change of state occurs.

The final link of the hydrogen value chain corresponds to the applications. Hydrogen can be used in different sectors for a wide range of purposes. In the refining sector, hydrogen plays a role in oil refineries, where it is used for processes such as desulfurization and hydrocracking. The chemical industries also make use of hydrogen, particularly, in the production of ammonia and methanol, among other chemicals. In the iron and steel sectors, hydrogen is extensively employed in the Direct Reduction of Iron (DRI), which is a vital process in the industry. Hydrogen is further used in the transportation sector, powering Fuel Cell Electric Vehicles (FCEVs) and providing a clean and efficient source of power. Hydrogen is also used in rail applications and shipping, offering alternatives to traditional fossil fuel-based propulsion systems. Moreover, hydrogen can be used as a clean fuel for a variety of applications, such as water and space heating, providing an alternative to traditional fossil fuel-based systems. This is considered, by literature, one of the most promising applications. Finally, hydrogen can serve as a storage medium for renewable energy sources in the generation of electricity during periods of low demand or when renewable sources are not available (Germescheidt et al., 2021; IEA, 2021; Sgarbossa et al., 2023).

2.1 Feedstock and hydrogen production

When it comes to hydrogen production, it can be achieved through a wide variety of feedstocks, specifically classified into two broad categories: fossil fuel-based, such as coal and hydrocarbons; and renewable energies (Forghani et al., 2023). In agreement with Pinsky et al. (2020), in 2020, 96% of generated hydrogen used fossil fuels as feedstock: 48% originated from natural gas, 30% from heavy oils and naphtha, and 18% from coal. The remaining 4% of hydrogen production was attributed to renewable energies, encompassing biomass, water, and electricity derived from renewable power plants.

2.1.1 Feedstocks for water electrolysis

The process of water electrolysis requires a supply of electricity and water to continuously generate hydrogen and oxygen. Moreover, the electrical energy required can be obtained from electric grid or by a renewable power plant. When considering only renewable sources to produce electricity, the main sources include solar, hydro, wind, and geothermal energies (Sgarbossa et al., 2023).

Furthermore, the cost of hydrogen generation is intrinsically connected to the price of the energy source (Moradpoor et al., 2023). In literature, the renewable sources that are the most used with electrolyser production are solar and wind energy. Therefore, the behaviour of these sources as energy suppliers in the electrolysis process is studied in several articles (Riera et al., 2023b).

According to Riera et al. (2023b), the levelized cost of hydrogen per kilogram, when produced with solar as the energy source, is approximately 41% to 55% more expensive than when it is produced with wind and nuclear sources, respectively. Table 2 presents the levelized cost of hydrogen, for different energy sources, from literature.

According to literature, when considering the impact of renewable energy sources unpredictability, it becomes evident, that wind speed has a greater influence than the solar radiation on hydrogen production prices (Moradpoor et al., 2023). Additionally, as expressed in Table 2, reducing the fluctuation of the energy source leads to a decrease in the levelized cost of hydrogen. In other words, when combining PV and wind power plants, the power supply becomes less unstable, because it relies on two climate conditions instead of one. Consequently, the cost of hydrogen production decreases accordingly (Moradpoor et al., 2023). Sgarbossa et al. (2023) specifies that the expense reductions vary from 30% to 63%,

when integrating multiple discontinuous energy sources, in contrast to systems that rely on a single dedicated renewable energy source.

Regarding wind power, higher costs for wind electricity result in higher costs for producing hydrogen. Besides that, there is an important correlation, known as the capacity factor of wind turbines. This correlation is represented by the ratio of generated wind power to the turbine capacity and is directly linked to hydrogen costs. Lower hydrogen costs are associated with higher capacity factors (Riera et al., 2023b; Saur & Ramsden, 2011).

It should be noted that there is a substantial difference between a renewable off-grid power plant and a renewable on-grid power plant when it comes to their role as an electricity supplier for electrolysis. According to Moradpoor et al. (2023), the levelized cost of hydrogen production through electrolysis is twice as high connected to a standalone power plant when compared to a grid-tied plant.

Additionally, it is important to mention that nuclear power and geothermal energy have the potential to produce cheaper green hydrogen, competing with grey hydrogen price (hydrogen classification by colour is presented in subchapter 2.1.3.). However, the current draft of the European Union does not allow nuclear power as a source of producing green hydrogen.

Table 2 – Electrolysis process feedstocks and the corresponding levelized cost of hydrogen

| Input | Reference | Year | Nuclear electrolysis | PV electrolysis | Wind electrolysis | | PV + Wind electrolysis |
|---------------------|--------------------------|---------------|----------------------|-----------------|-------------------|------------|------------------------|
| | | | | | Onshore | Offshore | |
| Electricity [kWh] | (Riera et al., 2023b) | - | 54.2 | 54.2 | 54.2 | | - |
| Water [kg] | (Riera et al., 2023a) | - | 10 | 10 | 10 | | - |
| LCOH [US\$ or €/kg] | (Riera et al., 2023a) | 2019 | 4.3 | 9.49 | 5.6 | | - |
| | (Moradpoor et al., 2023) | 2020 (Europe) | - | (US\$) 7.5 | (US\$) 4.4 | (US\$) 4.2 | 3.5(€) |

An additional crucial factor to consider in the hydrogen supply chain is the availability of water. For wind and solar electrolysis, ten kilograms of water are required to produce one kilogram of hydrogen. Because of this, the use of water electrolysis technology is constrained

in some geographic places. According to Riera et al. (2023b), for an efficient hydrogen supply chain, it is necessary to take into account all the raw materials involved.

Considering this, countries like Saudi Arabia are exploring the possibility of integrating water desalination with renewable power systems. This integration aims to reduce the overall system cost and allows for increased flexibility between the sectors, as they are designed to complement each other. Ignoring the water supply can lead to misleading cost estimations, making the production appear cheaper than it actually is. Furthermore, choosing a production method without considering the local conditions of a particular region may result in an unsuitable approach for that specific area.

Overall, structuring a hydrogen supply chain sourcing plan must consider two primary hurdles. The first hurdle concerns the availability, quality, location, and accessibility of different energy sources and their cost in relation to the energy market and long-term supplier agreements. The second hurdle involves the unpredictable nature of renewable sources.

2.1.2 Production methods

Regarding hydrogen production, there are a wide variety of methods to its production. To illustrate this, in Figure 6 the general hydrogen production strategies are represented.

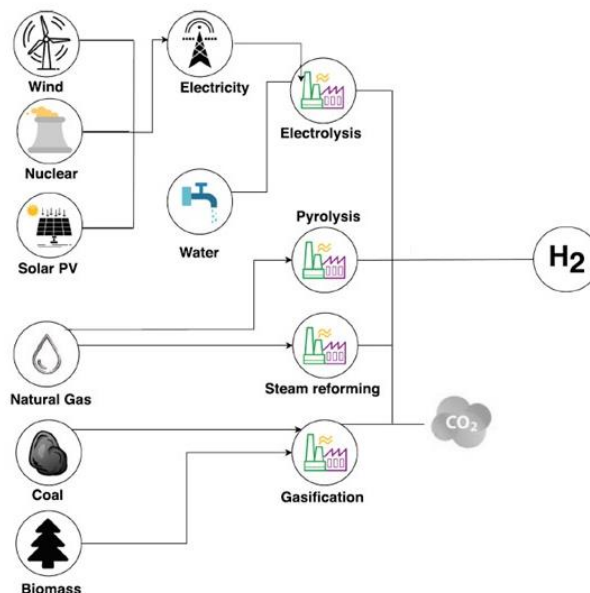


Figure 6 – General hydrogen production processes. Adapted from Al-Qahtani et al. (2021a).

Hydrogen production pathways can be distinguished based on the energy source, catalyst and raw materials used. A diversity of sources of energy and raw materials can be

used in hydrogen production. Different hydrogen production methods require distinct input products, which include water, fossil fuels, and biomass, as can be observed in Table 3.

Table 3 – Inputs of general hydrogen productions methods. Adapted from F. Zhang et al. (2016)

| Method | Input raw material | Source of energy |
|--------------------|--|------------------|
| Water electrolysis | Water | Electrical |
| Gasification | Water, fossil fuels (coal), biomass | Thermal |
| Reforming | Water, fossil fuel (natural gas) or biofuels | Thermal |
| Thermolysis | Water | Thermal |
| Methane Pyrolysis | Methane | Thermal |

Moreover, depending on which production method is used, byproducts, such as oxygen, carbon dioxide, and other environmentally harmful gases, can be generated. All these characteristics are intrinsically connected to the carbon footprint of the hydrogen production chain (European Commission, 2020). The description of general hydrogen production methods are summarized in Table 4.

Table 4 – Description of general production method. Adapted from Zhang et al. (2016)

| Method | Description |
|--------------------|--|
| Water electrolysis | Water decomposition into oxygen and hydrogen by passing a direct current that drives electrochemical reactions |
| Gasification | Converts solid carbonaceous materials into carbon monoxide and hydrogen by reacting them with oxygen and/or steam |
| Reforming | Reacts carbon-based liquid or gaseous fuels with steam at high temperature to produce carbon dioxide and hydrogen |
| Thermolysis | Uses thermal energy to decompose water molecule at very high temperature, approximately 2500 °C |
| Methane Pyrolysis | Decomposes hydrocarbons into solid carbon and hydrogen at high temperatures, either thermally or catalytically, without the presence of oxygen |

Despite the potential categorization of hydrogen, there is currently no universal standardization. Consequently, several interpretations and classifications are allowed (Lagioia et al., 2023). One of the possible distinctions is proposed by a diversity of stakeholders, such as research institutions, organizations, agencies, and companies. This

categorization involves associating colours with hydrogen to reflect the degree of sustainability in its production process (Dawood et al., 2020). However, hydrogen classified under the same colour may still be associated with different GHG emissions, because of discrepancies in production parameters (Noussan et al., 2021). Further information will be clarified in subchapter 2.1.3. Another classification, that differs from the previously presented, regards to the European Commission, as will be delved in subchapter 2.1.4.

2.1.3 Classification of hydrogen by colours

Firstly, there is green hydrogen, also known as clean hydrogen, which is derived from water electrolysis. As previously seen in chapter 2.1.1, the energy source for the separation of water molecule is electricity generated from renewable sources. Therefore, this process results directly in zero-carbon emissions. Although green hydrogen is the cleanest and has the lowest environmental impact, its production is still costly compared to the remaining alternatives. In 2021, approximately 120 Mt of hydrogen were produced and less than 1% of this amount was obtained through water electrolysis using renewable energy sources (Lagioia et al., 2023). Therefore, research in the field of green hydrogen focuses on the economic aspect, aiming to achieve a cost-effective production method (Lee et al., 2022).

Notwithstanding, the hydrogen produced with the use of fossil fuels are classified in turquoise, grey, or brown. To explain, the differences between them are based on the amount of GHG emissions that each one generates.

Currently, a percentage of 75% of the produced hydrogen is originated through the process of Steam Reforming (SMR). This kind of production originates a product that is categorized as grey hydrogen. Although is not the most pollutant method, it does not have a threshold regarding carbon emissions. Moreover, another problem of this process is reflected on its incomplete combustion. To be specific, the unburned methane escape into the atmosphere leads to an increase in carbon emissions of 42.1 gCO₂eq/MJ of H₂. In fact, this type of gas is responsible for approximately 25% of the present global warming.

Brown hydrogen stands out for having the higher carbon dioxide emissions. This method is based on the gasification of coal and is characterized with the worst environmental performance.

Finally, from methane pyrolysis, turquoise hydrogen and solid carbon are originated. One of the benefits of turquoise hydrogen when compared with grey or brown hydrogen,

remains in the fact that solid carbon is easier to store and transport than carbon dioxide gas. In other words, there is not carbon emission directly associated with this process. As a result, this method is labelled as being more sustainable than the two previously presented. However, its Technological Readiness Level (TRL)² ranges from 3 to 5, in a scale from 1 up to 9, as can be seen in Figure 7 (Al-Qahtani et al., 2021b; Germscheidt et al., 2021; Howarth & Jacobson, 2021; IEA, 2019b).

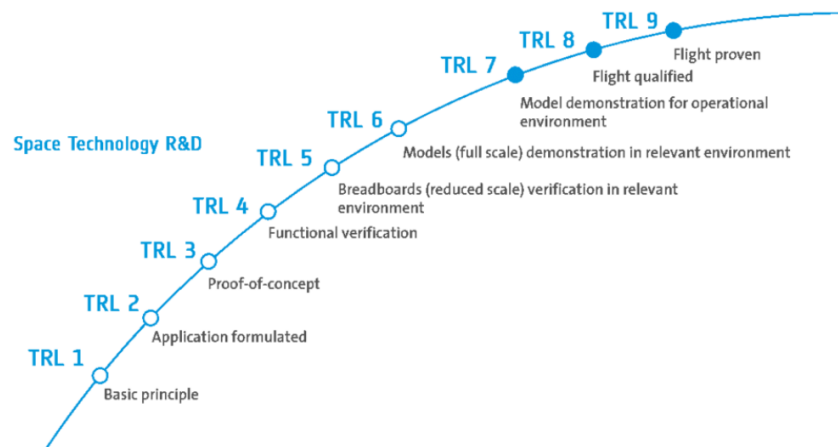


Figure 7 – Scale of TRL (European Space Agency, 2023).

Furthermore, with the current sustainable concerns, technological advancements emerge with the aim of mitigating CO₂ emissions. One of the developed solutions is based on the capture of carbon dioxide through absorption and adsorption. According to European Commission (2020), the maximum GHG capture has a maximum efficacy of 90%. Additionally, captured CO₂ can be stored and then be used in several industrial processes, which increases the potentiality of this method, known as CCUS (IEA, 2023).

Therefore, when the CCUS technology is integrated with grey or and brown hydrogen production, the environmental impacts are significantly reduced. Consequently, a new classification of hydrogen was originated, the blue hydrogen. This method has a TRL ranging from 7 to 8, with steam methane reforming and coal gasification serving as the base processes, respectively. It should be noted that there is no need to construct new facilities, as the carbon capture device can be applied in the existing facilities. In 2021, only two installations were in operation, one in Canada ran by Shell and another in the United States,

² TRL - method for estimating the maturity of technologies.

managed by Air Products. Both installations are based on the steam methane reforming process (Howarth & Jacobson, 2021; Noussan et al., 2021).

Other colour classifications of hydrogen emerge when its production method is electrolysis, but the energy is not supplied by PV or wind power plants. For instance, if the energy supply comes from the nuclear industry, it is classified as pink hydrogen. On the condition that has an energy source from a mixture of fossil fuels and renewable energy, it is considered yellow hydrogen. Both pink and yellow hydrogen are associated with lower environmental impacts when compared to the production pathways of grey and brown hydrogen.

To conclude this categorization, white hydrogen is presented. It is associated with the natural hydrogen, which is generated through geochemical processes below the Earth's crust. For this reason, it is considered to be a perpetual and sustainable source. However, due to the economic impracticality of detection and subsequent extraction, there is currently no commercial interest in natural hydrogen. Furthermore, there are some papers in literature that attribute the white colour to hydrogen obtained from biomass, waste and from processes based on the separation of water molecules using concentrator collectors. Therefore, this categorization is not totally defined, which open space to interpretation (Germescheidt et al., 2021; Recupera, n.d.). The information about the categorization of hydrogen by colours is summarized in Figure 8. It is also presented a comparison of CO₂ emissions and environmental impacts for different hydrogen categories.

| Color Code | Process | CO ₂ Emission | Environmental Impact | Cleanliness Level of the H ₂ |
|--------------------------------|---|--------------------------|----------------------|---|
| Fossil Fuels H ₂ | Coal → H ₂ ; Gasification process, syngas, T=700°C. CO ₂ emitted directly | ● | ● | ○ |
| | Natural gas (CH ₄) → H ₂ ; Steam Reforming. Most common process | ● | ● | ○ |
| | Natural gas (CH ₄) → H ₂ ; Steam reforming with capture and store of CO ₂ | ◐ | ◐ | ◐ |
| | Natural gas (CH ₄) → H ₂ ; Methane pyrolysis with production of solid carbon | ○ | ◐ | ◐ |
| Electrolysis H ₂ | H ₂ production from water electrolysis through nuclear energy | ○ | ◐ | ● |
| | H ₂ production from water electrolysis through mixture of sources (FF and RE) | ○ | ◐ | ● |
| | H ₂ production from water electrolysis through renewables sources | ○ | ○ | ● |
| Alternative H ₂ | Natural occurrence, rare on Earth. H ₂ is found in clathrates or in the atmosphere (1 ppm) | ○ | ○ | ● |
| | Thermochemical water splitting produced by concentrated solar energy | ○ | ○ | ● |
| | H ₂ produced from garbage, plastic or biomass | ◐ | ◐ | ◐ |

○ low ◐ medium ● large

Figure 8 – Summary of the categorization of hydrogen by colours, and comparison of its carbon dioxide emissions, environmental impact, and cleanliness of the compound produced. FF stands for fossil fuels and RE for renewable energies (Germescheidt et al., 2021).

2.1.4 Classification of hydrogen by European Commission

In accordance with the European Commission classification, hydrogen types are named based on the energy source. Firstly, is identified the electricity-based hydrogen, which is obtained through water electrolysis. The environmental impact of this type of hydrogen depends directly on how the electricity was generated.

If the electrolyser input electricity is from renewable sources, such as wind and solar, the classification is designed by renewable or clean hydrogen. It should be noted that, this classification also includes biogas reforming and biochemical biomass conversion (European Commission, 2020).

If fossil fuels are used as the energy source for water electrolysis or as the feedstock for steam reforming or gasification processes, the resulting hydrogen is categorized as fossil-based hydrogen. Currently, fossil-based hydrogen represents the higher share of hydrogen production, approximately 96% (Howarth & Jacobson, 2021). Nevertheless, when a CCUS

technology is implemented in combination with the fossil-based hydrogen pathway, it is classified as fossil-based hydrogen with carbon capture (European Commission, 2020).

Lastly, a wide category includes the production processes that emit fewer GHG than the most used at present. These include, specifically, the low carbon hydrogen molecules obtained through processes that use fossil fuels and incorporate a Carbon Capture System (CCS), as well as, the production pathways based on electricity, such as water electrolysis (European Commission, 2020).

To sum up, the absence of a universal categorization for each type of hydrogen constitutes an obstacle for commercialization and establishment of international policies and standards. As a result, it becomes more difficult to conduct the hydrogen technology development (Lagioia et al., 2023). In order to solve this problem, the CertiHy Steering Group proposed a limit of CO₂ emissions to classify the hydrogen production pathway. This measure, implemented in Europe, aims to attain a clear and worldwide definition of the low carbon hydrogen and high carbon hydrogen. The emissions limit calculation considers a 60% reduction in GHG release compared to the SMR process, which serves as the reference, with a value of 91 gCO₂e/MJ of hydrogen. Therefore, to the final product be classified as low-carbon hydrogen, the process that lead to its generation cannot emit more than 36.4 gCO₂e/MJ of hydrogen (Noussan et al., 2021).

2.1.5 Categories comparison

To assess the least economically favourable type of hydrogen, Al-Qahtani et al. (2021a) conducted an economic evaluation covering several hydrogen categories. This assessment considered the levelized cost and relevant externalities, including human health indicators, the monetized ecosystem quality and the monetized resource depletion. The reported conclusion was that the gas reforming process, combined with CCUS, offers the most accessible option, with a final cost of US\$ 4.67 per kilogram of hydrogen. Thus, blue hydrogen will be of significant interest in the short and medium term, serving as a substitute for the green hydrogen production process until the green methods meet the necessary conditions for intensive use.

However, social barriers and indirect economic costs should be taken into consideration. Despite being derived from matured and widely used processes, blue hydrogen requires the implementation of CCS in existing production units. This often requires

the construction of CCS facilities, which require space and economic investment. Additionally, the application of CCS may lead to a reduction of 5 to 14% in the energy efficiency of the steam methane reforming process (Noussan et al., 2021). Furthermore, there are another fact that requires attention: the high-water consumption of the gasification and steam methane reforming processes, which can reach levels of 38 and 24 litres of water per kilogram of hydrogen, respectively (Al-Qahtani et al., 2021a; Noussan et al., 2021).

Another fundamental issue is the social acceptance of processes involving the valorisation of CO₂ emissions (Lagioia et al., 2023). In this case, the GHG is taken as a raw material for industrial processes rather than an undesirable byproduct, creating a market that undermines initiatives for green hydrogen production. Furthermore, current blue hydrogen facilities do not have the capability to capture all the direct emissions, neither to reduce indirect emissions. Among the indirect emissions, methane is included, which has a significant environmental impact. To conclude, the hydrogen production pathway can compromise the achievement of environmental goals and agreements (Lal & You, 2023).

2.2 Hydrogen storage

One of the foremost stages in the strategic analysis of hydrogen value chain is related with the leakage of the lightest elemental substance on the planet, 0.0837 kg/m³ at NTP conditions. The low volumetric energy density of this energy carrier presents a significant challenge for its handling. Therefore, for any undertaking which incorporate hydrogen, a crucial aspect lies upon determining the appropriate method to increase the volumetric energy density for its efficient storage (Palys & Daoutidis, 2022).

Figure 9 shows a variety of fuels and their respective energy densities. Even when hydrogen is compressed up to 300 bar, its density remains lower than all the represented fuels, including methanol, ethanol, and ammonia. When compared with methanol at the same pressure, hydrogen exhibits a comparatively modest energy density. With respect to other hydrogen storage pathways, such as in liquid state (cryogenic) or solid (metal hydride), they have higher energy density. Nonetheless, they are not able to be used in large-scale installations (Escamilla et al., 2022).

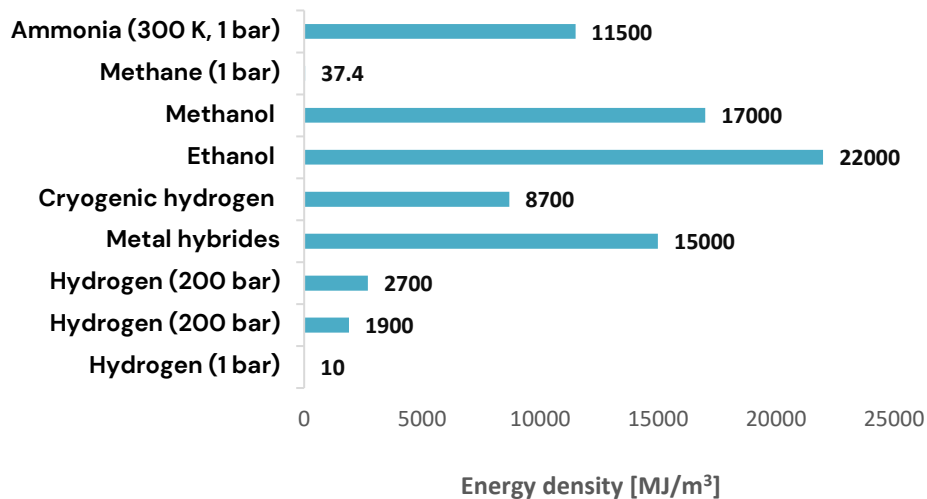


Figure 9 - Energy density for different fuels. Adapted from Escamilla et al. (2022).

According to Sgarbossa et al. (2023), hydrogen storage serves two purposes. Firstly, it can address the intermittencies of renewable energy by enabling seasonal energy storage. Secondly, it should be noted that stockpiling has the potential to overcome the mismatch between the renewable energy production and unsynchronized demand profiles. Besides, when comparing hydrogen with other energy storage options, in terms of mitigating the renewable energies intermittency, hydrogen storage stands out positively due to its characteristics as an energy carrier. The versatility of ways that hydrogen can be stored for extended periods is a significant advantage over other storage technologies (Escamilla et al., 2022).

According to Hassan et al. (2021), hydrogen storage can be categorized into two wide classes. Through observation of Figure 10, it becomes clear that these categories refer to physical and material-based storage. Physical storage predominates, primarily using compressed and liquefied hydrogen, as explained in Sgarbossa et al. (2023). It is worth noting that, according to Escamilla et al. (2022), the temporal domain wherein hydrogen energy storage presents maximal desirability is within the range of days to months.

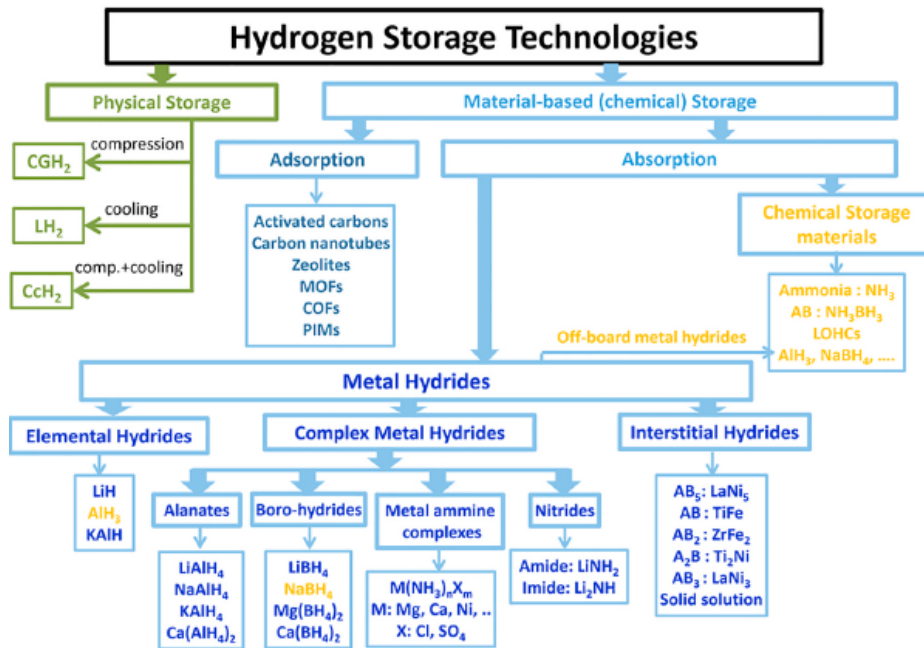


Figure 10 - Hydrogen storage technologies (Hassan et al., 2021).

2.2.1 Compression and liquefaction: methods comparison

As previously mentioned, one of the ways to achieve higher volumetric energy density is through hydrogen gas compression. However, by analysing the Figure 9 it became evident that storing hydrogen in the form of gas is a very complex task. One of the alternatives to attain a greater volumetric power density is to perform the liquefaction of hydrogen (Hassan et al., 2021).

Typically, hydrogen is produced within the range of 1 to 30 bar of pressure and 303 to 333 K of temperature. Nevertheless, the liquid state of hydrogen can only be attained at temperatures ranging from below 20.37 K, at a pressure of 1 bar, to 33.14 K, at a critical pressure of 12.79 bar. Thus, it is required a facility that employs cryogenic technology so the temperature can be lowered to ultra-low levels (Escamilla et al., 2022).

The process of transforming hydrogen into a liquid state involves four primary stages. The first stage is precompression, which is performed at ambient conditions. The second stage is precooling, where the hydrogen temperature is decreased from ambient to around 80 K. In the third stage, cryo-cooling is implemented, which further reduces the temperature from 80 K down to 30 K. The fourth and final stage involves liquefaction, achieved by reducing the temperature from 30 K to around 22.8 K or 20.37 K, depending on whether the hydrogen

pressure is 2 bar or atmospheric pressure. This results in the conversion of hydrogen from a gas to a liquid form.

A diagram of a liquefaction plant is represented in Figure 11, where it is possible to observe these four main stages (Escamilla et al., 2022). Furthermore, according to Palys & Daoutidis (2022), the storage conditions for liquid hydrogen require a temperature of 20.15 K and a pressure of 4 bar.

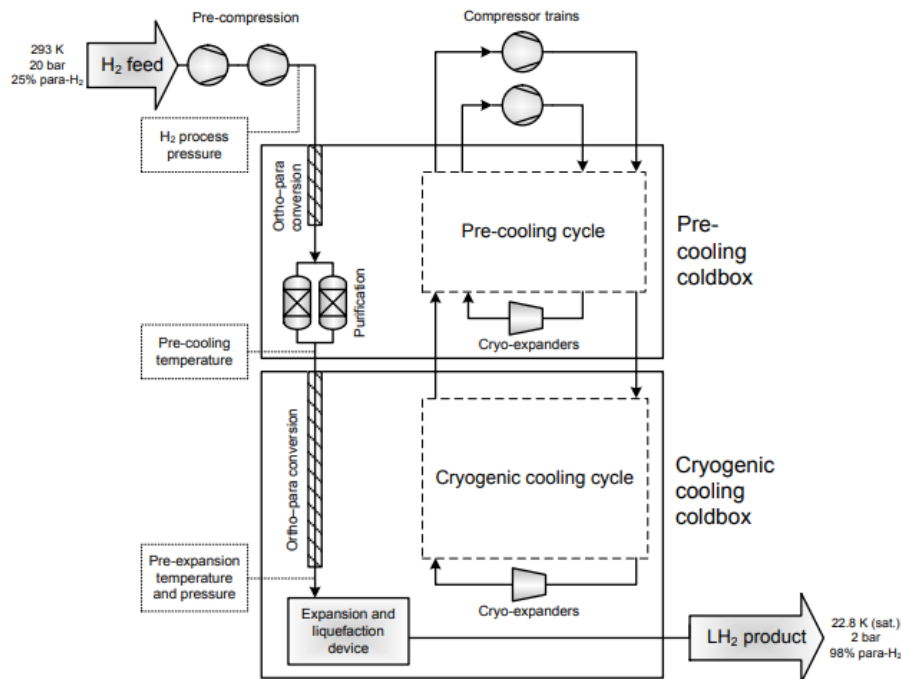


Figure 11 – Example of a hydrogen liquefaction facility (T & Ch, 2012).

On one hand, there is a beneficial return from applying this process, which is reflected in achieving greater mass and energy densities compared to gaseous hydrogen. Specifically, at conditions of 15 K or 20 K (for a pressure of 1.013 bar), hydrogen possesses a density of 76.2 or 70.9 kg/m³, respectively, which is significantly higher than the density of gaseous hydrogen at the same pressure.

Even if hydrogen gas is compressed up to 700 bar, its density only reaches 42 kg/m³, which is almost 1.7 times lower than the density of liquid hydrogen (Bondarenko et al., 2022; Escamilla et al., 2022; Hassan et al., 2021).

On the other hand, handling liquid hydrogen can come at a significant economic expense. For instance, the investment in a refuelling station that provides hydrogen at 700 bar is three times higher than providing it at 350 bar (Maroufmashat & Fowler, 2017). Furthermore, during the process of liquefaction, a significant amount of energy is needed (Bondarenko et al., 2022). There exists a diversity of values in the literature that depict the

amount of energy used in the process of liquefaction. For instance, according to Reuß et al. (2017), the energy consumed in this process is estimated to be 12 to 15 kWh/kg, whereas, for He et al. (2021), the value is lower, of about 11 kWh/kg.

Conversely, Bondarenko et al. (2022) declares that the energy consumption is about 25 to 45% of the hydrogen energy. In this context, IDEALHY³ conducted a comprehensive analysis of the stages involved in the liquefaction process, with the objective of reducing specific energy consumption and lowering investment costs. The outcomes of this project revealed that the aggregate energy consumption incurred during the liquefaction process was approximately 6.7 kWh/kg, the equivalent to 20% of the LHV of hydrogen (Escamilla et al., 2022; Stolzenburg & Mubbala, 2013).

Despite the previously mentioned study, it is widely acknowledged in the literature that the energy consumption of liquefaction is higher than that used for the compression of gaseous hydrogen. For instance, compressing hydrogen gas from 1 up to 1000 bar demands 4 kWh/kg (Escamilla et al., 2022). According to Hassan et al. (2021), the compression of hydrogen to 700 bar, which is the minimum required for automotive applications, consumes approximately 10% of the gas energy content. At lower pressures, it is required 0,7 to 1 kWh/kg (Matute et al., 2022).

Another downside of storing liquid hydrogen regards its low heat of vaporization. As reported by Reuß et al. (2017), high-volume liquid hydrogen tanks exhibit a boil-off ratio of 0.03% for each diurnal cycle, due to the exchange of heat with the surrounding environment. In other words, one preeminent attribute of projecting a storing liquid hydrogen tank is the losses obtained from evaporation. They are expressed as a percentage of the internal tank volume per unit of time. Therefore, more energy is consumed to mitigate the loss of liquid hydrogen that may occur during long periods of storage.

There are two main strategies to minimize this problem. The first one is to maintain the temperature of the liquid hydrogen below its boiling point.

The second is to use the cryogenic technology equipped with a condensation system of the evaporated hydrogen. Hydrogen vapour is typically condensed using gaseous helium, which serves as a colder cryoagent (Bondarenko et al., 2022; Escamilla et al., 2022).

³ IDEALHY was a project that aimed to make hydrogen liquefaction economically viable in Europe.

Besides, the utilization of a cryogenic fluid inherently entails losses along the liquid hydrogen route. To be specific, the losses occur in the transportation of hydrogen from a liquefaction facility to a mobility option, in transferring hydrogen from a mobility option to a storage station, the conveyance of hydrogen from a storage station to an end-user utilizing a pump or compressor, and finally during the utilization of hydrogen in a fuel cell or other power generation apparatus (Escamilla et al., 2022).

The processing of hydrogen after production significantly affects the storage and transportation stages. For mobile applications, it is crucial to have high energy density, which is associated with higher costs. Conversely, when considering stationary applications, it becomes vital to ensure a substantial reduction in costs and, simultaneously, an increase in storage capacity (Bondarenko et al., 2022; Escamilla et al., 2022; Hassan et al., 2021).

2.2.2 Technical considerations for gaseous hydrogen storage

In the literature, several publications are focused on the technical data of gaseous hydrogen storage. This type of storage can be divided into two categories based on pressure: low-pressure and high-pressure (Guilbert et al., 2017; Maroufmashat & Fowler, 2017).

The low-pressure group has a maximum compression capacity of 200 bar, while the high-pressure group has a maximum compression capacity of 700 bar (Maroufmashat & Fowler, 2017). The pressure range in which the hydrogen can be compressed vary between 50 and 400 bar for stationary applications, and up to 900 in mobility applications (Escamilla et al., 2022). In Bondarenko et al. (2022) it is stated that, storing hydrogen in standard steel cylinders at a pressure of up to 206.65 bar is the most straightforward approach, which enables approximately 16 kg of hydrogen to be stored in a one cubic metre tank (Figure 12). Similarly, Reuß et al. (2017) consider the same tank form, but the pressure threshold varies between 200 and 350 bar.

Regarding high-pressure storage, Reuß et al. (2017) considers a range of 350 up to 700 bar. Kim et al. (2023) studied the feasibility of offshore wind turbines coupled with hydrogen production. The authors consider storing hydrogen in a tank with compression ranging from 15 bar to 250 bar as the most conventional method. This narrow pressure range is also considered by Forghani et al. (2023). Finally, Crespi et al. (2022) take into account a pressure ranges from 30 up to 200 bar.



Figure 12 - Example of a cylinder storage tank for hydrogen gas (India Hydrogen Alliance, 2021).

Conversely, Palys & Daoutidis (2022) indicates a wider storage pressure range. Specifically, the authors state that hydrogen storage pressure can vary from 200 to 1000 bar. It also highlights that storage vessels designed for energy and transportation purposes typically have a tolerance for 700 bar pressure. To further explain, this high-pressure hydrogen storage, which ranges between 350 and 700 bar, is normally used to provide fuel for vehicles equipped with fuel cells (Kotowicz et al., 2017; Maroufmashat & Fowler, 2017).

2.2.3 Technical considerations for underground storage

An alternative approach for storing gaseous hydrogen involves underground storage. This subterranean retention can be achieved by using exhausted oil and gas fields, cavernous excavated from hard rock or salt deposits. This technique facilitates the storage of large quantities of hydrogen gas over substantial periods (Maroufmashat & Fowler, 2017). Based on Maroufmashat & Fowler (2017) work and considering only technical aspects, salt caverns are the preferred option for hydrogen storage. This is owing to inertness of salt towards hydrogen, which, in turn limits its diffusivity from the storage cave (Kotowicz et al., 2017; Palys & Daoutidis, 2022). An illustration of underground storage is represented in Figure 13. However, the availability of suitable geological formations for this kind of storage constitutes a significant obstacle (Maroufmashat & Fowler, 2017).

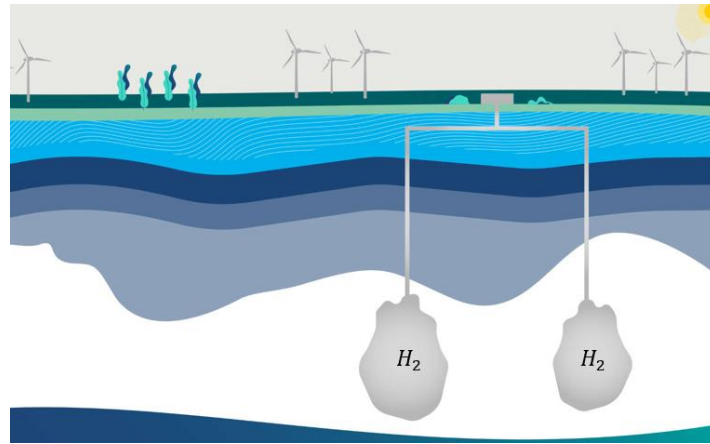


Figure 13 – Illustration of underground hydrogen storage through a salt cavern (Wolter, 2020).

According to Kotowicz et al. (2017), these underground tanks can also be produced with human intervention. For example, leaching salt reservoirs with a capacity of 750,000 cubic metres would cost between 20 and 30 million euros. Therefore, from an economic perspective, using this storage technique is more cost-effective when the quantity of hydrogen to be stored exceeds 20 tons. This is due to the specific investment involved, which can result in costs up to ten times lower for a storage capacity of 100 tons of hydrogen, when compared to storing it in vessels (Palys & Daoutidis, 2022). Moreover, when considering economical aspects, another limitation of this storage method emerges. This limitation is related with the expensive transportation costs of hydrogen to and from these caverns, even in the case of reduced distances between the storage point and the production or application facilities (Palys & Daoutidis, 2022).

Regarding the technical parameters, the compression pressure thresholds for subterranean storage may fluctuate within a range of 20 to 180 bar (Maroufmashat & Fowler, 2017). In contrast, Palys & Diopitids (2022) states that the pressure of hydrogen can achieve 200 bar in this type of storage. Also, the salt cavern storage can operate with hydrogen compressed between 60 to 150 bar (Forghani et al., 2023). On other hand, Kotowicz et al. (2017) states that for a 500,000 cubic metre, hydrogen must be compressed to pressures that vary from 60 to 180 bar. Hence, underground tanks require lower pressure compared to above-ground storage. Table 5 presents a summary about compressed hydrogen storage technical data.

Table 5 – Technical information of compressed hydrogen storage

| Reference | Type of storage | Type of compression | | Geological Storage |
|-------------------------------|----------------------|--|---|--|
| | | Low pressure | High Pressure | |
| (Maroufmashat & Fowler, 2017) | Pressure range [bar] | Up to 200 | Up to 700 | 20 up to 180 |
| | Type of vessel | Based on SA516 Grade 70 carbon steel | - | Salt caverns, depleted oil and gas fields and aquifers |
| | Application | Stationary applications | Transportation fuel (refuelling stations) | Stationary applications |
| (Escamilla et al., 2022) | Pressure range [bar] | 50 up to 400 | Up to 900 | - |
| | Type of vessel | - | Carbon fibres composite pressure vessels | - |
| | Application | Stationary applications | Mobility applications | - |
| (Bondarenko et al., 2022) | Pressure range [bar] | Up to 206.65 | | - |
| | Type of vessel | Standard steel cylinders | | - |
| | Application | - | | - |
| (Reuß et al., 2017) | Pressure range [bar] | 200 up to 350 | 350 or 700 | - |
| | Type of vessel | - | | - |
| | Application | Stationary tube systems | Automotive applications (on-board hydrogen storage) | - |
| (Palys & Daoutidis, 2022) | Pressure range [bar] | 200 up to 1000 | | Up to 200 |
| | Type of vessel | Composite shell associated with a permeation barrier * | | - |
| | Application | Transport applications (700 bar) | | - |
| (Forghani et al., 2023) | Pressure range [bar] | 15 bar up to 250 | | 60 up to 150 |
| | Type of vessel | - | | Salt cavern |
| | Application | - | | - |
| (Kim et al., 2023) | Pressure range [bar] | 15 bar up to 250 bar | | - |
| | Type of vessel | - | | - |
| | Application | - | | - |
| | Pressure range [bar] | 30 to 200 | | - |

| Reference | Type of storage | Type of compression | | Geological Storage |
|-------------------------|----------------------|---|--|--------------------------------------|
| | | Low pressure | High Pressure | |
| (Crespi et al., 2022) | Type of vessel | - | | - |
| | Application | - | | - |
| (Kotowicz et al., 2018) | Pressure range [bar] | - | | - |
| | Type of vessel | Cylindrical or spherical pressure tanks | | - |
| | Application | - | | - |
| (Kotowicz et al., 2017) | Pressure range [bar] | | Up to 700 | 60 up to 180 |
| | Type of vessel | Cylindrical or spherical tanks | | - |
| | Application | | Electrical energy production (through fuel cell devices) | Rock caverns, and coal or salt mines |

* The vessel is constituted by two components, one to perform robustness, a composite shell of carbon or glass fibre insert in resin, and a permeation barrier constituted by a metal or polymer layer (Palys & Daoutidis, 2022).

2.2.4 Technical considerations for cryo-compressed storage

With the aim of maximizing the potential of storage, a new technology has been developed. The innovation incorporates compression processes from gaseous storage and heat removal processes, which is associated with liquid storage. The main purpose is to attain optimal hydrogen density, while reducing energy consumption during operation. This is achieved by increasing pressure and reducing temperature. To determine the most efficient point, it must take into account the balance between energy expended in the process and the achieved density.

According to research conducted in this field, the ideal temperatures and pressures for cryo-compressed hydrogen vary from 35 up to 110 K and from 50 up to 700 bar, respectively. These values correspond to hydrogen densities of 60 to 71.5 kg/m³. Furthermore, the maximum energy consumption recorded in this new process was 25% of the LHV of hydrogen, which is lower than the maximum reached by the liquefaction process, but higher than what is required for gaseous storage (Hassan et al., 2021; Palys & Daoutidis, 2022).

In conclusion, the optimal method for storing and transporting hydrogen is dependent on the specific task at hand, and the most critical factor to consider is the amount of hydrogen

that needs to be managed. When dealing with substantial quantities of hydrogen exceeding 10 kg, the optimal approach is to store it in a liquid state, which necessitates the utilization of cryogenic storage. For quantities within the range of 100 g to 10 kg, the most efficient option is to employ compressed gaseous hydrogen stored in cylinders. Lastly, for quantities up to 100 g, hydrogen can be encapsulated within metal-hydride structures. As a result, it is imperative to meticulously define project objectives to ensure the selection of the most energy and cost-efficient solution (Bondarenko et al., 2022).

2.2.5 Characteristics of hydrogen storage vessels

Regarding to storage vessels, there is a clear distinction between gaseous and liquid hydrogen. High-pressure containers consist of a metallic or polymeric layer that makes contact with the gas, functioning as a shield to prevent hydrogen permeation. Additionally, it is common to use a composite shell made of carbon or glass fibres embedded in resin to increase mechanical strength (Palys & Daoutidis, 2022). This type of tank can be in cylindrical or spherical form (Kotowicz et al., 2017, 2018), and have higher costs than medium pressure tanks (Reuß et al., 2017).

Due to the need of using specialized tanks, storing liquid hydrogen has more stringent requirements than storing gaseous hydrogen at high pressures. In other words, the use of specialized tanks is what makes the storage of liquid hydrogen more complex.

The usual method of constructing these tanks is by placing several metal vessels within each other in a concentric way. Several methods, including high vacuum, vacuum-powder or multilayer technologies are used between the inner and outer vessels to create an insulation barrier that minimizes heat transfer to the inner vessel (Bondarenko et al., 2022). Figure 14 and Figure 15 provide two different possible constructive examples of the liquid hydrogen storage tank.

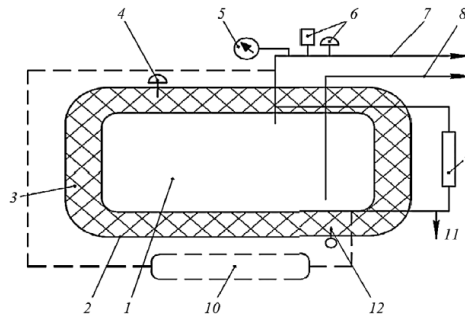


Figure 14 - Example of a common vessel for liquid hydrogen: (1) inner vessel (tank) for liquid hydrogen; (2) outer vessel (casing); (3) thermal insulation; (4) casing safety diaphragm; (5) pressure gauge; (6) safety devices (valve and diaphragm) of the inner vessel; (7) pipe for gas discharge; (8) drain and fill pipe; (9) level indicator; (10) evaporator (or receiver with compressed gaseous hydrogen or helium); (11) branch pipe for sampling liquid hydrogen; (12) vacuum control in the insulating space (Kotowicz et al., 2017).



Figure 15 – Example of a spherical liquid hydrogen storage tank (Kyodo, 2023).

Hassan et al. (2021) categorizes the gaseous pressure vessels based on different characteristics, resulting in four types of vessels, as shown in Figure 16. A type I cylinder, which is the most used, has a volume of 50 L. However, the energy storage capacity of these tanks falls significantly below the targets required for practical energy applications. Regarding pricing, this type of tank usually costs between €100 to €200. The price variation is due to delivery, as the tanks are typically shipped in packs, and transportation methods.

Type II vessels have higher pressure thresholds due to its reinforcement with carbon fibre. This composition is also associated with higher prices. Additionally, types III and IV have a full composite over-wrap, enabling them to achieve a higher gravimetric performance than the two previous tank types mentioned (Hassan et al., 2021).






| Type | | | I | II | III | IV | V | |
|---|-----------|---------|--|---|---|--|---|---------------------|
| Schematic | | |  |  |  |  |  | |
| Components and related failures | Metallic | part | Fully metallic | Metallic enclosure | Metallic liner | Boss | - | |
| | | Failure | - Hydrogen Embrittlement, mechanical properties degradation and premature cracks. - Premature failure for fatigue for metal liner and liner damage ^a . Reason: contact between metal and Hydrogen, surface impact ^a . | | | | | |
| | Composite | part | | Some fibre over-wrap | Full composite over-wrap | | Fully composite | |
| | | Failure | Not applicable | Fiber breaks, delamination and matrix cracking, composite thickness decrease. Reason : accidental mechanical impacts and subsequent pressure loads. | | | | |
| | Polymer | part | not applicable | | | | Polymer liner | Under consideration |
| | | Failure | | | | | Permeation, leakage Reason : contact between polymer and H ₂ charge/discharge conditions | |
| Pressure limit | | | ≤ 50 MPa | Not limited | ≤ 45 MPa | ≤ 100 MPa | | |
| Vessel price | | | ++ | + | - | - | | |
| Gravimetric capacity wt. % or tank mass | | | - | ± | + | ++ | | |
| Popularity & maturity | | | **** | ** | * | * | | |

Figure 16 - Categorization of pressure vessels (Hassan et al., 2021).

Furthermore, Hassan et al. (2021) suggests that including composite filaments in these storage systems increases resistance to corrosion, reduces weight and increases strength. Thus, these tanks can accelerate the commercialization of hydrogen in the automotive industry.

Currently, the industrial cylinders are constructed to withstand 300 bar of pressure. Nevertheless, many cylinders still in use only accommodate a pressure of 200 bar, because they were designed according to the most popular pressure rating used in the past. In Table 6 is presented the technical information about these two storage systems (Hassan et al., 2021).

Table 6 – Information about storage cylinders from the past and the present (Hassan et al., 2021).

| Description of the system | Gravimetric density kgH ₂ /kg system | Volumetric density kgH ₂ /L system | Content, standard m ³ (kg) |
|---|--|--|--|
| Old standard, 200 bar, cylinder weight 67 kg | 0.37 (0.011) | 0.38 (0.011) | 8.9 (0.75) |
| New standard, 300 bar, cylinder weight 63 kg | 0.55 (0.0166) | 0.51 (0.015) | 12.6 (1.07) |

2.3 Hydrogen transportation

Regarding transportation, two primary procedures are involved: transmission and distribution. As can be seen in Figure 2, the transmission process usually incorporates the transport of hydrogen over long distances, connecting the production facilities to the storage stations. This transportation can occur across regions or even countries. Notwithstanding, the distribution is characterized by the transport of hydrogen from storage to the point of use (Riera et al., 2023a). In order to meet the need, multiple methods of transporting hydrogen in large-scale production systems were developed. It is worth noting that certain literature describes hydrogen transportation as a form of mobile storage (He et al., 2021).

Nowadays, hydrogen can be transported either in a liquefied state or as a compressed gas. In the first scenario, the main approaches of transport are tanks which are implemented in road vehicles, ships, and trains. This last two transport options are presented in Figure 17 and Figure 18, respectively.



Figure 17 - Example of liquid hydrogen being transported via ship (Collins Leigh, 2022).



Figure 18 - Example of hydrogen being transported via train (Diermann, 2020).

Hydrogen can also be transported via high-pressure pipelines, tube trailers or railway tube cars. Moreover, tube trailers, which have been widely studied in hydrogen supply chain models, are one of the commonly used modes for transporting smaller quantities of hydrogen. Alternative methods, such as pipelines and shipping vessels, may be more cost-effective for larger quantities (Collins Leigh, 2022).

Therefore, the selection of hydrogen transportation method is substantially affected by investment and operation costs. Another crucial factor to take into account is the distribution of hydrogen demand, which determines the distance to be covered. For instance, a pipeline may be impractical or prohibitively expensive for transporting hydrogen across the ocean.

Additionally, the transportation of hydrogen can be accomplished through the use of a hydrogen carrier, such as ammonia, liquid organic hydrogen carriers, or metal hydrides (Bondarenko et al., 2022; Forghani et al., 2023; Riera et al., 2023b; Sgarbossa et al., 2023; Yang et al., 2021).

2.3.1 Technical considerations for gaseous hydrogen transportation

As previously mentioned, the transportation of hydrogen gas relies on the utilization of trailers coupled with cylinders or bundled tubes. This well-established methodology, presented in Figure 19, has been extensively embraced for transporting small quantities over short distances, up to 200 km. Furthermore, the fraction of hydrogen dispatched through this mode of transportation is contingent upon the degree of compression imposed on the product. To be precise, the pressure gradient oscillates between 220 and 500 bar, which corresponds to 420 and 1,100 kg of hydrogen, respectively.



Figure 19 – Example of a truck trailer coupled with hydrogen gas storage bundled tubes (AIChE Academy, 2020).

Conversely, the transport of hydrogen in a liquid state is believed to be more effective for larger quantities or longer distances (Hassan et al., 2021). According to analyses of Reuß et al. (2017), liquid hydrogen is exclusively lucrative compared to gaseous hydrogen for transporting distances over 500 km (in other words, for remote transportation).

Nevertheless, an extensive array of technical data related to the transportation of gaseous hydrogen via trailers can be found in the literature. This fact highlights a considerable degree of diversity in this matter. He et al. (2021) stated that stored hydrogen transported via trucks, generally is performed under a pressure of 180 bar. This pressure is lower in comparison to the pressure levels noted in stationary pressure vessels. There exist two distinct types of tube trailers (Forghani et al., 2023). One variation consists in a tube of steel that manages hydrogen at 162 bar, whereas the other category, which was previously disclosed by Hassan et al. (2021), comprises a tube trailer manufactured with composite materials, possessing the ability to transport and store up to 1100 kg of gaseous hydrogen under a pressure of 500 bar.

In concordance with the previous information, both Escamilla et al. (2022) and Yang et al. (2021) state that the prevalent technique employed to accumulate and distribute hydrogen in modest amounts is the gaseous compression. Evidently, the pressure of compression varies depending on the final use of the product. According to Escamilla et al. (2022), the range of this variation for mobility applications spans from 50 bar to 900 bar. Yang et al. (2021) mention a hydrogen compression up to 200 bar and a transportation via truck. Moreover, Hassan et al. (2021) specifies a spectrum of compression from 200 up to 500 bar, which and are transported in cylinders or bundled tubes on tube trailer on trucks.

In accordance with Reuß et al. (2017), the economic costs incurred for the transportation of gaseous hydrogen via truck trailers solely depend on the distance traversed, as a result of the constrained capacity of each transported batch. Therefore, there is no consequential benefit to be derived from an escalation in demand. To be more precise, the expenditure of this transportation model can be calculated considering multiple factors, such as the velocity during transportation, the duration of the loading and unloading process and the fuel consumption of the truck. Additionally, the study also supports that composite tube trailers enable higher storage capacity when compared with steel tubes trailers. To be more specific, is stated that the storage capability of this composite equipment reaches 1,150 kg of hydrogen gas, despite their higher cost compared to steel tubes. The study also concludes that one of the viable options for gaseous transportation is a composite tube trailer capacity of 680 kg. Forghani et al. (2023) declares that, regardless the modest capital cost of traditional tube trailers, their storage capacity is not substantial. To illustrate this statement, the

researcher presented a conventional tube trailer priced as US\$ 300,000 with a capacity of 300 kg of hydrogen.

2.3.2 Technical considerations for pipeline transportation

The infrastructures assigned to the distribution of natural gas are widely dispersed. This fact, coupled with the fact that energy transmission through natural gas pipelines is more efficient and results in lower energy losses, encourages the use of these infrastructures for the distribution of hydrogen. Blending green hydrogen, which is generated from renewable energy sources, with natural gas in the pipelines, creates hydrogen-enriched natural gas (Maroufmashat & Fowler, 2017). Furthermore, in accordance with the exposition presented by Maroufmashat & Fowler (2017), the admixture of hydrogen into natural gas at a maximum concentration of 10%, would result in no remarkable impact on the pre-existing natural gas infrastructure or terminal equipment. However, Riera et al. (2023b) suggests a higher admissible flow of hydrogen. With less than 15% of hydrogen concentration, this technology can be implemented with solely slight alterations. This means that, with the minimal initial investment, the operation of pipelines can be carried out promptly.

Moreover, the production of hydrogen can be integrated into the natural gas grid, and the resulting hydrogen can be directly supplied to the grid or, in specific circumstances, be stored in gas tanks. In this case, the main function of storage tanks is to guarantee the uninterrupted integration of the necessary volume of hydrogen into the natural gas pipeline, consequently balancing its supply and demand (Kotowicz et al., 2017; Maroufmashat & Fowler, 2017).

Thus, this grid can perform two vital roles, namely, storage and transmission, within the hydrogen supply chain owing to its construction designed for the conveyance of substantial volumes. The operational mechanism of this versatile infrastructure is straightforward, i.e., hydrogen may be withdrawn from or injected into pipeline terminals, similar to the procedure of storage charging or discharging (He et al., 2021). For these reasons, the literature reveals the benefits of deploying pipeline transportation in the hydrogen supply chain. According to He et al. (2021) and Maroufmashat & Fowler (2017), this approach can satisfy the required energy storage capacity, avoiding the energy loss originated by renewable energy. The determination of the hydrogen flow rate can be predicated upon the maximum admissible concentration of hydrogen in natural gas, a threshold which has

been established in the existing literature, depending on the application (Kotowicz et al., 2017; Maroufmashat & Fowler, 2017). For instance, the region, the country policies and grid components technical requirements are also constraints.

Despite the benefits and practicality of using gas grid pipelines for the transportation and storage of hydrogen, any potential project must take several constraints into consideration. These include pipeline longevity and potential leakage, given that many of the existing pipes are over 100 years old and may pose safety risks, for instance, the possibility of ignition. Another concern is reflected in limitations on the permissible proportion of hydrogen into natural gas pipelines, which is associated to uncertain effects around end-point devices. If the permissible limits typically lie between 5% and 20% hydrogen concentration, higher hydrogen blending may result in additional costs for the final users. Furthermore, hydrogen blends exceeding a 40% threshold require the substitution of compressors, which represents a major drawback (Maroufmashat & Fowler, 2017; Riera et al., 2023b).

An alternative approach is based on the projection of a grid of pipelines solely for hydrogen rather than a mixture, as can be observed in Figure 20. This solution is currently in use, but the networks are still in a small scale.

The United States currently has approximately 2,600 km of pipelines intended for the transport of hydrogen, compared to the 300,000 km of transmission lines that make up its natural gas network (Riera et al., 2023a). According to Forghani et al. (2023), a pipeline that has a diameter of 20 cm can transfer up to 120 tons a day and costs around US\$ 285.000 per kilometre.



Figure 20 – Illustration of a hydrogen pipeline (Nguyen, 2023).

Regarding cost-effectiveness, pipeline transportation proves to be a more lucrative option than electricity transportation when the distance exceeds 1,000 km. This is due to the

significant initial capital investment required for pipeline transportation, which is offset by lower operational costs (Hassan et al., 2021; Reuß et al., 2017).

Apart from the considerable upfront capital outlay, this technology requires a larger number of turbines and compressors compared to the natural gas pipeline grid. This is essential for delivering hydrogen at an appropriate volumetric flow that matches its volumetric energy density (Riera et al., 2023a). Therefore, an increase in equipment quantity leads to a transmission cost for hydrogen that is approximately 1.5 to 1.8 times higher than that of natural gas.

Moreover, the other dissimilarities between the natural gas and hydrogen grid, which unfavourably impact the hydrogen distribution system, involve embrittlement, sealing complications, fatigue stress, larger diameter piping, and the need for more compression power (Hassan et al., 2021). Table 7 provides a summary of technical data related to the transportation of hydrogen gas.

Table 7 - Technical information of hydrogen gas transportation found in literature

| Type of transportation | Reference | Conditions |
|------------------------|--|--|
| Trailer truck | (Hassan et al., 2021) | 220 and 500 bar (420 and 1100 kg) |
| | (He et al., 2021) | 180 bar |
| | (Forghani et al., 2023) | 162 or 500 bar (depending on the type of tube trailer) |
| | (Escamilla et al., 2022) | 50 up to 900 bar |
| | (Yang et al., 2021) | Up to 200 bar |
| Pipelines | (Kotowicz et al., 2017; Maroufmashat & Fowler, 2017) | Blended with natural gas, with hydrogen concentration ranging from 5 up to 20% |
| | (He et al., 2021) | A 0,2-metre diameter pipeline with hydrogen at 100 bar (transport 0,3 tons of H2 per mile) |

2.3.3 Technical considerations for liquid hydrogen transportation

The transportation of liquid hydrogen over extensive distances can be accomplished via specialized tanks fitted onto truck trailers and semi-trailers, such as the illustrated in Figure 21. These tanks have a volumetric capacity ranging from 25 to 55 m³ (Bondarenko et al., 2022). However, as stated in Hassan et al. (2021), the volumetric capacity can achieve values up to 60 m³. Additionally, He et al. (2021) report that the hydrogen carrying capacity

of commercially available liquid trucks is usually four tonnes, whereas the Reuß et al. (2017) states a wider range, which is from 4.0 to 4.5 tons of hydrogen. These mass values correspond to 133 and 149 MWh of hydrogen, respectively. Therefore, the hydrogen liquid transportation via truck exceeds the capacity of hydrogen gas trucks, which is 1.15 tons (38.3 MWh).



Figure 21 – Example of a truck trailer coupled with liquid hydrogen storage tank (Furui CIT, 2022).

Furthermore, these liquid hydrogen tanks operate at slightly elevated pressures compared to the atmospheric pressure in order to prevent air from infiltrating the hydrogen environment while in transit through rail or road transportation (Bondarenko et al., 2022). Table 8 summarizes the technical information about the liquid transportation pathway.

Table 8 – Technical information of liquid hydrogen transportation found in literature

| Reference | Trailer truck |
|---------------------------|----------------------------|
| (Bondarenko et al., 2022) | 25 up to 55 m ³ |
| (Hassan et al., 2021) | Up to 60 m ³ |
| (He et al., 2021) | 4 tons |
| (Reuß et al., 2017) | 4 up to 4.5 tons |

2.4 Hydrogen applications

According to IEA (2021) and IEA (2022), the demand for hydrogen has been growing, with an increase of approximately 50% when comparing the data from the year 2000 to 2020. Besides that, in the year 2021, there was a post-pandemic economic recovery that allowed a 5% increase in hydrogen demand. Thus, the demand reached 94 Mt in 2021, whereas only 60 and 90 Mt were requested in the years 2000 and 2020, respectively.

The application of hydrogen is essentially divided into two sectors, as can be seen in Figure 22. Specifically refining processes (in refineries) and the industries, such as chemical industry, with the production of chemical compounds, and steel industry (IEA, 2022; Zou et al., 2022).

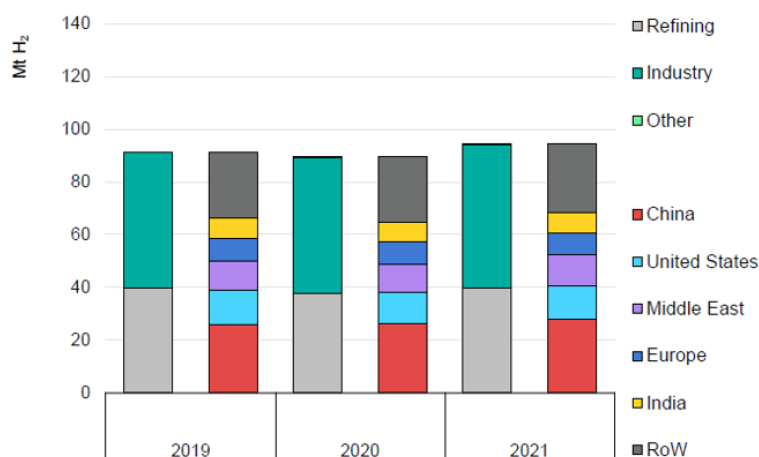


Figure 22 - Hydrogen demand across sectors and regions. Adapted from IEA, (2022).

Nowadays, many policies and commitments by governments are inciting the hydrogen industry to develop and expand into more sectors of the society, such as transportation and as a final energy supplier in industrial processes and steel manufacturing. The main goal is through sustainable hydrogen, to promote the decarbonization in these sectors. In addition, the combination of hydrogen-related technologies with primary energy sources such as solar and wind promotes the energy storage and enhances its utility (Fonseca et al., 2019; Kojima et al., 2023; Von Zuben et al., 2022b).

2.4.1 Petrochemical industry

Hydrogen is one of the main raw materials for the petrochemical industry, particularly in refinery operations. In 2021, around 40 Mt of hydrogen were used. It is foreseen that by 2030, the consumption of hydrogen in this field will double when compared to the amount consumed in 2005 (IEA, 2022; Sazali, 2020). The main processes are hydrodesulfurization, hydroisomerization, dearomatization, and hydrocracking (Kovač et al., 2021; Von Zuben et al., 2022b).

The hydrodesulfurization arises from the increasing need to limit sulphur quantities equal to or less than 10 ppm in motor vehicle fuels. Therefore, hydrogen is used to react with sulphur, contained in organic molecules. This leads to a generation of hydrogen sulphide, which is eliminated from the fuel in question, removing approximately 70% of its sulphur (Von Zuben et al., 2022b).

Regarding hydroisomerization, it is used to reduce paraffin in hydrocarbon chains. In other words, saturated hydrocarbons are converted into branched ones with the same number of carbon atoms, resulting in improved combustion properties. The presence of

hydrogen is necessary to prevent the formation of unsaturated hydrocarbons, and to prevent catalyst deactivation. Dearomatization is a process in which aromatic compounds, in the presence of hydrogen, generate unsaturated structures that are important in industrial processes, such as pharmaceutical and materials chemistry industries. As for hydrocracking, it converts high-carbon chains and heavy oils into smaller chains.

Nowadays, the high demand for hydrogen in the aforementioned processes is met primarily by hydrogen derived from fossil fuels. This reliance on fossil fuel constitutes a big share in carbon emissions regarding refining processes. Therefore, by decarbonizing hydrogen, which means producing hydrogen without emitting carbon dioxide, it becomes possible to attain a substantial reduction in GHG emissions in the respective sector. For this reason, there is a wide and attractive market for green hydrogen in refinery sector (Sazali, 2020; Von Zuben et al., 2022b).

2.4.2 Chemical industry

According to IEA (2022), the production of chemical compounds such as methanol and ammonia through the Haber-Bosch process, consumed 15 and 34 Mt of hydrogen, respectively. In terms of percentage, methanol production corresponds to 10%, while ammonia formation process accounts for 55% of the global hydrogen demand (Kovač et al., 2021). A significant share of the produced ammonia acts directly in food production through fertilization of agricultural fields (Fonseca et al., 2019; Von Zuben et al., 2022b).

For this reason, several projects with the purpose to reduce carbon emissions in ammonia production are under development. These initiatives focus on the adoption of CCUS systems, as well as water electrolysis as a productive method for hydrogen generation. Based on IEA (2022), there was a 200% increase in water electrolysis projects and a 40% rise in CCUS projects in 2021, when compared to 2020.

Synthetic fuel methanol can be obtained by the reaction of carbon dioxide with hydrogen. This compound has a wide range of applications, for instance, it can be blended with diesel or gasoline, increasing their octane rating. As a result, when occurs the combustion of the mixture, the carbon emissions are reduced. Additionally, it can be used directly in fuel cells, specifically designed for this operation. Moreover, due to the lack of carbon emissions in its liquid state, methanol proves to be an excellent compound for storing and transporting energy produced from renewable sources (Von Zuben et al., 2022b; Zou et

al., 2022). Therefore, methanol can be used for storing and transporting renewable energy. In other words, the presented method to produce methanol from hydrogen and CO₂, demonstrates to be an excellent way to transport and store hydrogen produced from renewable energy. Since the methanol energy density, 5.53 kWh/kg, is higher than hydrogens (Zou et al., 2022).

Notably, some projects of this character are being developed. As an example, the Chinese group Henan Shuncheng has initiated a project using emissions-to-liquids technology developed by the Icelandic company Carbon Recycling International (CRI). This project targets to hydrogenate one hundred thousand tons of carbon dioxide, resulting in methanol and other hydrocarbons as reaction products (Zou et al., 2022).

Similar to methanol, ammonia can also serve as an energy carrier for renewable power plants through green hydrogen. In this way, some challenges that are being experienced in the energy transition, imposed by decarbonization measures, can be solved (Von Zuben et al., 2022b; Zou et al., 2022).

2.4.3 Steel industry

Another important application of hydrogen is in the steel industry. This industry alone accounts for 7% of the total CO₂ emissions. Therefore, efforts have been made to transform it into a more sustainable production chain. One of the proposed solutions consists in the use of green hydrogen instead of fossil fuels (Kovač et al., 2021; R. Li & Kawanami, 2023; Von Zuben et al., 2022b).

Firstly, hydrogen can be used as an energy source for production processes through a fuel cell. Additionally, it can be used to facilitate iron reduction (H-DR). It is worth noting that, the full or partial implementation of low-emission hydrogen in the steel production process is still in a developmental phase and it is not even close to the same level of maturity of the conventional DRI process, which uses coal and natural gas (Von Zuben et al., 2022b; Zou et al., 2022).

Several projects are under development in this field, with the most significant one being designated by HYBRIT. This project has been responsible for the production of several tons of steel using this new production method. It is predicted that, by 2030, 1.8 Mt of environmentally friendly hydrogen will be available for this industry. Despite the

environmental benefits associated with the hydrogen metallurgical industry, the final cost of steel rises by 20% to 30%, making it economically less attractive (IEA, 2022; Zou et al., 2022).

2.4.4 Emerging applications

Regarding the unconventional applications of hydrogen, it is forecasted that hydrogen will performance an important role in the shifting of the energy market, enabling a revolutionary transition. All the mentioned peculiarities are closely linked to the decarbonization path (Von Zuben et al., 2022b).

One of the main applications of this category has already been presented. It consists in the use of hydrogen as a storage medium for renewable energy power plants. The objective is to store the surplus energy generated by these intermittent power plants and utilize it during periods of non-production (Li & Kawanami, 2023; Maroufmashat & Fowler, 2017). It should be noted that, this application is the most discussed in literature, as can be analysed in Figure 23.

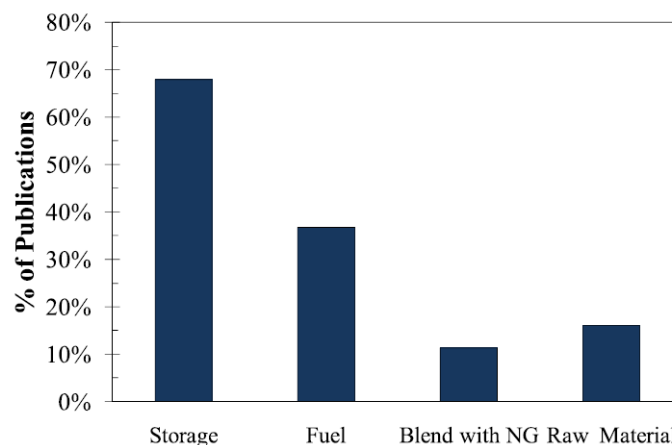


Figure 23 - Dissemination of hydrogen applications (Fonseca et al., 2019).

To achieve the aforementioned application, the integration of water electrolysis into the renewable energy power plant is required. This integration allows to produce hydrogen using renewable energy during periods of low consumption and high renewable energy production. Consequently, energy is stored and not wasted.

In addition, the chemical energy stored as hydrogen can be converted back to electricity and be used during periods of higher energy demand, such as peak consumption. As a result, it is possible to mitigate peaks in electricity demand and minimize the overall expenses associated with energy consumption (Crespi et al., 2022).

Alternatively, hydrogen can be used as fuel in different systems. However, due to its highly flammable and volatile nature, as well as its HHV, 141.9 kJ/g, hydrogen exhibits a powerful and rapid combustion. These characteristics represent a risk associated with its combustion in an engine. Moreover, the requirement of a complex system to ensure the safety of this combustion would result in high costs (Von Zuben et al., 2022b). To overcome this problem, several solutions have been explored. One of them involves blending hydrogen with natural gas, resulting in what is designated as hydrane. Its constitution consists in 20% of hydrogen and the remaining fraction is methane. In summary, it reduces the risk and cost of hydrogen combustion and increases the efficiency of internal combustion of natural gas. Nevertheless, this fuel is associated with pollutant emissions, which make them an unusable fuel in the path of decarbonization (Von Zuben et al., 2022b).

Hence, the clean solution consists in a device known as fuel cell. To be specific, its operating principle is based in the conversion of chemical energy into electricity, with water and heat as a byproduct. As a corollary, this technology is a way to use hydrogen as a sustainable fuel (R. Li & Kawanami, 2023).

Despite its high investment cost, this technology reveals numerous qualities, such as: its high efficiency that can exceed 90% when considering the recovery of 30% to 40% of emitted heat; its low operating cost; its high reliability with a degradation lower than 0.1% in a thousand hours of operation; and its silent operation. Furthermore, its abundant range of power ratings, from a few watts to several gigawatts, allows for its application in distinct environments. If the hydrogen supplied to the fuel cell has been produced from renewable energy sources, the direct emissions associated with the entire process will be approximately zero (Abdelkareem et al., 2021).

Due to its excellent advantages, this technology proves to be one of the solutions to be adopted to achieve the environmental goals set for 2050. Therefore, it has been the subject of study by many researchers to decrease its economic costs and expand its field of applications (Von Zuben et al., 2022b).

Currently, fuel cells can be used in transportation sector, commercial and service buildings that need uninterrupted energy supplies, such as hospitals and industries, but also in portable devices, such as mobile phones, and space applications (Huang, 2022; Khlifi et al., 2022).

Furthermore, 90% of the energy needed in transportation is supplied with the combustion of fossil hydrocarbons. As a result, this sector is responsible for a significant share of carbon emissions, approximately 23%. Thus, transportation is one of the main sectors aimed for achieving decarbonization (Boldrin & Brandon, 2019; IEA, 2022). The demand for hydrogen in the mobility sector is still insipient, accounting for only 0.003% of all energy consumed in transportation. Despite this fact, a growth of 60% in the requirement for this fuel was registered in 2021 compared to the previous year. As for the stock of fuel cell vehicles, it exceeded 59,000 units in June 2022, reflecting a 15% increase compared to the end of 2021. All the aforementioned data is in accordance with the (IEA, 2022).

Several projects have been announced in the field of vehicles. As an example, Renault plans to launch a hydrogen-powered electric car by the end of 2024. Toyota and Hyundai are already with vehicles available in the market. Additionally, Great Wall Motors is planning to develop a range of luxury cars equipped with fuel cell technology. Regarding buses, the West Midlands in the United Kingdom will deploy 124 new fuel cell buses (IEA, 2022).

3. COMPONENT CHARACTERIZATION OF A PV POWER PLANT INTEGRATED WITH HYDROGEN PRODUCTION

In this chapter, it is presented a full characterization of each component of a PV power plant integrated with hydrogen production, taking into account the possible options for the system under modelling. Since the goal is to model a solar-powered system, a characterization of PV power production is presented. Afterwards, the processes of green hydrogen production based on water electrolysis are fully described, as well as the alternative options for hydrogen compressing and fuel cells operation. Finally, it is explained the PV-electrolyser system design connection.

3.1 PV power production unit

3.1.1 PV panels and solar tracker system

A solar panel converts sunlight into electricity by using PV cells. PV cells are manufactured with materials that produce excited electrons that flow through a circuit and produce electricity, which can be directly used or stored. A PV power production unit consists of one or more solar panels, an inverter that converts DC electricity to AC electricity, and other components such as controllers and trackers.

Solar trackers confer movement to the solar panels. This component has the purpose to track the sun's movement throughout the day. In other words, the tracker is designed to optimize sunlight exposure for the PV panel by maximizing the amount of sunlight received and minimizing any potential shading effects. This is achieved with the use of a mechanism that rotates the axis, varying the tilt angle, in order to reduce the angle at which sunlight hits the plane of PV panels (Kang et al., 2019; Martínez-García et al., 2021).

There are three types of solar trackers: (a) fixed rack tracker, (b) single-axis tracker and (3) double-axis tracker (c). All these systems are represented in Figure 24.

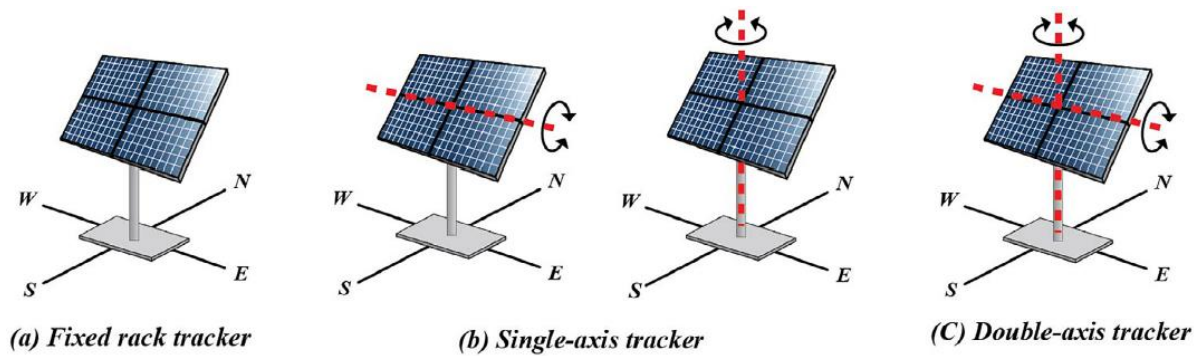


Figure 24 – Types of trackers for PV system (Kang et al., 2019).

The fixed rack tracker has the advantage of lower initial and maintenance costs. However, power plants equipped with this type of tracker are associated with the lowest electricity production among the three types. This is primarily due to its fixed position, which avoids any movement of the PV cell to track the daily trajectory of the sun.

Single-axis tracker provides mobility to the PV cells due the fact that the tracker possesses an axis of rotation. This allows the tracking of the sun’s movement, but only in one direction, either north- south or east-west. Nonetheless, the cost of this single-axis tracker exceeds the fixed equipment (type a) due to the higher installation complexity.

Finally, the double-axis tracker differs from type b) because it has the capacity of tracking the sun movement in two directions, simultaneously. This comes as a result of the incorporation of two axes with rotational abilities. Despite being associated with higher electricity production, it is also the most expensive in terms of maintenance and initial costs (Kang et al., 2019).

3.1.2 Combiner string box

The string combiner box is an essential component placed between the PV modules and the inverter or DC converter. This equipment performs two functions, and it is represented in Figure 25. Firstly, it has the capacity simplify the system by consolidating the multiple DC outputs of the PV panels in one output. Secondly, the combiner string box avoids the PV components to degrade with, for instance, an overload from a lightning strike. In addition, it works as circuit breaker for short circuit protection. In other terms, this equipment isolates the PV energy production system, with the purpose of preventing the risk of propagating electrical accidents.



Figure 25 – Example of a string combiner box.

According to manufacturers, there are boxes with or without a monitoring unit. This additional component allows the analysis of the input current of each PV string, monitoring the inside temperature, checking the status of lightning protection, circuit breakers, and summarizing the output voltage (ABB group, 2023; MOREDAY SOLAR, 2023).

3.1.3 Maximum power point tracking

Regarding the PV panel output power, it depends essential on cell temperature, irradiance, and load impedance (Salas et al., 2006). The effect of the first two presented factors on the operation conditions of the PV module, can be seen in Figure 26.

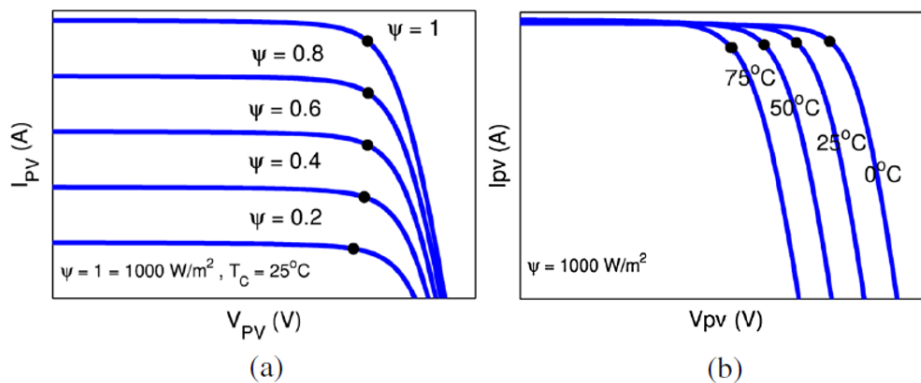


Figure 26 – I-V curves for different a) irradiance, and b) temperature. Adapted from (Tajuddin et al., 2015).

It should be noted that, the operation condition associated to the higher production power is marked in Figure 26 with a spot, and it is known as Maximum Power Point (MPP). To put it differently, for each combination of irradiance and temperature, the system has an optimum combination of current and voltage, which represents the maximum output power (IEEE Staff, 2019; Tajuddin et al., 2015). Besides, it is possible to understand that temperature variations influence the output voltage, and the radiation affects mostly the output current of the PV panel (Salas et al., 2006).

The algorithm responsible for identifying and extracting the maximum power from a PV system is identified as the Maximum Power Point Tracker (MPPT). Its purpose is to optimize the power output of the PV panels, which oscillates with the variation of temperature and irradiance, as explained previously. Furthermore, the MPPT can be implemented in a device, for instance in a DC-DC converter, inverter, or a standalone controller.

Regarding the MPPT, it consists in the calculation of the power output of the system through the detection of voltage and current. The process continues until the MPP is determined, at which point the converter's operating point is adjusted accordingly (Tajuddin et al., 2015; Węcel et al., 2020). This controller draws a line of the maximum power points, known as the Maximum Power Points Line (MPL) of the PV panels (Phan Van et al., 2023).

Furthermore, the load impedance is an important factor that affects the performance of the PV system. This relation can be seen on a I-V graph, such as Figure 27, which has an electrolyser as a load. The operation point of the PV panel is point where occurs the interaction of its I-V curve and the load line.

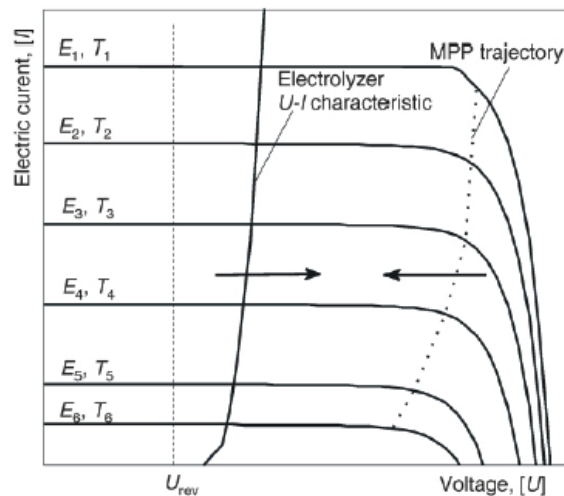


Figure 27 – Example of varying conditions and MPP trajectory response (Firak & Djukić, 2010).

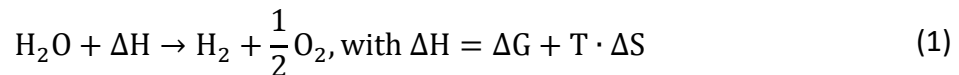
By analysing the Figure 27, the operating points for different pairs of temperature and solar irradiance may not match with the maximum power point trajectory, defined by the MPPT for the PV system (Firak & Djukić, 2010). To achieve a higher energy efficiency of the system, the load line of the electrolyser must be as closer as possible of the MPL (Paul & Andrews, 2008).

3.2 Green hydrogen production systems based on electrolysis

Although there are several methods for producing green hydrogen, this bibliographic research is exclusively focused on water electrolysis. This endothermic process uses renewable energy sources to generate electricity, which is then used to power an electrolyser that splits water into hydrogen and oxygen (Noussan et al., 2021). The process described does not release any GHG (Hussain, 2021; Palys & Daoutidis, 2022; Shiva Kumar & Lim, 2022).

3.2.1 Electrolysis process

The energy required for the electrolysis process, as shown in equations (1) and equation (2), can be divided into two parts: thermal energy ($T \cdot \Delta S$), which accounts for system irreversibility and electric energy (ΔG), energy available to generate useful work. It should be noted that, the variation of enthalpy value (ΔH) presented in the equation (1) is verified under standard conditions, specifically at 25°C and 1 bar (Hussain, 2021; Kotowicz et al., 2017, 2018).



Furthermore, understanding the behaviour of the electric and thermal energy is crucial as electrolysers operate under varying conditions. According to Hussain (2021), increasing the temperature at which electrolysis occurs reduces the electricity demand (ΔG). As for the thermal energy results, the main change is observed at 100 °C, which is caused by water vaporization. Except for this abrupt variation, thermal energy gradually increases with the rise in temperature. The pressure variation has minimal impact on the enthalpy required for the process. The aforementioned information regarding temperature variations is depicted in Figure 28.

The efficiency of the electrolysis process is an important factor in comparing different types of electrolysers, which are devices used to perform the chemical reaction described in equation (2). There are several kinds of performance ratios, which include Faraday efficiency, voltage efficiency, and overall energy efficiency. The first two are factors that impact the overall energy efficiency of the electrolysis.

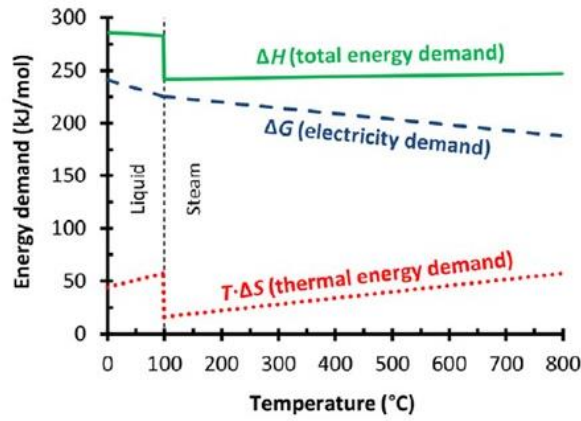


Figure 28 - Influence of temperature on thermodynamic parameters of water electrolysis. Adapted from Hussain (2021).

According to the Faraday law, in an ideal scenario, the amount of hydrogen produced during the electrolysis process should be directly proportional to the current value. Nevertheless, this assertion is not verified by experimental results, which has led to the use of two variables to express the performance ratio: (i) the theoretical electrical current (I_{Th}) required to drive the electrolysis reaction and (ii) the actual current (I) circulating through the cell. This discrepancy in currents is mainly attributed to hydrogen leakage through the membrane, as well as undesired reactions and electrolyte leakage currents. It is worth to mention that these phenomena are more pronounced at low current values (Hussain, 2021; Kotowicz et al., 2017, 2018; Yodwong et al., 2020).

Equation (3) introduces the concept of Faraday efficiency, which pertains to the proportion of current that is effectively utilized in the intended electrochemical process. Thus, Faraday efficiency (η_F) can be defined as the ratio between the actual amount of hydrogen produced ($p m_{H_2}$) and the maximum amount of hydrogen that could be generated in theory ($c m_{H_2}$) based on the electrical energy input (Hussain, 2021; Yodwong et al., 2020).

$$\eta_F = \frac{p m_{H_2}}{c m_{H_2}} \quad (3)$$

Through the observation of equation (2), it can be understood that the electrolysis process requires not only electricity, but also an adequate amount of heat. The heat is obtained from the entropy variation and the necessity to rise the temperature of the water that is supplied to the electrolysis. Moreover, the heat source is determined according to the type of device used. For instance, for high temperature electrolysis, an external heat supplier is employed to provide the necessary energy. In contrast, low-temperature electrolysis relies

on the flow of electric current across the electrolytic cell to provide the necessary thermal energy (Kotowicz et al., 2017).

In this last case, the voltage needed for electrolysis surpasses the standard voltage, which is known as reversible voltage (V_{rev}). Voltage is required for the decomposition of water molecules into hydrogen and oxygen (Hussain, 2021; Kotowicz et al., 2018; H. Zhang et al., 2012). According to Kotowicz et al. (2018), this higher voltage is called neutral thermal voltage (V_0). It should be noted that, in standard conditions (25°C, 1 bar), reversible voltage and neutral thermal voltage assume a value of 1.229 V and 1.48 V, respectively (Hussain, 2021; Kotowicz et al., 2018).

However, the total potential of an electrolysis cell (V) must account for energy dissipation. These energy losses can be expressed in overpotentials such as ohmic (V_{ohm}), activation (V_{act}), and concentration overvoltage (V_{con}). Therefore, the real voltage is higher than the neutral thermal voltage, as can be seen in equation (4).

$$V = V_{rev} + V_{act} + V_{ohm} + V_{con} \quad (4)$$

That being said, the correlation between neutral thermal voltage (V_0) and real voltage (V) can be established, and labelled as voltage efficiency (η_V), which is expressed through equation (5) (Hussain, 2021; Kotowicz et al., 2018).

$$\eta_V = \frac{V_0}{V} \quad (5)$$

The energy overall efficiency of the electrolysis process (η_{ele}) can be quantified using equation (6), which considers the input energy to the electrolyser cell (E_{DC}) and the resulting output energy in the form of hydrogen (Hussain, 2021).

$$\eta_{ele} = \frac{HHV_{H_2} \cdot m_{H_2}}{E_{DC}} \quad (6)$$

It also important to note that, in the case of low-temperature electrolysers where electricity is the only form of energy supplied to the cell, the overall efficiency can be calculated using equation (7) (Hussain, 2021).

$$\eta_{ele} = \eta_F \cdot \eta_V \quad (7)$$

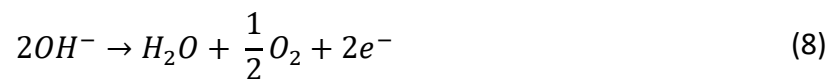
3.2.2 Types of electrolysers

One of the most important aspects of the green hydrogen production is the electrolyser selection, as it impacts subsequent stages of hydrogen handling. Multiple devices are capable of conducting water electrolysis, which can be categorized into two major groups based on their operating temperature: low temperature technologies and high temperature technologies. The alkaline and proton exchange membrane electrolysis cells are the primary representatives of the former group, while the latter group comprises solid oxide electrolysis cells (Nami et al., 2022).

Alkaline electrolyser

Alkaline electrolysers have been the most used devices for water electrolysis. This technology has achieved a multi-megawatt scale in commercial applications worldwide (Shiva Kumar & Lim, 2022). Part of the reason for their high market dominance is the elevated cost-benefit ratio when compared with other technologies. This is due to the utilization of affordable Nickel based metals electrodes, that are non-noble metal and usually have a prolonged lifespan and exhibit exceptional efficiency (Amireh et al., 2023). It is important to mention that the process occurring in this type of cell derives its name from the electrolyte utilized, namely sodium hydroxide or potassium hydroxide, both of which are alkaline solutions (Devbalan & Yadav, 2022).

Nonetheless, these types of devices are associated with several drawbacks that pose challenges to their continued dominance in the electrolysers market (Devbalan & Yadav, 2022). Firstly, these devices are classified under Amireh et al. (2023) as massive and bulky equipment, primarily due to their large size. These characteristics are related to the low electron density flux allowed in this type of electrolyser. To gain a comprehensive understanding of the disadvantage, it is necessary to examine the anode and cathode reactions, respectively presented in equation (8) and (9), and in Figure 29.



Initially, the cathode reaction takes place, equation (9), in which the alkaline solution is reduced, resulting in the production of hydrogen and hydroxide ions (OH⁻). These ions are then transported to the anode due to the application of an electric field. Lastly, the oxidation

of hydroxide ions occurs, leading to the release of water and oxygen, as represented by equation (8). Due to their size and interactions with the solution, hydroxide ions have low mobility. As a result, the electrolyte experiences higher internal resistance (ohmic resistance), leading to lower current densities and slower reaction rates. This negatively affects the efficiency and performance of the electrolysis process. Therefore, electrolysis cells require larger dimensions to compensate the reduced mobility of hydroxide ions and maintain satisfactory electrolysis performance. Compared to other types of electrolyzers, the 0.2 to 0.4 A/cm² current density of alkaline devices is relatively modest (Amireh et al., 2023; Shiva Kumar & Lim, 2022). Additionally, it is important to note that this equipment utilizes an electrolyte that is susceptible to corrosion. This corrosion can lead to the degradation of its components (Kim et al., 2023).

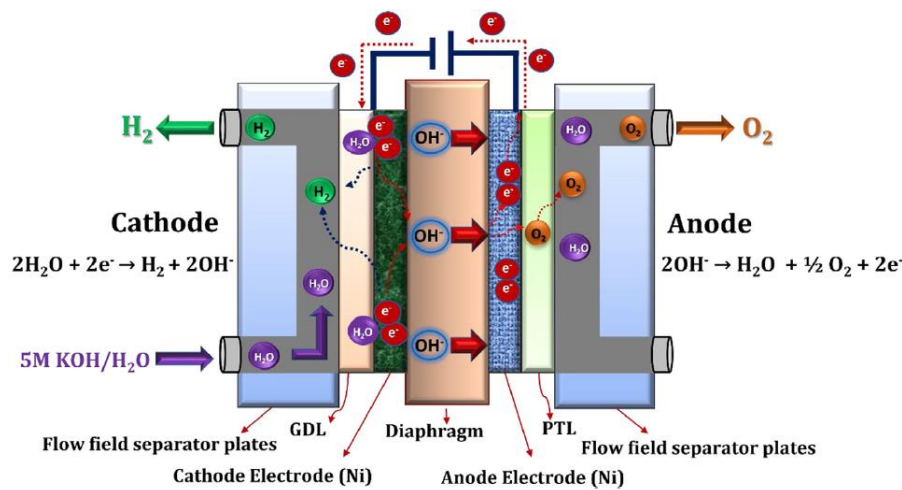


Figure 29 – Example of an alkaline electrolyser cell functional principle (Shiva Kumar & Lim, 2022).

Another drawback associated with the use of alkaline electrolyzers is that the electrolytes used are sensitive to the presence of carbon dioxide in the surrounding environment. When the electrolyte is exposed to the atmosphere, it reacts and forms a salt, either K₂CO₃ or Na₂CO₃, depending on whether the device uses KOH or NaOH solution, respectively. These circumstances give rise to two main challenges. Firstly, there is a decrease in the number of hydroxide ions (OH⁻) present in the electrolyte, which consequently leads to a reduction in ionic conductivity. Secondly, the formation of potassium or sodium carbonate salt can block the pores in the anode's gas diffusion layer. This obstruction limits the ions transferability. Ultimately, all these factors are responsible for the decrease in hydrogen

production (Shiva Kumar & Lim, 2022). Another drawback is related with the existence of a reverse current in the electrolyser when the device is powered off (Amireh et al., 2023).

Proton exchange membrane electrolyser

Proton Exchange Membrane (PEM) water electrolyser cells, unlike alkaline devices, accommodate higher current density and have a more compact system design, leading to the production of purer hydrogen. These electrolysers were developed as an attempt to overcome the drawbacks of alkaline devices. For instance, Crespi et al. (2022) chose PEM electrolyser because of its capacity of adjustment for energy fluctuations throughout the day. In other words, have effective load-adjustment capabilities, due to its speeds of start-up and shut-down (Crespi et al., 2022; Devbalan & Yadav, 2022; Kim et al., 2023).

However, these devices rely on precious catalysts such as platinum and iridium. Given the scarcity and subsequent high cost of these metals, the worldwide expansion across different industries, as well as the widespread adoption of these devices in the energy market, are expected to face numerous challenges (Riera et al., 2023b). At the present, around five tons of iridium are produced per year. According to the information presented in (Nami et al., 2022), this level of production corresponds to an annual capacity of around 25 GW. Therefore, it is important to note that this falls significantly below the required capacity of 3 to 4 TW per year.

For a more comprehensive understanding of the economic aspect associated with these devices, Shiva Kumar & Lim (2022) provides a practical example. It highlights that operating a 10 MW PEM water electrolyser at a current density of 1 A/cm² requires approximately 15 kg of Iridium. In August 2021, this quantity equated to approximately 2,503,462 euros. Moreover, the membrane present in the PEM electrolyser requires a sophisticated architecture to perform correctly (Riera et al., 2023b). There are some differences between PEM and the alkaline electrolyser. These disparities can be seen in Figure 30.

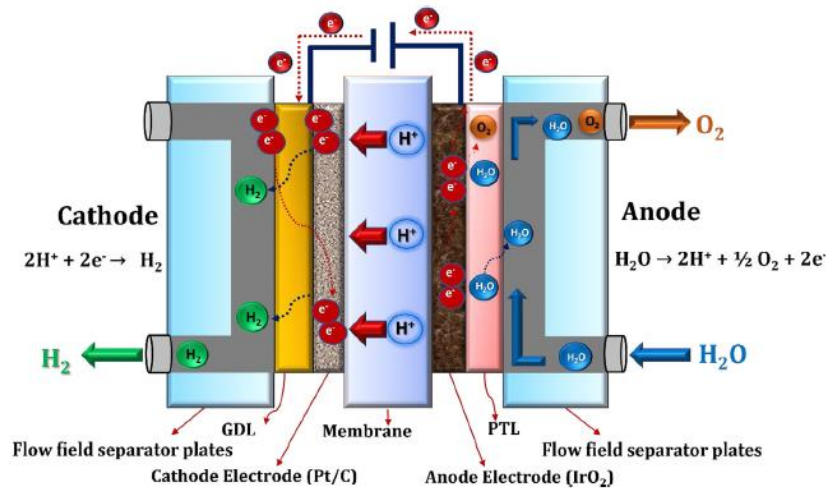


Figure 30 - Example of an PEM electrolyser cell functional principle (Shiva Kumar & Lim, 2022).

The process in the device involves the decomposition of water on the anode side, resulting in the generation of hydrogen ions, oxygen, and electrons. Subsequently, the polymeric membrane permits the passage of hydrogen ions while acting as a barrier to electrons, which travel through the external circuit. On the cathode side, the hydrogen ions combine with the electrons to form hydrogen. It should be noted that, hydrogen ions have higher mobility compared to hydroxide ions in the alkaline. This characteristic is one of the reasons why these PEM electrolyzers can be more compact and capable of accommodating higher current density, as previously mentioned (Devbalan & Yadav, 2022; Shiva Kumar & Lim, 2022).

Solid oxide electrolyser

When it comes to high-temperature electrolysis, Solid Oxide Electrolysis Cells (SOEC) are extensively discussed in literature. Still, this technology is not widely adopted in industry due to the specific operating conditions, lack of long-term stability and, because it is presently undergoing developmental stages (Escamilla et al., 2022; Kotowicz et al., 2017; Shiva Kumar & Lim, 2022).

SOECs require operation temperatures ranging from 700 to 1000 °C. Therefore, a continuous supply of heat is required to achieve these working temperatures. For this reason, this technology is economically viable only if there is access to a cost-effective or free available source of steam for heating purposes. For instance, implement in sites such as oil refining, steelmaking industry, production of methanol and ammonia with surplus of flows.

For this reason, the position expected for the hydrogen production is downstream the chemical or metallurgical industry (Kotowicz et al., 2017; Moradpoor et al., 2023; Shiva Kumar & Lim, 2022).

The amount of electrical energy required to break the water molecule in this specific type of device is significantly lower compared to low-temperature technologies. This is primarily because the water supplied to the electrolyser is in the form of steam. As a result, the efficiency of the electrolyser, represented by the division of the energy contained in hydrogen by the electricity used to break the water molecules, is higher than that of alkaline and PEM electrolysis. Another advantage is that this high temperature process reveals favourable thermodynamics and reaction kinetics, which also provides the opportunity to achieve higher efficiency (Shiva Kumar & Lim, 2022). SOEC (Figure 31) does not require the use of noble metals in their electrode constitution (Shiva Kumar & Lim, 2022).

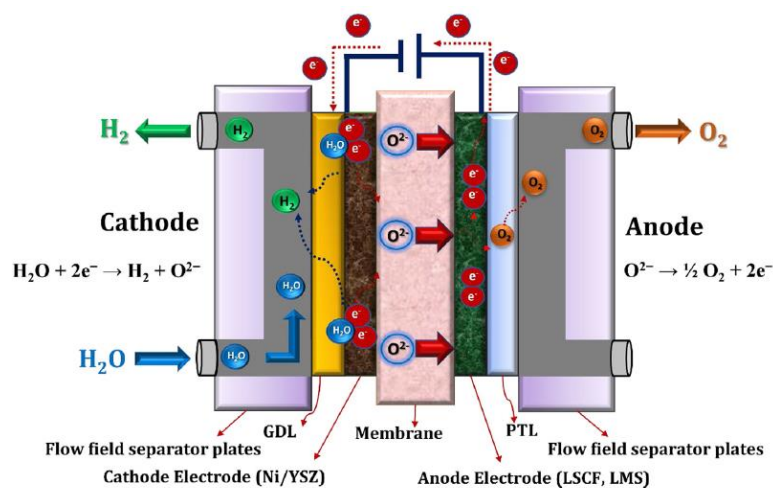


Figure 31 - Example of a solid oxide electrolyser cell functional principle (Shiva Kumar & Lim, 2022).

An oxide ion O^{2-} is formed at the cathodic surface through the oxidation reaction of water molecules. Simultaneously, hydrogen is also generated in this part of the device through the same reaction. Subsequently, the oxide ion travels to the anodic site where it is reduced, resulting in the production of oxygen and electrons. The electrons then flow through the external circuit back to the cathodic site, driven by the positive attraction (Kotowicz et al., 2017). A summary of the overall characteristics of water electrolysis technologies is presented in Table 9.

Table 9 – General characteristics of water electrolysis technologies (Shiva Kumar & Lim, 2022)

| Parameter | Alkaline | PEM | Solid Oxide |
|-------------------------------------|---|---|--|
| Electrolyte | KOH/NaOH (5M) | Solid polymer electrolyte (PFSA) | Yttria stabilized Zirconia (YSZ) |
| Separator | Asbestos/Zirfon/Ni | Nafion | Solid electrolyte YSZ |
| Electrode/Catalyst (Hydrogen: side) | Nickel coated perforated stainless steel | Iridium oxide | Ni/YSZ |
| Electrode/Catalyst (Oxygen side) | Nickel coated perforated stainless steel | Platinum carbon | Perovskites (LSCF, LSM) (La,Sr,Co,FE) (La,Sr,Mn) |
| Gas Diffusion layer | Nickel mesh | Titanium mesh/carbon cloth | Nickel mesh/foam |
| Bipolar Plates | Stainless steel/Nickel coated stainless steel | Platinum/Gold-coated Titanium or Titanium | Cobalt coated stainless steel |
| Nominal current density | 0.2-0.8 A/cm ² | 1-2 A/cm ² | 0.3-1 A/cm ² |
| Voltage range (limits) | 1.4-3 V | 1.4-2.5 V | 1.0-1.5 V |
| Operating temperature | 70-90 °C | 50-80 °C | 700-850 °C |
| Cell pressure | <30 bar | <70 bar | 1 bar |
| H ₂ purity | 99.5-99.9998% | 99.9-99.9999% | 99.9% |
| Efficiency | 50%-78% | 50%-83% | 89% (laboratory) |
| Lifetime (stack) | 60,000 h | 50,000-80,000 h | 20,000 h |
| Development status | Mature | Commercialized | R & D |
| Electrode area | 10,000-30,000 cm ² | 1,500 cm ² | 200 cm ² |
| Capital costs (stack) minimum 1 MW | 270 US\$/kW | 400 US\$/kW | > 2,000 US\$/kW |
| Capital costs (stack) minimum 10 MW | 500-1,000\$/kW | 700-1,400\$/kW | Unknown |

3.2.3 Auxiliary components of electrolysis

Notwithstanding, more equipment beyond the electrolyser is necessary for hydrogen production. For demonstrative purposes, Figure 32 provides an example of the components needed for a hydrogen production unit. This auxiliary equipment can be divided into three main groups: converters, monitoring and control systems and complementary equipment.

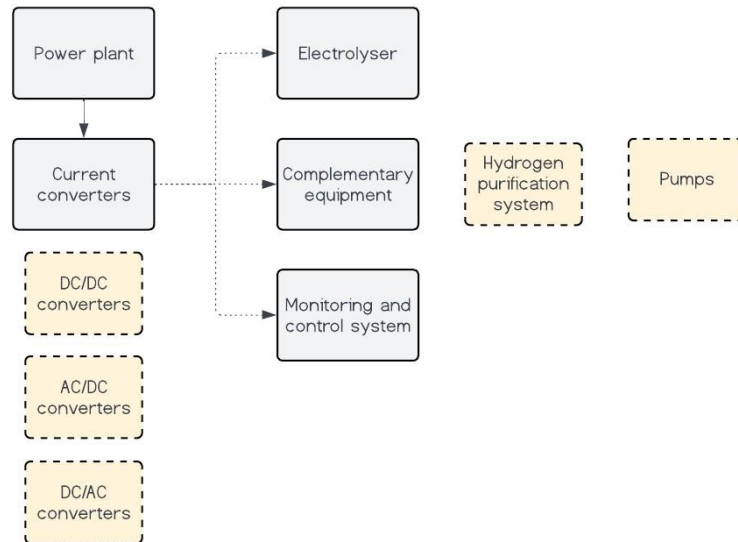


Figure 32 – Example of an electrolyser installation supplied by a power plant. The blocks with dashed borders represent examples of elements that integrate some categorization of the auxiliary components and may be present in the installation.

The auxiliary components include, the gas handling system, which is responsible for collecting and purifying the hydrogen and oxygen gases produced, pumps for water continuous supply, cooling systems, and heaters to guarantee desirable temperatures for the electrolysis process.

Furthermore, there are three converters that can be used for the installation, taking into account the conversion of Direct Current (DC) and the Alternate Current (AC), DC-DC, DC-AC, and AC-DC converters. Firstly, DC-DC converters are used when the electrolyser is connected to the renewable source power plant, such as to the PV cells. Secondly, DC-AC converters can be employed when is necessary to supply with DC power the auxiliary components, that operate with alternating current.

Finally, AC-DC converters can be applied when the electrolyser installation is connected to the power grid. Regarding monitoring and control systems, their role is to regulate the electrolyser operation (Brauns & Turek, 2020; Kotowicz et al., 2018).

3.2.4 Behaviour of electrolyzers connected to renewable energies

When using renewable energy sources for water electrolysis, it is important to consider the fluctuation in power supply as a crucial factor. The electricity input must be within the working thresholds of the electrolyser, so it can work. As an illustration, alkaline electrolyzers have several limitations that must be accomplished. For instance, the minimum load required is usually between 10% up to 40% of the nominal load and the supply of the electricity must be with a current density of 0.2 up to 0.4 A/cm² (Amireh et al., 2023).

The process of water electrolysis with an instable input energy causes a much wider range of operating parameters compared to using electricity from the grid. Therefore, it is important to list the main variables and understand the trend of evolution in relation to the rate of energy supply (Kojima et al., 2023). Kojima et al. (2023) states that the operating temperature of the electrolyser increases with an increase in the power supplied from renewable energy sources and decreases with a decrease in power provided. Besides, when the outlet flux of the electrolyser is low due to a limited supply of renewable power, the purity of the hydrogen decreases.

Thus, low load capacities can be problematic when fuel cells are the end destination of the output, as they require high purity hydrogen. Consequently, coupling the electrolyzers with intermittent renewable electricity presents numerous hurdles (Amireh et al., 2023). This variation is presented in Figure 33.

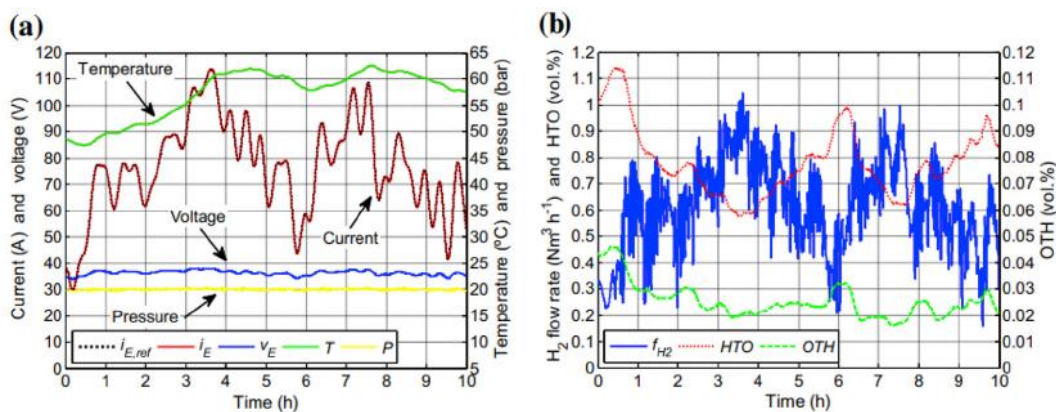


Figure 33 – Experimental results of an electrolyzer for different operation conditions. a) variation of current, voltage, temperature, and pressure over time. b) Evolution of hydrogen flow f_{H_2} , hydrogen transferred to the oxygen current (HTO), and oxygen transferred to the hydrogen current (OTH) over time (Kojima et al., 2023).

Another important aspect to consider when providing renewable energy to electrolyzers is the cyclic start-up and shutdown which can lead to device degradation. Matute et al. (2021) highlights the three significant states that an electrolyzer can assume: idle, standby, and production mode.

In standby mode, only a few systems, such as monitoring and anti-freezing units, are functioning. Therefore, this state is recognized for its lower energy consumption. On the other hand, in standby state the electrolyzer stands at pressure and temperature that allows for a promptly transition, within seconds, to the production state. It should be noted that this transition consumes a specific energy. Lastly, the production state is the only that can generate hydrogen through the supply of water and electricity. To conclude, the dynamic nature of the electrolyzer allows the transition between different states, resulting in energy and time consumption.

Moreover, these state options can make an installation more profitable and flexible. For instance, in cases where the demand for hydrogen is under the capacity of the electrolyzer, it can be advantageous to maintain the electrolyzer in a standby state during periods of high electricity prices and produce hydrogen when prices are low. By keeping the electrolyzer in standby, the need for frequent cold starts is reduced, which helps prevent degradation of the system over its lifetime. However, there may also be instances where it is preferable to shut down the unit once the hydrogen demand for a specific period has been fulfilled to avoid the electricity consumption associated with hot standby (Matute et al., 2021).

As a result of the potential challenges and disadvantages associated with pairing electrolyzers with intermittent renewable energy sources, several studies have been carried out to assess the feasibility.

Regarding alkaline water electrolyzers, a durability test was performed by supplying a constant current for 10 hours each day, followed by a shutdown period for the rest of the day. The potentials of both electrodes remained relatively stable during continuous operation. However, each start and stop cycle causes an increase in the overpotentials of both electrodes. In other words, the electrodes must overcome a higher activation voltage each time they are stopped and restarted. In addition, the reverse current that occurs when alkaline electrolyzers are turned off can cause the devices to degrade faster than it would

under normal operating conditions, leading to a decrease in overall efficiency and lifespan (Amireh et al., 2023; Kojima et al., 2023).

Some researchers have investigated the capability of electrolyzers to respond to short-term, one and three hours, fluctuations in renewable energy supply. Their findings suggest that these systems can adapt to large power fluctuations without requiring start and stop operations. Experimental results showed that cell voltage remained stable throughout the test periods, indicating that the electrolyzers could maintain a consistent level of performance even when energy inputs change (Kojima et al., 2023).

Thus, for the best possible use of alkaline electrolyzers, they should be associated with large-scale PV power plants, since they have a greater capacity to supply enough energy to prevent recurrent stoppages and restarts (Kojima et al., 2023).

Concerning PEM electrolyzers, a study was conducted to compare the degradation of the devices under various current supply scenarios. The study specifically examined the effects of constant current, alternating current with values above zero, and a combination of constant and no flow of electric current. The researchers concluded that significant performance degradation was observed in tests where constant currents of 1 and 2 A/cm² were alternated every 6 hours or where constant currents of 0 and 2 A/cm² were alternated every 10 minutes.

Conversely, from the two scenarios observed in the study presented above, a constant current of 1 A/cm² and alternating operation between 0 and 2 A/cm² for 6 hours, conclude that connecting the device to the electrical grid or a photovoltaic system that can provide a stable current for a certain period does not pose a significant risk of damaging the electrolyser (Kojima et al., 2023).

Regarding SOEC electrolyzers, they have the capacity to easily absorb the load changes over time. Due to their high operating temperature, their response time and start-up/shutdown durations extend from minutes to hours. This is necessary to prevent equipment degradation caused by the temperature gradients that arise when there are alterations in working conditions of the electrolyser (Escamilla et al., 2022).

3.3 Compressor

The compressor serves as the primary element in gaseous hydrogen storage, being responsible for rising gas density by pressure increase. Two main types of compressors are applied in the present context, namely dynamic compressors and positive displacement compressors. Regarding positive displacement compressors, they operate by reducing the volume of a gas within a confined space, while dynamic compressors operate by continuously increasing the velocity of a gas as it passes through them, without relying on a confined space. As presented in Figure 34, it is evident that there are a wide variety of sub-categories within the two main compressor groups. However, due to the specific hydrogen compression requirements, not all of them can be used (Brun & Kurz, 2019).

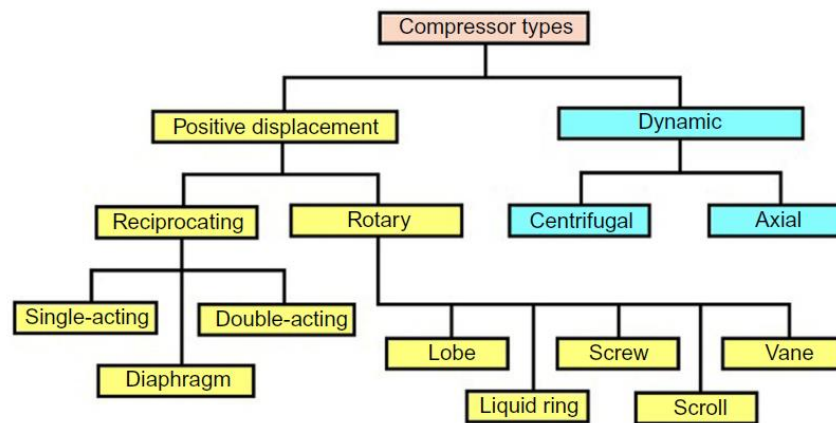


Figure 34 – Family tree of compressors categorization (Brun & Kurz, 2019).

An important characteristic is the pressure ratio of the compressor. At stationary state, the discharge pressure of the compressor must be approximately within the range of 180 to 250 bar. If the electrolyser hydrogen output pressure is 20 bar, then the maximum pressure ratio required is 12.5:1. Additionally, another factor that impacts the selection of the compressor is the requirement for high-purity hydrogen for fuel cells. According to Kotowicz et al. (2018), a PEM fuel cell requires a minimum purity of 99.95% hydrogen, although 99.999% is recommended. Consequently, the risk of contamination must be mitigated as much as possible. In this regard, the preeminent alternative is to employ compressors that are oil free.

Escamilla et al. (2022) proposes two distinct solutions: the diaphragm compressors and the hydraulically driven dry-running reciprocating compressors. The authors' recommendation was based on operational criteria, which can be either continuous or discontinuous. This parameter has distinct consequences on the compressors' longevity.

Compressors equipped with a diaphragm enjoy a prolonged lifespan under conditions of uninterrupted operation, as frequent starts and stops have a negative impact on their temporal endurance. The dry-running reciprocated compressors are comparatively less susceptible to the influence of intermittent operational modes.

Therefore, due to the inherent volatility in the production of renewable energies, the most practical option is to use a dry running piston reciprocated compressor. This type of compressor allows for longer operation times without the need for frequent equipment replacements (Escamilla et al., 2022).

3.3.1 Compression efficiency

The overall efficiency of a compressor is a result of a product of a several aspects. For instance, Hollingsworth et al, (2018) states that the reciprocated compressor power consumption can be divided in isentropic efficiency, valve losses, and mechanical losses.

Firstly, the compression efficiency is defined by isentropic efficiency (η_{isen}), expressed in equation (10). It quantifies the relationship between the adiabatic power (P_{adb}) and the actual power (P_R) involved in the compression process. This efficiency typically varies between 80% up to 95% for a reciprocated compressor (Hollingsworth et al., 2018).

$$\eta_{isen} = \frac{P_{adb}}{P_R} \quad (10)$$

Moreover, a part of the energy supplied by the electric motor is lost due to compressor mechanical losses. To be precise, there are several components that contribute to this energy loss, such as energy consumed at the crank pin (E_{MS}), piston pin (E_{MT}), crank journal (E_{MQ}) and energy dissipated between the cylinder walls (E_f). That being the case, the equation (11) can express the mechanical compressor efficiency (Tsuji et al., 2012). It should be noted that, E_T which represents the energy supplied to the compressor, include, beyond the friction losses, gas compression energy.

$$\eta_m = \frac{E_T - (E_f + E_{MT} + E_{MS} + E_{MQ})}{E_S} \quad (11)$$

In regard of mechanical losses, valve losses are also integrated, which are responsible for pressure losses and, therefore, energy losses. This occurs during the inlet and the outlet of the fluid flow at the cylinder (Bauer, 1988; Hollingsworth et al., 2018). Additionally, and

according to Hollingsworth et al. (2018), the mechanical losses of a reciprocated compressor can vary in a range of 95% up to 98%.

Regarding electric motor, this component plays a crucial role in the compressor system by transforming electric power into mechanical power, which drives the compressor. It is an indispensable component of the system without which the compressor cannot operate. Basically, there are two main types of electric motors: the induction motor and the DC motor (Gonzalez, 2017). According to Banerjee (1998), AC and DC driven systems have distinct characteristics, with DC motors needing extra components for proper cooling at different speeds, and AC drives being able to achieve the same range using a motor that is designed for adjustable-frequency duty and does not require additional components.

Another important parameter is the performance of the equipment (η_{elec}), that can be evaluated through equation (12). This ratio is defined by the mechanical output power (P_{out}) per electrical input power (P_{in}).

$$\eta_{elec} = \frac{P_{out}}{P_{in}} \tag{12}$$

Furthermore, AC drive systems are slightly more efficient than DC drive systems, especially at lower speeds. As the speed of a steady torque DC drive system is decreased below 100%, its efficiency drops off faster than that of an AC drive system, as can be seen in Figure 35. However, the efficiency of any drive system is influenced by several factors such as the application's nominal power, operating speed, load, and other characteristics. Thus, it is important to consider all these aspects when evaluating the efficiency of a drive system (Banerjee, 1998).

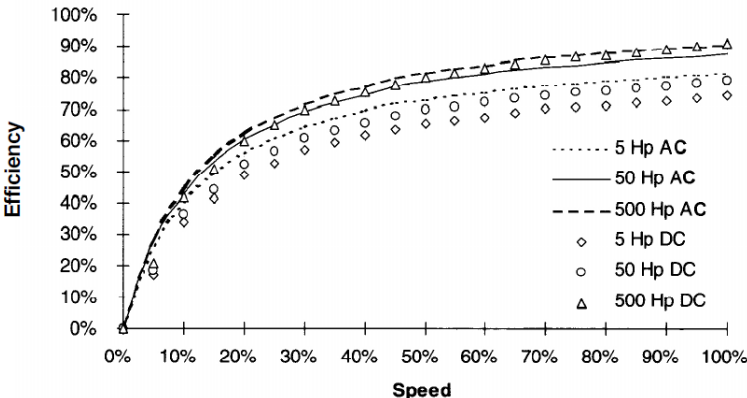


Figure 35 – Comparison of the efficiency of drive systems for a steady torque application (Banerjee, 1998).

Other important aspect that influences the choice is the life cycle cost of the product. The overall expenses incurred throughout the lifetime of a DC-driven system exceed those of an AC-driven system (Banerjee, 1998).

Calzada-Lara & Álvarez (2015) explores the potential for improving the performance of control systems, including direct torque control, when used in conjunction with induction motors. The research findings indicate that alterations to these control structures can lead to a considerable improvement in the performance of applications that have previously relied only on DC servomotors. In other words, the AC motors efficiency can be significantly higher to DC motors in certain applications, as in Figure 35.

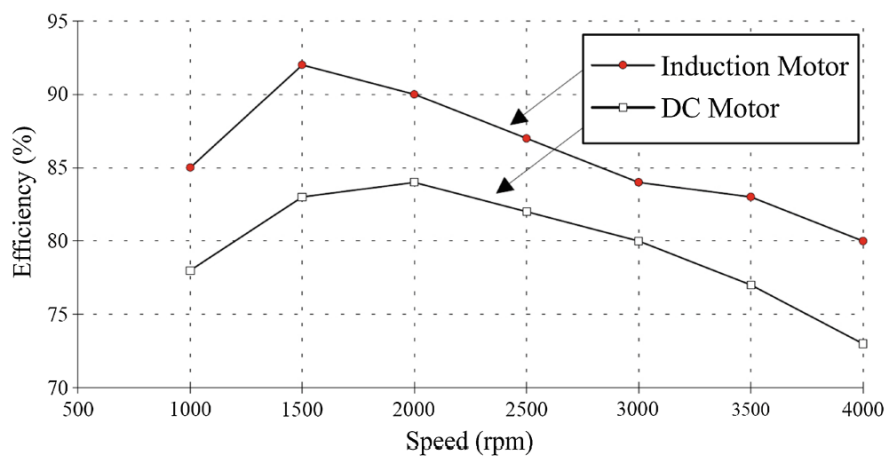


Figure 36 – Induction motor and a DC motor efficiency for the same application (Calzada-Lara & Álvarez, 2015).

In conclusion, other important subsystem that consumes energy is the cooling system, which prevents the overheating of the compressor cylinders and respective components during operation. Therefore, the efficiency of the compressor is maintained, and its lifespan is prolonged (Hollingsworth et al., 2018; P. Li et al., 2023).

3.3.2 Performance characteristics of a reciprocating compressor

Regarding reciprocating compressors, Figure 37 represents the variation of the isentropic efficiency with a pressure ratio for a specific compressor working with hydrogen fluid. It can be concluded that the compression efficiency slightly increase with a raise of the compression ratio.

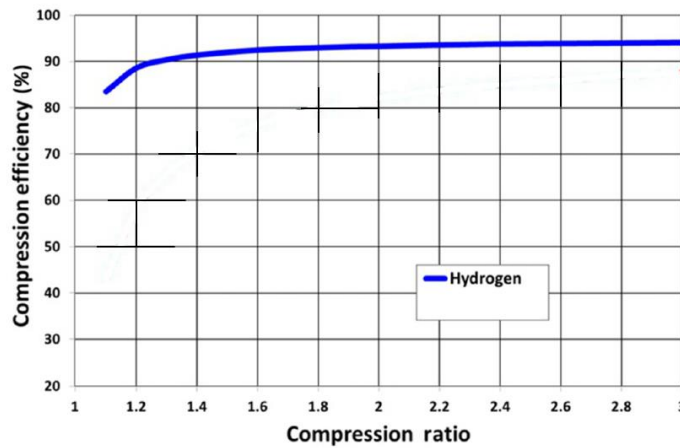


Figure 37 – Reciprocating compressors efficiency. Adapted from (Hollingsworth et al., 2018).

In Figure 38 presents the variation of mass flow capacity for a range of compressor speeds, expressed in rotation per minute (rpm). It can be observed that the mass flow of the gas increases almost linearly with the rise in compressor speed (Mccovern, 1988).

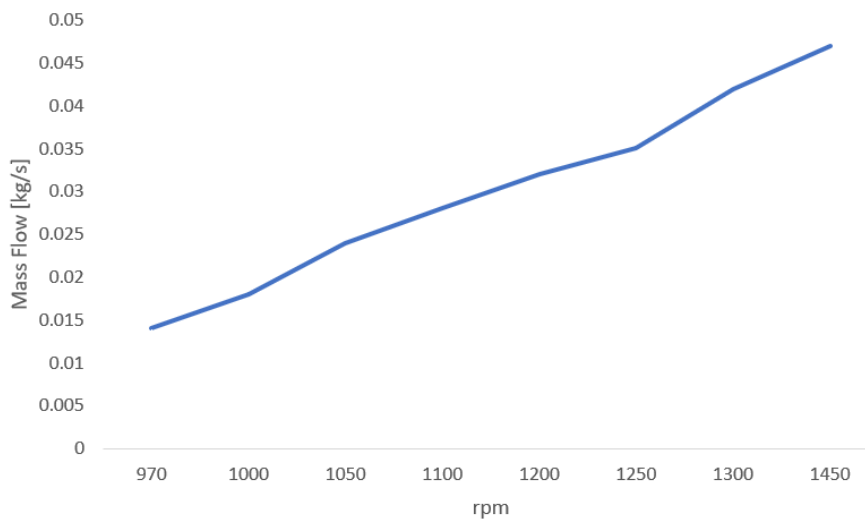


Figure 38 – Example of mass flow variation over a range of speeds of a reciprocating compressor operating with R-12 refrigerant. Adapted from (Mccovern, 1988).

Thus, understanding how the compressor efficiency behaves with variations in mass flow becomes of utmost importance. It was not found this variation for an R-12 refrigerant fluid compressed in a reciprocating compressor. However, the respective variation exists for a compression of carbon dioxide used as a refrigerant (Ma et al., 2012). This correlation is represented in Figure 39.

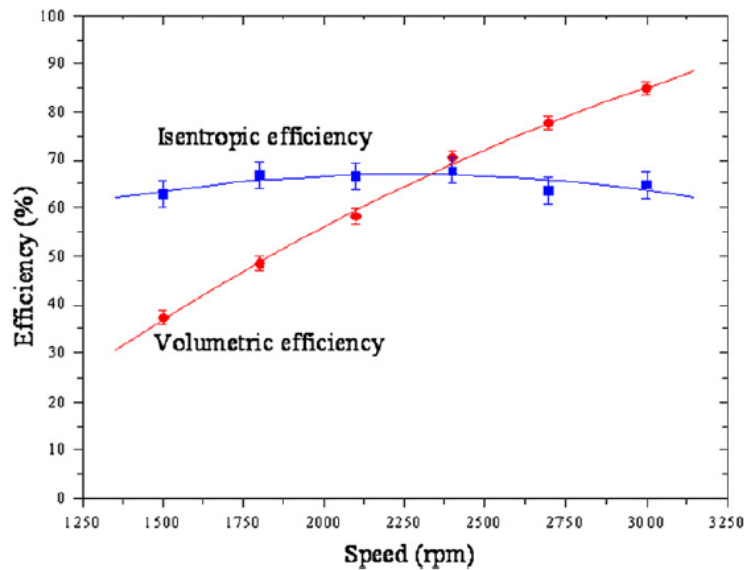


Figure 39 – Example of isentropic efficiency variation over a range of speeds of a reciprocating compressor operating with carbon dioxide as a refrigerant (Ma et al., 2012).

It is possible to conclude that, although the maximum isentropic efficiency is in the range of 2,000 up to 2,400 rpm, the efficiency is not significantly affected by the speed of the compressor.

3.4 Fuel cell

Fuel cells are a Power-to-Power technology that enables the conversion of chemical energy into electricity. It is characterized by the wide variety of fuels, including: hydrogen, natural gas, methanol and several hydrocarbon fuels (Kotowicz et al., 2018; Maroufmashat & Fowler, 2017). When it comes to hydrogen conversion, it is devoid of GHG. For this reason, this device constitutes an important role in the seasonal storage of energy produced in renewable power plants. In other words, the fuel cells become a tool that can be used in the construction of a more sustainable world. (Amin et al., 2022; Brouwer, 2010; Huang, 2022). According to Brouwer (2010), there has been a growing demand in renewable and low-emission power generation solutions. Because of this, significant advancements in hydrogen and fuel cell technologies have been observed, accompanied by notable market trends. These developments have had a profound impact on the field, driving it to progress and innovation.

3.4.1 Fuel cell general operation

The fuel cells have a lot of similarities with electrolyzers, being practically manufactured with the same components, whereas, working reversibly. The main components of fuel cells are electrodes, which can be divided in a cathode and an anode, and an electrolyte, which can be solid or liquid, and either acidic or alkaline. The electrolyte is characterized by its ionic permeability, and it functions as a medium for their movement between the electrodes. Additionally, a catalyst is also present to facilitate the electrochemical reactions within the fuel cell (Gechev & Punov, 2022; Palys & Daoutidis, 2022).

The working principle can be observed in Figure 40. The hydrogen, fuel, reacts with the oxygen contained in air, oxidant, and generates electrical work (W), water, and heat (Q). Therefore, without a combustion, electricity can be produced through a fuel that can be obtained using environmentally friendly methods (Bavane et al., 2023).

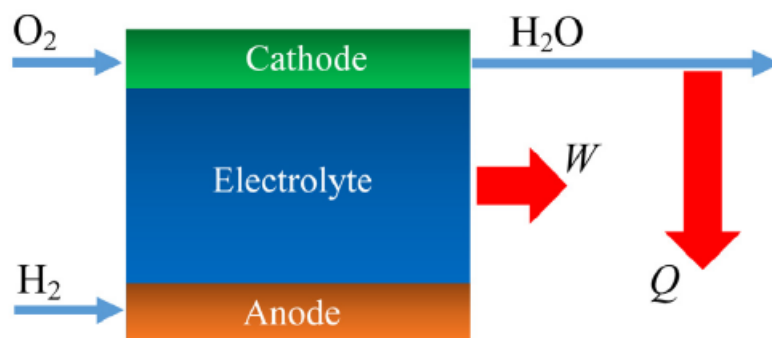


Figure 40 – Scheme of the working principle of hydrogen fuel cell (Haseli, 2018).

Hydrogen is provided to the negative electrode and the oxidation reaction occurs. This originates hydrogen protons transferred to the positive electrode through the electrolyte, and electrons transported through external wiring. This process can be found in equation (13). Then, as can be noted in equation (14), takes place a combination of the hydrogen proton with oxygen and electrons in the cathode side that generate water, and heat. The flow of electrons from the anode to the cathode creates an electric current, that can be hardness to power electrical devices. In other words, electricity is generated (Bavane et al., 2023; Palys & Daoutidis, 2022). The general reaction of the fuel cell is represented in equation (15). For a visual illustration, these events are represented in Figure 41.



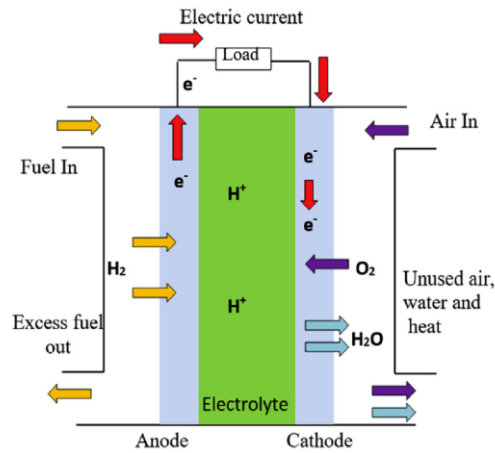


Figure 41 – Example of the proton exchange fuel cell in operation (Li et al., 2019).

While the working principle is shared across all types of fuel cells, the reduction and oxidation reactions vary amongst them. The aforementioned equations and functionality pertain to a specific type of fuel cell, namely the proton exchange fuel cell. Nowadays, hydrogen fuel cells are primarily utilized in stationary power plants and the transportation sector (Brouwer, 2010). Because of the fact that the reaction that generates water is exothermic, this equipment can be implemented in a combined heat and power installation. In this case, the main objective is to make the most of the energy generated by the device (Kotowicz et al., 2018; Palys & Daoutidis, 2022).

3.4.2 Types of fuel cells

Similar to electrolyzers, fuel cells have equivalent categorisation of devices with identical designations. The most commonly discussed types in literature include alkaline fuel cells (AFC), proton exchange membrane fuel cells (PEMFC), solid oxide fuel cells (SOFC), and phosphoric acid fuel cells (PAFC). This categorization is based on variations in the components that compose each fuel cell, including the electrolyte, as well as the operational configuration of each device (Palys & Daoutidis, 2022).

Alkaline fuel cells

In Figure 42 is presented a low temperature fuel cell, AFC. This device utilizes potassium hydroxide solution as electrolyte (i.e., the hydroxide ions go from the cathode to the anode). The reactions present in this type of fuel cell are described in equations (16) and (17).



These devices can operate with temperatures in a range from 60 °C to 70 °C, the startup time is very short when it is compared to high temperature fuel cells. However, when it is drawn a comparison with other low temperature fuel cells, such as PEMFC, it is clear that they have less flexibility and waste more time on the startup. Another disadvantage of this kind of technology is the low power output density. The value is approximately one-tenth of that found in PEMFC (Huang, 2022; Palys & Daoutidis, 2022).

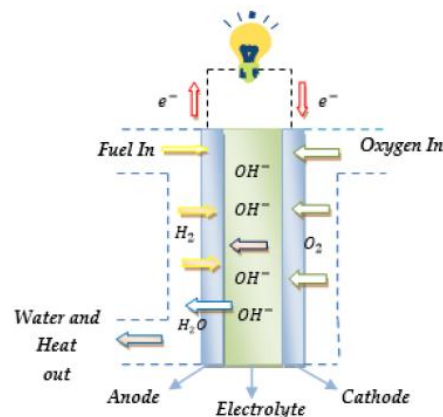


Figure 42 – Working principle of an alkaline fuel cell (Khlifi & Toukebri, 2022).

Despite all these disadvantages, alkaline fuel cells are still in use in some applications. The low cost of the materials used in this technology, which represents a low initial investment, and a low production cost, allied with its maturity, make this equipment one of the most affordable within its market. Because of that, these devices represent the best option for some implementations, for instance, a small-scale stationary power generation (Huang, 2022).

The power output of this devices can be increased by scaling up the number of fuel cells unites. Beyond the increase in the energy transformation process, this can also lead to an optimization of the balance of plant components, which consist in auxiliary systems that are required for the fuel cell operation (Palys & Daoutidis, 2022).

Proton exchange membrane fuel cells

The PEMFC, presented in Figure 43, exhibits a solid electrolyte, which reduces the risk of corrosion phenomena. Additionally, advantages of this fuel cell include high current density, compact system, and a dynamic system, which is associated with a fast respond to the different operation conditions. However, the devices integrate high-cost materials in the electrodes, such as platinum (Palys & Daoutidis, 2022). This constitutes huge obstacle in the implementation of this kind of fuel cell over the lower cost AFC.

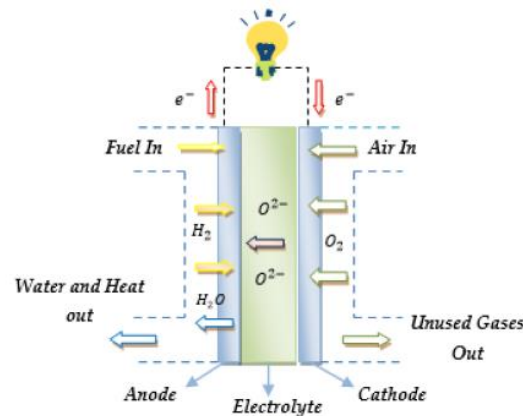


Figure 43 – Working principle of a PEMFC (Khelifi & Toukebri, 2022).

Regarding operational conditions, these type of fuel cells can be divided into two subgroups: (i) the low temperature (LT-PEMFC), which operational temperatures are below 100°C, normally vary from 60°C up to 80°C; (ii) and the high temperature (HT-PEMFC), which comprises temperatures from 120 °C to 200 °C. The distinct components enable the difference in operating conditions. The LT-PEMFC has electrolyte membrane made of perfluorosulfonic acid (Nafion), which can be damage with temperatures above 100 °C. Conversely, the HT-PEMFC incorporate a polybenzimidazole membrane infused with phosphoric acid, which has the capacity to operate at temperatures reaching up to 200°C (Palys & Daoutidis, 2022; Rosli et al., 2017).

The high temperature category can achieve a higher efficiency in Combined Heat and Power (CHP) applications over a low temperature group. Nevertheless, the vaporization that occurs at temperatures above 100°C can escalate the degradation rates and reduce the lifespan of the device, as a result of membrane dehydration (Palys & Daoutidis, 2022; Rosli et al., 2017).

Furthermore, the LT-PEMFC has another advantage, namely, their flexibility for dynamic operations (Palys & Daoutidis, 2022). This kind of fuel cell is characterized with a fast startup, which constitutes an important aspect when dealing with dynamic installations.

Phosphoric acid fuel cells

With respect for PAFC, illustrated in Figure 44, they have the same working principle of PEMFC. Therefore, their reactions are represented in equations (13) and (14). Despite this fact, the electrolyte of PAFC, which is a phosphoric acid (H_3PO_4), differ from PEMFC electrolyte. Moreover, this intermediate temperature process has a low efficiency when compared with low temperature fuel cells, but their reaction is faster than PEMFC (Gechev & Punov, 2022; Huang, 2022).

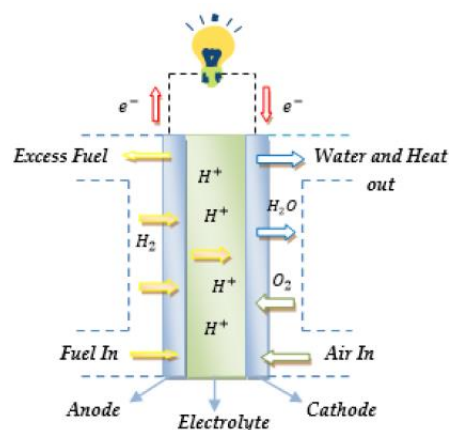


Figure 44 – Working principle of a PAFC (Khelifi & Toukebri, 2022).

As the alkaline technology, the PAFC has a corrosive electrolyte, which can represent a structural problem to the equipment (Gechev & Punov, 2022). Furthermore, the presence of platinum in the electrodes results in fuel cells having a high cost. This investment can be reduced if the equipment is scaled up, allowing a lower investment when compared with PEMFC. Despite this reduction, this type of fuel cell is not economically competitive when compared with AFC (Palys & Daoutidis, 2022).

When dealing with dynamic installations, such as the renewable energy power plants, one of the most relevant operational parameters is the energy input intermittency. This requires components with a flexible work capacity. Since, the PAFC have startups of four hours, according to Palys & Daoutidis (2022) they are not indicated for this type of application.

This type of fuel cell should be applied in cogeneration power plants, because of their easily installation and good performance when compared with traditional power plants

(Huang, 2022). Notwithstanding, as a pioneering in the market, represents the most mature fuel cell (Gechev & Punov, 2022). According to Palys & Daoutidis (2022), a single module has the capacity of 400 to 1000 kW, being mainly used for electrical energy production.

Finally, care must be taken into consideration about the fact that these fuel cells might degrade in the presence of carbon monoxide, that can be produced by reforming process of steam. This can occur when the heat generated in the process is used for heating water (Huang, 2022).

Solid oxide fuel cells

Regarding the high temperature fuel cells, the most discussed in literature are SOFC, which is represented in Figure 45. These devices incorporate a metallic oxide solid ceramic electrolyte that can endure high temperatures (Huang, 2022; Palys & Daoutidis, 2022).

Despite sharing the same operational principles as other fuel cells, some differences can be evidenced. The air containing oxygen is supplied to the cathode side, originating a reduction reaction of oxygen forming oxygen ion. Similar to other fuel cells, the electrons formed are conducted to an external circuit to the cathode side. On the anode, hydrogen combines with oxygen ions, which migrate from the cathode due to chemical potential, and produces water (Huang, 2022).

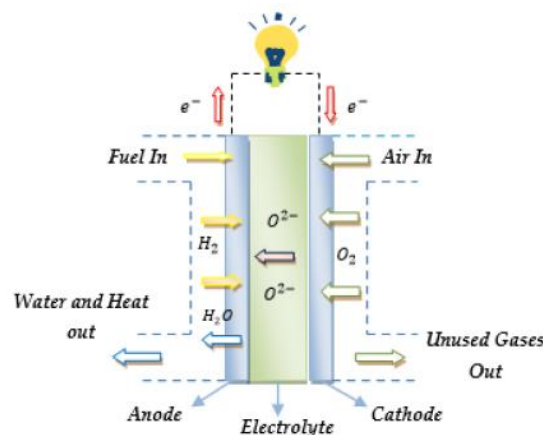


Figure 45 – Working principle of a SOFC (Khelifi & Toukebri, 2022).

These types of fuel cells possess advantageous characteristics, with the most distinctive feature being their ability to operate not only as fuel cells but also as electrolyzers. In other words, these cells have the capacity to perform electrolysis and power generation through a hydrogen fuel (Palys & Daoutidis, 2022). It is worth to note that these two operating modes cannot be used simultaneously.

Furthermore, precious metal as catalytic component is not required, reducing the investment costs. When used in combined heat and power installations SOFC can accomplish 90% of efficiency, which make them suitable for this kind of applications.

Conversely, high operation temperature can lead to a faster degradation of the fuel cell. Additionally, this operation parameter obligates that the startups and shutdowns take a duration of hours. In simple terms, this technology does not have the capacity to adapt to an intermittent load demand (Palys & Daoutidis, 2022).

This kind of fuel cell is applicable in large scale energy demand, because the modules of SOFC can attain 1,000 kW of power (Palys & Daoutidis, 2022). For instance, in marine or truck of long distance, where the startup times doesn't have much importance. In addition, their flexibility size also constitutes an important parameter for these kinds of applications (Huang, 2022). A summary of the advantages and disadvantages of each type of fuel cell is presented in Table 10.

3.4.3 Fuel cells efficiency

Fuel cells generate two forms of energy: electrical energy and thermal energy. Thus, three distinct efficiencies can be taken into consideration to evaluate and compare fuel cell devices. Nevertheless, the main objective of a fuel cell is to convert chemical energy into electricity, in other words, the primary performance criterion to take into account is the electrical efficiency (Environmental Protection Agency et al., 2015). To further explore the issue, equation (18) defines the electrical efficiency ($\eta_{FC_{elec}}$) as follows:

$$\eta_{FC_{elec}} = \frac{out E_{FC}}{E_{H_2}} \quad (18)$$

Being $out E_{FC}$ the output electric power of the fuel cell, and E_{H_2} represents the chemical energy of the hydrogen. Therefore, the evaluation of the efficiency can be determined as the ratio of the electrical energy produced to the energy contained in the hydrogen that is supplied to the fuel cell (Kotowicz et al., 2018). The general values of this fraction vary between 40 and 60% (Blaabjerg et al., 2004; Wang et al., 2011).

Table 10 – Fuel cell advantages and disadvantages and application (Gechev & Punov, 2022; Hadi Tawil & Hareb, 2008)

| Type | Electrolyte | Advantages | Disadvantages | Application |
|-------|---|---|--|--|
| AFC | Aqueous Potassium hydroxide – KOH | <ul style="list-style-type: none"> - High efficiency and low start-up time, low operating temperature; - Easy to operate and easy thermal management; - Inexpensive materials; | <ul style="list-style-type: none"> - Very high intolerance to CO and CO₂; - Prone to leakage liquid electrolyte; - Lower power output density; | Portable and stationary |
| PEMFC | Solid polymer membrane, acidic | <ul style="list-style-type: none"> - Low operating pressure, temperature and start-up time (dynamic); - Simple and compact design; - High current, voltage and output power density; - Solid electrolyte; | <ul style="list-style-type: none"> - Requires constant stack humidification and thus water management; - Requires platinum catalyst (which is expensive), and high fuel purity; - Intolerance to CO and sulphur; | Portable, transportation, and small-scale stationary |
| PAFC | Liquid phosphoric acid – H ₃ PO ₄ | <ul style="list-style-type: none"> - Cheap electrolyte; - Low operating temperature and reasonable start-up times; - Mature technology, with market presence; | <ul style="list-style-type: none"> - Stack must be kept above 42°C – the freezing point of electrolyte, requires extra hardware which makes it heavier and larger; - Low efficiency; - Liquid corrosive acidic electrolyte which requires careful handling; | Stationary |
| SOFC | Solid yttria stabilizer zirconia YSZ | <ul style="list-style-type: none"> - Internal fuel processing; - Inexpensive catalyst; - High efficiency; - Generation of a lot of waste heat; - Solid electrolyte; | <ul style="list-style-type: none"> - Need of heat management due to high operating temperature; - Brittle electrolyte, strict material requirements; - Longer start-up times and immaturity; - High cost of the technology | Stationary |

Regarding thermal energy, its efficiency ($\eta_{FC_{th}}$) can be observed in equation (19). It is important to note that $_{th}E_{FC}$ represents the thermal energy that is emitted from the fuel cell on the cathode side. Therefore, the thermal efficiency can be obtained by the division of the heat generated in the fuel cell by the total chemical energy contained in the supplied hydrogen (Zarzycki et al., 2018).

$$\eta_{FC_{th}} = \frac{_{th}E_{FC}}{E_{H_2}} \quad (19)$$

Finally, it is presented in equation (20) the overall efficiency ($\eta_{FC_{OV}}$) of the fuel cell. This ratio can reach a value of 80%. As mentioned earlier, these two energy components can only be harnessed if the fuel cell device is incorporated into a combined heat and power installation (Blaabjerg et al., 2004; Wang et al., 2011).

$$\eta_{FC_{OV}} = \frac{(_{out}E_{FC} + _{th}E_{FC})}{E_{H_2}} \quad (20)$$

Table 11 summarizes the values of electrical and overall efficiencies of fuel cells, presented in literature.

Table 11 – Efficiencies of each type of fuel cell, according to literature

| Reference | Type of fuel cell | Electrical efficiency ($\eta_{FC_{elec}}$) [%] | Overall efficiency ($\eta_{FC_{OV}}$) [%] |
|--|-------------------|--|---|
| (Khlifi & Toukebri, 2022) (Palys & Daoutidis, 2022) (Gechev & Punov, 2022) (Wang et al., 2020) | AFC | Up to 60 Up to 60 50 a 65 70 | Up to 80 |
| (Khlifi & Toukebri, 2022) (Gechev & Punov, 2022) (Wang et al., 2020) | PEMFC | 40 a 50 40 a 60 65 a 72 | |
| (Huang, 2022) (Khlifi & Toukebri, 2022) (Palys & Daoutidis, 2022) (Gechev & Punov, 2022) (Wang et al., 2020) | SOFC | | Up to 60 90-100 90 85 |
| (Palys & Daoutidis, 2022) (Gechev & Punov, 2022) (Wang et al., 2020) | PAFC | 40-45 35-45 45 | 80 85 |

3.5 PV-electrolyser connection system design

The connection between the energy supply, the PV system, and the electrolyser can be performed by a direct or indirect method. As presented in Figure 46, the PV panels can be straightly connected with the electrolyser, or a DC-DC converter can be placed between these two units (Phan Van et al., 2023).

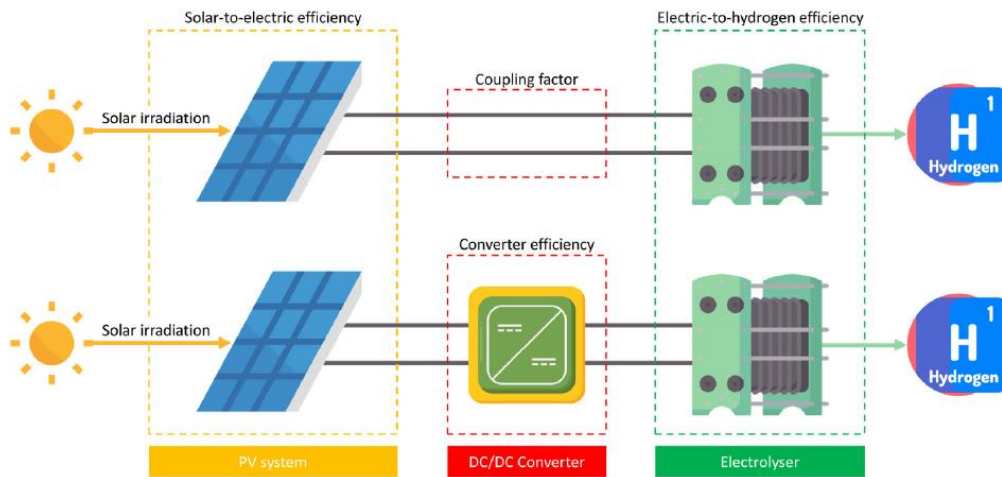


Figure 46 – Representation of direct and indirect PV-electrolyser connection. Adapted from Phan Van et al. (2023).

3.5.1 Direct connection

The installation with a direct connection, without a DC-DC converter, is a simpler installation with lower energy losses and lower costs when compared with the indirectly connection. However, since the PV system is directly linked to the electrolysis device, the output voltage and current of the combiner string box are the same as the electricity that enters the hydrogen production unit. This results in a lack of flexibility due to the strong dependence of the electrolyser operating current and voltage on the current-voltage curves of the PV panels.

Consequently, careful consideration must be given to these two components sizing, considering the limited range of energy production and supply flexibility of this setup. To achieve a higher coupling factor, which is the energy transfer efficiency, is necessary to position the load line of the electrolyser as near as possible to the maximum power line. To accomplish this, it is necessary choosing the most suitable configuration for the installation. To clarify, it involves modifying the arrangement of electrolyser and PV panels by adjusting

their connections in series and parallel. In Figure 47, can be noticed some possible adjustments in electrolyser the cells configuration.

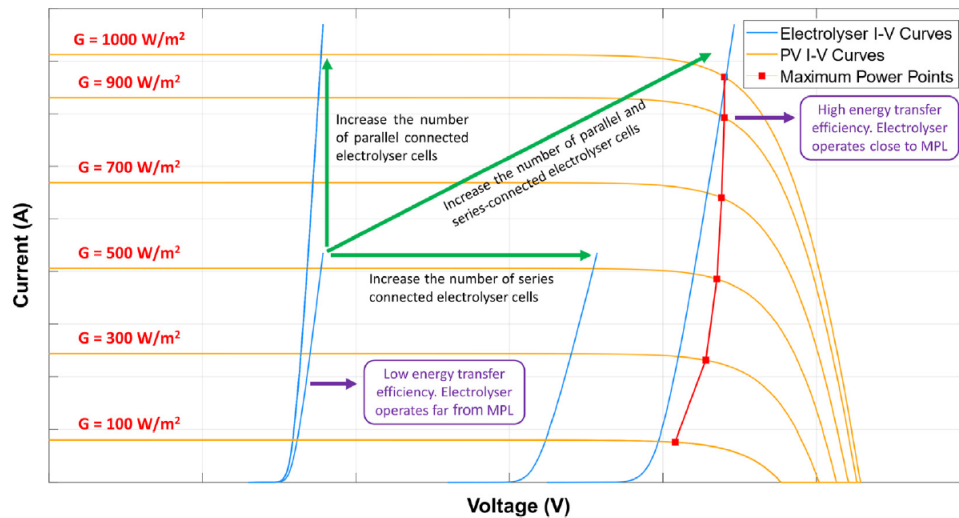


Figure 47 - Examples of possible adjustments in the series-parallel electrolyser cells configuration that can be made to achieve a match between the MPL with the electrolyser load line (I-V) (Phan Van et al., 2023).

In addition, adjusting some operating conditions, such as temperature, water activity, and pressure, can also increase the energy transfer efficiency (Phan Van et al., 2023).

3.5.2 Indirect connection

As previously presented, there are some limitations associated to the straight connection between the PV system and the electrolyser. The voltage delivered by the renewable power plant is usually beyond the acceptable levels of the water electrolyser. Therefore, as can be seen in example of Figure 48 a), the operation of the PV panels is not at the maximum power. To achieve the matching between the operation and the MPL, it is possible to apply the techniques presented in chapter 3.5.1 or to incorporate a DC-DC converter into the system.

A DC-DC converter can be implemented with an algorithm, which perform the maximum point tracking of the PV system over the time and ensures that the energy produced can be supplied to the electrolyser. In consequence, the solar energy is efficiently captured by the PV and transported to the electrolyser. This scenario is represented in Figure 48 b).

Furthermore, other advantage of integrating the DC-DC converter in the installation is reflected in higher operational flexibility since the component has the ability to provide power regulation. This component also reduces the voltage and current output ripple, which

is crucial for enhance the efficiency of the electrolyser. Notwithstanding, this implementation increases installation investment costs (García-Valverde et al., 2008; Garrigós et al., 2014; Guilbert et al., 2020).

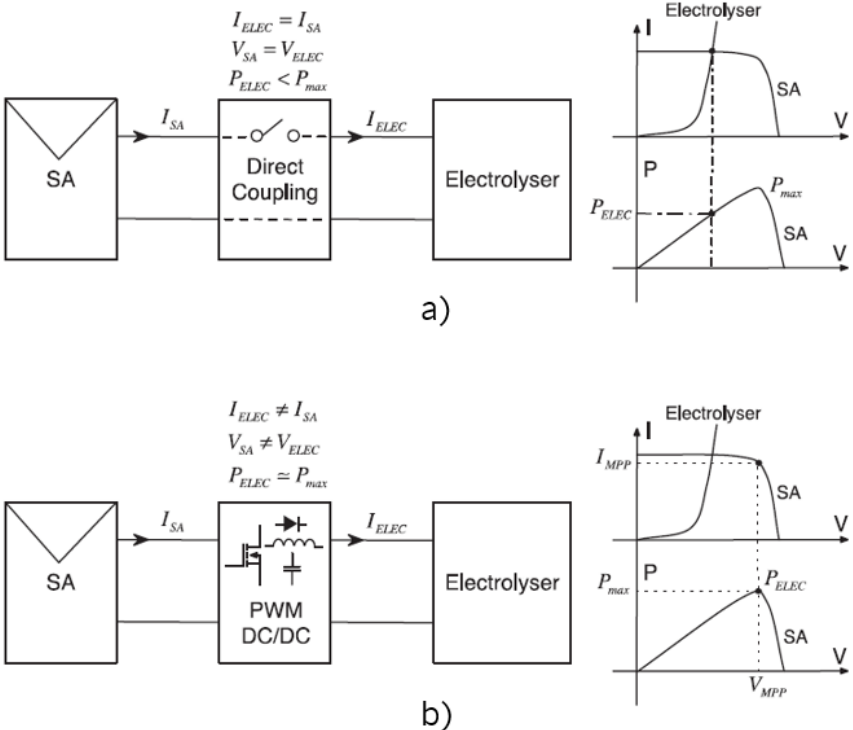


Figure 48 – Representation of a direct a) and indirect b) connection between the PV system and the electrolyser. Adapted from (Garrigós et al., 2014).

According to literature, there are three types of DC-DC converters, buck, boost, and buck-boost converter. The buck converter is characterised for reducing the input voltage to a lower output voltage and increasing the input current to a higher output current. Conversely, the boost converter performs an increase in the input voltage to a higher output voltage, which decreases the input current to a lower output current. Finally, the buck-boost converter is capable of lowering or increasing the input voltage to a lower or higher output voltage (García-Valverde et al., 2008; Guilbert et al., 2020).

The converter selection depends on its application. In literature, to connect a PV system to an electrolyser there are a variety of choices. For instance, (García-Valverde et al., 2008) proposes a buck-boost DC-DC converter, because it can handle a variety of voltage input values with a minimum energy loss. Contrarily, Guilbert et al. (2020) perform an experimental validation of a DC-DC buck converter placed between a renewable energy source and an electrolyser. Identically, Ergin Şahin (2020) realized a simulation in MATLAB (Simulink) an installation with a PV powered buck converter for electrolysis load.

Furthermore, (Crosa et al., 2006) decided to model a PV system, which powers an electrolysis device, but incorporates two DC-DC converters. The first converter works as maximum power point tracking, and the second controls the electrolyser operation voltage and current.

4. SYSTEM DESCRIPTION AND MATHEMATICAL MODEL

As mentioned previously, in an increasingly sustainable world, renewable energy generation from wind turbines and solar panels is reliant on environmental factors. Furthermore, establishing large-scale plants for storage battery production can be unfeasible due to their high costs and the inappropriateness of batteries for seasonal energy storage. As a result, these sources are intermittent and cannot consistently meet the electricity grid's demands, which have consumption peaks regardless of weather conditions (Kojima et al., 2023). Therefore, the model developed aims to solve this problem.

The thermodynamic model presented in this chapter couples a renewable power plant with a hydrogen production (i.e., water splitting using an electrolyser) and storage units. The system should be able to suppress the electricity demand of an industrial facility, according to its energy consumption profile. Moreover, the surplus energy can be stored in the form of hydrogen.

The main objective is to study the use of surplus energy, over the course of one year, with an hourly time interval analysis, considering the energy production from a PV power plant. The problem is modelled to maximize the system's self-sufficiency, thereby avoiding energy purchasing from the national electrical grid. The outline of the PV plant integrated with hydrogen production model is presented in Figure 49.

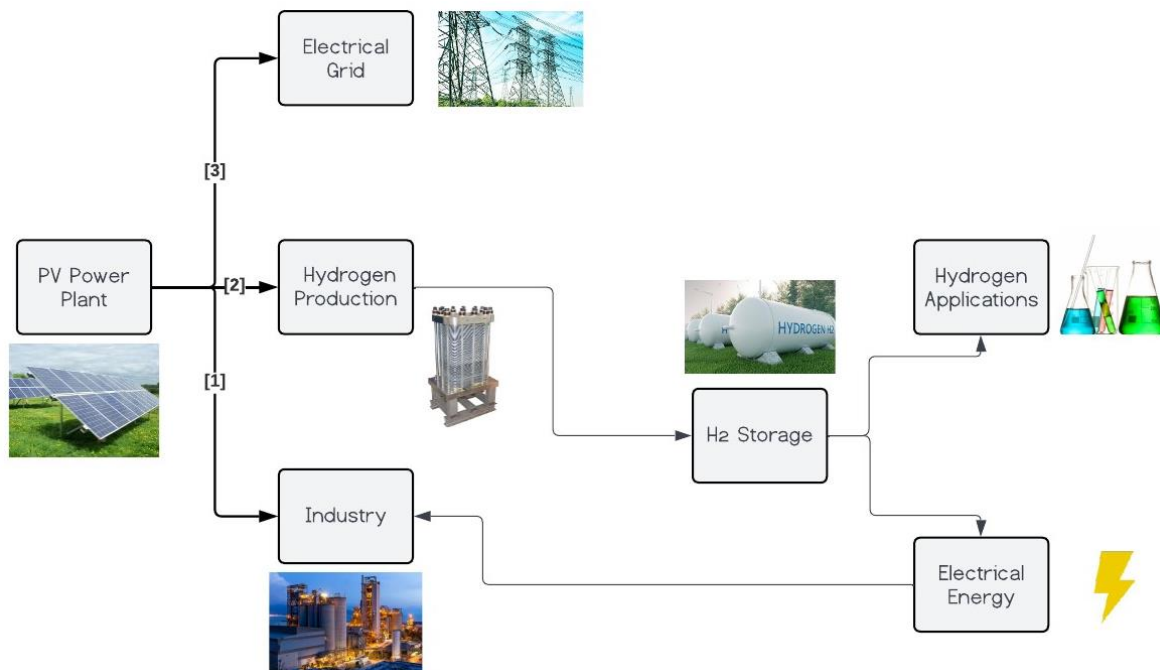


Figure 49 – Outline of the PV plant integrated with hydrogen production model.

The electricity generated by the power plant has three possible paths. It should be noted that, the energy from the PV system is distributed according to the order of significance of each application, and to their respective minimum and maximum limits of energy absorption.

The first path, highlighted as [1], is the most important path because it corresponds to the industry energy supply. The second path [2] is the second most significant because it supplies the energy to the hydrogen production unit. The last path [3] corresponds to the electricity selling to the grid. Thus, the priority of the system is to suppress the industry electricity demand with renewable energy. In the case of excess of energy production, after the primary need is fulfilled, the energy is directed to the electrolyser to proceed with hydrogen production. As hydrogen acts as an energy carrier, it allows energy to be stored for long periods, avoiding energy waste. If the surplus energy is higher than the maximum amount that the electrolyser can handle, the energy is sold to the grid to increase the cash revenues.

As hydrogen is produced, it can be stored at the same location of its production, namely a centralized water electrolysis facility. Furthermore, hydrogen can be stored for days to months, depending on its destination. There are two main routes for stored hydrogen. One involves selling the sustainable fuel to its applications, previously mentioned in subchapter 2.2.2. The other potential route is taken when the energy generated by the PV power plant is not sufficient to meet the industry energy demand. In this case, the hydrogen is converted in electricity and supplied to industry.

4.1 Profile of industry energy consumption

The model was defined taking into account the industry energy consumption profile. For this study, it was selected a factory that works with a single shift, characterized by its continuous production process, operating daily from 8:00 AM to 6:00 PM. For simplification, the energy requirement is considered constant throughout the working hours. It is essential to highlight that the factory experiences a start-up period from 7:00 AM until 8:00 AM and a shut-down period from 6:00 PM until 7:00 PM. The typical daily profile of the electrical demand of the industry is represented in Figure 50.

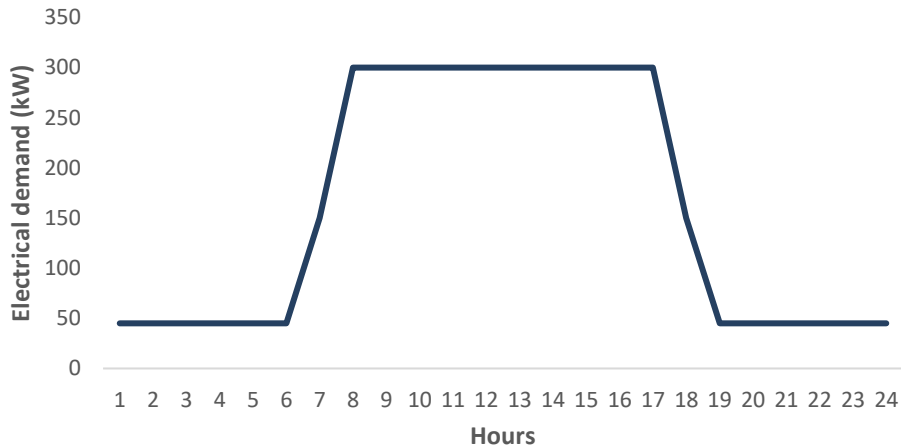


Figure 50 - Daily profile of the electrical demand of the industry.

It should be noted that, during the start-up and shutdown periods, only half of the energy required in the continuous production (300 kW) is consumed. Regarding the night period, a constant value of 45 kW is considered, which is 15% of the production consumption.

4.2 Location of the power plant installation

The modelled facilities are situated in the village Canha, which is a Portuguese village belonging to the municipality of Montijo, Setubal. This location is represented in Figure 51.



Figure 51 – Location of the modelled installation, from a general and close distance.

The location was chosen due to the existence of a real PV power plant at this site. It is worth mentioned that the precise spot of the power plant was provided by the Voltalia company. Further characteristics about this matter are summarized in Table 12.

Table 12 – Summary of the location characteristics of the installation

| Installation location characteristics | |
|---------------------------------------|------------|
| Village | Canha |
| Region | Setubal |
| Country | Portugal |
| Latitude | +38.73 ° |
| Longitude | -8.60 ° |
| Altitude | 91.05 amsl |

*amsl means above mean sea level.

4.3 Input of meteorological data

One of the inputs of the model is the hourly meteorological data over a full year, which is necessary to calculate the energy produced by the PV power plant. As weather conditions during a particular period vary from year to year, selecting a specific year can potentially introduce meteorological data containing deviations from the typical conditions. Such discrepancies have the potential to result in erroneous study conclusions. Therefore, a Typical Meteorological Year (TMY) was considered in this study. A TMY comprises meteorological data values for a specific global location defined by altitude and latitude. This data can be found in Table 13, and is provided for each hour of the year. The values are from a timeframe that can surpass ten years. To be specific, the meteorological values for each month of the TMY are the most representative for that specific time of the year.

Table 13 – Output data from a TMY

| Typical meteorological year data | |
|----------------------------------|-------------------------------|
| T2m [°C] | Dry bulb (air) temperature |
| RH [%] | Relative Humidity |
| G(h) [W/m ²] | Global horizontal irradiance |
| Gb(n) [W/m ²] | Direct (beam) irradiance |
| Gd(h) [W/m ²] | Diffuse horizontal irradiance |
| IR(h) [W/m ²] | Infrared radiation downwards |
| WS10m [m/s] | Windspeed |
| WD10m [°] | Wind direction |
| SP [Pa] | Surface (air) pressure |

In this study, the selected years correspond to PVGIS-SARAH2, which covers the timeframe from 2005 to 2020. The data is obtained through satellites covering Europe, Africa, and Asia. For the specific location of the projected power plant, the years from which the used meteorological values are presented in Table 14. It should be noted that this tool is available online at the European Commission website.

Table 14 - Information about which year provided the meteorological data for each month of the TMY

| Mouth | Year |
|--------------|-------------|
| January | 2018 |
| February | 2019 |
| March | 2011 |
| April | 2008 |
| May | 2007 |
| June | 2019 |
| July | 2011 |
| August | 2007 |
| September | 2014 |
| October | 2013 |
| November | 2006 |
| December | 2012 |

4.4 System description

In order to define the proposed model, it is necessary to select and size all the system components. Figure 52 schematically presents the parts of the main system. It is worth noting that, the auxiliary system of the fuel cell is not presented, because it is similar to the electrolyser support system, which is already represented in the scheme. Additionally, some of the auxiliary systems of PV power plant and storage unit have been suppressed due to graphical simplification purposes. Nevertheless, all the considerations will be further explored in the respective subchapter.

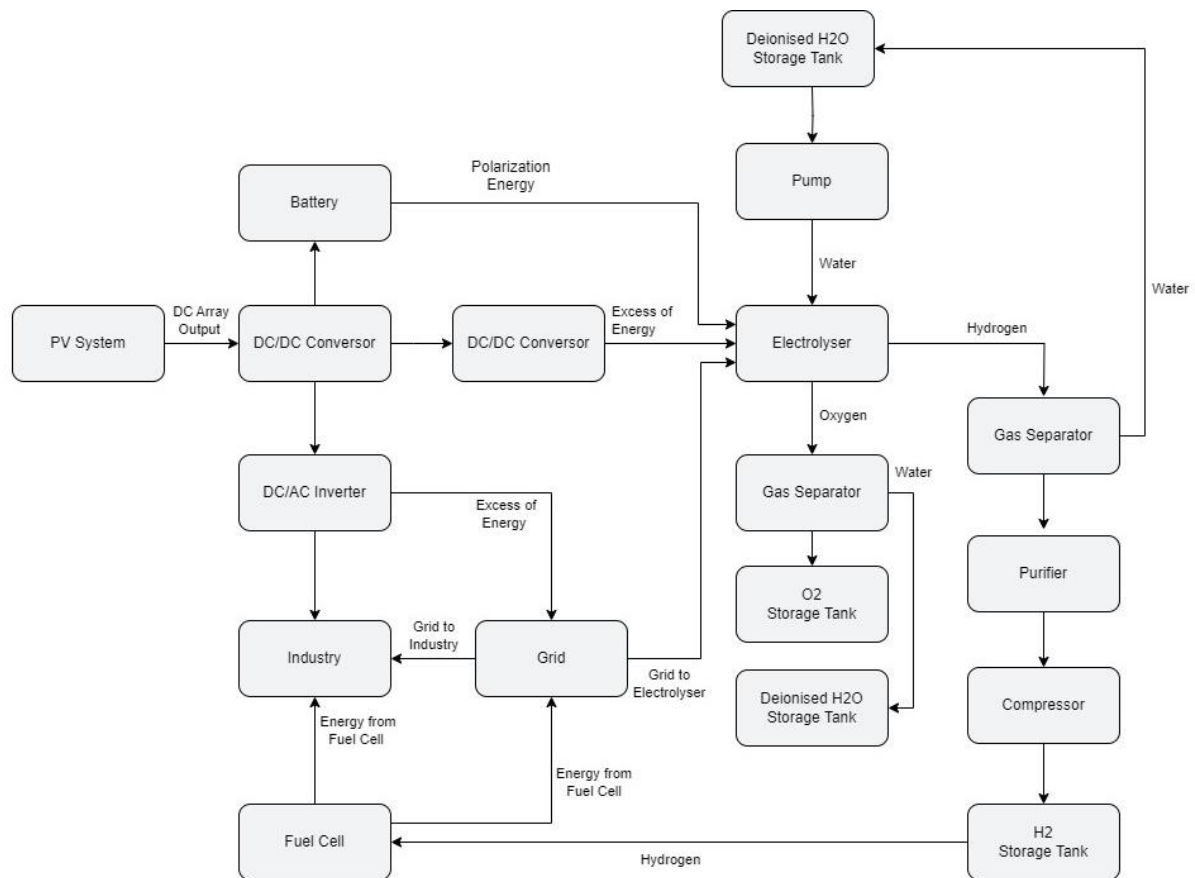


Figure 52 – System main components.

4.4.1 PV power plant

The pivotal subsystem of this model is the PV power plant. This unit captures the solar energy and produces electricity. Figure 53 illustrates the projected structure and the connection of the PV system to external components.

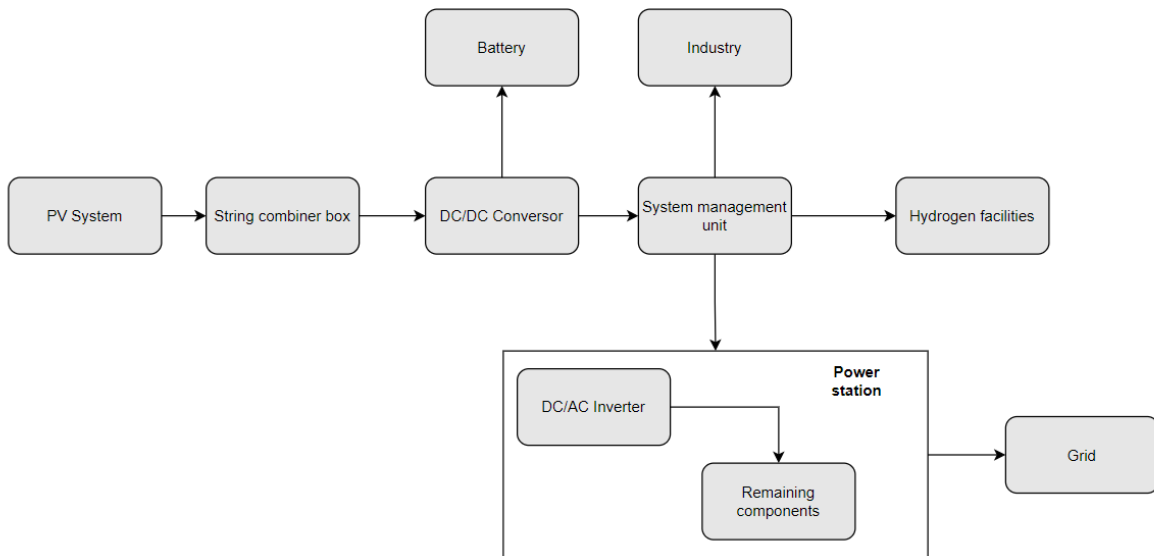


Figure 53 - Representation of the most important components of the photovoltaic plant and their respective connections.

It is important to emphasize that this power plant was planned based on an existing installation. Therefore, careful consideration was given to select components that closely replicated those used in the real configuration. In this work, the selected PV panel was the JKMS285M-60V Maxim Monofacial model. An example of this can be observed in Figure 108, presented at Appendix 1. With a peak power of 285 W, this component is manufactured by Jinkosolar, further information is featured in Table 15.

Table 15 – PV panel characteristics

| Main characteristics | |
|----------------------|--------------------|
| Module model | JKMS285M-60V Maxim |
| Manufacturer | Jinkosolar |
| Technology | Si-mono |
| Type of module | Monofacial |
| Maximum voltage | 1000 V |
| Peak Power | 285 W |
| Efficiency | 17.4 % |

Furthermore, these modules are assembled in a single axis' solar tracker, oriented in north south. An illustration of this configuration is presented in Figure 109, presented at Appendix 1. The structure model is a SkySmart with a configuration of 2V from Arctech Solar. The choice was based on the fact that this single-axis solar tracker is the most balanced in terms of solar capture and investment costs. To be specific, the single-axis solar tracker has better solar capture than the fixed tracker and lower CAPEX and OPEX than the two-axis tracker. Additionally, the two-axis tracker is associated with lower reliability and a larger occupied area.

The PV power plant must incorporate one or more string boxes. In Figure 110, presented at Appendix 1, is illustrated a string box that can be implemented in this model. Another component is the DC-DC controller, its function was already explained in the literature revision. The chosen device it is characterised for having an efficiency of 98%. The monitoring system is responsible for receiving data corresponding to the energy produced by the PV panels and making decisions, based on specific criteria, about the distribution of this energy. As shown in Figure 53, there are four possible pathways for the energy: the industrial sector, hydrogen facilities, battery, or the grid. The guidelines that control this system will be explained in chapter 4.5.

The power station also incorporates several components such as current inverters and transformers. This allows the connection between the PV system and other subsystems, by inverting the type of current and increasing or decreasing its voltage. These subsystems can be contemplated in Figure 111 and Figure 112, which are presented at Appendix 1.

As pointed out, this PV system was based on an existing installation. Nonetheless, the number of PV panels has been reduced to meet the requires energy output. The final number accounts for 7056 PV modules, which are mounted on 98 single-axis trackers (72 PV panels per structure). In Figure 54, it is possible to identify the projected PV power plant and the reduction in the number of PV panels.



Figure 54 – Representation of the real PV power plant and the projected power plant. The blue rectangle represents the projected PV panels, while the black ones represent the actual PV panels.

Concerning the projected power plant, as can be analysed in Figure 55, it is divided into two primary sections: the grey area signifies the space available for PV panels, while the purple area represents the location of the substation. The grey area can be further subdivided into the red region, which is unsuitable for PV panel installation due to the field's topography, and the blue rectangles that denote the area occupied by PV modules.

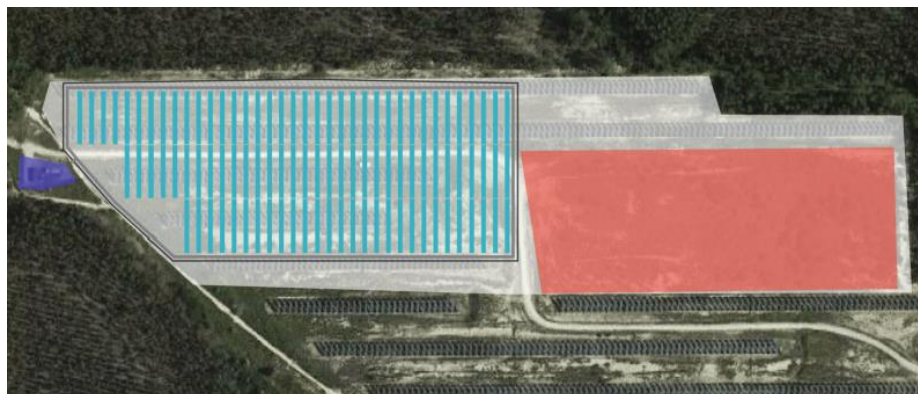


Figure 55 – Layout of the PV system. The grey area represents the available area for the PV panels implementation. The red area was designated as a restricted zone. The blue rectangles represent the PV panels. The purple area represents the substation. The black lines represent the fences, and the grey lines represent the roads.

4.4.2 Hydrogen production unit

The electrolyser was selected considering the PV energy output, the energy required to supply the factory facility and the excess energy on sunny days with the insurance that the device is not oversized. Therefore, it was necessary to estimate how much energy is produced during the days of abundant solar radiation. For this purpose, several days from the TMY were

analysed to study the magnitude of the unused energy. The industry energy demand was subtracted to the energy output of the PV power plant. Table 16 present the application of this calculation for June 2nd of the TMY. The difference represents the excess or deficit of energy generated by PV plant to supply the industry.

Table 16 –The electricity produced by the PV power plant, and the energy demand required by industry on June 2nd of 2019.

| Hour | DC Array Output [kWh] | Industry Demand [kWh] | Energy excess/ deficit |
|------|-----------------------|-----------------------|------------------------|
| 6 | 411.9 | 45 | 366.9 |
| 7 | 1155.6 | 150 | 1005.6 |
| 8 | 1470.7 | 300 | 1170.7 |
| 9 | 1583.1 | 300 | 1283.1 |
| 10 | 1608.0 | 300 | 1308.0 |
| 11 | 1600.3 | 300 | 1300.3 |
| 12 | 1610.8 | 300 | 1310.8 |
| 13 | 1607.4 | 300 | 1307.4 |
| 14 | 1597.4 | 300 | 1297.4 |
| 15 | 1584.1 | 300 | 1284.1 |
| 16 | 1469.7 | 300 | 1169.7 |
| 17 | 282.3 | 300 | -17.7 |
| 18 | 330.3 | 300 | 30.3 |
| 19 | 58.3 | 150 | -91.7 |

With the analysis, it was understood that out of the thirteen hours analysed, ten had a slight excess of 1 MWh of electrical energy. Moreover, it is highlighted with yellow the hour with highest electricity produced by the PV system, which was approximately 1.3 MWh. It should be noted that, in this analysis, the transportations efficiencies of the electrical energy and the energy consumption and efficiency of auxiliary components of the system were not taken into account, which means that, in absolute value, the excess/deficit of energy. As a result, it is estimated that the electrolyser should have a capacity close to 1 MWh.

Another factor is the adaptability of the electrolyser to the instability of renewable energies. As previous analysed, the PEM electrolysers have the most dynamic operation

capacities, and therefore are the best option for this application. Based on the selected capacity and type of the electrolyser for the model, a survey was conducted among the several manufacturers. Despite there being more than one electrolyser presented in the studies conducted, the electrolyser used in the main analysis is the ME 450/1400 from H-TEC Systems. Further information about this device is summarized in Table 17. In Figure 56 is represented the core elements of this electrolyser.

Table 17 – Technical information of electrolyser ME 450/1400 from H-TEC Systems

| Technical Parameter | Value |
|--------------------------------------|--------------------------------------|
| H ₂ nominal production * | 210 Nm ³ /h (450 kg/day) |
| H ₂ production range | 42 – 210 Nm ³ /h |
| H ₂ purity | 99.998 % |
| Nominal energy consumption | 4.7 kWh/ Nm ³ (53 kWh/kg) |
| Nominal load | 1 MW |
| Nominal system efficiency | 75% |
| Operating pressure of H ₂ | 20-30 bar |
| Water supply | 260 kg/h |

* It should be noted that the information is defined based on standard conditions (STP).

As the volume production varies with temperature and pressure conditions, it is considered that the mass of hydrogen does not change with these conditions. Therefore, the hourly calculations will be based on the mass of hydrogen rather than its volume. However, for the accurate sizing of the system, it is essential to be aware of the hourly hydrogen volume production, as some component manufacturers only specify the capacity of the components in volume. Furthermore, based on the analysis of Table 17, it can be concluded that the maximum hourly nominal hydrogen mass production is 18.75 kg. Therefore, using equation (21), the maximum nominal hydrogen volume production at 30 bar and 65 °C, which is the hydrogen outlet conditions of the electrolyser, can be calculated. The calculation relies on the density of hydrogen (ρ), which is equal to 2.104 kg/m³ in the previously stated conditions and the mass of the produced hydrogen (m_{H_2}), which is equal to 18.75 kg/h. The result is 8.91 m³/h.

$$V = \frac{m}{\rho} \tag{21}$$

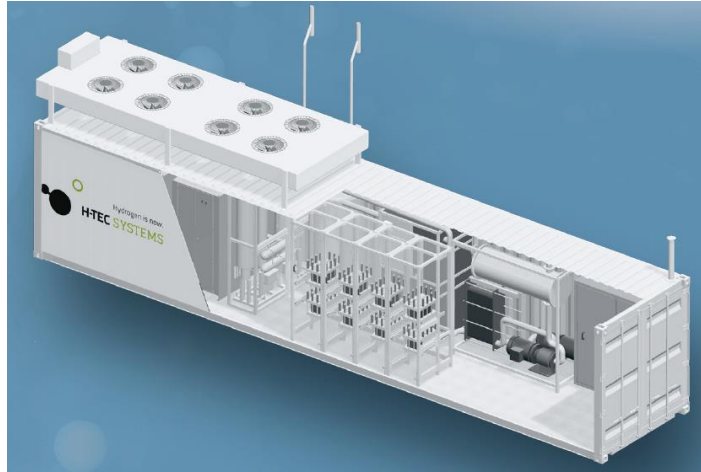


Figure 56 – Representation of the core elements of the electrolyser ME 450/1400 from H-TEC systems.

4.4.3 Compressor

The compressor is a fundamental part of this model, allowing the seasonal storage of renewable energy. In the thermodynamic model, the produced hydrogen comes out the electrolyser at 30 bar. Thus, it was considered the hydrogen compression of up to 250 bar.

When deciding which compressor type to be used, several factors were evaluated. Firstly, it is important to prevent, as much as possible, the contamination of hydrogen because a high level of hydrogen purity is required. As a result, an oil-free compressor was a priority choice. Secondly, it is necessary to consider the inherent intermittency of the PV power plant, so, the compressor must be adaptable for an intermittent operation. Therefore, as previously stated, the dry running piston reciprocated compressor is the best suitable option for this kind of application.

The complete sealing of hydrogen is crucial, given its flammable and explosive properties. Thus, it is of utmost importance to ensure compressor complete sealing. Piston compressor has a potential drawback in terms of gas leaks, because as the piston directly contacts with the gas being compressed, deterioration or imperfect seals can lead to gas leakage. Thus, dry piston reciprocated compressor is not considered as a viable solution. Conversely, the diaphragm compressor separates the gas from the drive mechanism, creating a completely sealed system, reducing the risk of gas leakage and potential hazards. Ergo, this type of compressor is the mostly used in the hydrogen application.

Besides, another important parameter is the compressor capacity. Thus, it was necessary to consider the fact that this component is dependent on the electrolyser's output. Since it is extremely difficult to perfectly match the optimal operating point of each device

over time, one of them has to be oversized. In this case, the equipment chosen to have an exceeded capacity is the compressor because all the hydrogen generated must be compressed before its storage.

Therefore, there is no point in having the electrolyser produce more hydrogen than the compressor can compress. Conversely, if the compressor is oversized all the hydrogen produced can be compressed and stored. Accordingly, the compressor selected to incorporate into the model is a diaphragm reciprocated oil-free compressor constructed by Minnuo Group, which is represented in Figure 57. Technical information about the selected compressor can be observed in Table 18.



Figure 57 - Representation of the chosen hydrogen diaphragm compressor option from the Minnuo Group.

Table 18 - Technical characteristics of the compressor provided by Shanghai Sollant

| Technical Parameter | Value |
|---------------------------|------------------------|
| Type of compressor | Diaphragm Compressor |
| Model | GD134-212/30-250 type |
| Inlet temperature | 25 °C |
| Inlet pressure | 30 bar |
| Outlet pressure | 250 bar |
| Maximum inlet flow | 212 Nm ³ /h |
| Nominal power consumption | 37 kWh |
| Motor speed | 420 rpm |
| Cooling style | Water cooling |
| Water consumption | 3 m ³ /h |

The hydrogen is compressed up to 250 bar and subsequently cooled to a temperature of 15 °C, resulting in a density of 18.131 kg/m³. By using equation (21), it is possible to obtain the maximum hourly mass flow in the conditions that the inlet flow is measured, 20°C and 1 bar. The result is 20.75 kg. It is noteworthy that the hydrogen mass is considered to remain

unchanged with the temperature and pressure. Therefore, it is assumed that all the produced hydrogen can be correctly stored. The maximum flow allowed in the compressor inlet can be calculated, which is 30 bar and 25 °C. The result is 8.722 m³, considering the hydrogen density as 2.379 kg/m³.

Regarding energy consumption, the mass of hydrogen compressed per hour is taken into account, being independent of the hydrogen's specific conditions. Thus, the maximum compression energy is determined by dividing the maximum hydrogen produced by the electrolyser and the compression energy consumed when compressing the same quantity of hydrogen. As data regarding compressor energy consumption as a function of the hydrogen mass was unavailable, the nominal consumption value was considered, as 0.506 kg/kWh.

4.4.4 Hydrogen storage

Regarding hydrogen storage, the selected method was to compress hydrogen gas, until it achieves a satisfactory energy density, which is required to its storage. This pathway was chosen due to the higher technology maturity and lower cost. Underground storage is not available in all locations worldwide and their access proves to be difficult. Therefore, it is not considered as a storage solution to be implemented in the model. The liquid storage consumes more energy than the compression storage, which constitutes a crucial factor for the selection of hydrogen gas storage.

Additionally, the model does not include transportation and, as a result, the storage is stationary and not couple with distribution. Given that liquid hydrogen attains higher levels of energy density, which is more relevant for transportation than for stationary storage, there are no advantages in selecting liquid storage from this perspective.

As previously stated, the cylindrical vessels are the common way to store hydrogen in gas state. This was the type of tank chosen to perform the seasonal storage of hydrogen in the model. After a meticulous market research, the manufacturers advised, based on the characteristics presented by the model, that the stationary storage should be organized in groups of three cylinders. In Figure 58 it can be observed the tube vessels with a complete manifold that are considered in the present work.



Figure 58 - Representation of the chosen hydrogen storage option from the Honghua (Shandong) Steel Group.

Further technical information can be analysed in Table 19. It should be noted that in Annex 2 is presented the technical data sheet provided by Honghua (Shandong) Steel Group, the manufacturer of the selected storage technology. At a pressure of 250 bar and a temperature of 15 °C, the hydrogen is stored in the tube vessels until is needed to produce electricity, or when it is sold as a commercial product.

Table 19 – Technical characteristics the selected storage tank

| Technical Parameter | Value |
|-----------------------------|-------------------------------------|
| Operation temperature | 15 °C |
| Operation pressure | 250 bar |
| Tube quantity | 51 |
| Total volume | 2.210 m ³ per tank |
| Hydrogen filling weight * | 40.07 kg of H ₂ per tank |
| Total installation capacity | 2,043.57 kg of H ₂ |

*At operating pressure and temperature.

4.4.5 Fuel cell

In terms of hydrogen end use, there are two possible applications. The first involves selling the stored hydrogen, assuming the buyer is responsible for transportation (the transportation stage will not be considered in this model).

The second possibility is to use the stored hydrogen in a fuel cell to generate electrical power. In this case, another component must be considered, which is the fuel cell. As previously analysed, there is a wide range of fuel cell types. For this study, the PureCell Model 400 was considered. The technical information about this device is presented in Table 20.

Table 20 – Technical information of the utilised fuel cell provided from Doosan

| Technical Parameter | Value |
|---------------------|-------------------------------------|
| Output power | 440 kW |
| Output water | 0.03 – 0.13 m ³ /h |
| Water temperature | 120 °C |
| Total efficiency | 85 % (49% electricity and 36% heat) |

Given this information it is possible to apply the equation (18) to obtain the fuel cell output power per kilogram of hydrogen consumed. With a HHV of 39.41 kWh/kg and an electrical efficiency (η_{FC}) of 0.49, the required inlet mass flow to achieve an energy output of 440 kWh is 22.79 kg/h. Consequently, the energy output per kilogram of hydrogen input is 19.31 kWh/kg, considering that the fuel cell is operating at maximum capacity.

4.4.6 Battery

Regarding the battery, this component has the role of storing part of the excess of the PV energy, in order to fulfil the energy needs of the electrolyser and compressor, if necessary. The chosen battery (Figure 59) has a storage capacity of 200 kWh and it is provided by Hebei Ecube New Energy Technology manufacturer.



Figure 59 – Illustration of a battery GRES-225-100.

4.4.7 Hydrogen flow parametrization

In summary, Figure 60 presents a comprehensive depiction of hydrogen flow, with numbered references indicating the conditions to which hydrogen is subjected along its path.

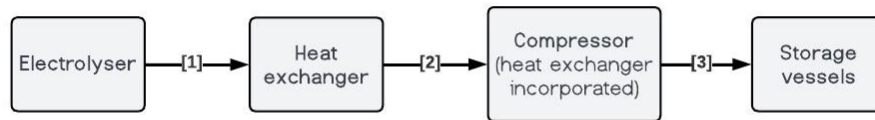


Figure 60 – General representation of the hydrogen flow.

The corresponding information for numbers [1] to [3] is provided in Table 21. It should be noted that the standard conditions represent the specific set of conditions that were employed by the manufacturers for calculating the inlet flows. These conditions serve as a reference point to ensure consistent and accurate calculations.

Table 21 - Representation of hydrogen of mass and volume flow at different conditions

| Conditions | Hydrogen density, ρ [kg/m ³] | Maximum hourly volume of hydrogen [m ³] | Maximum hourly mass of hydrogen [kg] |
|--|--|---|--|
| (Standard compressor) - 1 bar and 20 °C | 0.083 | 225.9 | 18.75 |
| (Standard electrolyser) - 1 bar and 0 °C | 0.089 | 210.7 | 18.75 |
| [1] - 30 bar and 65 °C | 2.104 | 8.911 | 18.75 |
| [2] - 30 bar and 25 °C | 2.379 | 7.881 | 18.75 |
| [3] - 250 bar and 15 °C | 18.13 | 1.034 | 18.75 |

4.5 Mathematical modelling

In order to analyse the behaviour of the system from a thermodynamic perspective, all the components were modelled in MATLAB®. In this section, the mathematical formulation that supports the model is presented as well as the interrelationships and decision-making processes are explained.

Figure 61 identifies the distribution of the generated electricity from the PV power plant. The industry holds the highest priority, while selling electricity to the grid is the least priority.

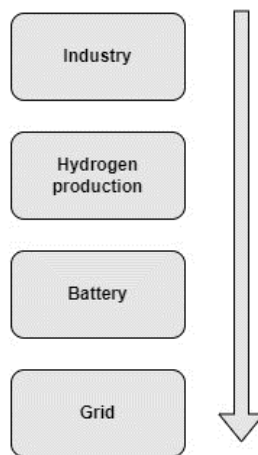


Figure 61 – Illustration of the order of importance regarding the energy application.

4.5.1 Energy pathway efficiency

The network depicted in Figure 52 illustrates the different pathways through which electricity energy may be used. The transmission of energy is intrinsically associated to energy losses, which can be characterized by efficiencies. Firstly, these routes encompass components that are required for regulating energy conditions, each possessing inherent efficiency coefficients. Secondly, the connection of these components is made by cables that inevitably result in the dissipation of energy. Consequently, based on the intended energy destination, distinct efficiencies serve as quantifiable indicators of the corresponding energy losses sustained across these diverse pathways.

Table 22 presents all the potential pathways that electricity can follow from the PV panels to terminal components. Terminal components refer to the final destinations of the electricity, such as the electrolyser, where the electrical energy is converted into hydrogen. In this context, each column corresponds to a distinct route, while each row represents an

efficiency applicable to that route. The final energy efficiency of every single route is defined by the product of the lines highlighted with an “x”. For example, the route connecting the PV power plant to the grid is determined by multiplication of all the represented efficiencies.

It is important to emphasize that the coefficients presented exclusively take into account the energy losses along the route. The calculations do not integrate the end components and the respective auxiliary equipment.

Table 22 – Efficiencies of photovoltaic power plant to components

| | | $\eta_{PV,grid}$ | $\eta_{PV,ele}$ | $\eta_{PV,comp}$ | $\eta_{PV,ind}$ | Value |
|---------------------------|------------------------|------------------|-----------------|------------------|-----------------|-------|
| Solar field | η DC cable | x | x | x | x | 0.992 |
| | η DC/DC converter | x | x | x | x | 0.980 |
| Power Station | η Inverter | x | | x | x | 0.984 |
| | η AC cable | x | | x | x | 1.0 |
| | η Transformer | x | | | | 0.980 |
| Total efficiencies values | | 0.937 | 0.972 | 0.956 | 0.956 | |

In Table 23, the efficiencies of routes that start from the grid and end in diverse components are depicted.

Table 23 - Efficiencies of grid to components

| | | $\eta_{Grid,ind}$ | $\eta_{Grid,ele}$ | $\eta_{Grid,comp}$ | $\eta_{Grid,fc}$ | Value |
|---------------------------|------------------------|-------------------|-------------------|--------------------|------------------|-------|
| Solar field | η DC cable | | x | | | 0.992 |
| | η DC/DC converter | | | | | 0.98 |
| Power Station | η Inverter | | x | | | 0.984 |
| | η AC cable | x | x | x | x | 1 |
| | η Transformer | x | x | x | x | 0.991 |
| Total efficiencies values | | 0.99 | 0.967 | 0.99 | 0.991 | |

4.5.2 Electrolyser state

As previously mentioned, the electrolyser device has three states, idle, standby and production state. Since the electrolyser plays a crucial role in this model, it is imperative to define its state, S_{ele} , in every hour, i , of the study.

In order to correctly consider the stages of operation, it is necessary to verify if the PV panels produce electricity, which is defined by E_{PV} . If the condition verifies, it is considered that the hour i is an hour with enough solar availability to activate the PV production, which is defined by $D^{(i)}=1$. This can be attained by the equation (22).

$$D^{(i)} = \begin{cases} 1, & E_{PV}^{(i)} > 0 \\ 0, & \text{Otherwise} \end{cases} \quad (22)$$

Next, it is necessary to understand if the electricity produced is sufficient to supply the industry needs, E_{ind} , because when there is an excess of energy, it is directed towards the electrolyser. As illustrated in Figure 61, the hydrogen production is second most important path.

For this purpose, equation (23), which gives the excess of energy (E_{xs}), is solved for each hour, i . If the result is a negative number, the PV power plant cannot satisfy the industry requirements in the hour i . If the result is higher than zero, there is an excess of energy that needs to be distributed. It also worth mentioning that if there is an excess of energy, there is obligatory energy production from the PV panels, which means $D^{(i)}=1$.

$$pc E_{xs}^{(i)} = pc E_{prod}^{(i)} - pc E_{ind}^{(i)} \quad (23)$$

Furthermore, another important factor is the state of the device in the previous hour, $S_{ele}^{(i-1)}$. All the aforementioned factors affect the definition of the electrolyser state in each hour of the study. The following systems of equations demonstrate how these variables determine the electrolyser's operational state. It is analysed the case in which the electrolyser remained in an idle state during the preceding hour, denoted as $S_{ele}^{(i-1)} = 0$.

$$S_{ele}^{(i)} = \begin{cases} 2, & E_{xs}^{(i)} > crit E_{ele}^{idl,prod} \\ 0, & \text{Otherwise} \end{cases} \quad (24)$$

As shown in equation (24), the only possible transition is from the idle state to the production mode. This occurs when the excess of energy surpasses the threshold defined by

the criteria defined for the transition, $_{crit}E_{ele}^{idl,prod}$. Additionally, it should be noted that transitioning from an idle state to a standby state is not logical, even if the energy required for this transition is available. This is because the electrolyser does not produce in either of these states but consumes more energy when in standby mode rather than when in idle mode. The second case reflects the context where the electrolyser stayed in a standby state during the previous hour, $S_{ele}^{(i-1)} = 1$.

$$S_{ele}^{(i)} = \begin{cases} 0, & D^{(i)} = 0 \\ 1, & E_{xs}^{(i)} < {}_{crit}E_{ele}^{sby,prod} \wedge D^{(i)} = 1 \\ 2, & E_{xs}^{(i)} > {}_{crit}E_{ele}^{sby,prod} \end{cases} \quad (25)$$

Analysing equation (25), it can be understood that from the standby state, the electrolyser can transition to the other two possible modes. If the radiation is not sufficient for the PV panels to produce electricity, the electrolyser shifts into the idle mode. If the irradiance is sufficient for the PV panels to generate electricity but the excess of energy does not exceed the criteria defined for the transition from standby to production, the electrolyser remains in standby state. Conversely, if the excess of energy surpasses this threshold, the electrolyser shifts to the production mode. The last scenario consists in electrolyser being in production mode in the preceding hour, $S_{ele}^{(i-1)} = 2$.

$$S_{ele}(i) = \begin{cases} 0, & D^{(i)} = 0 \\ 1, & E_{xs}^{(i)} < {}_{crit}E_{ele}^{maint,prod} \wedge D^{(i)} = 1 \\ 2, & E_{xs}^{(i)} > {}_{crit}E_{ele}^{maint,prod} \end{cases} \quad (26)$$

Equation (26) follows the same reasoning as previously presented. If the power plant does not produce energy in hour i , the electrolyser shifts to the idle state.

When the power plant is operational, two possibilities arise. Firstly, if the excess of energy is insufficient to sustain the electrolyser in production mode, it transitions to standby mode. The second case refers to the maintenance of the electrolyser in the production state, because the excess of energy is sufficient to satisfy the criteria of maintenance.

4.5.3 Transition criteria

The electrolyser state depends on the energy available to its own supply, and its outline by the transition criteria. These thresholds are defined by a specific quantity of

energy, which may or may not be attained on an hourly basis. There are three criteria, whereas, the first one is the necessary energy that an electrolyser must receive to transit from an idle state to production mode is defined. This is represented in equation (27).

$${}_{crit}E_{ele}^{idl,prod} = {}_{pr}E_{ele}^{min} + E_{ele}^{cs} \quad (27)$$

The term ${}_{pr}E_{ele}^{min}$ stands for the minimum energy required by the electrolyser to produce hydrogen. As for E_{ele}^{cs} , represents the energy consumed by the electrolyser during the transition from idle to production conditions, primarily influenced by factors such as temperature and pressure of the device.

Regarding the transition from a standby to a production state, it is aligned with the process presented in the aforementioned criteria, as can be seen in equation (28). In this case, the energy consumed to change the electrolyser conditions (from standby to production mode), E_{ele}^{hs} , is lower, as the temperature and pressure characteristic of the standby state are higher than those in idle mode.

$${}_{crit}E_{ele}^{sby,prod} = {}_{pr}E_{ele}^{min} + E_{ele}^{hs} \quad (28)$$

Lastly, it is presented, in equation (29), the criteria that is necessary to sustain the electrolyser in the production state. It is essential to emphasize, that in this scenario, the electrolyser is already in the specific temperature and pressure conditions to perform the production of hydrogen.

$${}_{crit}E_{ele}^{maint,prod} = {}_{pr}E_{ele}^{min} \quad (29)$$

As explained in the literature review, the systematic transition of the electrolyser from an idle state to a production mode (cold start) can promote the degradation of the device. Therefore, it is important to register the number of cold starts that occur in the study conditions. This is record as the variable Ct_{cs} .

4.5.4 Energy distribution

Subsequent to the delineation of the electrolyser states, it is imperative to have a complete characterization of the energy distribution system. As can be easily understood, this allocation highly depends on the quantity of electricity produced by the powerplant.

In this context, a control point (pc) is defined, which enables the model to assess the available energy at a specific location of the installation, as can be observed in Figure 62. Additionally, an equipment point (eq) is identified, signifying the point at which energy is introduced into the device.

This point exclusively receives the energy destined to power the electrolyser itself, excluding its associated accessories. Thus, by considering energy transport efficiencies and the auxiliary accessory consumptions, it becomes possible to determine the precise amount of energy at both the control point and the entrance of each equipment. This allows the correct comparison and distribution of energy throughout the system.

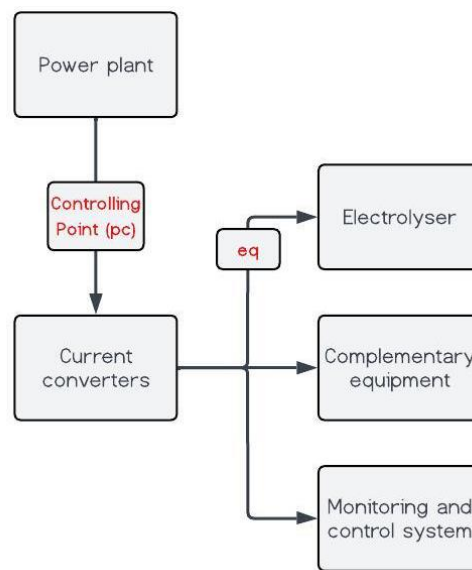


Figure 62 – Representation of the energy measurement points of the electrolyser device.

In the equation (30), is exemplified the relationship between the energy dedicated to the electrolyser measured at the controlling point (pc), and at the equipment point (eq). It is also noteworthy to mention that there is one more point of energy measurement, the grid point (gp), which is the assumed entry point for grid energy into the model.

$${}^{pc}E_{DH_2} = \frac{{}^{eq}E_{DH_2}}{\eta_{PV,ele} \cdot \eta_{ele,aux}} \quad (30)$$

Electrolyser at production state

If the electrolyser at a certain hour is in a condition to be in a production state, there are some conditions that need to be verified in order to correctly conduct the energy

allocation throughout the system. Through equation (31), the energy that can be conducted to the electrolyser is calculated, following the order of importance regarding the energy application represented in Figure 61.

$${}^{eq}E_{ele}^{(i)} = {}^{pc}E_{xs}^{(i)} \cdot \eta_{PV,ele} \cdot \eta_{ele,aux} \quad (31)$$

After that, the lower and upper energy limit of the electrolyser must be well defined in the model. Therefore, it is important to verify if the energy that could potentially be allocated to hydrogen production falls within the limits defined by the lower and the upper energy thresholds of the device. In the case of surpassing the lower limit and not exceeding the upper limit, all potential dedicated energy to hydrogen production is utilised in the hydrogen facilities. Conversely, if the energy potential dedicated to the production transcends the upper limit, only the energy corresponding to the upper limit can be used for production.

In the event that the available energy does not meet or exceed the lower energy limit, the electrolyser will not remain in the production state during hour i . These possible situations are expressed in equation (32). It should be noted that, the energy dedicated to the hydrogen production facilities is denoted as ${}^{eq}E_{DH_2}^{(i)}$.

$${}^{eq}E_{DH_2}^{(i)} = \begin{cases} {}^{eq}E_{ele}^{(i)}, & {}^{pr}E_{ele}^{min} \leq {}^{eq}E_{ele}^{(i)} \leq {}^{pr}E_{ele}^{max} \\ {}^{pr}E_{ele}^{max}, & {}^{pr}E_{ele}^{min} < {}^{eq}E_{ele}^{(i)} \\ 0, & \text{Otherwise} \end{cases} \quad (32)$$

The second step is based on the calculation of the mass of hydrogen that can be produced with the energy that is dedicated to the hydrogen production facilities. This is attained by solving the system of equations (33). Firstly, it is presented the load ratio of energy that is dedicated to the hydrogen production facilities and the maximum energy that can be absorbed by the electrolyser. The second equation represents an approximate expression for the electrolyser efficiency based on the load ratio (Lr) during hour i . This expression was obtained by comparing efficiency data curves from theoretical literature of electrolysers with the nominal efficiency provided by the manufacturer of the chosen component, which can be analysed in Table 17. Finally, the third equation calculates the potential hydrogen production mass, ${}^{pr}m_{H_2}^{(i)}$. It considers the high heating value, the previously mentioned electrolyser efficiency, and the energy available for the device, ${}^{eq}E_{DH_2}^{(i)}$.

$$\left\{ \begin{array}{l} Lr^{(i)} = \frac{eqE_{DH_2}^{(i)}}{prE_{ele}^{max}} \\ \eta_{ele}^{(i)} = -0.1537 \cdot e^{3.4302 \cdot Lr^{(i)}} + 78.5826 \cdot e^{0.0274 \cdot Lr^{(i)}} \\ pm_{H_2}^{(i)} = \frac{\eta_{ele}^{(i)} \cdot eqE_{DH_2}^{(i)}}{HHV_{H_2}} \end{array} \right. \quad (33)$$

As already mentioned, there is no point of producing hydrogen if it cannot be stored. Therefore, the final requirement that needs to be checked is the tank capacity. In the beginning of each hour, the storage capacity ($cp_{st}m_{H_2}$) is obtained by the subtraction of the total storage capacity ($cp_{tk}m_{H_2}$) with the storage occupancy in the beginning (defined by index s) of the hour i , $sm_{H_2}^{(i)}$. This calculation is represented in equation (34).

$$cp_{st}m_{H_2}^{(i)} = cp_{tk}m_{H_2} - sm_{H_2}^{(i)} \quad (34)$$

If the storage capacity exceeds the amount of hydrogen that can be produced ($pm_{H_2}^{(i)}$), with energy dedicated to the hydrogen production ($eqE_{DH_2}^{(i)}$), all this available electricity will be used to generate hydrogen. If there is an absence of space in the tanks, only the hydrogen corresponding to the remaining storage capacity can be produced. Therefore, the hydrogen produced is defined as $m_{H_2}^{(i)}$. This is expressed in equation (35).

$$m_{H_2}^{(i)} = \begin{cases} pm_{H_2}^{(i)}, & cp_{st}m_{H_2}^{(i)} \geq pm_{H_2}^{(i)} \\ cp_{st}m_{H_2}^{(i)}, & \text{Otherwise} \end{cases} \quad (35)$$

In the case of the storage capacity being lower than the hydrogen that can be produced ($pm_{H_2}^{(i)}$) a minor quantity of energy is allocated to the hydrogen production facilities. As a result, the load ratio of the hour i , will not be the same as in the previous calculation. Therefore, the electrolyser efficiency must be recalculated according to the systems of equations (36). The unknown variables that must be updated are: the load ratio, the electrolyser efficiency and the energy dedicated to hydrogen production. In fact, as previously mentioned, the mass of hydrogen produced is defined by the storage capacity.

$$\left\{ \begin{array}{l} Lr^{(i)} = \frac{eqE_{DH_2}^{(i)}}{prE_{ele}^{max}} \\ \eta_{ele}^{(i)} = -0.1537 \cdot e^{3.4302 \cdot Lr^{(i)}} + 78.5826 \cdot e^{0.0274 \cdot Lr^{(i)}} \\ eqE_{DH_2}^{(i)} = \frac{HHV_{H_2} \cdot m_{H_2}^{(i)}}{\eta_{ele}^{(i)}} \end{array} \right. \quad (36)$$

To ensure proper control of the hourly storage tank capacity, it is required the application of equation (37). This expression represents the sum of the hydrogen stored in the beginning of the hour with the hydrogen that is produced and stored in same hour, with the subtraction of the hydrogen consumed by the fuel cell device ($fc m_{H_2}^{(i)}$), obtaining the total hydrogen stored in the tanks at the end of each hour, $st m_{H_2}^{(i)}$. It should be noted that the hydrogen stored in the tanks at the end of each hour ($st m_{H_2}^{(i)}$) is equal to the storage occupancy in the beginning of the next hour, $st m_{H_2}^{(i+1)}$

$$st m_{H_2}^{(i)} = st m_{H_2}^{(i)} + m_{H_2}^{(i)} - fc m_{H_2}^{(i)} \quad (37)$$

On the one hand, as it was seen before, the energy that is potentially dedicated to hydrogen production can surpass the electrolyser upper power threshold. On the other hand, it is also possible that the excess energy is not enough to activate the production mode of the electrolyser. In both cases the total, or a part of the excess energy cannot be absorbed by the hydrogen facilities. Therefore, this energy, that cannot be absorbed by the electrolyser, is defined as the potential energy that can be used to charge the battery, $pE_{bat}^{(i)}$. This can be justified due to the next destination of the energy, after the electrolyser, being the battery, as noticeable by the observation of Figure 61. These conditions are depicted in expression (38).

$$pE_{bat}^{(i)} = \begin{cases} > 0, & pcE_{xs}^{(i)} - pcE_{DH_2}^{(i)} > 0 \\ 0, & Otherwise \end{cases} \quad (38)$$

The same logic, that was used at the hydrogen production facilities, is now applied to the battery charging process. Firstly, it is calculated the potential energy that can be used to charge the battery, $pE_{bat}^{(i)}$. It is obtained the energy that was produced by the PV panels and was neither absorbed by the industry and hydrogen production facilities, as it can be analysed in equation (39).

$${}^pE_{bat}^{(i)} = {}^pcE_{xs}^{(i)} - {}^pcE_{DH_2}^{(i)} \quad (39)$$

For the calculation of the actual energy supplied to the battery, the device remaining capacity (${}^{cp}E_{bat}^{(i)}$) must be verified. Therefore, the same reasoning that was applied in the hydrogen storage tanks is used in this case, as can be seen in equation (40).

$$E_{bat}^{(i)} = \begin{cases} {}^pE_{bat}^{(i)}, & {}^{cp}E_{bat}^{(i)} > {}^pE_{bat}^{(i)} \\ {}^{cp}E_{bat}^{(i)}, & \text{Otherwise} \end{cases} \quad (40)$$

Based on the equation (40), there is a possibility in which the battery cannot absorb all the exceeding energy that was not consumed by the hydrogen production facilities. Hence, the surplus electricity is forwarded to its final use.

The last use of the PV energy is its sale to the electrical grid, as in concordance to Figure 61. In other words, when the battery does not have more storage capacity and it still exceeds energy from the power plant, it is forwarded to the grid. Equation (41) presents the calculation of the energy that can be injected into the grid. If the final result is zero, there won't be any energy sold to the grid in hour i .

$$E_G^{(i)} = {}^pcE_{xs}^{(i)} - {}^{eq}E_{DH_2}^{(i)} - E_{bat}^{(i)} \quad (41)$$

Additionally, the model must consider the energy demand during hydrogen compression process. The calculation of the energy required to compress the produced hydrogen in hour i (${}^{pc}E_{comp}^{(i)}$) is expressed in equation (42).

$${}^{pc}E_{comp}^{(i)} = \frac{(m_{H_2}^{(i)} \cdot consE_{comp})}{\eta_{PV,comp} \cdot \eta_{comp,aux}} \quad (42)$$

This demand can be met either by utilizing the energy stored in the battery or by procuring electricity from the grid. The parameters governing this energy supply are represented in equation (43) and equation (44).

The model is programmed to verify if the battery has a sufficient stored energy reserve to power the device. On the one hand, if there is sufficient energy stored in the battery, defined by ${}^sE_{bat}^{(i)}$, it is used to fulfil the compressor needs. On the other hand, if there is not enough energy, it is necessary to buy it from the grid, as it is expressed in equation (44).

$$E_{bat,comp}^{(i)} = \begin{cases} {}^{pc}E_{comp}^{(i)}, & {}^sE_{bat}^{(i)} > {}^{pc}E_{comp}^{(i)} \\ {}^sE_{bat}^{(i)}, & \text{Otherwise} \end{cases} \quad (43)$$

The battery will never simultaneously supply energy to both the electrolyser and the compressor. When the battery powers the compressor, the electrolyser is supplied with energy from PV sources. Conversely, when the battery's energy is allocated to the electrolyser, the compressor is deactivated due to the absence of hydrogen for compression. Thus, it is avoided the battery does not became overloaded.

$$E_{G,comp}^{(i)} = \begin{cases} 0, & stE_{bat}^{(i)} > pcE_{comp}^{(i)} \\ pcE_{comp}^{(i)} - E_{bat,comp}^{(i)}, & Otherwise \end{cases} \quad (44)$$

To conclude, the total energy that is applied to the hydrogen facilities is denoted as $E_{Hf}^{(i)}$, as shown in Equation (45).

$$E_{Hf}^{(i)} = pcE_{DH_2}^{(i)} + pcE_{comp}^{(i)} \quad (45)$$

Electrolyser at idle or standby state

In the case of the electrolyser being in standby or idle state, the consumption of the device is 0.025 and 0.005%, respectively, of the maximum power that can be consumed in the production mode. There is a scenario, where the excess of energy is not being sufficient to fulfil the consumption of the electrolysis device. When this happens, the system is programmed to solve this problem. According to Figure 63 the model prioritizes the supply of electrical energy for the electrolyser from the battery and only buy energy from the grid if there is no energy stored in the battery.

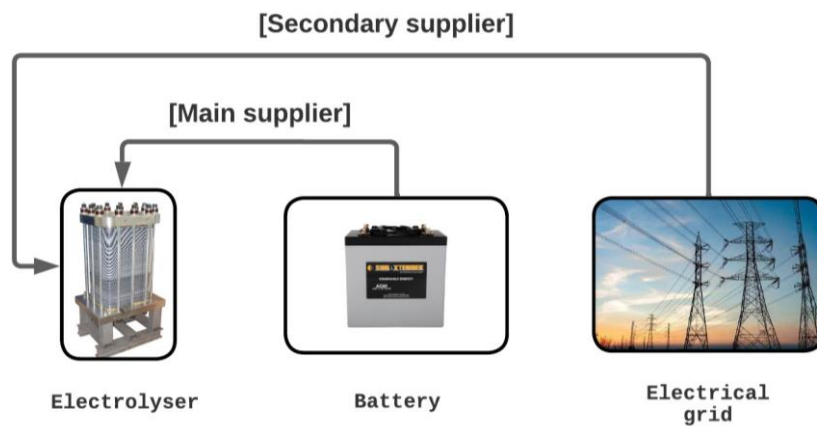


Figure 63 – Electrolyser energy supply when the PV power plant cannot meet the energy demand.

The lack of energy, $pcE_{ele}^{(i)}$, imposed by the electrolyser demand is calculated according to equation (46).

$${}^{pc}E_{L,ele}^{(i)} = \frac{{}^{cons}E_{ele}^{(i)}}{\eta_{PV,ele}} - {}^{pc}E_{xs}^{(i)} \quad (46)$$

In the system of equations (47), the aforementioned model logic to meet the electrolyser's energy consumption when there is a lack of energy greater than zero is represented.

$$\left\{ \begin{array}{l} E_{bat,ele}^{(i)} = {}^{st}E_{bat}^{(i)} - {}^{pc}E_{L,ele}^{(i)}, \quad {}^{st}E_{bat}^{(i)} > 0 \wedge {}^{st}E_{bat}^{(i)} > {}^{pc}E_{L,ele}^{(i)} \\ E_{bat,ele}^{(i)} = {}^{st}E_{bat}^{(i)}, \quad {}^{st}E_{bat}^{(i)} > 0 \wedge {}^{st}E_{bat}^{(i)} < {}^{pc}E_{L,ele}^{(i)} \\ E_{G,ele}^{(i)} = \frac{{}^{pc}E_{L,ele}^{(i)} - E_{bat,ele}^{(i)}}{\eta_{Grid,ele}}, \quad {}^{st}E_{bat}^{(i)} > 0 \wedge {}^{st}E_{bat}^{(i)} < {}^{pc}E_{L,ele}^{(i)} \\ E_{G,ele}^{(i)} = \frac{{}^{pc}E_{L,ele}^{(i)}}{\eta_{G,ele}}, \quad \text{Otherwise} \end{array} \right. \quad (47)$$

If the energy stored in the battery (${}^{st}E_{bat}^{(i)}$) is sufficient to meet the electrolyser's energy demand that is not fulfilled by the PV power plant (${}^{pc}E_{L,ele}^{(i)}$), no energy is purchased from the grid for the electrolyser. However, if the battery is insufficient to meet the required energy, it is purchased from the grid ($E_{G,ele}^{(i)}$).

It is worth mentioning that the fuel cell is not considered an energy supplier for the electrolyser and compressor for two reasons. Firstly, during the day, the fuel cell must remain available to meet the industry's energy demands in case the PV system is insufficient. Secondly, at night, the electrolyser's energy consumption is very low as the device remains in an idle state. Consequently, it is not expected to be cost-effective to keep the fuel cell device and all its auxiliary equipment operational.

Another important notion is the calculation of the energy that is stored in the battery at each hour of the study. The energy stored at the beginning of the hour (${}^{st}E_{bat}^{(i+1)}$) is represented in the equation (48) and the energy stored at the end (${}^eE_{bat}^{(i)}$) of the hour is explicit in equation (49).

$${}^{st}E_{bat}^{(i+1)} = {}^eE_{bat}^{(i)} \quad (48)$$

$${}^eE_{bat}^{(i)} = {}^sE_{bat}^{(i)} + E_{bat}^{(i)} - E_{bat,comp}^{(i)} - E_{bat,ele}^{(i)} \quad (49)$$

When experiencing reduced or even zero energy production from the PV panels, it is understandable that if the industry is in its operating hours, there will be an energy deficit. To solve this issue, the model is programmed to use hydrogen stored in the tanks, which can be converted into electricity through the fuel cell. Therefore, the requirement for electrical energy is calculated through equation (50).

$${}^pE_{fc}^{(i)} = \left| E_{xs}^{(i)} \right| \quad (50)$$

Additionally, it is important to confirm if the hydrogen stored at hour i can surpass the fuel cell's minimum operational input (${}^{pr}m_{fc}^{min}$) and meet the industry's power demand (${}^pE_{fc}^{(i)}$). If this threshold is reached, the fuel cell can shift into the production mode. It also should be noted that the remaining need from the industry, ${}^pE_{fc}^{(i)}$, has also to be superior to the minimum operational power of the fuel cell. In equation (51) it is represented the conditions regarding the minimum power limit of the fuel cell. It should be noted that the absolute value corresponds to the mass of hydrogen required to meet the industrial facility energy needs by supplying the fuel cell.

$${}^{pr}m_{fc}^{min} < {}^s m_{H_2}^{(i)} \wedge \left| \frac{{}^pE_{fc}^{(i)}}{{}_{out}\dot{E}_{fc}^{(i)}} \right| > {}^{pr}m_{fc}^{min} \quad (51)$$

If the previous stated equation is confirmed, another condition needs to be examined. This involves verifying whether there is enough hydrogen to generate the necessary energy for the industry. If the stored hydrogen is not sufficient, the remaining energy must be purchased from the grid. This can be observed in equation (52).

$$E_{fc}^{(i)} = \begin{cases} {}^pE_{fc}^{(i)}, & {}^{cp}m_{H_2}^{(i)} > \left(\frac{{}^pE_{fc}^{(i)}}{{}_{out}\dot{E}_{fc}^{(i)}} \right) \eta_{fc,ind}^{-1} \\ {}^{cp}m_{H_2}^{(i)} \cdot {}_{out}\dot{E}_{fc}^{(i)}, & \text{Otherwise} \end{cases} \quad (52)$$

In the second possibility, as previously presented, the remaining energy must be bought from the grid, as it is expressed in equation (53).

$$E_{G,ind}^{(i)} = \left| {}^pcE_{xs}^{(i)} \right| - E_{fc}^{(i)} \quad (53)$$

In this specific scenario, if a fuel cell is used, it becomes necessary to provide electrical energy to the auxiliary components of this device. Two potential energy source alternatives are available, a battery and the electrical grid. In the event of a shortage of PV energy to meet the industrial demand, the battery will already be tasked with supplying energy to the electrolyser, which will be in an idle or standby state. In order to prevent overloading of the battery, the chosen electrical source for the fuel cell device is solely the electrical grid. Furthermore, the energy consumption of the fuel cell auxiliary devices is minimal, resulting in a low impact on the overall electricity bill. The calculation of the mandatory energy is defined in relation of its energy efficiency and the output power of the fuel cell, as can be observed in (54).

$$E_{G,ind}^{(i)} = E_{fc}^{(i)}(1 - \eta_{fc,aux}) \quad (54)$$

As previous mentioned, the purchase of electricity from the grid is an available option to supply all the integrant components of the system. Therefore, it is important to well define the power purchase contract, which in Portugal, is divided into three main tariffs that vary with the hourly cycles. The single tariff is based in a constant tariff during all hours of the day. Bi-hourly tariff is based into two moments: off-peak (cheaper tariffs) and on-peak hours (expensive tariffs). Lastly, the tri-hourly tariff, it divides into three periods: off-peak, peak, and full hours. The consumption is cheaper during off-peak hours and more expensive during peak hours.

Since electricity purchasing can occur at any time during the day and not restricted to specific hours, choosing the simple tariff is expected to be cost-effective. The other two options bring a risk of purchasing electricity during a period of high electrical costs.

5. RESULTS AND DISCUSSION

This chapter presents the one-year energy analysis results of the study. The distribution of electrical energy produced by the PV power plant and the system's performance is analysed. Additionally, it reports on the hydrogen production and investigates the feasibility of seasonal hydrogen storage as a means to mitigate the need for grid energy purchases.

Firstly, the study introduces the standard model, corresponding to the modelled system. Subsequently, a sensitivity analysis of selected variables was undertaken to refine the model definition. This process involved incorporating feedback from ongoing results, ensuring logical coherence and aiming for an accurate representation of real-world complexities. The goal is to pursue and develop a comprehensive, realistic, and optimized representation of the case study.

For simplicity, detailed descriptions are provided only for the initial and final models. Regarding sensitivity studies, the focus will be on elucidating the reasons that prompted additional analyses. Furthermore, Table 24 presents a summary of the studies conducted, along with the respective model alterations when compared to the standard model.

Table 24 – Presentation of the designed models and corresponding studies conducted.

| Model | Study | Description of the alterations | |
|---|------------------------|---|---|
| Standard conditions for the reference case | | | |
| Sensitivity analysis | 2 | Decrease of 10% in the electrolyser capacity. | |
| | 3 | Increase of 389.3% in hydrogen storage facility capacity - 250 tanks. | |
| | 4 | Increase of 100% in industry demand – 600 kWh per hour of operation. | |
| | 5 | Combination of the two models presented above. | |
| Improved operating scenario (Final model) | 6 (high demand) | The study lasted for one year, beginning in April; The tanks were designed to hold the maximum hydrogen production capacity. | Industry demand of 600 kWh per hour of operation. |
| | 6 (low demand) | | Industry demand of 400 kWh per hour of operation. |

Furthermore, it is important to emphasize that when it comes to the quantitative energy analysis, it was conducted at the source output level. This means that the values of energies that are dedicated to other components presented in the model, not only take into account the energy supplied to the component, but also consider energy losses during transmission and the energy required to supply the auxiliary devices of the component.

5.1 Reference case simulation

In the following subchapters, the study of the standard model will be presented.

5.1.1 Energy distribution analysis

As illustrated in Figure 64, the critical months for irradiance, characterized by maximum and minimum solar irradiance, are August and December, respectively. Therefore, in the context of analysing the model’s behaviour in extreme scenarios in terms of irradiance, a study was conducted to examine the monthly energy balance and a daily profile analysis for those months. In order to facilitate the presentation of daily results, a single day from each month was selected to serve as a representative sample of the expected behaviour for a day within that particular month.

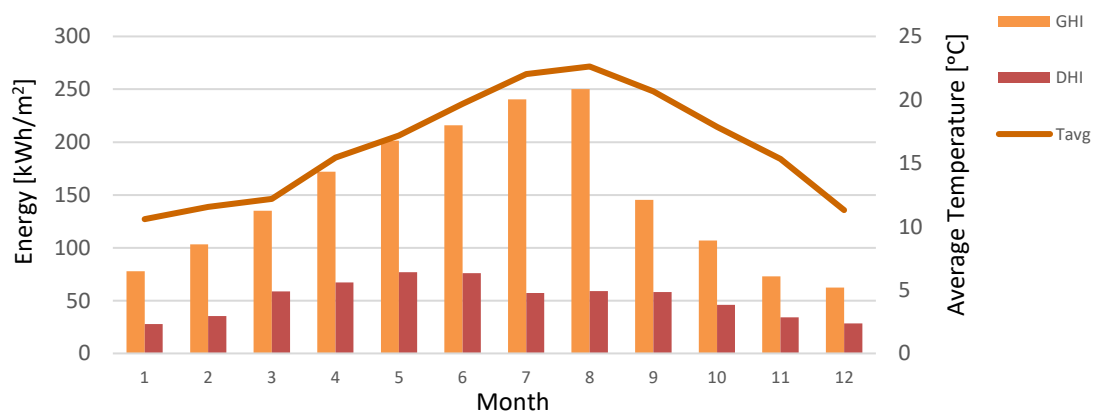


Figure 64 – Meteorological data for the power plant location. GHI stands for global horizontal irradiance, DHI represents the diffuse horizontal irradiance, and Tavg the average of temperature.

5.1.2 Simulation of a daily profile in December

The selected date for analysis was December 16th, chosen because it falls in the middle of the month, thus it is expected to provide a more representative depiction of typical monthly conditions.

First, the daily distribution of PV energy is analysed, which can be allocated to four destinations: industrial usage, hydrogen facilities, battery storage, and the grid, as illustrated in Figure 65.

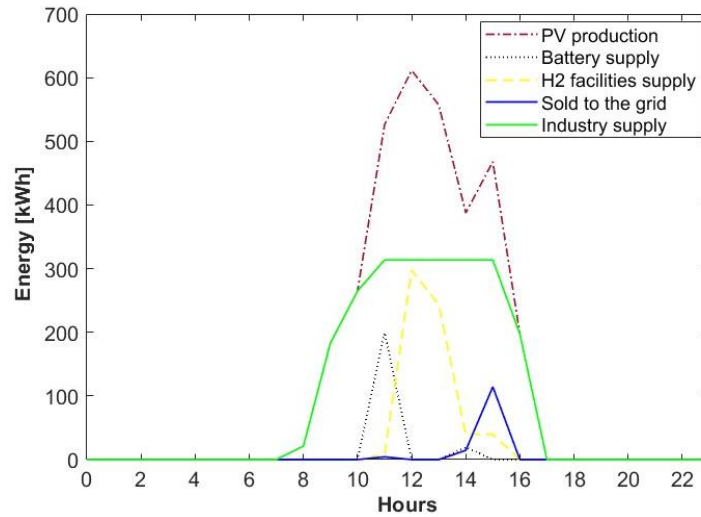


Figure 65 - Daily profile of energy distribution produced by the PV power plant. Data for December 16th.

Regarding the PV production, it starts at 8 AM and ends at 5 PM. The peak occurred at midday, and it is approximately 611.3 kWh. As expected, the primary proportion of energy absorption is attributed to the industrial sector, followed by hydrogen facilities, battery storage, and the grid. However, it is easily understood that only 5 hours of the industry operation were completely supplied by PV.

Furthermore, it is evident that the battery is charged before the hydrogen facilities, contradicting the previously established order of importance of the energy distribution. This arises because at 11 AM, the hour at which the battery was charged, the remaining energy after the industry supply does not surpass the minimum required for the electrolyser to start its operation, which is 205.7 kWh if the pathway efficiency is having into account, in other words, measured in the Control Point. It also should be noted that the battery was charge to its maximum capacity (200 kWh), only in one hour.

Finally, a significant energy injection into the grid was recorded at 3 PM, totalling approximately 114.3 kWh. Additionally, there were injections of 4 kWh and 14 kWh.

To delve deeper into the energy supply within the industrial sector, Figure 66 presents all the sources and illustrates the size of the slice that each of them contributes to the industry's energy supply.

The PV energy does not have the capacity to meet the industry facility energy demands throughout its entire operational timeframe. Consequently, from 7 AM to 11 AM and from 3 PM to 6 PM, the energy supply was complemented with the fuel cell production. The fuel cell was indeed the only supply in the last hours (5 PM to 7 PM) of industrial operations. It should be noted that there was no acquisition of electricity from the grid.

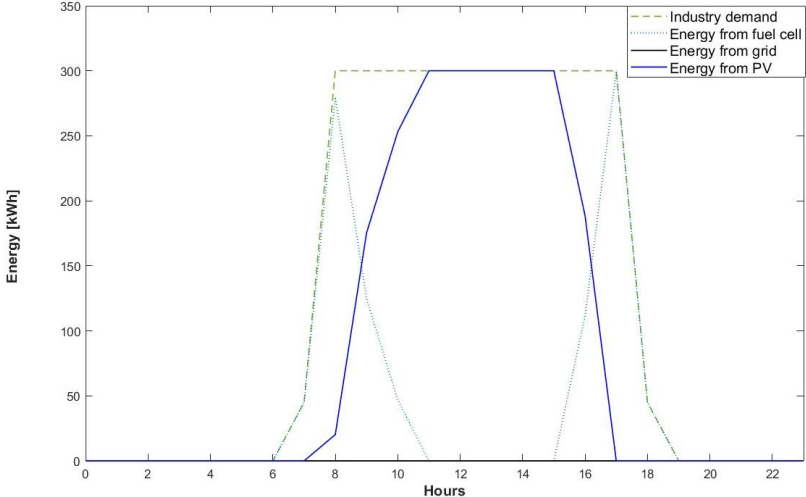


Figure 66 – Illustration of industry demand and its respective energy source supplier. Data for December 16th.

Furthermore, Figure 67 presents the hydrogen inlet, expressed in kilograms, required to supply the fuel cell in order to achieve the energy output represented in Figure 66. It is evident that the second peak in hydrogen supply, with a value of 15.9 kg, corresponds to the timeframe that the fuel cell was the only source of energy of the industry.

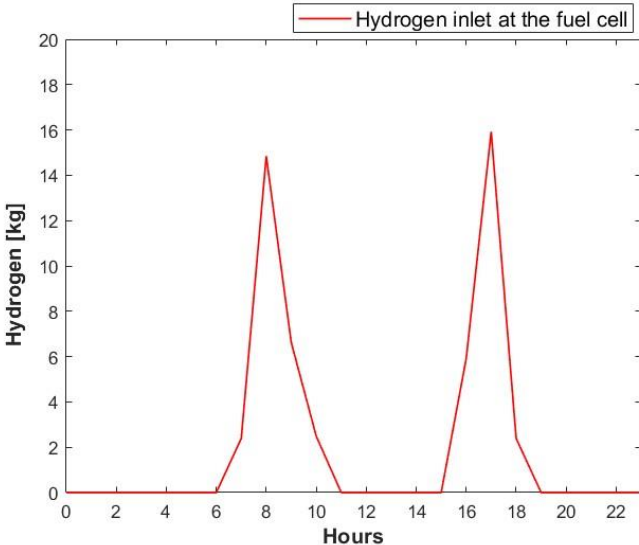


Figure 67 – The hydrogen inlet on the fuel cell device at each hour of the day. Data for December 16th.

In order to initiate fuel cell operation, it is necessary to have an adequate amount of stored hydrogen that exceeds the minimum input fuel requirement of the fuel cell, which is 2.3 kg/h. As it can be observed in Figure 68 a), it is evident that the storage tanks contained enough hydrogen to fulfil the industry's requirements in the absence of PV power.

However, if there were less than 2.3 kg available in the tanks, the line in Figure 66 corresponding to the fuel cell's output energy would remain the same, but it would correspond to energy drawn from the grid instead.

In Figure 68 a) and b) are represented the evolution of the storage tanks occupation in the beginning of each hour and the hourly hydrogen production, respectively.

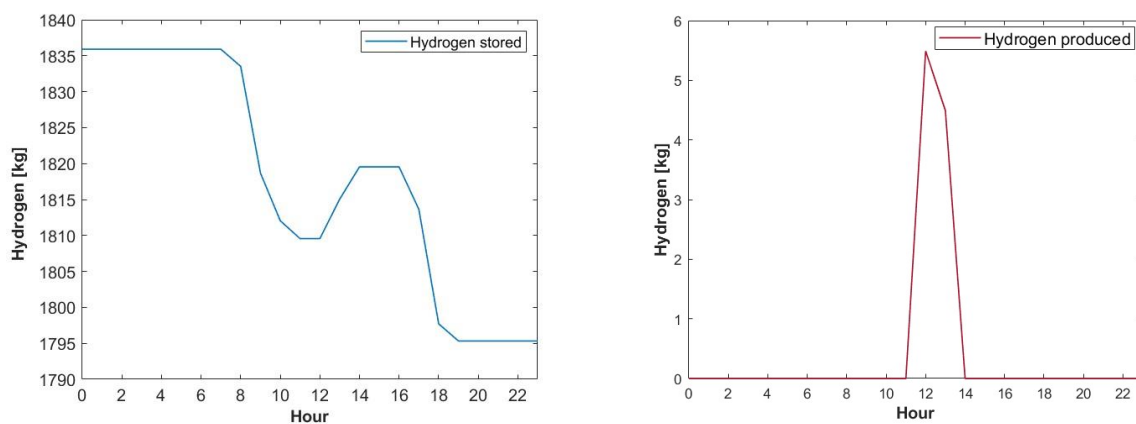


Figure 68 - a) The hydrogen that is stored at the beginning of each hour in the stationary storage tanks. Data for December 16th. b) The electrolyser hydrogen produced each hour.

It was noted a 2.2% reduction in hydrogen storage represented in Figure 68 a). Whereas, in the hydrogen production, it was registered a peak of 5.5 kg, which can be observed in Figure 68 b). To a complete comprehension of these graphs is necessary to have in attention the hydrogen consumption, which was already represented in Figure 67.

In Figure 68 a), there is a decrease in stored hydrogen of 26.3 kg from 7 AM to 11 AM, and a reduction of 24.2 kg from 4 PM to 7 PM. This corresponds to the fuel cell consumption to fulfil the industry demand. From 12PM to 2PM hour it was registered an increase in the hydrogen storage, which corresponds to the hydrogen production presented in Figure 68 b) at 12PM and 1PM, in which were produced 5.5 and 4.5 kg of hydrogen, respectively.

Furthermore, there is a timeframe that the hydrogen storage remains the same from 2PM to 4PM. It was neither hydrogen production nor consumption. As a result, it is possible to conclude that the PV power plant had the capacity to fulfil the industry demand, but not sufficient energy to start the electrolysis process. This can be verified in Figure 65.

It is imperative to note that, it is impossible to have hydrogen production and consumption at the same time. This due to the fact that to occur hydrogen production the energy from the PV power plant has to exceed the sum of industry demand and the minimum power requirement from the electrolyser. Therefore, when the electrolyser is in operating mode, the industry is complete fulfilled with the PV energy, which makes unnecessary the consumption of hydrogen to generate electricity.

Concerning the compressor energy supply, it is presented in Figure 69 all the sources that meet this requirement.

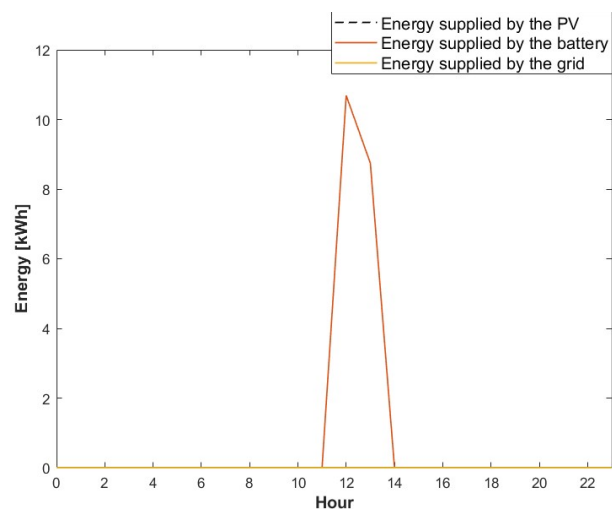


Figure 69 – Representation of the source and its respective amount of energy to meet the compressor's demand. Data for December 16th.

As can be observed, the compressor only requires energy from 12AM to 1PM, which corresponds to the hours that the electrolyser is in production mode. The peak of consumption is approximately 11.3 kWh. The energy consumed is supplied by the battery, being the PV and grid supply equal to zero. This is possible because of the available energy stored in the battery, as can be confirmed by observation of Figure 70.

It is important to note the absence of PV power. That occurred because after supplying the industry all the PV energy were directed to the electrolyser device. Since there was not sufficient energy to exceed the electrolyser capacity, there was not remaining energy to supply the compressor. In the scenario of the unavailable energy in the battery, the curve presented in Figure 69 would be the same but corresponding to energy bought to the grid (energy supplied by the grid). Furthermore, in Figure 70 it is represented the energy stored at the battery in the beginning of each hour of the 16th of December.

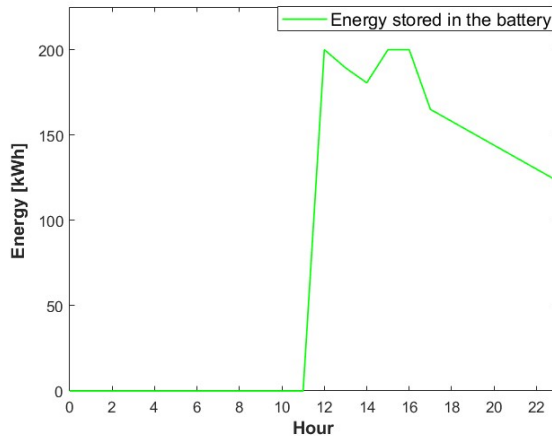


Figure 70 – Energy that is stored at the beginning of each hour in the battery. Data for December 16th.

It can be observed that at 11 AM, the battery reaches a full charge, followed by a discharge of 20.5 kWh, corresponding to the compressor's operation, and subsequently another full recharge. After that, from 5 PM to 11 PM, there is a discharge with varying energy loss rates, corresponding to consumptions of the electrolyser of 35 kWh and 7 kWh, which represent its standby and idle state, respectively. Regarding the electrolyser's energy consumption, it is essential to first analyse the device's state for each hour. For this reason, in Figure 71 it is presented the electrolyser state throughout the day.

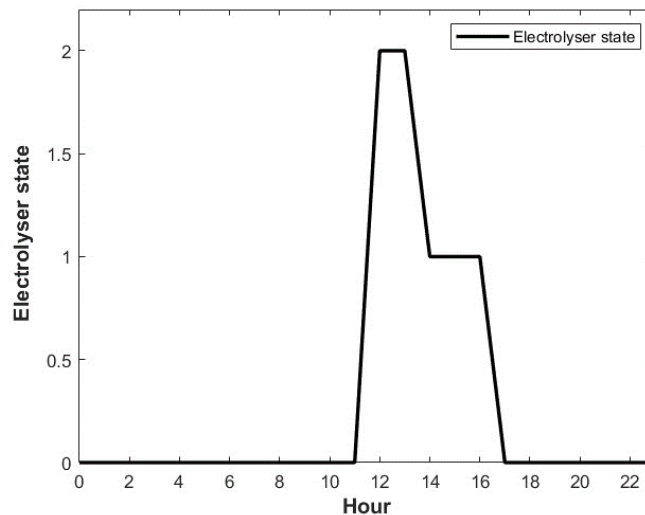


Figure 71 – Representation of the electrolyser state in each hour of the day. Data for December 16th. The values are coded as: 0 for idle, 1 for standby, and 2 for the production state.

It is evident that from midnight to 11 AM, the electrolyser was in an idle state, corresponding to the device's minimum energy consumption. The production mode becomes active from 12 AM to 1 PM, transitioning to standby mode from 2 PM to 4 PM, and subsequently returning to an idle state.

Another critical parameter to consider is the occurrence of cold starts over time. On this specific day, there is only one, which is the minimum possible in a day in which hydrogen production occurs, as the electrolyser remains in idle mode during the night.

The electrolyser does not shift from production to idle mode, when the available energy is insufficient to sustain it, due to the ongoing PV production, coupled with the limitation of the model to forecast meteorological conditions. In other words, the model takes into account the potential increase in energy availability in the subsequent hours, allowing the electrolyser to return to production mode. Therefore, if the electrolyser remains in standby mode when PV production is ongoing but insufficient to activate the production mode of the device, it avoids the necessity for another cold start.

Regarding the electrolyser's energy supply sources (Figure 72), it follows the same reasoning process that is applied in the compressor energy supply. However, in this case, all the three sources of energy were utilised.

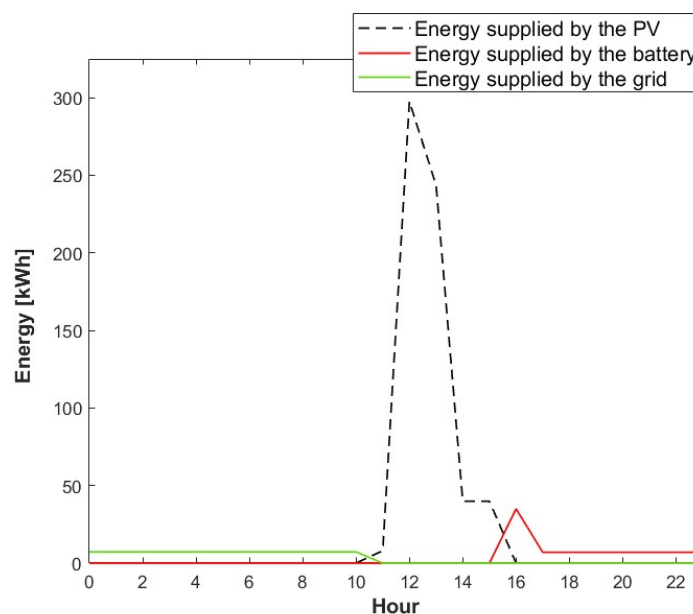


Figure 72 - Energy available to meet the electrolyser's demand. Data for December 16th.

From 12 AM to 10 AM the energy was supplied by the grid. This energy corresponds to the idle state of the electrolyser. From 11 AM to 3 PM the electrolyser was supplied by the PV system, with a peak of 297.6 kWh, and after that, from 4 PM to 11 PM it is fulfilled by the battery, which, as previously mentioned, was recharged at 11 AM.

It is observed that, for the same electrolyser state, the energy supplied is not uniform when the energy source varies. An illustrative instance of this disparity can be observed between 3 PM and 4 PM, where the electrolyser's consumption at an equipment level is 35

kWh. Nevertheless, the PV system supplies 36 kWh, and the battery only provides the 35 kWh. This discrepancy arises from the distinct routes that the energy must traverse from each source to the device. As previously explained, each pathway exhibits varying energy efficiencies. Consequently, to ensure the equipment receives the necessary energy, an adequate energy supply must account for losses during transmission.

Lastly, in Figure 73, it is presented the electrical energy that was supplied to the fuel cell's accessories. Despite the fuel cell being a device that utilizes fuel to generate electrical energy, its operation necessitates auxiliary components that consume electricity.

As can be observed, the supply is exclusively performed by the electrical grid. The two peaks, which have the values of 28.7 and 30.7 kg, correspond to the fuel cell period of operation, as already explained.

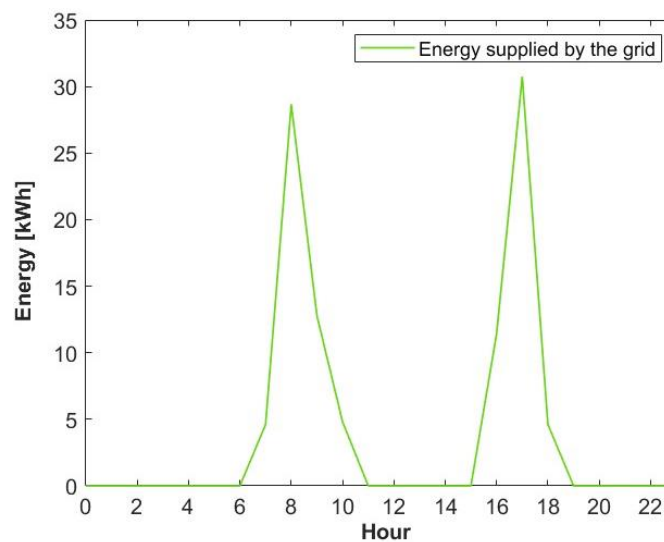


Figure 73 - Energy available to meet the fuel cell's demand. Data for December 16th.

5.1.3 Simulation of a daily profile in August

To better comprehend the model's behaviour during the summer period, the following chapter will analyse the daily profile of a day in August similar to the one held in December. The selected day is the 16th of August, chosen due to its status as the median of the month. It is expected that this day will more accurately represent the typical conditions of the month. The PV energy distribution is illustrated in Figure 74.

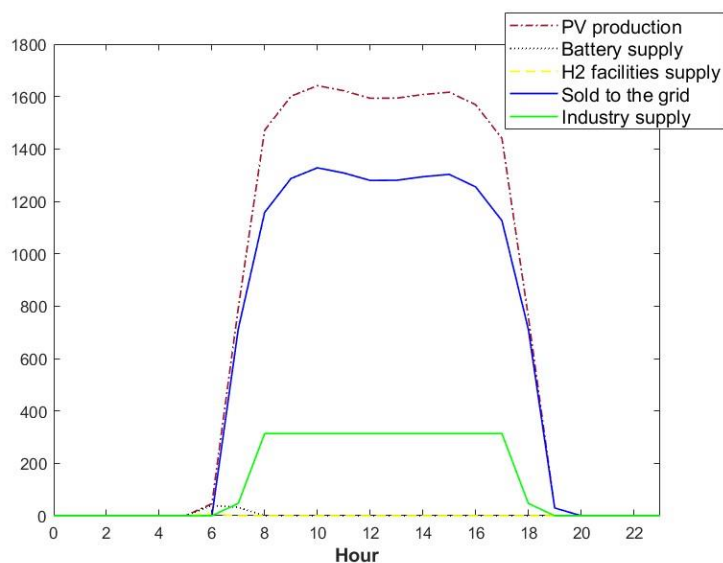


Figure 74 - Daily profile of energy distribution produced by the photovoltaic power plant. Data for August 16th.

The PV production starts at 6 AM and finishes at 7 PM. The production is above 1 MWh from 8 AM to 5 PM, having a peak of 1.64 MWh at 10 AM, which is 168.54% higher than the obtained on the 15th of December.

Another important aspect that must be mentioned is the absence of energy dedicated to the hydrogen production, and the high electrical energy sold to the grid. More precisely, the energy that is injected into the electricity grid, reaches a peak of 1.33 MWh, and maintains a level higher to 0.7 MWh from 7 AM to 6 PM.

To comprehensively elucidate why energy is directed to the grid rather than the hydrogen facilities, it is essential to refer to Figure 75. This plot illustrates that, by the second hour of the 16th of August, the hydrogen storage tanks have already achieved their maximum capacity, which is 2,043.6 kg. Owing to this fact, there no point of producing hydrogen since it cannot be stored. Additionally, with the battery achieving full charge in the second hour of the day, the subsequent step involves transmitting the energy towards its ultimate destination, namely, the sale to the grid.

Moreover, delving deeper into the details of Figure 75, it is evident that the storage tanks maintain the same quantity of hydrogen throughout the day. Thus, in addition to the electrolyser not producing any hydrogen, the fuel cell does not consume any either. Therefore, it can be concluded that the fuel cell accessories do not consume electrical energy during this day, neither the compressor device.

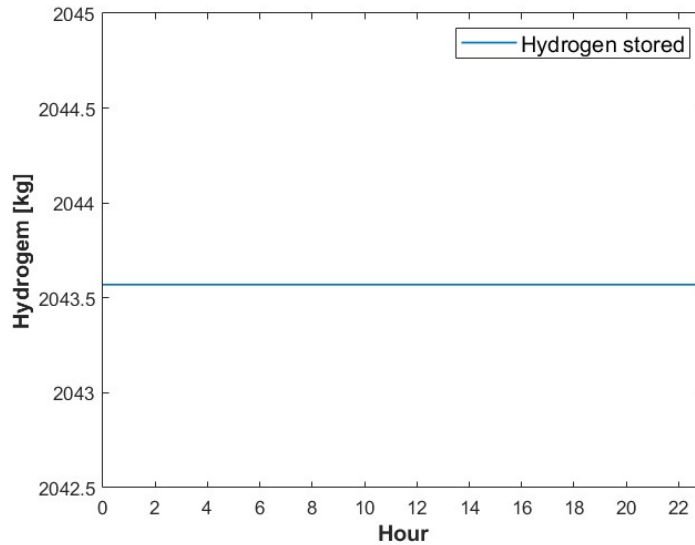


Figure 75 - The hydrogen stored at the beginning of each hour in the stationary storage tanks. Data for August 16th.

In Figure 76, it is presented the industry demand and respective supply throughout the day. As can be observed, the PV production is capable of supplying enough energy to the industry in every hour of its operation. This differs from what was observed in the profile of the 16th of December, that has to use 3 different sources of energy to fulfil the industry energy demand. It should be noted that the absence of hydrogen flow to the fuel cell is a consequence of this device initiating its operation only in the event of an energy deficit of the industry, a condition that was previously explained as not being verified.

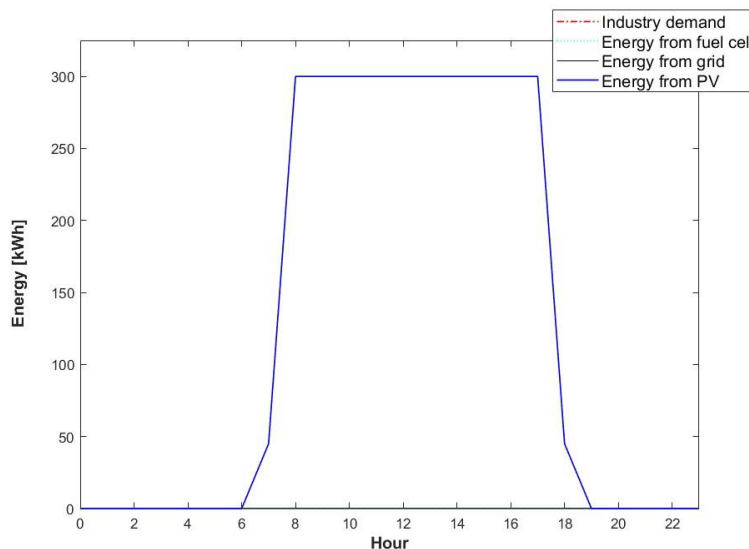


Figure 76 - Illustration of industry demand and its respective energy source supplier. Data for August 16th.

Lastly, regarding the energy supply to the electrolyser device, it's apparent that the device remains in idle mode during the daytime. This is because it doesn't make sense to transition to standby mode if the production mode won't be activated, as previously explained. Additionally, the energy sources that cover this idle consumption change throughout the day. Initially, during the nighttime period from 12 AM to 5 AM, the electrolyser is powered by the battery, and then it's supplied by the PV power plant. During the evening, from 8 PM to 11 PM, the battery returns supplying the electrolyser device.

5.1.4 Monthly analysis

In Figure 77, it is represented the hydrogen produced, consumed, and stored in the last day of August and December. Observing the data, it is evident that the mass of hydrogen produced in December exceeds that generated in August, with values of 1,198 kg and 95 kg, respectively. Furthermore, the amount of hydrogen stored in August, which is 2,044 kg, surpasses that stored in December, which amounts to 1,656 kg.

As evidenced in the analysis of August 16th, the hydrogen storage tank has already reached its maximum capacity. In other words, the hydrogen produced is to replace the amount consumed throughout the month, rather than filling empty tanks. Therefore, it becomes clear why there is a lower production in August, despite the higher solar irradiance available, when compared with December.

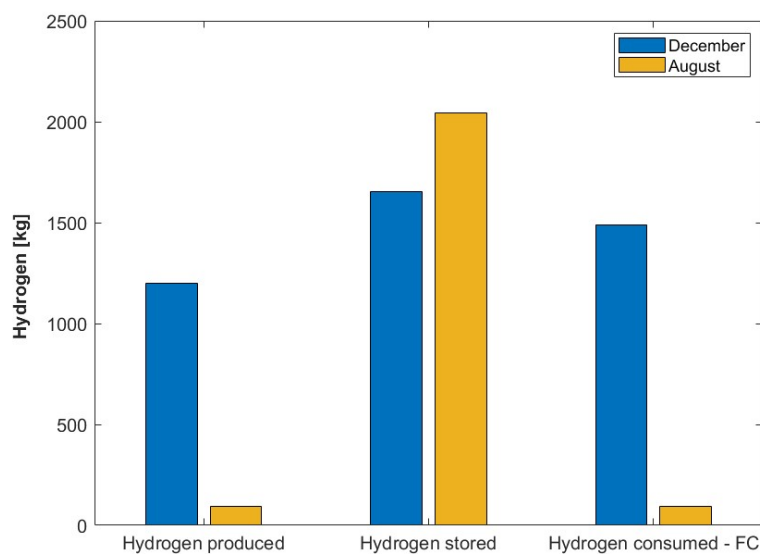


Figure 77 – Comparison of hydrogen production, storage, and consumption in December versus August.

The hydrogen consumption in December, which is 1,490.5 kg, is significantly higher than the consumption in August, which is 95.1 kg. This occurs because there is less solar availability in December compared to August, resulting in a lower PV capacity in December and, consequently, a higher demand for fuel cell output power.

Regarding the PV energy distribution, in Figure 78 it is represented its comparison between August and December. As it was expected, the available solar energy is much higher in August, approximately 220% greater than that in December. When it comes to the industry supplience in August is 39.25% higher than in December.

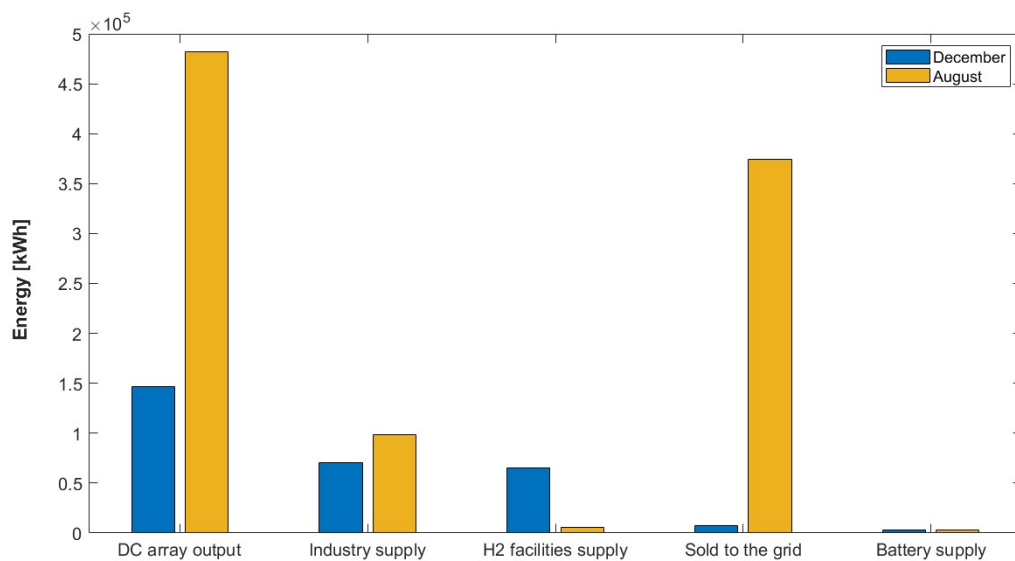


Figure 78 - Energy distribution comparison between December and August from the photovoltaic power plant.

Regarding battery supply, it is slightly higher in December, although it is not noticeable in the plot, due to the lower availability of solar energy. This shortfall of solar energy is offset by the energy stored in the battery, which is recharged whenever possible, thus is dedicated more energy to the battery. Moreover, the energy allocated to hydrogen facilities is 995.6% higher in December than in August, as previously discussed.

The bigger disparity pertaining to PV energy distribution, is the electricity that is sold to the grid. The energy injected into the grid in August is 374.5 MWh, whereas in December, it amounts to 7.2 MWh, corresponding to a deviation of 367.3 MWh. This is owing to the impossibility of utilizing a lot of solar energy in August for hydrogen facilities. Consequently, the majority of the surplus energy, defined as the energy remaining after meeting industrial demands, is sold to the grid due to the absence of alternative applications.

Figure 79 shows how the industry demand is fulfilled. It should be noted that the industry energy requirements are equal in both months, because they have the same number of days. The energy dedicated to industry from the PV power plant source is higher in August due to the days having more solar hours and more irradiance in each hour. In August, the value of energy dedicated to the industry was 98.3 MWh, whereas in December it was 70.6 MWh.

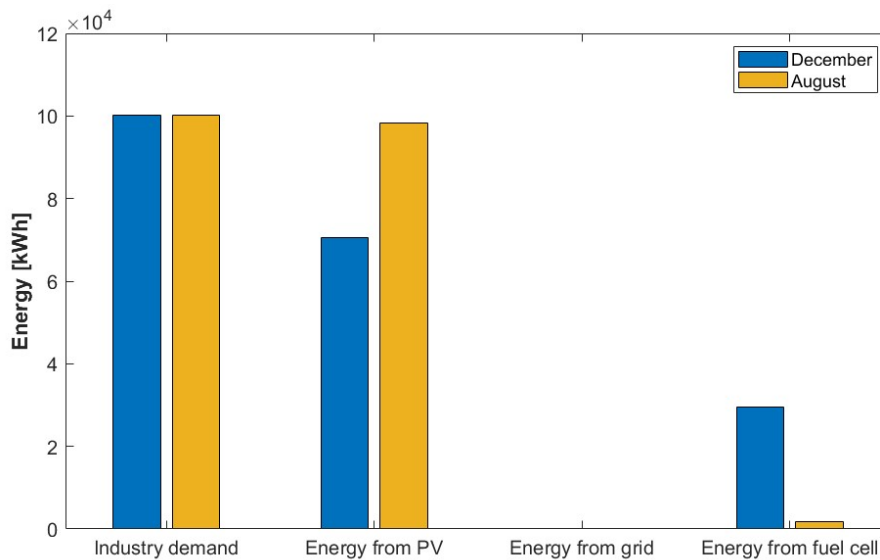


Figure 79 - Industry demand and its energy source supplier compared between December and August.

The second most influential energy source is the fuel cell device, which in August contributed with 1.9 MWh, and in December with 29.5 MWh. These values constitute, almost, the rest of necessary energy of the industry. This is possible, because the storage tanks in the analysed months have larger quantity of hydrogen, which is sufficient to generate the required energy.

Furthermore, the energy purchased to the grid constitutes a very low percentage of the total energy required. In December it was bought to the grid 221.6 kWh, while in August was 26 kWh. The operation of purchasing energy from the grid, when the tanks have hydrogen stored, pertains to situations where the energy deficit in the industry is below the minimum energy output required for the fuel cell to start its operation. In other words, the minimum amount of hydrogen accepted by the fuel cell to shift into its operational mode generates an electrical energy quantity surpassing the industry's required amount.

Since the objective of the model is to take advantage of the surplus solar energy in the sunny days, it was expected that the maximum hydrogen production occurred in the period between June and August. However, due to the fact of the tank capacity is achieved

before this period of high solar availability is over, the surplus PV energy cannot be utilized. Therefore, as was observed, in the month of December the hydrogen production was superior to the production in August.

5.1.5 Annual analysis

Regarding the annual simulation, the hydrogen production, consumption, and storage, at the end of the year is presented in Figure 80.

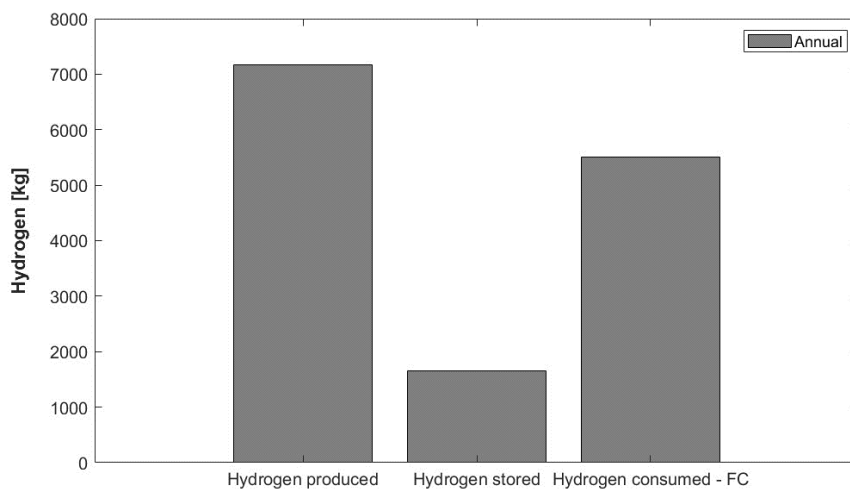


Figure 80 - Representation of annual hydrogen production, storage, and consumption.

There is a positive balance between the hydrogen that was produced (7,164.3 kg) and the hydrogen consumed (5,508.6 kg). However, according to Figure 81, the model bought 7.5 MWh from the grid to accomplish the correct operation of the industry.

Firstly, it suggests that despite the positive annual balance of hydrogen production and consumption, indicating an excess of hydrogen at the end of the year, there is an insufficient amount of hydrogen during certain periods to meet industry demand. This can be linked to the study, which starts in January, a month with limited irradiation, resulting in the system starting with a hydrogen deficit to meet industry demands during cloudy days.

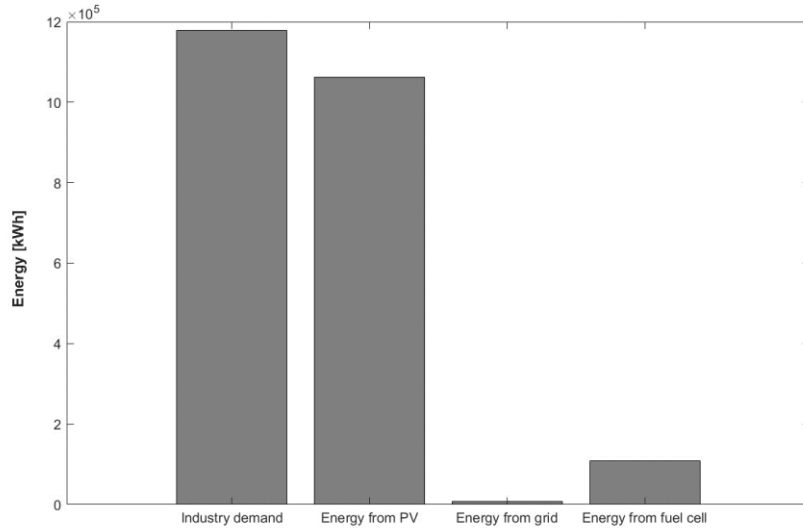


Figure 81 - Representation of the annual industry demand and its energy source supplier.

Moreover, it is possible to observe in Figure 82, which represents the annual energy distribution of the PV power plant, that 2.4 GWh were sold to the grid, and not used to produce and store hydrogen. Therefore, as previously mentioned in the monthly analysis, the model does not completely fulfil its purpose.

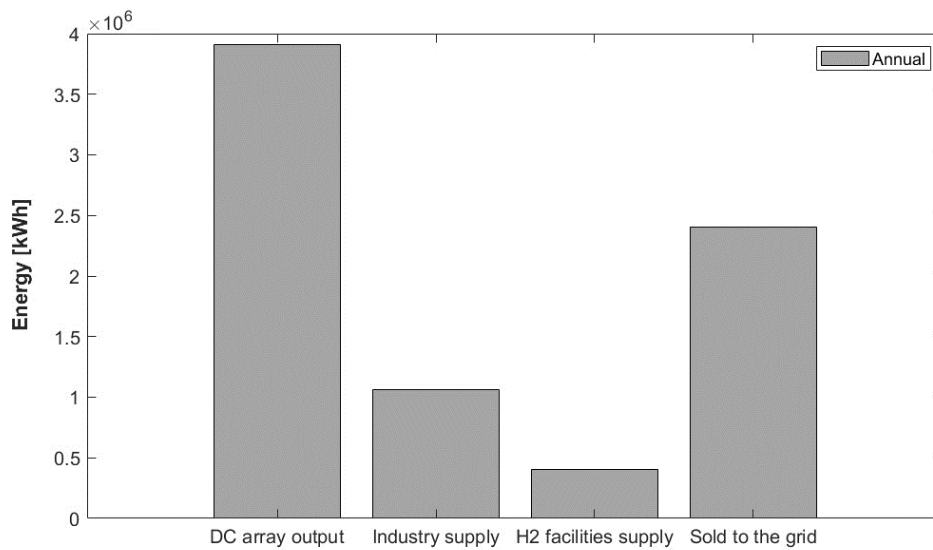


Figure 82 – Annual energy distribution from the photovoltaic power plant.

5.2 Sensitivity analysis

In this subchapter, it will be performed a sensitivity analysis of the model variables.

5.2.1 Analysis of electrolyser capacity

A critical parameter that was submitted to a sensitivity analysis was the electrolyser capacity since it is one of the most important components of the system. For a correct and effective evaluation, the standard electrolyser was compared with other with a reduced capacity. In Table 25 it is possible to observe the main disparities between the two electrolysers.

Table 25 – Representation of the main technical parameters of the standard and low-power electrolyser

| Technical Parameter | Standard Electrolyser | Low-Power Electrolyser |
|--|-----------------------|------------------------|
| H ₂ nominal production [kg/day] | 450 | 388.8 |
| H ₂ production range [kWh] | 200 – 1,400 | 100 - 900 |
| Nominal energy consumption [kWh/kg] | 53 | 57 |
| Nominal load [kW] | 1,000 | 900 |

It should be highlighted that the standard electrolyser operates in a wider power range and has a higher maximum capacity (1 MWh) compared to the low-power electrolyser (0.9 MWh). However, despite achieving a higher capacity, it only works with a minimum energy of 0.2 MWh, whereas the low-power electrolyser operates with only 0.1 MWh. Another important note is that the standby state is not considered, i.e., the electrolyser only has the idle and production mode in this study, in order to simplify the analysis.

There were two essential points analysed, the use of the surplus energy, and as a consequence the hydrogen produced, and the number of cold starts occurred. These studies are represented in Figure 83, Figure 84, and Figure 85, respectively.

As seen in Figure 83, which illustrates the annual energy sold to the grid, there is a significantly lower injection of energy into the grid regarding the standard electrolyser. The majority is directed towards hydrogen production due to the high energy absorption capacity of the electrolyser. This phenomenon is not observed in the low-power electrolyser, as the

equipment is unable to accommodate all excess energy, consequently selling it back to the grid. The disparity between these two energies is approximately 6.5 MWh.

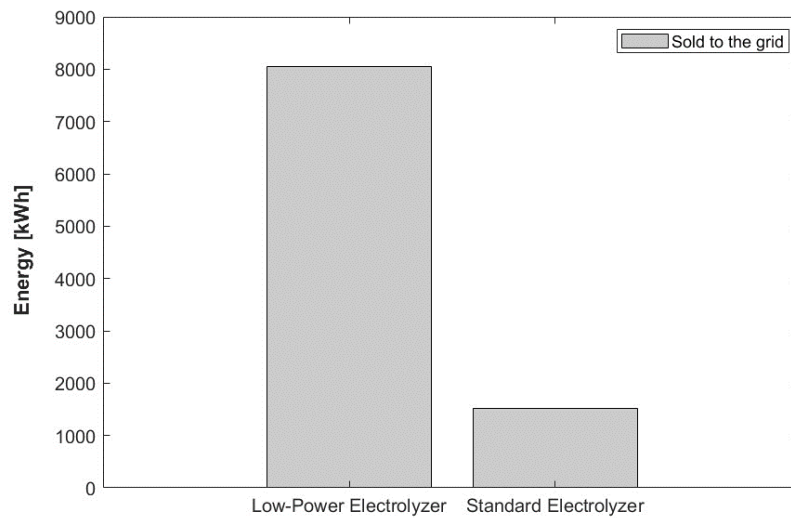


Figure 83 – Representation of the annual energy sold to the grid. Data from the electrolyzers study.

As it was expected, for the same PV production, if lower surplus energy is injected into the grid, more hydrogen is produced. Therefore, the standard electrolyser has more hydrogen production than the low-power electrolyser, being the discrepancy approximately 2,270.7 kg. This is represented in Figure 84.

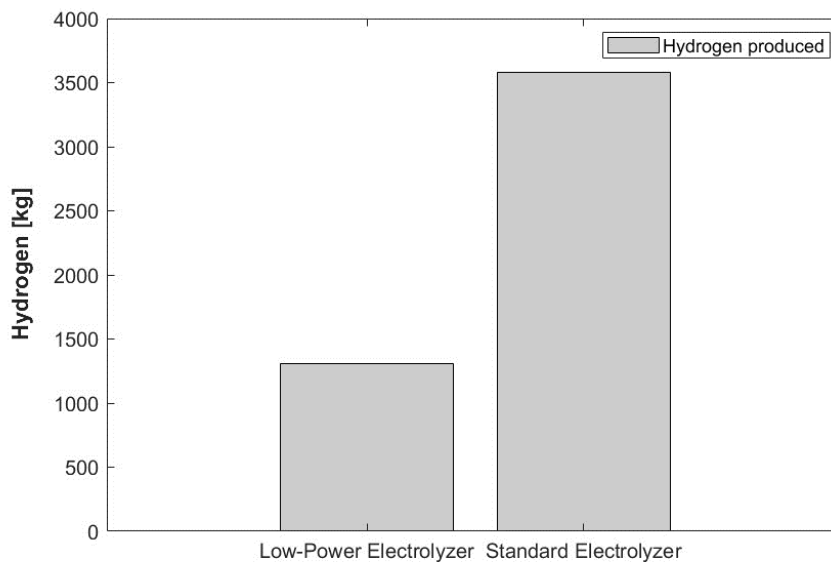


Figure 84 – Annual hydrogen production. Data from the electrolyser analysis.

Lastly, it is analysed the number of cold starts registered for both electrolyzers in December. This is illustrated in Figure 85. The electrolyser with lower capacity exhibits a higher frequency of cold starts compared to the standard electrolyser. This discrepancy is attributed to the lower minimum energy required to initiate the equipment's operation.

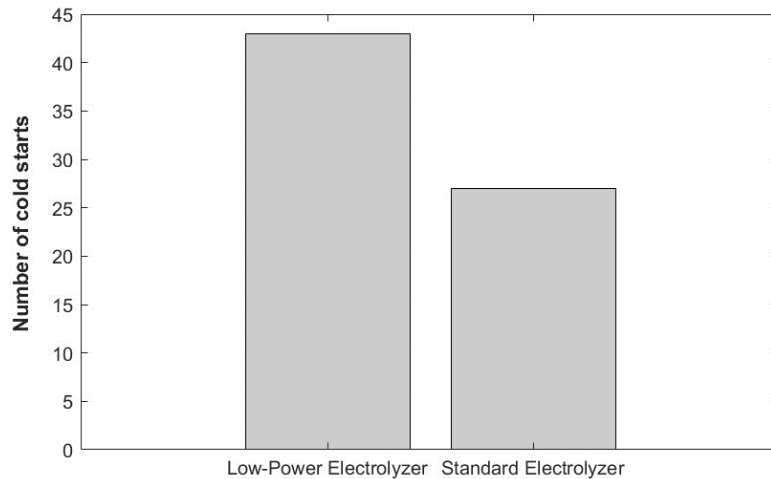


Figure 85 –Number of cold starts for low-capacity and standard electrolyser registered in December.

Table 26 provides a practical example of this model response. The lower capacity electrolyser, with its lower minimum energy requirement, shifts to operation mode, while the standard electrolyser requires more energy. Consequently, at 10 AM, the low-capacity electrolyser shifts to production mode, returning to idle mode at 11 AM. In contrast, the standard electrolyser remains in idle mode from 8 AM until 1 PM. This results in an increased number of cold starts for the lower capacity electrolyser. At the end of the day, the standard electrolyser accounts with four cold starts, while the low-capacity electrolyser accounts a total of six.

Table 26 - Model response concerning the operational state of the electrolyser throughout the day.

The “1” represents the operation mode and “0” the idle state

| Time | PV Production [kWh] | Excess/Deficit of Energy [kWh] | Electrolyser State [Low-Power] | Electrolyser State [Low-Power] |
|------------------|---------------------|--------------------------------|--------------------------------|--------------------------------|
| 2012-12-08T08:00 | 84.36 | -215.64 | 0 | 0 |
| 2012-12-08T09:00 | 350.2 | 50.12 | 0 | 0 |
| 2012-12-08T10:00 | 419.94 | 119.94 | 1 | 0 |
| 2012-12-08T11:00 | 390.48 | 90.48 | 0 | 0 |
| 2012-12-08T12:00 | 455.03 | 155.03 | 1 | 0 |
| 2012-12-08T13:00 | 519.4 | 219.4 | 1 | 1 |
| 2012-12-08T14:00 | 984.45 | 684.45 | 1 | 1 |
| 2012-12-08T15:00 | 1046.86 | 746.86 | 1 | 1 |
| 2012-12-08T16:00 | 500.06 | 200.06 | 1 | 1 |
| Total | | | 6 | 4 |

5.2.2 Analysis of hydrogen storage capacity

The first iteration involves upgrading the hydrogen storage facilities by increasing their storage capacity. Specifically, the new installations adopt the same technology as the standard model but incorporate more tanks, precisely 250 tanks, representing an increase of 389.3%, which corresponds to a storage capacity of 10,000 kg.

Figure 86 presents the comparison of the hydrogen production, storage at the start of the month, and consumption between December and August. It is concluded that the hydrogen production in December remains higher than in August. Moreover, the storage tank at the start of August is already full, which means that the problem identified in the standard model was not solved.

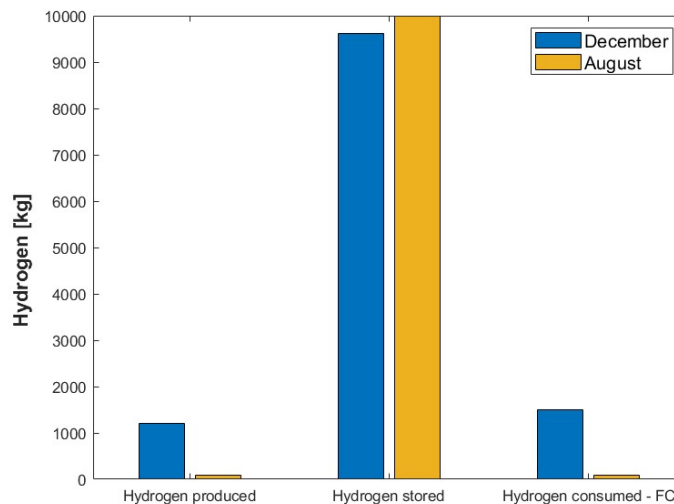


Figure 86 - Comparison of hydrogen production, storage and consumption between December and August.

Figure 87 shows that August has a lot more PV production than December, however, the most of its energy is sold to the grid, which is not the objective of the model. Therefore, it can be concluded that the absence of hydrogen production on sunny days, such as in August, and consequently, the inability to store the excess PV power, is attributed to the insufficient storage capacity. To solve the problem, it could be considered the increase the storage capacity or a higher energy demand from industry.

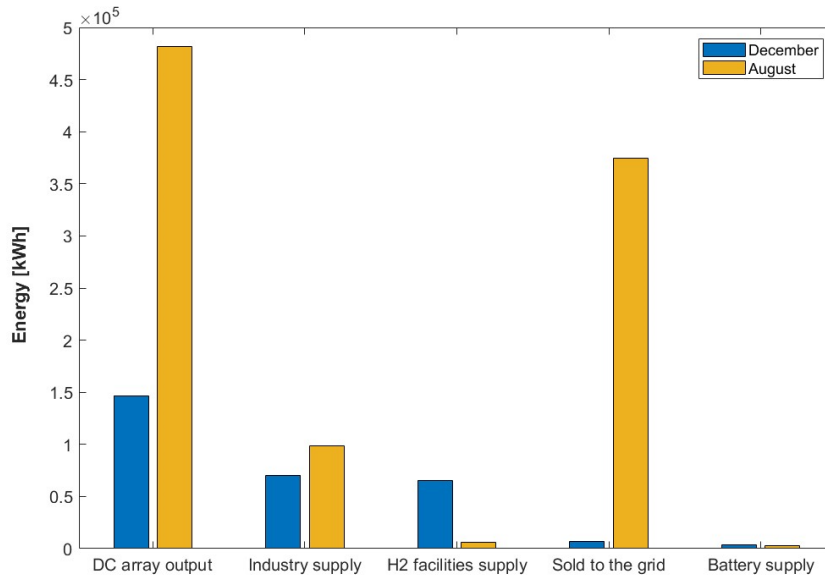


Figure 87 - Energy distribution comparison between December and August from the PV power plant.

5.2.3 Analysis of industry demand increase

In this model, it was adopted a higher industry demand, since in the previous studies, the tank was already full in the beginning of august. The new industry demand is expressed in Figure 88, and can be described as twelve hours of operation, from 7 AM to 7 PM, with a consumption of 600 kWh. It worths noting that the hydrogen facilities considered in this model are the same of the standard model.

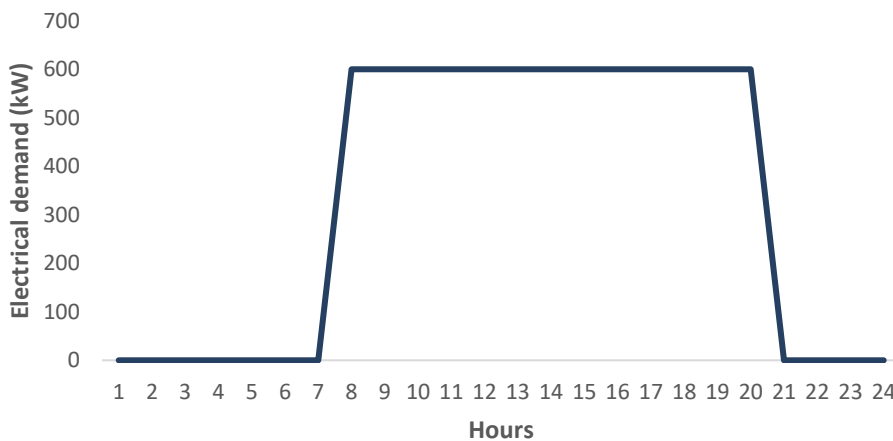


Figure 88 - Daily profile of the electrical demand of the industry.

Figure 89 shows that, in August, hydrogen production is superior to that in December. However, it is noticeable that the produced hydrogen is equal to the consumed hydrogen in December, and the same occurs in August. The difference between the two months is the hydrogen stored in its beginning.

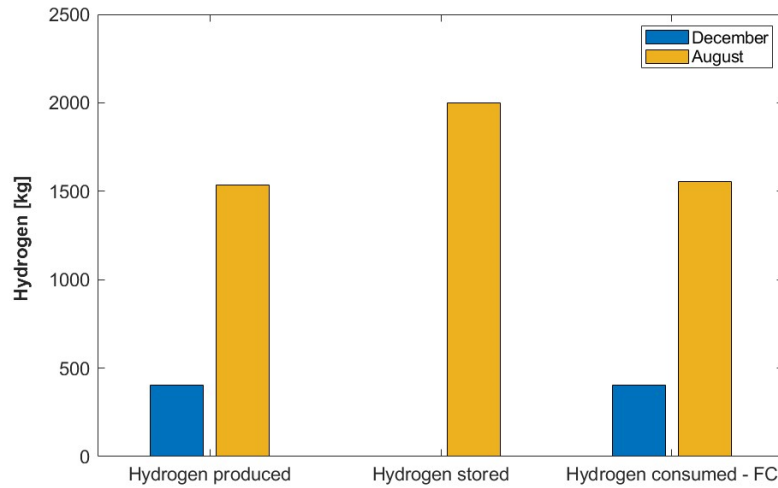


Figure 89 - Comparison of hydrogen production, storage and consumption between December and August.

In December the tank is empty, so the hydrogen that is used to contribute to fulfil the industry demand comes from the surplus energy that occur in a reduced number of days that possess hours with peaks of irradiance, that surpasses the industry needs and allows the daily storage of hydrogen.

In Figure 90, it is shown that a lot of energy is purchased from the grid, as the hydrogen and PV energy generated in December are not sufficient to meet the industry demand.

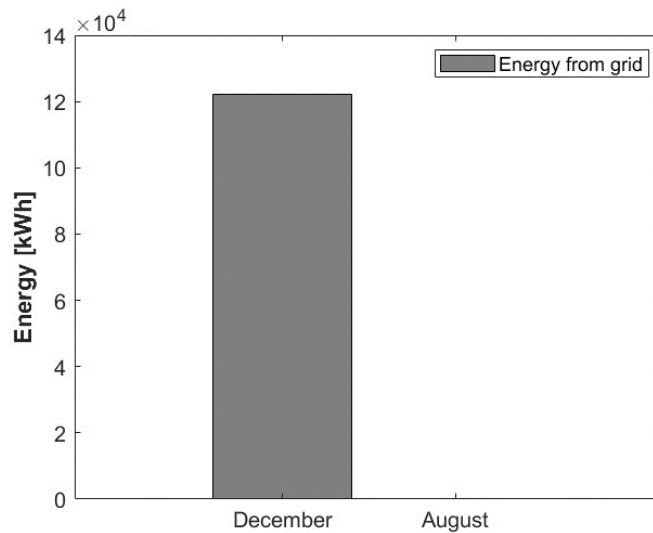


Figure 90 - Comparison of energy bought from the grid between December and August.

In August, there is no utilization of the total of the surplus energy to produce hydrogen, in order to perform its seasonal storage. This occurs because the tank is already full at the beginning of the month, as represented in the Figure 89. Part of the surplus energy at the periods with higher irradiance serves to replenish consumed hydrogen throughout the month, due to the high energy demand of the industry in hours of reduced irradiance. For

instance, at 7 PM in August, the PV production is usually zero or nearly zero. Owing to this fact, hydrogen is used in the fuel cell to fulfil the industry requirements.

The other fraction of the surplus PV energy is sold to the grid as can be analysed in Figure 91.

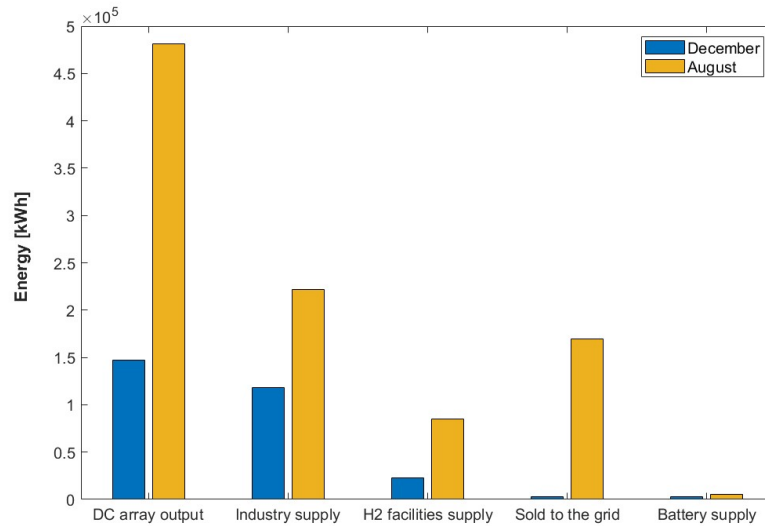


Figure 91 - Energy distribution comparison between December and August from the PV power plant.

5.2.4 Analysis of the increase in hydrogen storage capacity and industry demand

Another possibility analysed was the junction of the last two iterations. To clarify, the hydrogen facilities are considered to have a capacity of approximately 10,000 kg of hydrogen, and the demand taken into account was the 600 kWh per hour, expressed in Figure 88.

Despite the fact that the annual hydrogen produced is higher than in the previous iteration, a significant portion of the surplus energy remains unused, as it was sold to the grid, as can be observed in Figure 92.

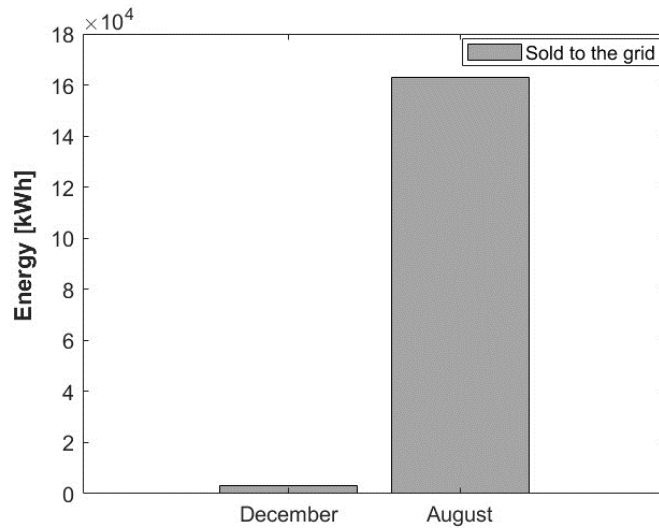


Figure 92 - Comparison between December and August of the energy sold to the grid.

This leads to the fact that there isn't enough hydrogen to avoid the purchase of electrical energy from the grid to fulfil the industry in the cloudy days, as it demonstrated in Figure 93.

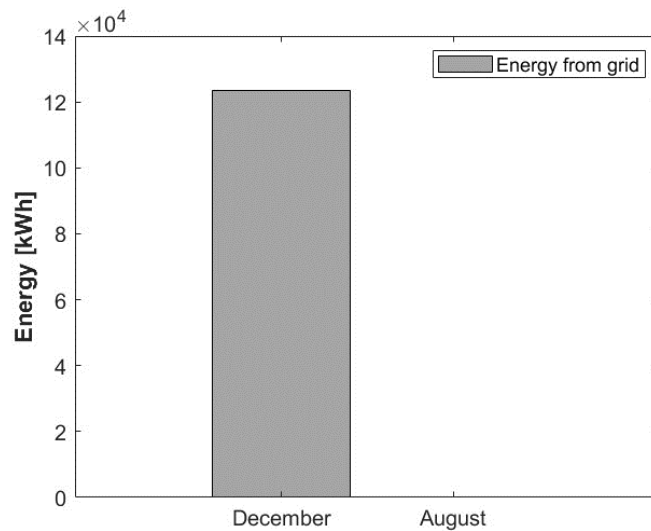


Figure 93 - Comparison between December and August of the energy bought from the grid.

It can be concluded that even if the demand of the industry is increased and the storage capacity is scaled up to 10,000 kg of hydrogen, is not enough to take advantages of all the surplus energy from the PV production. Therefore, another strategy has to be adopted.

5.3 Improved system operating scenario

As a result of the insights gained from the aforementioned iterations, the final model has been developed. This model demonstrates distinct characteristics in terms of storage facilities, which have been identified as posing a more significant challenge in achieving the predefined objectives. The final study is divided into two sub-studies, varying in the industry demand between 600 kWh, defined as high demand, and 400 kWh, defined as low demand. It should be highlighted that in these studies, the tanks were projected to accommodate all the hydrogen that can be produced.

Another important modification is the month in which the study begins and ends. As mentioned in the analysis of the results from the standard model, if the analysis starts from January, there is no evidence to show that the model, even if it takes advantage of all surplus energy, has enough hydrogen for all the months. This is because it begins in a period when hydrogen is already required to meet industry demands. Therefore, the study should start from sunny days to validate its capability to store surplus PV energy as hydrogen and fulfil industry needs during periods of low irradiation, when PV power is insufficient. Consequently, the month to start the study is April due to its already high irradiance, with a global horizontal irradiance that surpasses the 150 W/m² and a diffuse horizontal radiation that surpasses the 65 W/m².

5.3.1 High demand

In order to obtain a rough estimate of the number of tanks needed to store the surplus energy, the equation (55) is applied. This equation relates the energy produced by the PV power plant (E_{PV}), the energy required by the industry at the controlling point (E_{ind}), and the maximum hydrogen that can be produced by the electrolyser ($m_{H_2}^{(i)}$). All these variables correspond to annual values. To be specific, E_{PV} correspond to 3.9 GWh, the E_{ind} to 3 GWh, the $_{cons}\dot{E}_{ele}^{(i)}$ to 53kWh/kg, and the $\eta_{PV,ele}$ corresponds to 0.972.

$$m_{H_2}^{(i)} = \frac{(pc E_{PV}^{(i)} - pc E_{ind}^{(i)})\eta_{PV,ele}}{_{cons}\dot{E}_{ele}^{(i)}} \quad (55)$$

Finally, the maximum achievable hydrogen production is 17,125 kg. In consequence the number of tanks adopted for this study is 428, corresponding to a total capacity of 17,150 kg.

5.3.2 Monthly analysis

Similar to the analysis to the standard model, a monthly analysis will be conducted. Firstly, is presented in Figure 94 the hydrogen produced, consumed, and stored in the last day of August and December.

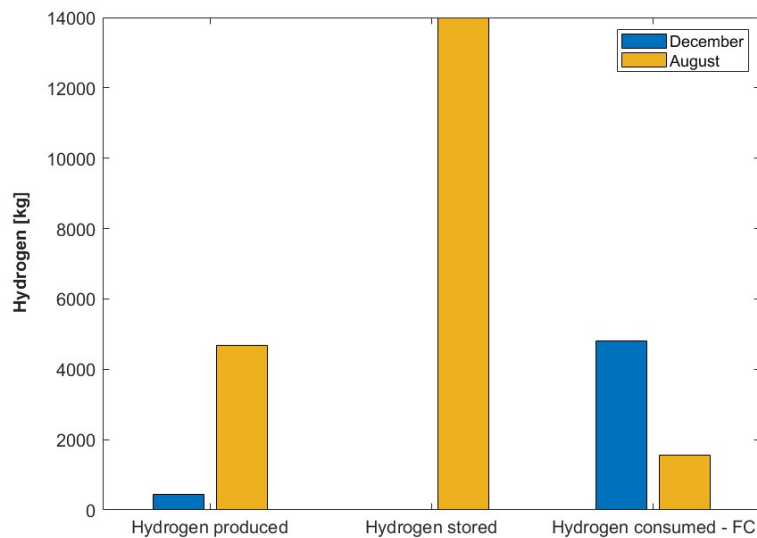


Figure 94 - Comparison of hydrogen production, storage and consumption between December and August.

It is possible to conclude that the mass of hydrogen produced in August exceeds that generated in December, with values of 4,670 kg and 452.6 kg, respectively. This differs from the standard study, since in this model the tanks are over dimensioned to store all the achievable hydrogen production. Regarding the fuel cell utilization, as it was expected, in December the hydrogen consumption is higher than in August, 4,802.1 kg and 1,555 kg, respectively. This is owing to the reduced PV production registered in December, when compared to August.

Furthermore, in August the tanks reach the 81.6% of storage capacity. As per December, the stored hydrogen is zero. This reflects that, at least by the end of December, the tank is already empty. It means that the hydrogen produced with the surplus solar energy is not sufficient to meet the industry demand throughout its timeframe of reduced irradiance.

It should be remembered that this study starts from April. Therefore, it can be already concluded that the model does not accomplish the self-sustaining level. Despite this, as observed in Figure 95, whether in August or December, the energy sold to the grid is nearly zero when compared to other energy applications.

This indicates the achievement of one of the stipulated goals. This plot also reinforces the conclusions from the preceding graph, as there is more energy allocated to hydrogen and industry facilities in August than in December.

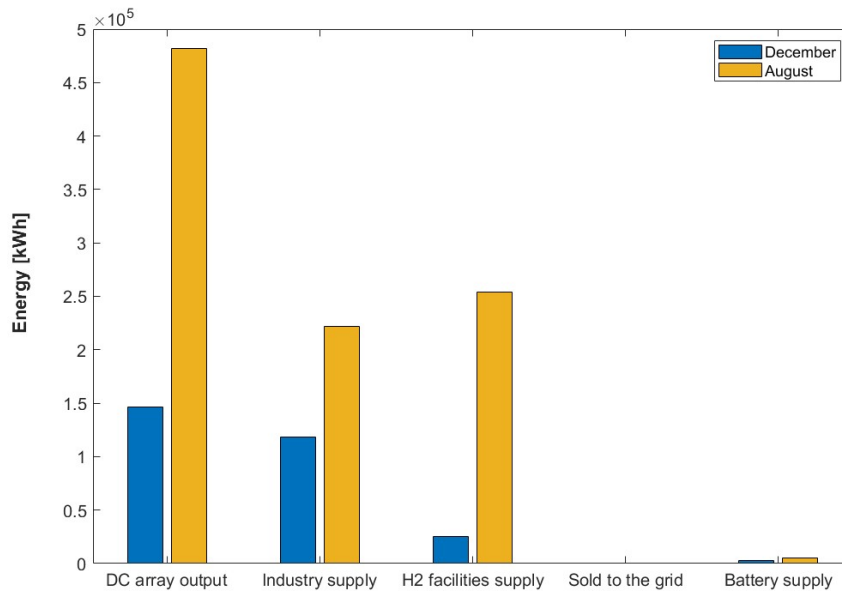


Figure 95 - Industry demand and its energy source supplier compared between December and August.

To conclude the monthly analysis, in Figure 96 is presented industry demands and its respective suppliers.

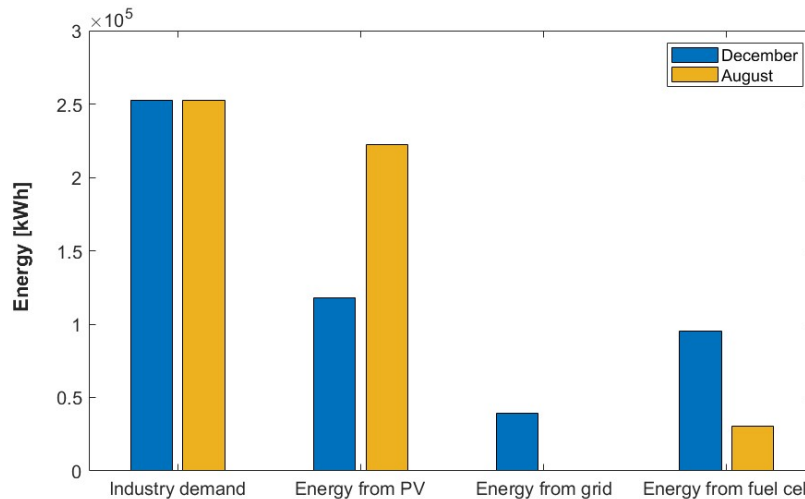


Figure 96 - Energy distribution comparison between December and August from the photovoltaic power plant.

To be specific, in August the value of energy from the PV power plant dedicated to the industry was 0.222 GWh, whereas in December was 0.1182 GWh. It can be observed a significantly higher utilization of the fuel cell in the month of December when compared to August, 95 MWh and 30.8 MWh, respectively.

In August, the energy purchased from the grid was nearly zero, amounting to only 109 kWh. In contrast, December saw a significant increase to 39 MWh, highlighting a substantial disparity between the two months. This can be elucidated by two reasons. On one hand, the increased solar radiation availability in August facilitates the maintenance of a minimized electricity purchase from the grid. On the other hand, beyond the low solar availability, the absence of stored hydrogen in December requires obtaining energy from the grid, since there is no other available supplier.

5.3.3 Annual analysis

Concerning the annual analysis, in Figure 97, Figure 100, and Figure 101, present the hydrogen production, storage, and consumption, as well as the energy distribution from the PV power plant. Additionally, they depict the annual demand of the industrial sector and its corresponding energy source supplier.

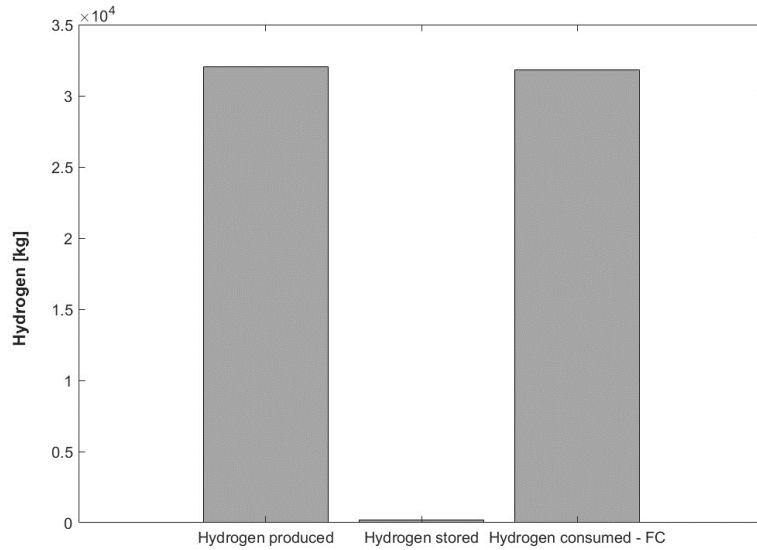


Figure 97 - Representation of annual hydrogen production, storage, and consumption.

As can be observed the practically all the produced hydrogen throughout the year, which accounts 32,018.1 kg, was consumed. The graphic exhibits that in the end of the last hour under analysis, the hydrogen stored in the tanks is 214.5 kg. Based in the previous observations, which indicated that the hydrogen tank was already empty in December, it can be inferred that this end-of-year value was generated in March. In essence, the minimal amount of stored hydrogen recorded at the conclusion of the study does not imply the self-sustainability of the model.

Previously, it was observed that in December, the hydrogen tank was already empty. To fully comprehend the variation in hydrogen storage throughout the year, the profile of tank's occupancy is presented in Figure 98.

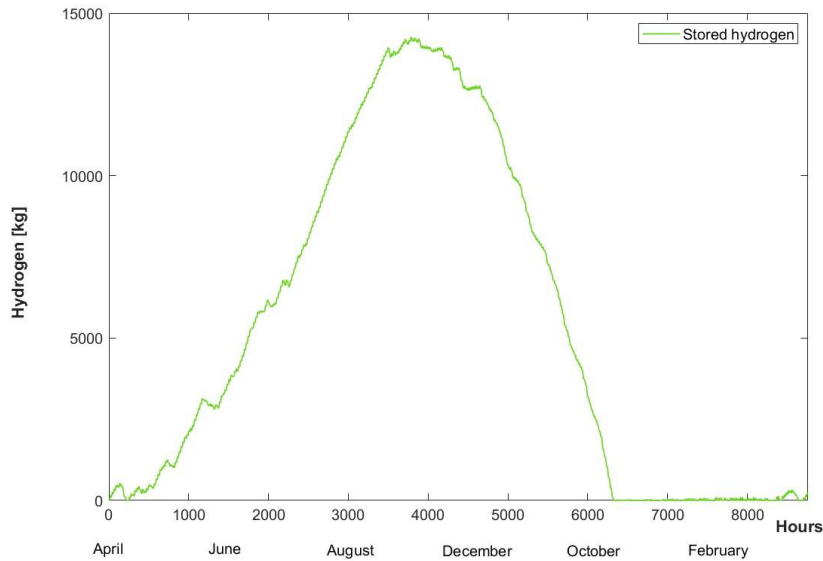


Figure 98 – Annual profile of tank of hydrogen tank’s occupancy of the final high demand model.

An increase in hydrogen levels in the storage tanks is observed from April to August, coinciding with the period of highest irradiance, resulting in an abundance of surplus energy. The maximum recorded hydrogen storage is 14,274 kg at the beginning of September. Following this peak, there is a notable decline in hydrogen levels within the tank from September to the end of March. This timeframe aligns with reduced solar availability and, consequently, diminished PV production.

Another important information obtained from Figure 98 is the point at which there is no more hydrogen available for electricity generation through the fuel cell device. In other words, this marks the point at which the acquisition of electrical energy from the grid rises, as depicted in Figure 99. To be precise, the day on which the tank registers zero hydrogen storage is the 20th of December.

Moreover, the observation of Figure 99 facilitates the identification of two distinct timeframes that can be correlated with the profile presented in Figure 98. The first corresponds to a period wherein the purchase of energy from the grid is approximately 100 kWh. This period aligns with high irradiance and hydrogen storage. In simple terms, the industry is primarily powered by the PV power plant, and in the event of its curtailment, the supply is ensured by the fuel cell device. The second relates to a period of purchase exceeding 600 kWh, corresponding to the absence of hydrogen in the storage tanks and insufficient PV energy to meet the industry demand. Therefore, the absence of hydrogen and low irradiance leads to the energy purchase from the grid.

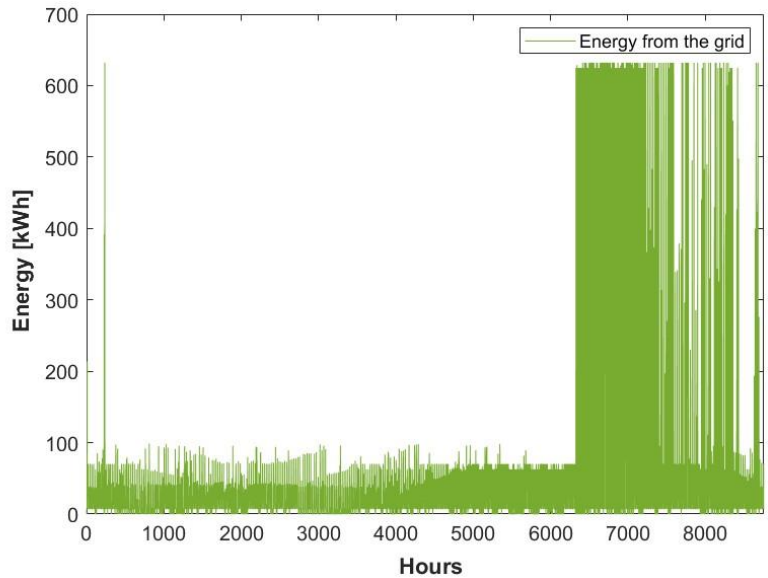


Figure 99 - Annual profile of Energy bought from the electrical grid.

It is important to note that the lower consumption of electricity from the grid is associated with various components. These include the electrolyser consumption at idle and standby mode, which sometimes cannot be fulfilled by the battery. Additionally, the auxiliary equipment of the fuel cell, the compressor system, and, during specific hours, usually at the start or end of the day, contribute to the electricity demand. In these instances, the PV production is very low, and the fuel cell, with its limited output of 440 kWh, is insufficient to meet the industry's energy requirements.

Regarding the annual PV energy distribution, it can be concluded by observation of Figure 100, that the large slice of energy was supplied to the industry, totalling 2.13 GWh of the 3.91 GWh generated by the power plant.

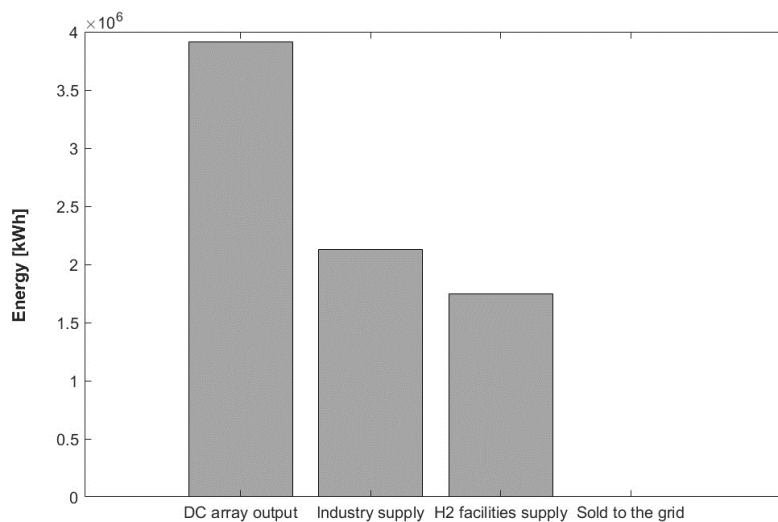


Figure 100 - Annual energy distribution from the PV power plant.

Furthermore, it can also be noted, as observed in the months of August and December, that the surplus energy ($E_{xs}^{(i)}$) is redirected to the hydrogen facilities, thereby preventing its sale to the grid. Specifically, 1.74 GWh were used to hydrogen production, and 4.97 MWh were injected in the grid, which reflects a massive disparity between these two energy possible destinations. Consequently, it is possible to conclude that the storage of the surplus energy is attained in this model.

It's worth noting that the substantial demand from the industrial sector demonstrates an obstacle for the electrolyser to receive an energy quantity that would enable it to attain its maximum capacity. Therefore, the injection of electricity to the grid occurs when the output of the solar array is inadequate to meet industrial requirements, thereby inhibiting the initiation of electrolyser production operations, and the battery reaches its maximum capacity. In this scenario, the remaining of the PV energy is sold to the grid.

The industry supply throughout the year is illustrated in Figure 101. It is observed that the primary supplier for the industry facilities is the PV power plant, providing 2.13 GWh. Following this, the fuel cell serves as the secondary supplier, generating 0.629 GWh, equivalent to 31,803.6 kg. The final source is the electrical grid, contributing 0.216 GWh, serving as the last resort.

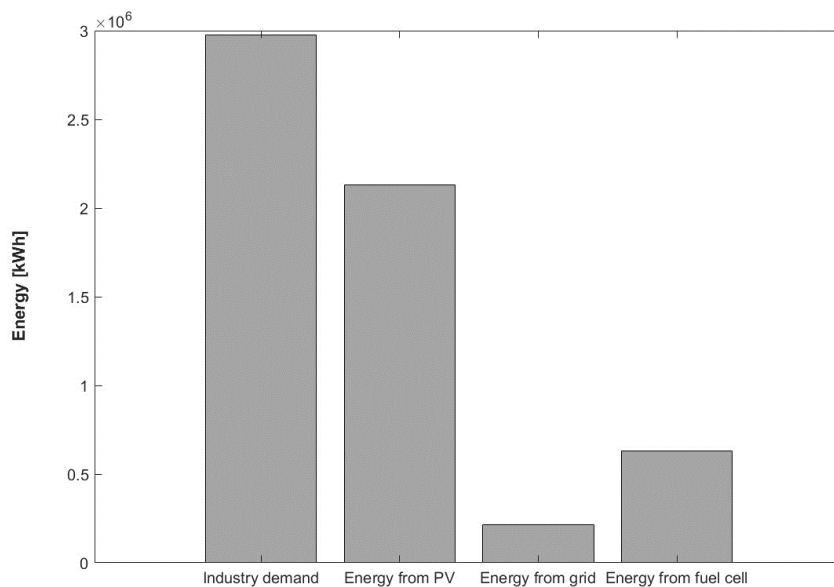


Figure 101 - Industry annual demand and its energy source supplier.

Figure 102 allows the analysis of the model's annual energy consumption, highlighting the portion acquired from the grid to meet requirements. The annual energy consumption of

the model was 4.85 GWh, being 7.68% of the suppliance of this energy bought from the grid, which accounts for 0.373 GWh.

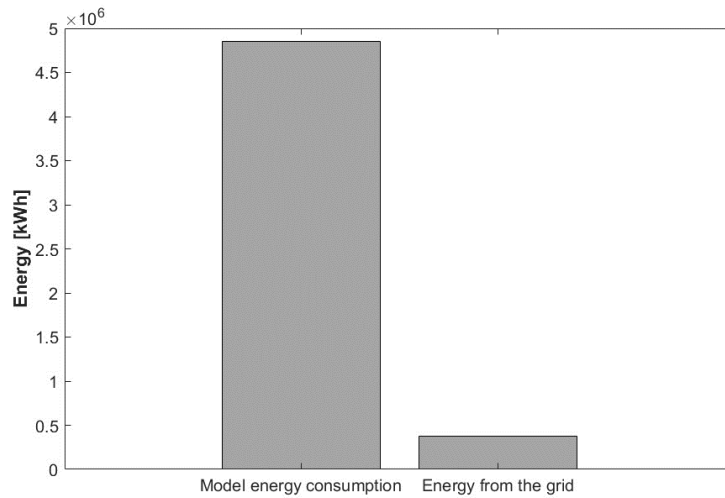


Figure 102 – Annual energy consumption of the model, and grid-acquired energy.

A comparison with the grid-dedicated energy value in Figure 101 indicates that the primary application of purchased electricity is for industrial purposes. Hence, aligning this conclusion with the data observed in Figure 98, it is expected that a reduction in industrial energy consumption will lead to a diminished reliance on grid energy. This aligns with one of the primary objectives of the model, which is to approach as closely as possible to achieving self-sufficient capacity (seasonal storage).

5.3.4 Analysis of industry demand

To assess whether the final model can achieve self-sustainability with a reduced industry demand, a study was conducted using identical data as before. However, in this study, the energy requirement is 400 kWh instead of 600 kWh.

This alteration resulted in a notable surplus energy increment, supplying additional electrical energy for hydrogen generation. Owing to this fact, the equation (55) must be recalculated, in order to calculate the maximum achievable hydrogen production ($m_{H_2}^{(i)}$). This makes possible the correct upgrading of the storage facilities. The maximum achievable hydrogen production obtained across a complete year was 35,300 kg, which results in 882 hydrogen storage tanks, an increase of 1,629.4% of the storage capacities, in comparison to standard model. This value is a gross estimative, that has to be corrected during the analysis of the results.

Another important note is the fact that the fuel cell has the capacity to meet industry requirements in the absence of PV power generation, which was not possible with the industry demand of 600 kWh, since the device maximum output is 440 kWh.

Figure 103 shows the total amount of hydrogen produced during the studied year, as well as, the quantity of hydrogen stored in the tank at the end of the study period, March 31st. To be specific, the hydrogen produced was 43,300 kg, which corresponds to an increase of 35.2% in relation to the high demand final study. In terms of hydrogen storage, it is evident that there is a substantial excess of stored hydrogen (19,200 kg), a phenomenon not observed in the previous study.

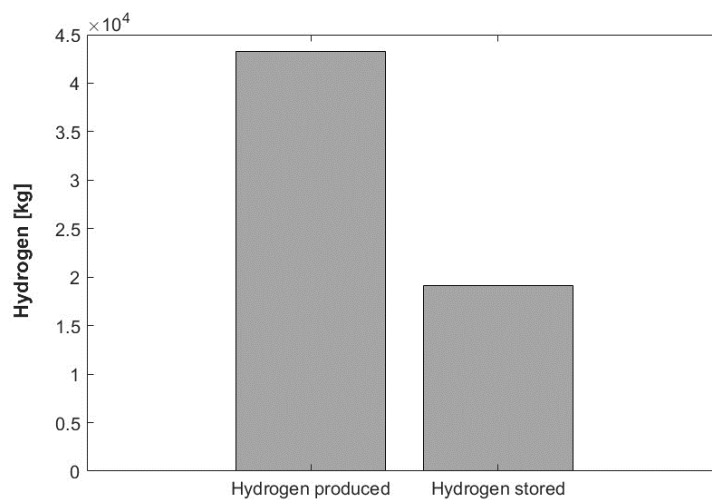


Figure 103 - Representation of annual hydrogen production and storage.

Nevertheless, it is crucial to ascertain whether hydrogen was consistently available throughout the entire year or if there were periods of hydrogen deficit. Therefore, in Figure 104 is analysed the variation of the occupancy on hydrogen storage tanks.

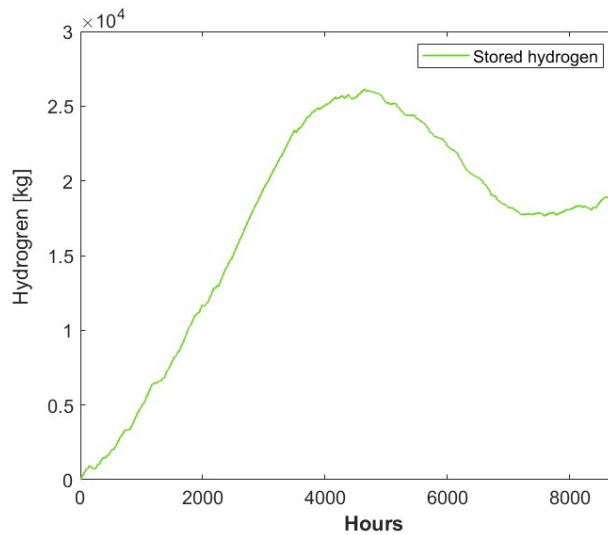


Figure 104 - Variation of hydrogen mass stored throughout the year.

There was no recorded period of hydrogen absence in the storage tanks. Consequently, in the event of insufficient PV energy to meet industrial needs, the fuel cell device can fulfil its energy requirements, given its ample fuel supply. As a result, it expected a drastic reduction of the energy that is bought to grid, when comparing with the high demand final study.

Figure 104 also shows the maximum simultaneous hydrogen storage, which is 26,200 kg and corresponds to 653 tanks, which is the tanks that are required by the final model. Figure 105 and Figure 106 depict the energy acquired from the grid to meet industry demands and the overall energy purchased from the grid, respectively.

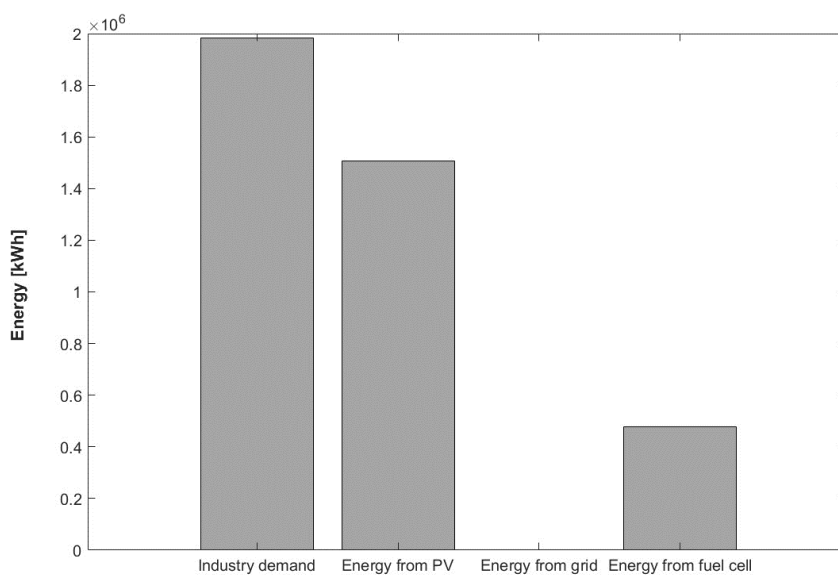


Figure 105 - Industry annual demand and its energy source supplier.

In Figure 105, it can be observed that the energy purchased from the grid remains at a magnitude level lower than that of other energy sources, as it was already seen in the high demand final study. The energy that was bought to the grid and dedicated to the industry was 1.6 MWh, which corresponds to a decrease of 0.214 GWh, when compared with the high demand of improved scenario.

One of the crucial analyses involves comparing the percentage of energy supplied to the industry by the electrical grid in this study with the previous one. In the current low-demand model, the electrical grid contributes only 0.08% to the total supplied energy to the industry, a stark contrast to the 7.43% recorded in the high demand final study. Therefore, it can be concluded that the industry's readjustment makes the current model approaching a higher level of self-sufficiency.

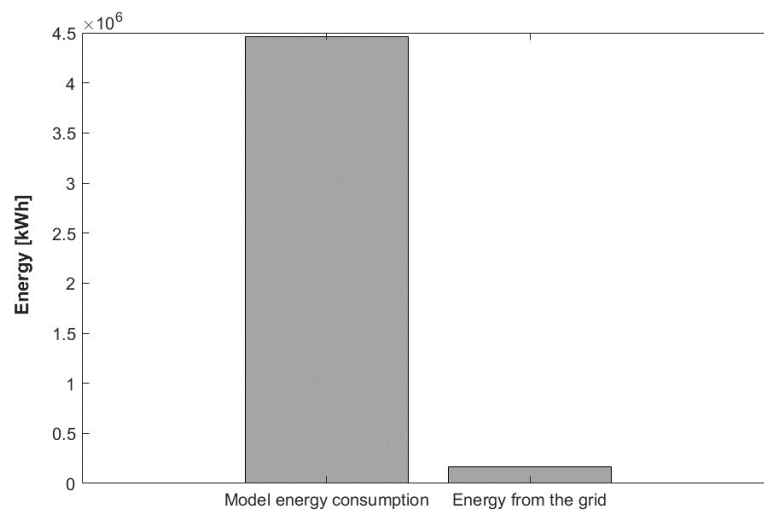


Figure 106 - Annual energy consumption of the model, and grid-acquired energy.

Regarding the total energy consumption from the grid, it accounts for 0.162 GWh, whereas the overall model consumption sums up a value of 4.46 GWh. When compared to the high demand final study, the overall model consumption suffered a decrease of 8%, while the energy bought from the grid decreased 129.8%. The reduced importation from the grid is attributed to both lower industry demand and an increased quantity of hydrogen available to meet industry requirements.

To conclude, the goal of achieving complete grid independence faces a wide range of challenges. These challenges are primarily related to the energy consumption patterns of the compressor, fuel cell, and electrolyser during their idle and standby modes, which are fought by the battery, a supplementary power source.

To further explain, one of the equipment's implemented to diminish the purchase of electrical grid is the battery. However, this battery can only store energy under specific conditions: when the electrolyser is not in production mode, and the industry is sufficiently powered, or the electrolyser reaches its maximum energy absorption capacity. Unfortunately, these scenarios are infrequent, and the battery frequently falls short of having enough stored energy to meet the power requirements of the devices.

Regarding the compressor, it primarily consumes energy from the electrical grid, as the battery doesn't always have enough energy to meet its demand.

Similarly, when the electrolyser is in standby or idle mode, it relies on PV energy. However, the electrolyser's energy demand can sometimes outstrip the available solar power. This scenario, combined with the lack of stored energy in the battery, leads the model to resort to the electrical grid to meet the electrolyser's needs.

As for the fuel cell, it enters in operation mode when PV energy is insufficient to meet the industrial energy demands. In essence, it serves as a backup during periods of limited solar power availability. That being the case, this equipment unavoidably relies on the electrical grid to supply its auxiliary equipment. Nonetheless, while attaining absolute self-sufficiency remains unfeasible, significant proximity to this goal has been reached.

Finally, it is necessary to ascertain whether the surplus energy generated by the PV power plant was efficiently utilized, as observed in the case of the high demand final study. In this case, the total energy injected into the grid was 5.58 MWh, an increase of 12.2% compared to the high demand final study. However, this injection accounts only for 0.13% of the total PV energy output over the year, indicating that the study's objective is essentially achieved. Additionally, the implementation of an electrolyser with a wider power range would probably result in near-zero energy injection into the grid.

6. ECONOMIC ANALYSIS

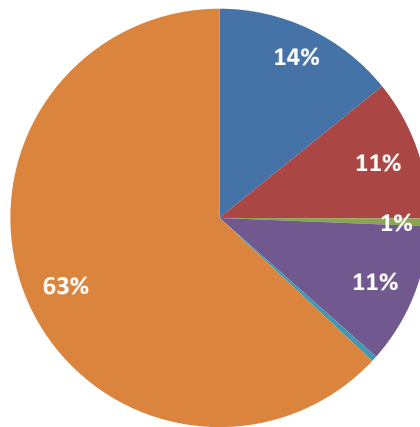
In this chapter, an economic analysis is presented. Firstly, an evaluation of the initial investment required to establish the final model will be discussed, alongside a study of the operating expenses and the Cost of Goods Sold (CoGS). It should be noted that the COGS includes all costs and expenses directly associated with the production of goods. It does not account for indirect expenses such as operation and maintenance. Secondly, a comparison will be made between the projected installation and a standard natural gas power plant. Furthermore, it is important to mention that for this economic analysis, the product for commercialization is the hydrogen for sale (goods). Therefore, the cost of goods sold are related to the water electrolysis process.

6.1 Assessing initial investment and operating costs

In Table 27, it is presented the CAPEX of the low demand final model. As can be observed the total initial investment has a value of 11.62 million of euros. It is important to note the higher cost of the hydrogen storage facilities, when compared to the rest of the equipment. To be specific, the hydrogen storage facilities account for 63% of the total initial investment, as can be observed in Figure 107. This is due to the number of tanks necessary to store the surplus energy of the PV power plant.

Table 27 - Summary of CAPEX of the low demand final model

| Component | CapEx [€] |
|-----------------------------|------------------------|
| PV power plant | 1 646 378.00 € |
| Electrolyser | 1 264 367.81 € |
| Compressor | 68 615.37 € |
| Fuel cell | 1 266 535.32 € |
| Battery | 51 007.75 € |
| Hydrogen storage facilities | 7 323 364.00 € |
| Total | 11 620 268.25 € |



■ PV power plant ■ Electrolyser ■ Compressor ■ Fuel cell ■ Battery ■ Hydrogen storage facilities

Figure 107 - Illustration of the distribution of CAPEX for each component of the final model.

Moreover, in Table 28, it is presented the OPEX. This are divided into Operation and Maintenance (O&M) cost of each equipment, the electricity that is spent in the projected power plant that is not directly used in the water electrolysis, and the labour expenses.

Table 28 - Summary of OPEX

| Parameter | | Opex [€/year] | Opex as % of CapEx |
|---------------------------------|-----------------------------|---------------------|--------------------|
| Operation and Maintenance (O&M) | PV power plant | 16 463.78 € | 1% |
| | Electrolyser | 37 931.03 € | 3% |
| | Compressor | 686.15 € | 1% |
| | Fuel cell | 25 330.71 € | 2% |
| | Battery | 510.08 € | 1% |
| | Hydrogen storage facilities | 73 233.64 € | 1% |
| Electricity for plant operation | | 20 095.02 € | |
| Labor costs | | 36 480.00 € | |
| Software and technology costs | | - | |
| Total | | 210 730.41 € | |

The O&M costs are determined as a percentage of the CAPEX. These values have resulted from the manufacturers' guidance, which has already been presented in the model description. For electricity, it is obtained from two different sources with distinct prices: the PV system and the electrical grid. This information can be found in Table 30.

Regarding the electricity expenses associated with the PV system, it is used the Levelized Cost of Electricity (LCOE) specific for the projected PV installation that is 0.0443 €/kWh. While the cost of electrical energy from the grid is estimated by a weighted average of the prices of the peak hour, off-peak hour and full hour given to an industrial consumer. The importance of each tariff period in the final price of grid electricity depends on when the highest electricity consumption occurs in the modelled scenario. Given that this period occurs between 7:00 AM and 6:00 PM, peak and full hours have a greater weight in the average price, representing 21% and 57%, respectively. This can be verified in Table 29. Therefore, the weighted price of grid electricity is 0.145 €/kWh.

Table 29 - Calculation of the weighted average price of electricity

| Hour | Price [€/kWh] | Number of hours [h] | % Weight | Weighted Price |
|-----------------------------------|---------------|---------------------|----------|----------------|
| Off-peak [00h-7h] | 0.235 € | 3 | 25% | 0.145 € |
| Peak [9:15h-12:15h] | 0.116 € | 8 | 67% | |
| Full [7h-9:15h and 12:15h-00h] | 0.102 € | 1 | 8% | |
| Total | | 12 | | |

Table 30 - Price of electricity and deionized water

| Price of deionized water [€/kg] | Price of renewable electricity [€/kWh] | Price of grid electricity [€/kWh] |
|---------------------------------|--|-----------------------------------|
| 0.01 | 0.0443 | 0.124 |

In order to gain a comprehensive understanding of electricity expenses, Table 31 presents a breakdown of consumption by component and the corresponding energy source responsible for meeting these demands.

Table 31 - Electricity demand by components and its supply source

| Component | Source | Total consumption of electrical energy [kWh] |
|----------------------|-----------------|--|
| Eletrolisador | PV | 2366400 |
| | Electrical Grid | 38622 |
| Remaining components | PV | 31518 |
| | Electrical Grid | 121890 |
| Industry | PV | 1506800 |
| | Electrical Grid | 1632.2 |

With regard to labour costs, this pertains to the salaries of four individuals essential for the correct operation of the power plant. Furthermore, it should be noted that the costs of the software used in the designed model are not considered in the economic analysis due to their reduced significance compared to other expenses.

Finally, the COGS is presented in Table 32, which, as previously explained, comprises the direct costs of water electrolysis.

Table 32– Annual COGS

| Cost of Goods Sold (COGS) [€/year] | |
|------------------------------------|---------------------|
| Deionized water | 6 007.65 € |
| Electricity | 173 230.72 € |
| Total | 179 238.37 € |

It can be observed that there are only two expenses, which are deionized water and PV electricity. Concerning the deionized water, the price is set at 0.01 €/kg_{H₂O}. This value is an estimate resulting from a middle-ground approach, as there is no available information on the price of deionized water for large quantities. This approach involved finding a midpoint between the price of deionized water for smaller amounts and the price of tap water. The quantity of water needed in this operation corresponds to 13.87 kg_{H₂O}/kg_{H₂} (Table 33). The PV energy is calculated based on the LCOE, as already was explained.

Table 33 - Water required in one year of hydrogen production

| Total of water consumption [kg] | Total of hydrogen produced [kg] | Water consumption [kgH ₂ O/H ₂] |
|---------------------------------|---------------------------------|--|
| 600765 | 43314 | 13.87 |

6.2 Revenues

The revenues can be divided into the hydrogen and PV electricity sell. In the context of the hydrogen selling price, market research was conducted, which led to the consideration of a selling price of 38 €/kg_{H₂}. The hydrogen is packaged in rechargeable 50-liter steel cylinders. Regarding the selling price of electricity, it was determined based on the average annual price provided by OMIE, which is 93.45 €/MWh. It is worth nothing that the OMIE is the electricity market operator responsible for managing the daily and intraday electricity market in the Iberian Peninsula. G

Table 34 presents the annual revenues originated by the system. The disparity in income originating from the two products is evident. This discrepancy is a result of the limited electrical energy injected into the grid, as previously analysed.

Furthermore, it should be noted that the hydrogen available for sale does not account for the total amount produced. In other words, the hydrogen for sale corresponds to the remaining hydrogen that was not utilized to fulfil the industry energy requirements.

Table 34 - Revenues originated by the sale of hydrogen and PV electricity

| Hydrogen to sell [kg] | Hydrogen price [€/kg] | Revenue [€/year] |
|-----------------------|-----------------------|------------------|
| 19156 | 38.00 € | 727 928.00 € |

| Electricity [€/kWh] - OMIE | Electricity injected into the grid [kWh] | Revenue [€/year] |
|----------------------------|--|------------------|
| 0.09345 € | 5230.8 | 488.82 € |

6.3 Calculation of avoided costs

In order to determine the avoided costs, it was considered the savings resulting from the replacement of a conventional natural gas thermoelectric plant, that meet the industrial facility energy demand, by the projected PV power plant with hydrogen production. The economic study takes into account both the initial costs and the additional expenses specific to this type of power plant. It is worth mentioning that the natural gas power plant is projected to produce the electrical energy equivalent to the electricity that is consumed in the projected model, with its peak power being 2 MW. Since the projected PV power plant with hydrogen production is a renewable energy system, the fuel costs are avoided.

In Table 35 are presented all the natural gas power plant expenses, which are divided in a similar way as it was presented for the modelled power plant. It is represented the CAPEX, secondly the OPEX and COGS.

Table 35 - Representation of the CAPEX, OPEX and COGS for the natural gas power plant

| Component | CapEx [€] | Parameter | Opex [€/year] | Opex as % of CapEx |
|------------------------------------|----------------|--|---------------------|--------------------|
| Natural Gas Power Plant | 2 000 000.00 € | Fixed Operation and Maintenance (O&M) | 60 000.00 € | 3% |
| | | Variable Operation and Maintenance (O&M) | 20 000.00 € | 1% |
| | | Labour costs | 51 840.00 € | |
| | | Total | 131 840.00 € | |
| Cost of Goods Sold (COGS) [€/year] | | | | |
| Natural Gas | 774 671.94 € | | | |

To the initial investment of 1000 €/kW of the power plant, which was based on the (Marcial, 2023). In the context of operational expenditures, these can be divided into Operation and maintenance costs, determined as a percentage of the capital expenditure, the labour costs of employment of six individuals, and a fee that is incurred due to carbon emissions. This fee is 23.9€/ton_{CO₂}, calculated based on an emission performance of 0.23 kg_{CO₂}/kWh, as published in the Portuguese legislation under the Decree nº 17313/2008 (Diário Da República, 2.a Série-N.o 122, 2008). Furthermore, Table 36 depicts the estimated carbon dioxide emissions for one year of power plant production.

Table 36 - Carbon dioxide emissions for one year of operation

| | |
|--|----------|
| CO2 Taxe [€/tonCO2] | 23.90 € |
| Emissions performance [kg/kWh] | 0.23 |
| Total CO2 emissions [tons/per year] | 1025.547 |
| Cost of CO2 emissions [€/year] | 235.88 € |

Finally, we present the cost of goods sold, which consists solely of natural gas, the primary fuel for the power plant. In Table 37, can be find the data related to the annual acquisition of the required kilograms of natural gas. The price of natural gas is set at 0.0834 €/kWh_{NG}, and it is based in the report (Observatório Da Energia et al., 2023), which is in compliance with Regulation (EU) 2016/1952.

Table 37 - Natural gas operating costs

| | |
|---|-------------|
| Price of Natural Gas [€/kWh] | 0.0834 |
| Energy Demand [kWh] | 4458900 |
| PCI of Natural Gas [kWh/kg] | 13 |
| Required Natural Gas [kg/year] | 714567.3077 |
| Natural Gas Power Plant Efficiency | 48% |

6.4 Analysis of economic viability

To have complete compression of the economic viability of the modelled project, it is calculated the Net Present Value (NPV) and the Internal Rate of Return (IRR). For these matters, the project economic study must be fully described, as it presented in Table 38.

The interest rate can be approximated as the nominal rate of return (i.e., the interest rate) minus the inflation rate (approximately 3.6% in Portugal for September 2023), plus owners' risk factor and correction for the method of compounding.

Table 38 - Economic study characterization

| Data | |
|--------------------|----|
| Lifetime [years] | 30 |
| Interest rate (ie) | 7% |

Moreover, it was performed the organization of the cash flows which are based on the expenses and revenues already presented. In investment year, only the capital expenditure of the projected modelled is taken into account. For the subsequent years, the parcels can be divided in positive and negative values. The operating expenditures and the cost of goods sold of the renewable power plant are assumed to be constant values and are represented as negative terms. The revenues are assumed to remain constant throughout the study years and are treated as positive income. Similarly, expenses associated with the natural gas power plant are considered as avoided costs. Additionally, the initial investment in the natural gas power plant generates a depreciation term equivalent to ten percent of the initial value, which is a constant positive factor in the cash flow calculation.

The NPV and the IRR are calculated according to equation (56) and (57), respectively. It is worth mentioning that the calculation of the two economic indicators was performed using MS Excel NPV and IRR functions.

$$NPV = \sum_{t=0}^{30} \frac{CF_t}{(1+c)^t} \quad (56)$$

$$IRR = \left(\frac{Future\ value}{Present\ value} \right)^{\frac{1}{Lifetime}} - 1 \quad (57)$$

As can be seen in Table 39, the NPV is, approximately, 5.2 million of euros, which means that the value of expected cash inflows is higher than the total present value of the initial investment and ongoing costs. Regarding the Internal Rate of Return, it is 11%, which is higher than the interest rate. Therefore, the project is likely to generate returns that surpass its initial costs, representing a financially appealing investment.

Table 39 - NPV and the IRR of the project

| NPV | IRR |
|----------------|------------|
| 5 236 134.69 € | 11% |

7. CONCLUSIONS AND PROSPECTS FOR FUTURE WORK

7.1 Conclusions

In the European context, sustainability takes centre stage, with active involvement from European countries in numerous protocols and initiatives. Notably, The European Green Deal stands as a substantial sustainability plan, backed by a one-trillion-euro investment to combat climate change, stimulate economic growth, and establish sustainable energy resource management. This steadfast commitment is demonstrated by investments in renewable energy, improved energy efficiency, decarbonization, and reduced reliance on fossil fuels, positioning Europe at the forefront of sustainable development initiatives.

In order to implement and achieve these sustainable objectives and policies, it is essential to address the harnessing of renewable energy and mitigate its volatility. In this context, hydrogen, which is the most prevalent element on Earth, emerges as a promising solution to address renewable instability. Its remarkable properties enable it to function as a versatile energy storage medium, adaptable for daily to seasonal energy demands. This adaptability positions hydrogen as a valuable asset in mitigating electricity instability and advancing renewable energy integration.

In this regard, it was developed a thermodynamic model which couples a renewable power plant with hydrogen production and storage facilities was studied, with the primary objective of maximizing the utilization of all generated renewable energy while minimizing the need to purchase energy from the grid. To achieve this, comprehensive research into the entire hydrogen value chain was required to design the aforementioned installation.

The principal objective of this study, which was maximize the utilization of renewable energy, has been successfully realized, with the final model injecting into the electrical grid a comparatively small fraction of the total energy produced by the PV power plant. To be precise, only 0.14% of the renewable energy is integrated into the grid.

Additionally, the industry exhibits a significantly reduced reliance on the grid, accounting for merely 0.08% of its energy needs sourced from the grid. Consequently, it can be deduced that the model demonstrates commendable thermodynamic performance, achieving the seasonal storage of renewable energy.

To achieve the aforementioned results, a sensitivity analysis was conducted on certain model components, such as the electrolyser. This analysis provided a deeper insight into its response to the proposed scenario and contributed to refining the model implementation.

In economic terms, the developed model demonstrates very attractive when compared to a natural gas power plant. This is evident through a substantial positive net present value and an internal rate of return that surpasses the chosen interest rate. Furthermore, it was verified that a significant portion of this favourable economic evaluation is attributed to the sale of the produced hydrogen generated from the surplus energy of the renewable power plant.

7.2 Prospects for future work

Regardless the initial objectives have been achieved, there remain certain matters that warrant further investigation in the context of future work, which are depicted in the following points:

1. Perform a delved and meticulous study about the connection between the electrolyser and the PV power plant to increase its efficiency.
2. Undertake an economical and technical evaluation of the possibility to store the produced hydrogen in a geological cavern and compare it with the presented storage solution.
3. Conduct a more comprehensive investigation into the impact of the electrolyser's power range on the utilization of PV energy.
4. Employ a mathematical model to individually optimize each component of the proposed system, aiming to enhance their performance in this specific application.
5. Conduct a comprehensive economic analysis of the system and the involved factors with the aim of reducing expenditures.

REFERENCES

- ABB group. (2023, July 13). *Solar string combiner boxes*. <https://New.Abb.Com/Low-Voltage/Products/Enclosures/Solar-Combiners>.
- Abdelkareem, M. A., Elsaid, K., Wilberforce, T., Kamil, M., Sayed, E. T., & Olabi, A. (2021). Environmental aspects of fuel cells: A review. *Science of the Total Environment*, 752. <https://doi.org/10.1016/j.scitotenv.2020.141803>
- AIChE Academy. (2020). *Hydrogen Safety: Transport*. https://www.youtube.com/watch?v=3ChDyDLpnfw&ab_channel=AIChEAcademy
- Al-Qahtani, A., Parkinson, B., Hellgardt, K., Shah, N., & Guillen-Gosalbez, G. (2021a). Uncovering the true cost of hydrogen production routes using life cycle monetisation. *Applied Energy*, 281. <https://doi.org/10.1016/j.apenergy.2020.115958>
- Al-Qahtani, A., Parkinson, B., Hellgardt, K., Shah, N., & Guillen-Gosalbez, G. (2021b). Uncovering the true cost of hydrogen production routes using life cycle monetisation. *Applied Energy*, 281. <https://doi.org/10.1016/j.apenergy.2020.115958>
- Amin, M., Shah, H. H., Fareed, A. G., Khan, W. U., Chung, E., Zia, A., Rahman Farooqi, Z. U., & Lee, C. (2022). Hydrogen production through renewable and non-renewable energy processes and their impact on climate change. In *International Journal of Hydrogen Energy* (Vol. 47, Issue 77, pp. 33112–33134). Elsevier Ltd. <https://doi.org/10.1016/j.ijhydene.2022.07.172>
- Amireh, S. F., Heineman, N. N., Vermeulen, P., Barros, R. L. G., Yang, D., van der Schaaf, J., & de Groot, M. T. (2023). Impact of power supply fluctuation and part load operation on the efficiency of alkaline water electrolysis. *Journal of Power Sources*, 560. <https://doi.org/10.1016/j.jpowsour.2023.232629>
- Banerjee, B. (1998). *An Assessment of High Performance AC Motor Drives Versus DC Motor Drives*. www.epri.com
- Bauer, F. (1988). *Valve Losses in Reciprocating Compressors*. <https://docs.lib.purdue.edu/icec>
- Bavane, V., Nawale, V., & Ingle, N. (2023). *Fuel Cell Based Future Power Supply for Remote Locations Protection of Crops from Wild Animals Using Intelligent Surveillance System View project International Journal of Scientific Research in Engineering and Management (IJSREM) Fuel Cell Based Future Power Supply for Remote Locations*. <https://www.researchgate.net/publication/370983255>

- Blaabjerg, F., Chen, Z., & Kjaer, S. B. (2004). Power electronics as efficient interface in dispersed power generation systems. *IEEE Transactions on Power Electronics*, *19*(5), 1184–1194. <https://doi.org/10.1109/TPEL.2004.833453>
- Boldrin, P., & Brandon, N. P. (2019). Progress and outlook for solid oxide fuel cells for transportation applications. In *Nature Catalysis* (Vol. 2, Issue 7, pp. 571–577). Nature Publishing Group. <https://doi.org/10.1038/s41929-019-0310-y>
- Bondarenko, V. L., Ilyinskaya, D. N., Kazakova, A. A., Kozlovsev, P. S., Lavrov, N. A., & Razenko, E. A. (2022). Hydrogen Storage. *Chemical and Petroleum Engineering*, *57*(11–12), 1026–1032. <https://doi.org/10.1007/s10556-022-01041-z>
- Brauns, J., & Turek, T. (2020). Alkaline water electrolysis powered by renewable energy: A review. In *Processes* (Vol. 8, Issue 2). MDPI AG. <https://doi.org/10.3390/pr8020248>
- Brouwer, J. (2010). On the role of fuel cells and hydrogen in a more sustainable and renewable energy future. *Current Applied Physics*, *10*(2 SUPPL.). <https://doi.org/10.1016/j.cap.2009.11.002>
- Brun, K., & Kurz, R. (2019). *Compression Machinery for Oil and Gas*.
- Calzada-Lara, G., & Álvarez, J. (2015). Reduced energy consumption in induction motors with possible mechatronic applications. *Mechanisms and Machine Science*, *25*, 219–228. https://doi.org/10.1007/978-3-319-09858-6_21
- Cohen, A. J., Brauer, M., Burnett, R., Anderson, H. R., Frostad, J., Estep, K., Balakrishnan, K., Brunekreef, B., Dandona, L., Dandona, R., Feigin, V., Freedman, G., Hubbell, B., Jobling, A., Kan, H., Knibbs, L., Liu, Y., Martin, R., Morawska, L., ... Forouzanfar, M. H. (2017). Estimates and 25-year trends of the global burden of disease attributable to ambient air pollution: an analysis of data from the Global Burden of Diseases Study 2015. *The Lancet*, *389*(10082), 1907–1918. [https://doi.org/10.1016/S0140-6736\(17\)30505-6](https://doi.org/10.1016/S0140-6736(17)30505-6)
- Collins Leigh. (2022). *SPECIAL REPORT | Why shipping pure hydrogen around the world might already be dead in the water*. <https://www.rechargenews.com/energy-transition/special-report-why-shipping-pure-hydrogen-around-the-world-might-already-be-dead-in-the-water/2-1-1155434>
- Crespi, E., Colbertaldo, P., Guandalini, G., & Campanari, S. (2022). Energy storage with Power-to-Power systems relying on photovoltaic and hydrogen: modelling the operation with secondary reserve provision. *Journal of Energy Storage*, *55*. <https://doi.org/10.1016/j.est.2022.105613>

- Crosa, G., Lubiano, M., & Trucco, A. (2006). *MODELLING OF PV-POWERED WATER ELECTROLYSERS*. <http://www.asme.org/about-asme/terms-of-use>
- Dawood, F., Anda, M., & Shafiullah, G. M. (2020). Hydrogen production for energy: An overview. In *International Journal of Hydrogen Energy* (Vol. 45, Issue 7, pp. 3847–3869). Elsevier Ltd. <https://doi.org/10.1016/j.ijhydene.2019.12.059>
- Devbalan, I., & Yadav, A. (2022). Green Hydrogen from Green Electricity. *2022 Advances in Science and Engineering Technology International Conferences, ASET 2022*. <https://doi.org/10.1109/ASET53988.2022.9735036>
- Diermann, R. (2020). *Hydrogen can be transported by rail, German railway company says*. <https://www.pv-magazine.com/2020/08/10/hydrogen-can-be-transported-by-rail-german-railway-company-says/>
- Dincer, I., & Acar, C. (2014a). Review and evaluation of hydrogen production methods for better sustainability. *International Journal of Hydrogen Energy*, 40(34), 11094–11111. <https://doi.org/10.1016/j.ijhydene.2014.12.035>
- Dincer, I., & Acar, C. (2014b). Review and evaluation of hydrogen production methods for better sustainability. *International Journal of Hydrogen Energy*, 40(34), 11094–11111. <https://doi.org/10.1016/j.ijhydene.2014.12.035>
- DNV. (2022). *Energy Transition Outlook 2022 - A global and regional forecast to 2050*.
- Energy Agency, I. (2021). *Statistics report Key World Energy Statistics 2021*.
- Environmental Protection Agency, U., Heat, C., & Partnership, P. (2015). *Catalog of CHP Technologies, Section 6. Technology Characterization – Fuel Cells*.
- Ergin Şahin, M. (2020). A photovoltaic powered electrolysis converter system with maximum power point tracking control. *International Journal of Hydrogen Energy*, 45(16), 9293–9304. <https://doi.org/10.1016/j.ijhydene.2020.01.162>
- Escamilla, A., Sánchez, D., & García-Rodríguez, L. (2022). Assessment of power-to-power renewable energy storage based on the smart integration of hydrogen and micro gas turbine technologies. *International Journal of Hydrogen Energy*, 47(40), 17505–17525. <https://doi.org/10.1016/j.ijhydene.2022.03.238>
- European Commission. (2023). *A European Green Deal*. https://commission.europa.eu/strategy-and-policy/priorities-2019-2024/european-green-deal_en

- European Commission. (2018). *A European strategic long-term vision for a prosperous, modern, competitive and climate neutral economy*.
- European Commission. (2019). *The European Green Deal*.
- European Commission. (2020). *A hydrogen strategy for a climate-neutral Europe*. <https://eur-lex.europa.eu/legal-content/EN/TXT/?uri=CELEX%3A52...>
- European Space Agency. (2023). *Technology Readiness Levels (TRL)*. https://www.esa.int/Enabling_Support/Space_Engineering_Technology/Shaping_the_Future/Technology_Readiness_Levels_TRL
- Firak, M., & Djukić, A. (2010). An investigation into the effect of photovoltaic module electric properties on maximum power point trajectory with the aim of its alignment with electrolyzer U-I characteristic. *Thermal Science*, 14(3), 729–738. <https://doi.org/10.2298/TSCI1003729F>
- Fonseca, J. D., Camargo, M., Commenge, J. M., Falk, L., & Gil, I. D. (2019). Trends in design of distributed energy systems using hydrogen as energy vector: A systematic literature review. *International Journal of Hydrogen Energy*, 9486–9504. <https://doi.org/10.1016/j.ijhydene.2018.09.177>
- Forghani, K., Kia, R., & Nejatbakhsh, Y. (2023). A multi-period sustainable hydrogen supply chain model considering pipeline routing and carbon emissions: The case study of Oman. *Renewable and Sustainable Energy Reviews*, 173. <https://doi.org/10.1016/j.rser.2022.113051>
- Frankowska, M., Rzczycki, A., Sowa, M., & Drożdż, W. (2023). Functional Model of Power Grid Stabilization in the Green Hydrogen Supply Chain System—Conceptual Assumptions. *Energies*, 16(1). <https://doi.org/10.3390/en16010154>
- Fuel Cells and Hydrogen 2 Joint Undertaking. (2019). *A sustainable pathway for the European energy transition - Hydrogen roadmap (Europe)*. <https://doi.org/10.2843/249013>
- Furui CIT. (2022). *Cryogenic Road Tanker*. https://en.frcit.cn/product/Cryogenic-Road-Tanker-704.html?gclid=CjwKCAjwtuOIBhBREiwA7agf1mIJDOQbEGzBZ6szdep3rBxS3RhjPCRuRRd8YYFPvJ4Q1XO8b5q1RoCduYQAvD_BwE
- Galli, S. (1997). *SAPHYS Project-Development and Testing of a Stand-Alone Photovoltaic HYdrogen energy System-Final Report View project Solid Polymer Electrolyte Fuel cells View project*. <https://doi.org/10.13140/RG.2.2.30307.58406>

- García-Valverde, R., Miguel, C., Martínez-Béjar, R., & Urbina, A. (2008). Optimized photovoltaic generator-water electrolyser coupling through a controlled DC-DC converter. *International Journal of Hydrogen Energy*, 33(20), 5352–5362. <https://doi.org/10.1016/j.ijhydene.2008.06.015>
- Garrigós, A., Lizán, J. L., Blanes, J. M., & Gutiérrez, R. (2014). Combined maximum power point tracking and output current control for a photovoltaic-electrolyser DC/DC converter. *International Journal of Hydrogen Energy*, 39(36), 20907–20919. <https://doi.org/10.1016/j.ijhydene.2014.10.041>
- Gechev, T., & Punov, P. (2022). *Popular Fuel Cell Types-A Brief Review*. <https://www.researchgate.net/publication/359732890>
- Germescheidt, R. L., Moreira, D. E. B., Yoshimura, R. G., Gasbarro, N. P., Datti, E., dos Santos, P. L., & Bonacin, J. A. (2021). Hydrogen Environmental Benefits Depend on the Way of Production: An Overview of the Main Processes Production and Challenges by 2050. *Advanced Energy and Sustainability Research*, 2(10), 2100093. <https://doi.org/10.1002/aesr.202100093>
- Gonzalez, C. (2017). *What's the Difference between AC, DC, and EC Motors?*
- Guilbert, D., Collura, S. M., & Scipioni, A. (2017). DC/DC converter topologies for electrolyzers: State-of-the-art and remaining key issues. In *International Journal of Hydrogen Energy* (Vol. 42, Issue 38, pp. 23966–23985). Elsevier Ltd. <https://doi.org/10.1016/j.ijhydene.2017.07.174>
- Guilbert, D., Sorbera, D., & Vitale, G. (2020). A stacked interleaved DC-DC buck converter for proton exchange membrane electrolyzer applications: Design and experimental validation. *International Journal of Hydrogen Energy*, 45(1), 64–79. <https://doi.org/10.1016/j.ijhydene.2019.10.238>
- Hadi Tawil, I., & Hareb, F. (2008). *FUEL CELLS –THE ENERGY KEY OF FUTURE - Review and Prospective Study*. <https://www.researchgate.net/publication/323401704>
- Haseli, Y. (2018). Maximum conversion efficiency of hydrogen fuel cells. *International Journal of Hydrogen Energy*, 43(18), 9015–9021. <https://doi.org/10.1016/j.ijhydene.2018.03.076>
- Hassan, I. A., Ramadan, H. S., Saleh, M. A., & Hissel, D. (2021). Hydrogen storage technologies for stationary and mobile applications: Review, analysis and perspectives. In *Renewable*

- and Sustainable Energy Reviews* (Vol. 149). Elsevier Ltd.
<https://doi.org/10.1016/j.rser.2021.111311>
- He, G., Mallapragada, D. S., Bose, A., Heuberger, C. F., & Gencer, E. (2021). Hydrogen supply chain planning with flexible transmission and storage scheduling. *IEEE Transactions on Sustainable Energy*, 12(3), 1730–1740. <https://doi.org/10.1109/TSTE.2021.3064015>
- Hollingsworth, J., Phillippi, G., Hinchliff, M., Kulhanek, C., Rimpel, A. M., & Maywald, F. (2018). Reciprocating compressors. In *Compression Machinery for Oil and Gas* (pp. 167–252). Elsevier. <https://doi.org/10.1016/B978-0-12-814683-5.00005-5>
- Howarth, R. W., & Jacobson, M. Z. (2021). How green is blue hydrogen? *Energy Science and Engineering*, 9(10), 1676–1687. <https://doi.org/10.1002/ese3.956>
- Huang, E. (2022). Design of Hydrogen Fuel Cell: Methods to Higher Efficiency. In *Highlights in Science, Engineering and Technology GEMFE* (Vol. 2022).
- Hussain, C. (2021). Renewable hydrogen production by water electrolysis. In *Sustainable Fuel Technologies Handbook* (pp. i–iii). Elsevier. <https://doi.org/10.1016/b978-0-12-822989-7.00021-4>
- IEA. (2023). *Carbon Capture, Utilisation and Storage*. <https://www.iea.org/energy-system/carbon-capture-utilisation-and-storage>
- IEA. (2019a). *The Future of Hydrogen*.
- IEA. (2019b). *The Future of Hydrogen (Seizing today's opportunities)*.
- IEA. (2021). *Global Hydrogen Review 2021*. www.iea.org/t&c/
- IEA. (2022). *Global Hydrogen Review 2022*. www.iea.org/t&c/
- IEEE Staff. (2019). *2019 International Conference on Electrical, Electronics and Computer Engineering (UPCON)*. IEEE.
- India Hydrogen Alliance. (2021). *Hydrogen Storage and Transport*. <https://ih2a.com/workgroup-2-hydrogen-storage-and-transport/>
- IPCC. (2019). *Global Warming of 1.5°C*.
- IRENA. (2021). *WORLD ENERGY TRANSITIONS OUTLOOK 1.5° C PATHWAY*. www.irena.org
- Jiang, H., Qi, B., Du, E., Zhang, N., Yang, X., Yang, F., & Wu, Z. (2022). Modeling Hydrogen Supply Chain in Renewable Electric Energy System Planning. *IEEE Transactions on Industry Applications*, 58(2), 2780–2791. <https://doi.org/10.1109/TIA.2021.3117748>
- Kang, H., Hong, T., Jung, S., & Lee, M. (2019). Techno-economic performance analysis of the smart solar photovoltaic blinds considering the photovoltaic panel type and the solar

- tracking method. *Energy and Buildings*, 193, 1–14.
<https://doi.org/10.1016/j.enbuild.2019.03.042>
- Khlifi, Z., & Toukebri, Y. (2022). *Fuel Cells: Operating Principle & Energy Issues*.
- Kim, A., Kim, H., Choe, C., & Lim, H. (2023). Feasibility of offshore wind turbines for linkage with onshore green hydrogen demands: A comparative economic analysis. *Energy Conversion and Management*, 277. <https://doi.org/10.1016/j.enconman.2023.116662>
- Kojima, H., Nagasawa, K., Todoroki, N., Ito, Y., Matsui, T., & Nakajima, R. (2023). Influence of renewable energy power fluctuations on water electrolysis for green hydrogen production. In *International Journal of Hydrogen Energy* (Vol. 48, Issue 12, pp. 4572–4593). Elsevier Ltd. <https://doi.org/10.1016/j.ijhydene.2022.11.018>
- Kotowicz, J., Bartela, Ł., Węcel, D., & Dubiel, K. (2017). Hydrogen generator characteristics for storage of renewably-generated energy. *Energy*, 118, 156–171.
<https://doi.org/10.1016/j.energy.2016.11.148>
- Kotowicz, J., Węcel, D., & Jurczyk, M. (2018). Analysis of component operation in power-to-gas-to-power installations. *Applied Energy*, 216, 45–59.
<https://doi.org/10.1016/j.apenergy.2018.02.050>
- Kovač, A., Paranos, M., & Marciuš, D. (2021). Hydrogen in energy transition: A review. *International Journal of Hydrogen Energy*, 46(16), 10016–10035.
<https://doi.org/10.1016/j.ijhydene.2020.11.256>
- Kyodo. (2023). *Japan to invest ¥15 trillion in hydrogen supply for decarbonization*.
<https://www.japantimes.co.jp/news/2023/06/06/business/economy-business/hydrogen-supply-investment-plan/>
- Lagioia, G., Spinelli, M. P., & Amicarelli, V. (2023). Blue and green hydrogen energy to meet European Union decarbonisation objectives. An overview of perspectives and the current state of affairs. In *International Journal of Hydrogen Energy* (Vol. 48, Issue 4, pp. 1304–1322). Elsevier Ltd. <https://doi.org/10.1016/j.ijhydene.2022.10.044>
- Lal, A., & You, F. (2023). Targeting climate-neutral hydrogen production: Integrating brown and blue pathways with green hydrogen infrastructure via a novel superstructure and simulation-based life cycle optimization. *AIChE Journal*, 69(1).
<https://doi.org/10.1002/aic.17956>
- Lee, H., Choe, B., Lee, B., Gu, J., Cho, H. S., Won, W., & Lim, H. (2022). Outlook of industrial-scale green hydrogen production via a hybrid system of alkaline water electrolysis and

- energy storage system based on seasonal solar radiation. *Journal of Cleaner Production*, 377. <https://doi.org/10.1016/j.jclepro.2022.134210>
- Li, C., Liu, Y., Xu, B., & Ma, Z. (2019). Finite time thermodynamic optimization of an irreversible proton exchange membrane fuel cell for vehicle use. *Processes*, 7(7). <https://doi.org/10.3390/pr7070419>
- Li, P., Li, G., Liu, J., Su, H., Han, X., & Han, Z. (2023). Performance comparison and multi-objective optimization of improved and traditional compressed air energy storage systems integrated with solar collectors. *Journal of Energy Storage*, 58. <https://doi.org/10.1016/j.est.2022.106149>
- Li, R., & Kawanami, H. (2023). A Recent Review of Primary Hydrogen Carriers, Hydrogen Production Methods, and Applications. *Catalysts*, 13(3), 562. <https://doi.org/10.3390/catal13030562>
- Luo, Z., Wang, X., Wen, H., & Pei, A. (2022). Hydrogen production from offshore wind power in South China. *International Journal of Hydrogen Energy*, 47(58), 24558–24568. <https://doi.org/10.1016/j.ijhydene.2022.03.162>
- Ma, Y., He, Z., Peng, X., & Xing, Z. (2012). Experimental investigation of the discharge valve dynamics in a reciprocating compressor for trans-critical CO₂ refrigeration cycle. *Applied Thermal Engineering*, 32(1), 13–21. <https://doi.org/10.1016/j.applthermaleng.2011.03.022>
- Marcial, O. (2023). *B. Combined Cycle GT (CCGT)*.
- Maroufmashat, A., & Fowler, M. (2017). Transition of future energy system infrastructure; through power-to-gas pathways. In *Energies* (Vol. 10, Issue 8). MDPI AG. <https://doi.org/10.3390/en10081089>
- Martínez-García, E., Blanco-Marigorta, E., Parrondo Gayo, J., & Navarro-Manso, A. (2021). Influence of inertia and aspect ratio on the torsional galloping of single-axis solar trackers. *Engineering Structures*, 243. <https://doi.org/10.1016/j.engstruct.2021.112682>
- Matute, G., Yusta, J. M., Beyza, J., & Correas, L. C. (2021). Multi-state techno-economic model for optimal dispatch of grid connected hydrogen electrolysis systems operating under dynamic conditions. *International Journal of Hydrogen Energy*, 46(2), 1449–1460. <https://doi.org/10.1016/j.ijhydene.2020.10.019>
- Matute, G., Yusta, J. M., Beyza, J., & Monteiro, C. (2022). Optimal dispatch model for PV-electrolysis plants in self-consumption regime to produce green hydrogen: A Spanish

- case study. *International Journal of Hydrogen Energy*, 47(60), 25202–25213. <https://doi.org/10.1016/j.ijhydene.2022.05.270>
- Mccovern, J. A. (1988). *Performance Characteristics of a Reciprocating Refrigerant Compressor Over a Range of Speeds*. <https://docs.lib.purdue.edu/icec>
- Moradpoor, I., Syri, S., & Santasalo-Aarnio, A. (2023). Green hydrogen production for oil refining – Finnish case. *Renewable and Sustainable Energy Reviews*, 175. <https://doi.org/10.1016/j.rser.2023.113159>
- MOREDAY SOLAR. (2023, July 13). *DC COMBINER BOX*. <https://www.moreday.com/moreday-solar-dc-6-in-1-out-6-strings-600v-1000v-ip65-dc-combiner-box-pv-solar-combiner-box-product/>.
- Nami, H., Rizvandi, O. B., Chatzichristodoulou, C., Hendriksen, P. V., & Frandsen, H. L. (2022). Techno-economic analysis of current and emerging electrolysis technologies for green hydrogen production. *Energy Conversion and Management*, 269. <https://doi.org/10.1016/j.enconman.2022.116162>
- Nguyen, N. (2023). *Hydrogen Blending as a Pathway Toward U.S. Decarbonization*. <https://www.nrel.gov/news/program/2023/hydrogen-blending-as-a-pathway-toward-u.s.-decarbonization.html>
- Noussan, M., Raimondi, P. P., Scita, R., & Hafner, M. (2021). The role of green and blue hydrogen in the energy transition—a technological and geopolitical perspective. In *Sustainability (Switzerland)* (Vol. 13, Issue 1, pp. 1–26). MDPI AG. <https://doi.org/10.3390/su13010298>
- Observatório Da Energia, DGEG, & ADENE. (2023). *Energia em Números*.
- Palys, M. J., & Daoutidis, P. (2022). Power-to-X: A review and perspective. *Computers and Chemical Engineering*, 165. <https://doi.org/10.1016/j.compchemeng.2022.107948>
- Panarello, D., & Gatto, A. (2023). Decarbonising Europe – EU citizens’ perception of renewable energy transition amidst the European Green Deal. *Energy Policy*, 172. <https://doi.org/10.1016/j.enpol.2022.113272>
- Paul, B., & Andrews, J. (2008). Optimal coupling of PV arrays to PEM electrolyzers in solar-hydrogen systems for remote area power supply. *International Journal of Hydrogen Energy*, 33(2), 490–498. <https://doi.org/10.1016/j.ijhydene.2007.10.040>
- Phan Van, L., Hieu Hoang, L., & Nguyen Duc, T. (2023). A comprehensive review of direct coupled photovoltaic-electrolyser system: Sizing techniques, operating strategies,

- research progress, current challenges, and future recommendations. In *International Journal of Hydrogen Energy*. Elsevier Ltd. <https://doi.org/10.1016/j.ijhydene.2023.03.257>
- Pinsky, R., Sabharwall, P., Hartvigsen, J., & O'Brien, J. (2020). Comparative review of hydrogen production technologies for nuclear hybrid energy systems. In *Progress in Nuclear Energy* (Vol. 123). Elsevier Ltd. <https://doi.org/10.1016/j.pnucene.2020.103317>
- Recupera. (n.d.). *Recupera: About us*. Recupera - About Us. Retrieved July 18, 2023, from <http://www.recupera.si/eng/>
- Reuß, M., Grube, T., Robinius, M., Preuster, P., Wasserscheid, P., & Stolten, D. (2017). Seasonal storage and alternative carriers: A flexible hydrogen supply chain model. *Applied Energy*, 200, 290–302. <https://doi.org/10.1016/j.apenergy.2017.05.050>
- Riera, J. A., Lima, R. M., & Knio, O. M. (2023a). A review of hydrogen production and supply chain modeling and optimization. In *International Journal of Hydrogen Energy*. Elsevier Ltd. <https://doi.org/10.1016/j.ijhydene.2022.12.242>
- Riera, J. A., Lima, R. M., & Knio, O. M. (2023b). A review of hydrogen production and supply chain modeling and optimization. In *International Journal of Hydrogen Energy*. Elsevier Ltd. <https://doi.org/10.1016/j.ijhydene.2022.12.242>
- Rosli, R. E., Sulong, A. B., Daud, W. R. W., Zulkifley, M. A., Husaini, T., Rosli, M. I., Majlan, E. H., & Haque, M. A. (2017). A review of high-temperature proton exchange membrane fuel cell (HT-PEMFC) system. *International Journal of Hydrogen Energy*, 42(14), 9293–9314. <https://doi.org/10.1016/j.ijhydene.2016.06.211>
- Salas, V., Olías, E., Barrado, A., & Lázaro, A. (2006). Review of the maximum power point tracking algorithms for stand-alone photovoltaic systems. In *Solar Energy Materials and Solar Cells* (Vol. 90, Issue 11, pp. 1555–1578). <https://doi.org/10.1016/j.solmat.2005.10.023>
- Saur, G., & Ramsden, T. (2011). *Wind Electrolysis: Hydrogen Cost Optimization*. <http://www.osti.gov/bridge>
- Sazali, N. (2020). Emerging technologies by hydrogen: A review. In *International Journal of Hydrogen Energy* (Vol. 45, Issue 38, pp. 18753–18771). Elsevier Ltd. <https://doi.org/10.1016/j.ijhydene.2020.05.021>
- Schneider Electric. (2016).

- Sgarbossa, F., Arena, S., Tang, O., & Peron, M. (2023). Renewable hydrogen supply chains: A planning matrix and an agenda for future research. *International Journal of Production Economics*, 255. <https://doi.org/10.1016/j.ijpe.2022.108674>
- Shiva Kumar, S., & Lim, H. (2022). An overview of water electrolysis technologies for green hydrogen production. In *Energy Reports* (Vol. 8, pp. 13793–13813). Elsevier Ltd. <https://doi.org/10.1016/j.egy.2022.10.127>
- Solar Heat for Industry*. (2017).
- Solar Industry*. (2023, August 21). <https://Solarindustrymag.Com/Sma-Introduces-480-Vac-Interconnection-for-Ground-Mount-Projects>.
- Solar Jinko*. (2023, September 16). <https://Www.Belgiansolar.Be/Wp-Content/Uploads/Simple-File-List/Jinko-300-Mono-Maxim-Silver-Frame.Pdf>.
- Stolzenburg, K., & Mubbala, R. (2013). *Integrated Design for Demonstration of Efficient Liquefaction of Hydrogen (IDEALHY)*.
- T, W. H., & Ch, H. (2012). *Principles for the liquefaction of hydrogen with emphasis on precooling processes*.
- Tajuddin, M. F. N., Arif, M. S., Ayob, S. M., & Salam, Z. (2015). Perturbative methods for maximum power point tracking (MPPT) of photovoltaic (PV) systems: A review. In *International Journal of Energy Research* (Vol. 39, Issue 9, pp. 1153–1178). John Wiley and Sons Ltd. <https://doi.org/10.1002/er.3289>
- Tsuji, T., Oku, T., Ishii, N., Anami, K., Knisely, C. W., Maeda, T., & Yamamoto, A. (2012). Calculated Optimal Mechanical Efficiency of a Large Capacity Reciprocating Compressor. In *International Compressor Engineering Conference at Purdue*. <https://docs.lib.purdue.edu/icec>
- United Nations. (2023). *Conference of the Parties (COP)*. <https://unfccc.int/process/bodies/supreme-bodies/conference-of-the-parties-cop>
- United Nations. (2017). *World Population Prospects (The 2017 Revision)*.
- United Nations. (2022). *The Sustainable Development Goals Report*.
- Von Zuben, T. W., Moreira, D. E. B., Germscheidt, R. L., Yoshimura, R. G., Dorretto, D. S., de Araujo, A. B. S., Salles, A. G., & Bonacin, J. A. (2022a). Is Hydrogen Indispensable for a Sustainable World? A Review of H₂ Applications and Perspectives for the Next Years. In *Journal of the Brazilian Chemical Society* (Vol. 33, Issue 8, pp. 824–843). Sociedade Brasileira de Quimica. <https://doi.org/10.21577/0103-5053.20220026>

- Von Zuben, T. W., Moreira, D. E. B., Germscheidt, R. L., Yoshimura, R. G., Dorretto, D. S., de Araujo, A. B. S., Salles, A. G., & Bonacin, J. A. (2022b). Is Hydrogen Indispensable for a Sustainable World? A Review of H₂ Applications and Perspectives for the Next Years. In *Journal of the Brazilian Chemical Society* (Vol. 33, Issue 8, pp. 824–843). Sociedade Brasileira de Quimica. <https://doi.org/10.21577/0103-5053.20220026>
- Wang, Y., Chen, K. S., Mishler, J., Cho, S. C., & Adroher, X. C. (2011). A review of polymer electrolyte membrane fuel cells: Technology, applications, and needs on fundamental research. In *Applied Energy* (Vol. 88, Issue 4, pp. 981–1007). Elsevier Ltd. <https://doi.org/10.1016/j.apenergy.2010.09.030>
- Wang, Y., Seo, B., Wang, B., Zamel, N., Jiao, K., & Adroher, X. C. (2020). Fundamentals, materials, and machine learning of polymer electrolyte membrane fuel cell technology. In *Energy and AI* (Vol. 1). Elsevier B.V. <https://doi.org/10.1016/j.egyai.2020.100014>
- Wappler, M., Unguder, D., Lu, X., Ohlmeyer, H., Teschke, H., & Lueke, W. (2022a). Building the green hydrogen market – Current state and outlook on green hydrogen demand and electrolyzer manufacturing. In *International Journal of Hydrogen Energy* (Vol. 47, Issue 79, pp. 33551–33570). Elsevier Ltd. <https://doi.org/10.1016/j.ijhydene.2022.07.253>
- Wappler, M., Unguder, D., Lu, X., Ohlmeyer, H., Teschke, H., & Lueke, W. (2022b). Building the green hydrogen market – Current state and outlook on green hydrogen demand and electrolyzer manufacturing. In *International Journal of Hydrogen Energy* (Vol. 47, Issue 79, pp. 33551–33570). Elsevier Ltd. <https://doi.org/10.1016/j.ijhydene.2022.07.253>
- Węcel, D., Jurczyk, M., Uchman, W., & Skorek-Osikowska, A. (2020). Investigation on system for renewable electricity storage in small scale integrating photovoltaics, batteries, and hydrogen generator. *Energies*, 13(22). <https://doi.org/10.3390/en13226039>
- Winter, C. J. (2005). Into the hydrogen energy economy - Milestones. *International Journal of Hydrogen Energy*, 30(7), 681–685. <https://doi.org/10.1016/j.ijhydene.2004.12.011>
- Wolter, R. (2020). *RWE researches large-scale storage for green electricity in salt caverns*. <https://www.rwe.com/en/press/rwe-gasstorage-west-gmbh/2020-09-30-rwe-researches-large-scale-storage-for-green-electricity-in-salt-caverns/>
- Xu, X., Zhou, Q., & Yu, D. (2022). The future of hydrogen energy: Bio-hydrogen production technology. In *International Journal of Hydrogen Energy*. Elsevier Ltd. <https://doi.org/10.1016/j.ijhydene.2022.07.261>

- Yang, Y., Ma, C., Lian, C., Zhang, Y., & Pang, X. (2021). Optimal power reallocation of large-scale grid-connected photovoltaic power station integrated with hydrogen production. *Journal of Cleaner Production*, 298. <https://doi.org/10.1016/j.jclepro.2021.126830>
- Yodwong, B., Guilbert, D., Phattanasak, M., Kaewmanee, W., Hinaje, M., & Vitale, G. (2020). Faraday's efficiency modeling of a proton exchange membrane electrolyzer based on experimental data. *Energies*, 13(18). <https://doi.org/10.3390/en13184792>
- Zarzycki, R., Kacprzak, A., & Bis, Z. (2018). The use of direct carbon fuel cells in compact energy systems for the generation of electricity, heat and cold. *Energies*, 11(11). <https://doi.org/10.3390/en11113061>
- Zhang, F., Zhao, P., Niu, M., & Maddy, J. (2016). The survey of key technologies in hydrogen energy storage. In *International Journal of Hydrogen Energy* (Vol. 41, Issue 33, pp. 14535–14552). Elsevier Ltd. <https://doi.org/10.1016/j.ijhydene.2016.05.293>
- Zhang, H., Su, S., Lin, G., & Chen, J. (2012). Efficiency Calculation and Configuration Design of a PEM Electrolyzer System for Hydrogen Production Solar cells; Fuel cells; Quantum heat engines; Thermoelectric devices, etc. View project Solar/Thermal energy driven thermoelectric system View project Efficiency Calculation and Configuration Design of a PEM Electrolyzer System for Hydrogen Production. In *Article in International Journal of Electrochemical Science* (Vol. 7). www.electrochemsci.org
- Zou, C., Li, J., Zhang, X., Jin, X., Xiong, B., Yu, H., Liu, X., Wang, S., Li, Y., Zhang, L., Miao, S., Zheng, D., Zhou, H., Song, J., & Pan, S. (2022). *Industrial status, technological progress, challenges, and prospects of hydrogen energy*. <https://doi.org/10.3787/j.issn.1000>

APPENDICES

Appendix 1 – Components of the projected model

In this appendix will be presented illustrations of some components that include the modelled system.



Figure 108 - Example of a Monofacial Si-mono photovoltaic module (Solar Jinko, 2023).

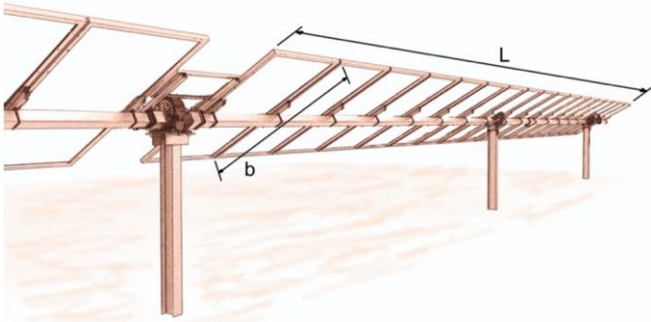


Figure 109 - Architectural design of a single axis's solar tracker. (Martínez-García et al., 2021).



Figure 110 – Example of a string box (Schneider Electric, 2016).



Figure 111 – Illustration of inverter devices (Solar Industry, 2023).



Figure 112 – Illustration of a power transformer.

Appendix 2 – Data base

With the goal of organizing all the input data, an Excel file with multiple spreadsheets is utilized. To elaborate, there exists a spreadsheet for each system component, enabling the incorporation of information concerning maximum flows, power operational range, start-up criteria, power and water consumptions, as well as the potential states of the device. An example of this can be found in Figure 113 and Figure 114.

| Electrolyser Data | | | | | | | | | | |
|-------------------|----------------|---------------------|------------------------|------------------------|--------------|--|--|--------------------------|--|--|
| Technology | Capacity | | | | Minimum load | Power range | | Water Consumption | | |
| | H2 mass output | H2 volume flow rate | Production consumption | Production consumption | | Input Power at maximum (nominal power) | Input Power at minimum (nominal power) | | | |
| | kg/day | Nm ³ /h | kwh/kg | kwh/Nm ³ | % | kWh | kWh | Liters/kg H ₂ | | |
| PEM | | | | | | | | | | |

| Electrolyser State | | | | | | | | | |
|----------------------------|---------------------|-----------------|----------------|------------------------------------|-----------------------------------|---|-------------------------------|------------------------------|--|
| Off Production Consumption | | Data to Start | | | | Criterion for transitioning to production | Number of Starts | | |
| Idle consumption | Standby consumption | Cold Start Time | Hot Start Time | Energy for cold start (transition) | Energy for hot start (transition) | | Maximum number of cold starts | Maximum number of hot starts | |
| kWh | kWh | min | seg | MWh | MWh | x every x hours | x every x hours | | |
| | | | | | | | | | |

Figure 113 - Example of a spreadsheet of the database with information about the electrolyser.

| η eletrolizador | | | | | |
|-----------------|--------------|-----------|-----------|------------------|---------------|
| Electrolyser | η HG (geral) | η voltage | η faraday | η overall energy | η accessories |
| | | | | | |

| Accessories | η pumps | η fan | η cooling system | η heaters | η purification system | η Filter | η separator |
|-------------|---------|-------|------------------|-----------|-----------------------|----------|-------------|
| | | | | | | | |

| Electrolyser efficiency curve | |
|-------------------------------|------------|
| Load ratio | Efficiency |
| x1 | η1 |
| x2 | η2 |
| x3 | η3 |

Figure 114 – Example of an electrolyser efficiency spreadsheet of the database.

Appendix 3 – Photovoltaic resolution methodology

The PV energy yield methodology, calculated by the pvDesign, can be resumed by the following steps:

1. Solar Position Calculation
2. Sun-Tracking Structures (if applicable)
3. Irradiance Conversion
4. PV Module Performance

The output of this methodology is the hourly energy produced by the PV power plant, for a period of one year.

Appendix 4 – Economic analysis

Cash flows

Table 40 represents every parameter that is included in the cash flow calculation.

Table 40 - Representation cash flow calculation of the year one and fifteen of the study

| | Year 1 | Year 10 |
|--|----------------|----------------|
| OpEx | - 210 730.41 € | - 210 730.41 € |
| COGS | - 179 238.37 € | - 179 238.37 € |
| Sale of electricity | 488.82 € | 488.82 € |
| Sale of Hydrogen | 727 928.00 € | 727 928.00 € |
| Depreciation of the natural gas plant | 200 000.00 € | - € |
| Avoided Costs/Savings | 906 511.94 € | 906 511.94 € |
| Environmental benefits | 235.88 € | 235.88 € |
| Cash Flow | 1 445 195.85 € | 1 245 195.85 € |

It should be noted that there are two different potential cash flows in the study. Specifically, the difference pertains to the depreciation of the natural gas plant, which becomes zero after ten years.

Moreover, to fully understand the calculation of NPV refer to the cash flows in Table 41.

Table 41 – Representation of annual cash flows in the economic study, and the respective accumulated values

| Year | Cash Flow | Accumulated | Year | Cash Flow | Accumulated |
|------|-------------------|-------------------|------|----------------|---------------|
| 0 | - 11 620 268.25 € | - 11 620 268.25 € | 16 | 1 245 195.85 € | 10 102 865.41 |
| 1 | 1 445 195.85 € | 10 175 072.40 € | 17 | 1 245 195.85 € | 11 348 061.27 |
| 2 | 1 445 195.85 € | 8 729 876.54 € | 18 | 1 245 195.85 € | 12 593 257.12 |
| 3 | 1 445 195.85 € | 7 284 680.69 € | 19 | 1 245 195.85 € | 13 838 452.97 |
| 4 | 1 445 195.85 € | 5 839 484.83 € | 20 | 1 245 195.85 € | 15 083 648.83 |
| 5 | 1 445 195.85 € | 4 394 288.98 € | 21 | 1 245 195.85 € | 16 328 844.68 |
| 6 | 1 445 195.85 € | 2 949 093.13 € | 22 | 1 245 195.85 € | 17 574 040.54 |
| 7 | 1 445 195.85 € | 1 503 897.27 € | 23 | 1 245 195.85 € | 18 819 236.39 |
| 8 | 1 445 195.85 € | 58 701.42 € | 24 | 1 245 195.85 € | 20 064 432.24 |
| 9 | 1 445 195.85 € | 1 386 494.43 € | 25 | 1 245 195.85 € | 21 309 628.10 |
| 10 | 1 245 195.85 € | 2 631 690.29 € | 26 | 1 245 195.85 € | 22 554 823.95 |
| 11 | 1 245 195.85 € | 3 876 886.14 € | 27 | 1 245 195.85 € | 23 800 019.80 |
| 12 | 1 245 195.85 € | 5 122 082.00 € | 28 | 1 245 195.85 € | 25 045 215.66 |
| 13 | 1 245 195.85 € | 6 367 277.85 € | 29 | 1 245 195.85 € | 26 290 411.51 |
| 14 | 1 245 195.85 € | 7 612 473.70 € | 30 | 1 245 195.85 € | 27 535 607.37 |
| 15 | 1 245 195.85 € | 8 857 669.56 € | | | |

It is possible to conclude that past 30 years of the study, the accumulated value is 27 535 607.37 €.

ANNEXES

Annex 1 – Conference of the Parties (COP)

Table 42 - History of Conference of the Parties (COP)

| Location | Session | Conference |
|---|---------|---|
| Sharm el-Sheikh, Egypt | COP 27 | Sharm el-Sheikh Climate Change Conference - November 2022 |
| Glasgow, United Kingdom of Great Britain and Northern Ireland | COP 26 | Glasgow Climate Change Conference – October-November 2021 |
| Madrid, Spain | COP 25 | UN Climate Change Conference - December 2019 |
| Katowice, Poland | COP 24 | Katowice Climate Change Conference – December 2018 |
| Bonn, Germany | COP 23 | UN Climate Change Conference - November 2017 |
| Marrakech, Morocco | COP 22 | Marrakech Climate Change Conference - November 2016 |
| Paris, France | COP 21 | Paris Climate Change Conference - November 2015 |
| Lima, Peru | COP 20 | Lima Climate Change Conference - December 2014 |

| | | |
|-------------------------|--------|--|
| Warsaw, Poland | COP 19 | Warsaw Climate Change Conference - November 2013 |
| Doha, Qatar | COP 18 | Doha Climate Change Conference - November 2012 |
| Durban, South Africa | COP 17 | Durban Climate Change Conference - November 2011 |
| Cancun, Mexico | COP 16 | Cancún Climate Change Conference - November 2010 |
| Copenhagen, Denmark | COP 15 | Copenhagen Climate Change Conference - December 2009 |
| Poznan, Poland | COP 14 | Poznan Climate Change Conference - December 2008 |
| Bali, Indonesia | COP 13 | Bali Climate Change Conference - December 2007 |
| Nairobi, Kenya | COP 12 | Nairobi Climate Change Conference - November 2006 |
| Montreal, Canada | COP 11 | Montreal Climate Change Conference - December 2005 |
| Buenos Aires, Argentina | COP 10 | Buenos Aires Climate Change Conference - December 2004 |

| | | |
|-------------------------|---------|--|
| Milan, Italy | COP 9 | Milan Climate Change Conference - December 2003 |
| New Delhi, India | COP 8 | New Delhi Climate Change Conference - October 2002 |
| Marrakech, Morocco | COP 7 | Marrakech Climate Change Conference - October 2001 |
| Bonn, Germany | COP 6-2 | Bonn Climate Change Conference - July 2001 |
| The Hague, Netherlands | COP 6 | The Hague Climate Change Conference - November 2000 |
| Bonn, Germany | COP 5 | Bonn Climate Change Conference - October 1999 |
| Buenos Aires, Argentina | COP 4 | Buenos Aires Climate Change Conference - November 1998 |
| Kyoto, Japan | COP 3 | Kyoto Climate Change Conference - December 1997 |
| Berlin, Germany | COP 2 | Berlin Climate Change Conference - December 1996 |
| Switzerland, Geneva | COP 1 | Geneva Climate Change Conference - December 1995 |

Annex 2 – Manufacturer's information

Electrolyser

INNOVATIVE PRODUCTS

for your supply of hydrogen.

→ The ME 450/1400 PEM Electrolyser belongs to H-TEC's Series-ME and is currently the most powerful electrolyser for decentralized applications in the megawatt class product range. New designs of the stack and the system allow the H-TEC electrolysers to achieve a very good price-performance ratio, with minimal

production costs for hydrogen. Apart from that, the design of H-TEC's Series-ME offers many advantages. Its compact construction makes its transport, connection and use possible almost anywhere. Thanks to heat extraction, electrolysers made by H-TEC achieve an overall efficiency of up to 95 %.

| Parameter | ME 450/1400 | |
|-----------------------------------|---|-------------------------------------|
| H ₂ nominal production | 450 kg d ⁻¹ | 210 Nm ³ h ⁻¹ |
| H ₂ production range | 25–210 Nm ³ h ⁻¹ | |
| H ₂ purity | 3.0, with adsorption drying: 5.0 | |
| Nominal energy consumption | 4.9 kWh Nm ⁻³ | |
| Nominal load | 1 MW | |
| Electrolyser power | 0.2–1.4 MW | |
| Nominal system efficiency | 74 % | |
| Load change | Partial load to nominal load = 30 s | |
| Heat extraction | max. 65 °C outlet temperature and 55 °C return temperature | |
| Operating pressure H ₂ | unpressurised – 30 bar | |
| Operating pressure O ₂ | unpressurised | |
| Feed water quality | Drinking water, nominal 350 kg h ⁻¹ | |
| Grid connection | Voltage: 3x 400 V/ 50 Hz + N + PE in accordance with IEC 60038. Connected load: 2 MVA | |
| Dimensions | 40' container, approx. – ca. 12 m x 3 m x 3.5 m | |
| Weight | approx. 25 t | |
| Ambient temperature | -15 °C to +35 °C | |

Compressor

| Compressor technical parameters | | | |
|---|---|--------------------|---------|
| Model | D type, water cooling, two cylinders, single acting | | |
| compressed media | Hydrogen | | |
| Model | GD134-212/30-250 | Compression levels | 2-stage |
| Condition | Rated condition | | |
| Rated flow Nm ³ /h | 212 | | |
| Inlet pressure MPa (G) | 3.0 | | |
| Exhaust pressure MPa(G) | 25 | | |
| Inlet air temperature °C | 30 | | |
| Temperature after cooling °C | ≤50 | | |
| Cooling water volume m ³ /h | 3 | | |
| Piston stroke mm | 130 | | |
| Crankshaft speed r/min | 420 | | |
| Piston average speed m/s | 1.82 (maximum) | | |
| Shaft power kW | ≤25 | | |
| Transmission mechanism lubrication method | Oil pump pressure circulation lubrication | | |
| oil pressure | 0.3~0.5 MPa (G) | | |
| Lubricating oil grade | L-HM32 | | |
| Lubricating oil consumption (Kg) | 150 | | |
| Noise sound pressure level dB(A) | ≤85 | | |
| Unit vibration intensity mm/s | 18 | | |
| Dimensions (length x width x height) mm | 3300X2900X1760 | | |
| Maximum part weight kg | 1500 | | |
| Unit weight: kg | 6000 | | |
| repair space | The maintenance space around and above the compressor shall not be less than 1.5 meters | | |

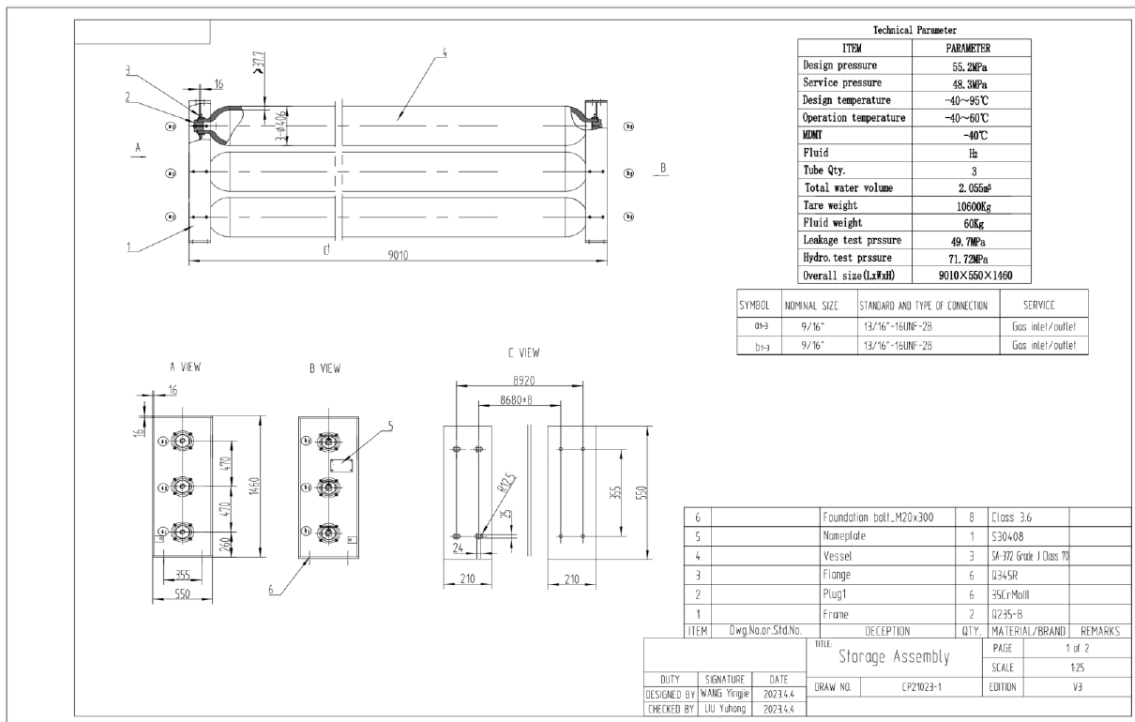
Utilities Consumption Index

| | use | Voltage | unit | normal value | working method |
|-------------|--|----------------|-------------------|--------------|----------------|
| electricity | main motor | 380V | kw | 37 | continuous |
| | oil pump motor | 380V | kw | 0.37 | continuous |
| | oil tank heater | 220V | kw | 2 | Intermittent |
| | motor space heater | 220V | kw | | Intermittent |
| Water | Total amount of cooling water for compressor | Recycled water | m ³ /h | 3 | continuous |

Electrical and Instrumentation Control

| | | | |
|------------------------|--|-----------------------|--------------|
| Motor parameters | | | |
| Motor form | YBX3 -14-37KW low voltage asynchronous motor | | |
| Motor Power | 37KW | Main motor voltage | 380V |
| Motor speed | 420r/min | frequency | 50Hz |
| Temperature rise level | Class B | Insulation class | F |
| degree of protection | IP55 | Explosion-proof grade | DIICT4 |
| Motor weight | kg | installation area | indoor |
| transfer method | direct connection | start method | Direct start |
| Oil supply system | | | |
| Motor Power | 0.37KW | Main motor voltage | 380V |
| Explosion-proof grade | DIICT4 | flow | 12L/min |
| Filtration accuracy | 100μm | work pressure | ≤0.8MPa |

Storage tank



Fuel cell

PureCell[®] Model 400 Hydrogen

This pollution free power generation solution, which uses hydrogen, boasts high production efficiency and also produces clean water as a byproduct.



Hydrogen



8.3 x 2.5 x 3.0m



440kW



HG (120°C)



30-130L/hr



Total 85%,
Electricity 49%, Heat 36%

